# Extraction of Endocrine–Disrupting Compounds from Aqueous Solutions using Ionic Liquids: Theoretical Predictions and Experimentations using Supported Liquid Membrane

*A Thesis Submitted in Partial*
*Fulfillment of the Requirements for the Degree of*

**DOCTOR OF PHILOSOPHY**

by

**SANTHI RAJU PILLI**


**Department of Chemical Engineering**
**Indian Institute of Technology Guwahati**

**August 2014**

*Dedicated*

*To*

*My Family,*
*My Grandma and*
*All My Teachers*

**Department of Chemical Engineering**

**INDIAN INSTITUTE OF TECHNOLOGY GUWAHATI**

---

# CERTIFICATE

---

This is to certify that **Santhi Raju Pilli** has been working under our supervision since June 2010. We are forwarding his thesis entitled **"Extraction of Endocrine–Disrupting Compounds from Aqueous Solutions using Ionic Liquids: Theoretical Predictions and Experimentations using Supported Liquid Membrane"** to be submitted for the award of the degree of Doctor of Philosophy. We certify that he has fulfilled all the requirements according to the rules of this institute and the investigations embodied in his thesis have not been submitted elsewhere for a degree or diploma.

**Dr. Kaustubha Mohanty**
Associate Professor
Department of Chemical Engineering
Indian Institute of Technology Guwahati

**Dr. Tamal Banerjee**
Associate Professor
Department of Chemical Engineering
Indian Institute of Technology Guwahati


**Department of Chemical Engineering**

**INDIAN INSTITUTE OF TECHNOLOGY GUWAHATI**

---

# STATEMENT

---

I hereby declare that the matter embodied in this thesis is the result of investigations carried out by me in the Department of Chemical Engineering, Indian Institute of Technology Guwahati, Assam, India under the supervision of ***Dr. Kaustubha Mohanty*** and ***Dr. Tamal Banerjee***.

In keeping with the general practice of reporting scientific observations, due acknowledgement has been made wherever the work described is based on the findings of other investigations.

Guwahati
August 2014

*Santhi Raju Pilli*

# ACKNOWLEDGEMENT

*First and foremost, with a deepest sense of gratitude, I would like to express my sincere thanks to my supervisors* ***Dr. Kaustubha Mohanty*** *and* ***Dr. Tamal Banerjee****, who had been a constant source of inspiration for me. Their timely help during the crucial phases of my Ph.D career has made possible to achieve my target. My special thanks to them for their valuable guidance, encouragement, inspiration, creative and scientific ideas which helped me to enhance my knowledge. I am also fortunate enough to have their guidelines to cultivate scientific thought. I would mention my heartfelt thanks for them for such a wonderful friendly nature that encouraged me to have many scientific discussions and for teachings for life, for which I remain indebted to them.*

*I would like to acknowledge my sincere gratitude to my doctoral committee chair, Dr. Chandan Das and all my doctoral committee members, Dr. G. Pugzhenthi, Dr. S. Sreedeep for their intuitive reviewing of my work, advices, constructive suggestions and criticism during due course my Ph.D progress seminars. I would like to thank all faculty members of the Department of Chemical Engineering of IIT Guwahati for their invaluable suggestions. I express my sincere gratitude and acknowledgement to IIT Guwahati for all the facilities that were made available to me. I am thankful to Mr. Lukumoni Borah, Mr. Prasun Bhattacharjee and Mr. Harsaraj Biswanath of Department of Chemical Engineering, Mr. S.P. Singh and Mr. Kulakamal Senapati of Central Instruments Facility and all the non-teaching staffs of Department of Chemical Engineering for their help during my Ph.D. tenure. I wish to thank our lab seniors Dr. Somen Jana, Dr. Anathraj Ramalingam, Dr. S. Murugavelh, Dr. A. Anantha Praveen Kumar, Dr. Soumya Sasmal for lending their hands of support whenever needed. I thank*

*all my lab members Amrita Difusa, Samarpita Basu, Madhusmita Dash, Krushna Prasad Shadangi, Dharamashi Rabari, Himadri Sahu, Sanjukta Bhoi, Basudhrity Banerjee and Anand Bharati for their invaluable cooperation and suggestions. I further take this precious opportunity to thank (Dr.) Venkata Swamy Nalajala and Mr. Venubabu Borugadda who have shared their thoughts and views with me and also for their endless support, friendship, joyful moments, for being my rest upon.*

*I thank all my IITG close friends, Sarede Yadav, China Malakondaiah Kaniganti, Anadbabu Desamala, Kamal Kumar, Yennam Rajesh, Arijit Das, A. Giri, Emani Sriharsha, Rajasekar Reddy, Manish Kamal, Murali Pujari, Amruta, Manna, Sanjeev, Ruhit, Chndra Sekhar, Anil Kumar, Ravi Bolledu, Rajeev, Seim T, Snigdha, Swaroopa Rani, Bhaskar Jothi Medhi, Kanchopogu Suresh, Kelothu Suresh and Satyanarayana for all the laughs, joyful moments, for their support and suggestions.*

*I also take this opportunity to thank all of my Ph.D. batch mates (June, 2010) and the other research scholars @ Chemical Engineering department and all my IITG friends, who have shared their thoughts and views with me. My M.Tech friends Ravi Kumar Bandaru, Sama Vijay Krishna, Venkateswara Reddy, Samuel Mekala, Balaji Chilukoti, Girish Madeti, Chenchaiah and other friends of M.Tech 2010 batch of IITG are grateful for their time and friendship and timely help.*

*My teachers, Mr. Pallikona Samuel, Mrs. Vijaya Kumari, Mrs. Kamala, Mr. Janaki Ram, Mr. T. Sambha Sivarao, Mrs. Mineni Vijaya Lakshmi, Mrs. K. Santhi Latha, Rev. M. Yesu Bhaktu and Mr. Partha Sarathi from which my scientific interest is generated and multiplied with time. Therefore, I wish to thank them for all their valuable teachings and emotional attachment.*

*Finally, my Ph.D. endeavor could not have been completed without the endless love, unending support, tolerance and blessings from my parents,* ***Pilli Nageswara Rao*** *and* ***Siromani,*** *who encouraged me to do my very best in everything. I wish to express my sincere gratitude to my sister (Prema Kumari), brother (Vinaya Babu). They are all the main soul and inspiration for each and every step that I achieve in my life. My highest sense of gratitude to my parents remains throughout my life.*

*Last but not the least, my most heartfelt thanks goes to my wife,* ***Sowjanya,*** *for her enormous amount of love and patience, abundant praise, constant and continuous affection, encouragement, unending support morally and financially. After proofreading my papers, listening to my presentations, and hearing me talk about my studies (all while taking care of our son and my mom), she should probably get a PhD too. Since, I mentioned my kid, thanks to my son, Satvik Raju (Cherry), for being parenthood.*

*For financial support of this research, I would like to thank the Department of Science and Technology (****DST****), Government of India vide sanction No. SR/FTP/ETA–56/2010 under the Fast Track Scheme.*

*Santhi Raju Pilli*

# ABSTRACT

Solvent based extraction processes are useful in the selective removal of endocrine disrupting compounds (EDCs) like Pentachlorophenol (PCP) and DichloroDiphenylTrichloroethane (DDT), Phthalic Acid (PA), Endosulfan (ES) and Bisphenol–A (BPA) from aqueous solution. Ionic liquids (ILs) are a very good alternative for the volatile organic solvent as extractant. This work reports the judicious screening of various ionic liquids for the extraction of EDCs from aqueous solutions. COSMO–RS (Conductor–like Screening MOdel for Real Solvents) method was used for the prediction of selectivity of these compounds in aqueous medium at infinite dilution. These screening results were used for the application of LLE and SILM processes. This work also emphasis on the experimental and COSMO–RS validation using the octanol–water partition coefficients ($K_{ow}$) of EDC's.

Additionally, HOMO–LUMO energy studies were predicted for systems such as: [PCP]+[$C_4$DMIM][$PF_6$] and [PA]+[$C_4$DMIM][$PF_6$] and individual species. DFT based B3LYP/6-31G* method was adopted to carry out geometry optimization. The experimental and theoretical $^1$H NMR chemical shifts of predicted systems were also carried out to benchmark our predictions. Further, an experimental investigation of LLE behavior of [$C_4$DMIM][$PF_6$](1)+PCP(2)+water(3) and [$C_4$DMIM][$PF_6$](1)+PA(2)+water(3) was carried. The selectivity and distribution coefficients determined from the tie line data, confirmed high values of selectivity ~ 24–29 for PA and ~106–293 for PCP. The UNIQUAC and NRTL models were then used to correlate the experimental data.

Through SILM experiments, the effect of operating parameters such as pH and feed concentration along with flux calculation and mechanism of separation were presented. The transport mechanism of Endosulfan, PCP and phenol through SILM was explained by hydrogen bonding interactions, hydrophobic interactions and carbon–π bonding interactions. The characterization of membrane was carried by SEM and EDX analysis. A maximum of 72% (at feed pH=6.5) of endosulfan permeation was observed using 0.1 M NaOH as stripping agent after 30 h. The rate of permeation of endosulfan decreases with increase in pH from 2 to 10 (87–55%). Highest PCP permeation of 86.74% was obtained by [TBP][$PF_6$] at feed of pH 4, whereas [$C_4$DMIM][$PF_6$] gave 78.82% after 30 h at feed of pH 4. The maximum phenol permeation rate of 75.63% was achieved over an experimental run of 24 h at pH 4. High permeation rate was obtained by [CYPHOS® 104] among all the six ionic liquids studied. The order of the permeation rates followed: [CYPHOS® 104] > [CYPHOS® 103] > [CYPHOS® 102] > [CYPHOS® 101] > [$C_8$MIM][$PF_6$] > [Aliquat 336®]. The operational stability and performance of the supported liquid membranes was studied via characterization techniques such as SEM, EDX and FTIR analysis. The transport mechanism of EDC through SILM was also proposed. SILM and LLE experiments have been shown potential for further development into a process for the removal of organic compounds from wastewater in the bench scale or in industry.

# CONTENTS

# LIST OF TABLES

# LIST OF FIGURES

# CHAPTER 1

## INTRODUCTION AND LITERATURE REVIEW

## 1.1. Introduction

In recent years, the contamination of the environment, especially water has led to a harmful impact on the physical system and living beings. Population growth, rapid urbanization and industrialization have further increased the problem particularly related to wastewater pollution.

Industries are a large promoter of economic growth and as India strive to maintain and accelerate its impressive GDP growth; the demand for water in industrial sector is also bound to increase. Moreover, the effluents generated by industries such as pulp and paper, thermal power plants, textiles, and the iron and steel is huge in quantity. Industries in India have also been criticized for taking inadequate steps to comply with existing environmental standards. Discharge criteria required the installation of facilities that performed what is now called primary treatment of wastewater. This involved using screens and sedimentation tanks to remove most of the contaminants in the wastewater that float or settle. As subsequent discharge criteria are tightened, secondary treatment became necessary. Secondary treatment is accomplished by bringing together waste, bacteria and oxygen in trickling filters or the activated sludge process. The advanced treatment processes go beyond conventional secondary treatment and include the removal of recalcitrant organic compounds like pentachlorophenol (PCP), dichlorodiphenyltrichloroethane (DDT), endosulfan (ES), phthalic acid (PA), and bisphenol A (BPA). In this work these very class of compounds also known as Endocrine Disrupting Compounds (EDCs) are considered. The section below explains a brief introduction of toxic chemicals studied in this work.

***PCP and DDT*** are some of the harmful environmental chemicals due to their toxicity and pollution with dioxins. PCP is found in two forms as a sodium salt of PCP and is produced by the chlorination of phenol in the presence of a catalyst. It dissolves in water easily. DDT produced by the reaction of $CCl_3CHO$ (chloral) with chlorobenzene ($C_6H_5Cl$) in presence of sulfuric acid acting as a catalyst is almost insoluble in water but has a superior solubility in most of the organic solvents, oils and fats. Further both PCP and DDT are commercially well–known synthetic pesticides or insecticides [Caralson et al., 2004; Wurl et al., 2006; Fan et al, 2008].

***Phthalic Acid*** (PA) and ***phthalic acid esters*** (PAEs) are environmental chemicals because of its toxicity and pollution with dioxins. Phthalic acid is extremely soluble in boiling water (18 g/100 mL), and is much less soluble in chilled (14 °C) water (0.54 g/100 mL). Phthalic acid and esters of the phthalic acids (PEAs) are common industrial chemicals and major raw material in polymer industries. PA is a commercially well–known synthetic chemical and is an important precursor for the synthesis of many other organic substances. Commonly used PEAs are dimethyl phthalate (DMP), diethyl phthalate (DEP), di–n–butyl phthalate (DBP), butylbenzyl phthalate (BBP), di(2–ethylhexyl) phthalate (DnOP), di–n–octyl phthalate (DnOP). The polymer materials from phthalic acid esters are extensively used for the manufacturing of large variety of products such as medical devices, lubricants, binders, adhesives and glues, personnel care products, detergents, toys, plastic films, insulating materials, paints, food and pharmaceuticals [Rudel and Perovich, 2009]. PAEs have also been used as plasticizers in various products [Rudolph, 1970]. PA esters have been listed as ‘priority pollutants’ by the US EPA [Keith and Telliard, 1979]. Recently, PAEs have

been suspected to cause estrogenic effects in mammals including humans leading to the damage of the reproductive system [Parmar et al., 1995; Toppari et al., 1995; Fukuoka et al., 1997]. It is also considered as endocrine disrupting in nature.

***Endosulfan*** (CAS Registry Number is 115-29-7) is an off–patent organochlorine pesticide and is used to kill insects and mites. There are several Persistent Organic Pollutants (POPs) among which endosulfan is one such chemical compound. Theo Colborn and co-workers are pioneers on endocrine gland disruption studies and have listed endosulfan as an EDC [Colborn et al., 1997]. Recently endosulfan became a highly controversial agricultural chemical because of its acute toxicity, possibility for bioaccumulation and its role as an EDC. Endosulfan usage is responsible for many fatal pesticide poisoning incidents around the world [PAN magazine, 2006]. Endosulfan spraying on cashew gardens resulted in a series of abnormalities reported in local children of Kasargod district of Kerala (India) in 2001 [Romeo and Quijano 2002]. Endosulfan has been found to contaminate diverse parts of the atmosphere, including ponds, lakes and drinking water sources. Endosulfan residues were detected from air, water (surface and ground water) and soil in India [Chowdhari et al., 2001].

***Bisphenol A (BPA)*** was first synthesized in eighteenth century and is usually found in detergents, resins, plasticizers and monomers in plastic packaging materials [Paris et al., 2002]. The major sources of human exposure to BPA occur through direct contact in the workplace or at home, or through intake of contaminated water, food, or air [Gomez et al., 2009]. In September 2010, Canada became the first country to declare BPA as a toxic

substance [http://en.wikipedia.org/]. In the European Union and the Canada, BPA use is banned in baby feeding bottles. Because of its adverse health effects and its carcinogenicity there is a need to remove BPA from aqueous phase. Evidently some of these chemicals are functional but at the same time many are toxic and they harm the environment, human as well as animal health.

Apart from the uses of above mentioned chemical compounds in daily life, there are concerns related to health effects due to their endocrine disruption nature. Various endocrine disrupting compounds along with their effect and potential source have been reported in recent years [Chang et al., 2009] and are presented in Table 1.1 [Daniel et al., 2011]. Water and wastewater are some of the main routes of exposure of these EDCs, it is essential to determine at what levels EDCs are found in these media and how these levels may be reduced. Section 1.2. briefly describes the health effects associated with EDCs.

## 1.2. Methods of EDC Removal

The conventional physico-chemical methods to remove EDCS include solvent extraction and micro-extraction [Valsaraj and Springer, 1986; Francisco et al., 2008; Lozano et al., 2011], sorption [Weber et al., 1968; Hu et al, 1994; Diaz-Flores et al., 2006; Akhtar et al., 2007; Comerton et al., 2007; Pilli et al., 2010; Luo et al., 2011], photolytic and photodegradation [Topalov et al., 2001; Qiaolin and Dionysiou, 2004; Subramanian et al., 2007], magnetic nanomaterials [Lin et al., 2010], composite membranes (surfactant–enhanced) [Kumara et al., 2008], ultrasonication [Pham et al., 2009] and advanced-catalytic oxidation processes. In literature [Fukushima et al., 2003; Saritha et al., 2007; Ning et al.,

2007], coagulation, sedimentation, and filtration were used for the minimal levels of removal [Zhang et al., 1999; Ternes et al., 2002]. Some other notable methods include biological and aerobic degradation [Zwiener et al., 1995; Murthy and Manonmani, 2007]. However, the above methods can be used either independently or on conjunction with others. Bioremediation process which is one of the widely used process, involves the action of live and active microorganisms to degrade or remove the organic pollutant by transmuting them into non-toxic substances, specifically, carbon dioxide and water [Susan et al., 1993]. Though the process is eco–friendly, low–cost and highly competent it cannot process the pollutants which are not readily biodegradable. Some of the EDCs are highly resistant to bioremediation also [Sato and Matsumura 2003; Ang et al., 2005]. In addition, many of these processes are pertain with their own inherent limitations such as emulsion formation, more energy requirement, generation of toxic and hazardous sludge which causes persistent solid wastes disposal problem, perceptive operating conditions, low reproducibility, labor intensive and have high capital and operating costs. In addition to the generated solid waste, carbon beds may leads to fire hazards incase activated carbons are used as adsorbents. Thus, it is essential for an alternate process which can deal with the various issues that are not addressed by other conventional techniques.

### 1.3. Membrane Technology

In recent years, membrane based technologies has shown potential application in process industries. This method has considerable advantages because of low energy consumption, low temperature of operation, no phase change and occurrence of simultaneous

concentration and purification of products [Paulson et al, 1987; Fan et al., 2008; Potdar et al., 2012]. Apart from these, membrane-based separation processes are getting appreciable attention due to easy scaling up, capability of integration with other process (hybrid processes), and adjustable characteristics of the membrane. Liquid membranes in general have certain advantages such as generation of large surface area in small equipment, simultaneous extraction, and stripping in single step and high selectivity [Pilli et al., 2014a]. Liquid membranes are divided into several groups such as bulk membrane (BLM), supported liquid membrane (SLM) and emulsion liquid membrane (ELM). Out of these, SLM technology is of much interest as it has high separation factor, easy scale up and low capital and operating costs. The SLM is simple in design and is used mostly in laboratory, but could not be scaled up for industrial use till date. Essentially, this is just a hydrophobic porous membrane whose pores are filled with the organic liquid and placed in between the source phase and receiving phase. By means of diffusional process, components of the aqueous solutions can move through SLM from one phase to another phase. The advantageous fact with SLM is that the amount of solvent needed in the process is minimum and the processes of extraction and stripping are combined into one single stage. The use of supported liquid membranes (SLMs) for the recovery of metal ions from aqueous solutions, the removal of contaminants from industrial effluents and the recovery of fermentation products, has been widely studied during the past 20 years [Magos, 1976; Keith and Walters, 1992; Pichichero et al., 2002; MHRA, 2003; Hviid et al., 2003; Fan et al., 2008]. However, industrial applications of SLMs are still scarce, mainly due to the concern with SLM stability and long–term performance [The European Agency for the evaluation of medical products, 2001],

leading to a reduction of solute flux and membrane selectivity. These effects result in the loss of solvent from the supporting membrane, either by evaporation or dissolution/dispersion into the adjacent phases [Doig et al., 1999]. Several approaches have been proposed to minimize instability problems, such as the use of mild operating conditions, protection of the SLM with a gel layer [Official Journal of the European Communities, 1986], and adequate design of both the supporting membranes and the contacting phases [Livingston, 1993]. Moreover, the choice of solvent as membrane phase in SLMs is very significant.

Extractants used in liquid membranes are mainly organic solvents such as aromatic and aliphatic hydrocarbons, amines, esters, ethers, ketones, and nitrated or chlorinated hydrocarbons. Most of these solvents are carcinogens as recognized by NIOSH, volatile at room temperature, non-biodegradable and are flammable. Search for better and greener solvents ends with room temperature ionic liquids (ILs), which have numerous advantages over the traditional organic solvents. ILs, which are well known as green solvents (only very few of them are mildly toxic in nature) [Pilli et al., 2014b] can be better solvents than traditional organic solvents. Due to the relatively high viscosity of the ionic liquids, the preparation of SLMs can play a significant role on the liquid immobilization and consequently on the membrane stability. Moreover, ionic liquids can be tailor made to target the separation of a particular pollutant.

### *1.3.1. Ionic liquid as a solvent*

Before considering a new solvent for incorporation into an industrial application, a fundamental understanding must be established for the chemical and physical properties of

the solvent. Ideally, if a new solvent is to be introduced as a 'green' solvent, it should be an improvement over the solvents currently available. Optimal physical properties would include low viscosity to facilitate mixing and a large density difference in comparison to other process fluids to hasten phase separation. Chemically, the solvent should have a high selectivity for the solute. To encourage widespread use of the solvent, it should be inexpensive to produce, recyclable, and robust to endure various processing environments. Of most interest to us at present are Ionic Liquids that are liquid at room temperature and represent potential replacements for traditional volatile organic solvents in separation processes [Brennecke et al., 2001]. ILs are composed solely of organic cations and organic or inorganic anions. They are usually comprised of nitrogen-containing organic cations and anions such as halogens, tetrafluoroborates and hexafluorophosphates. Relations between the properties and the chemical structure have been demonstrated for IL's. For example, increasing the size of the cation or anion decreases the melting point [Behar et al., 2001; Behar et al., 2002] and longer N-alkyl chain of the cation resulted in lower density [Huddleston et al., 2011].

IL's are used as a potential alternative medium in many organic reactions [Huddleston et al., 2011; Rogers and Seddon, 2002; Zhao and Malhotra, 2002]. Typical examples include Diels-Alder reaction [Earle et al., 1999; Xiao and Malhotra, 2004], Friedel-Crafts reaction [Earle et al., 1998], and polymerization [Zhang et al., 2002]. Other applications include nanostructured material fabrication [Zhou et al., 2004], separation and extraction [Bartsch et al., 2002], biotechnology [Park and Kazlauskas, 2003] and electrochemistry [Mazurkiewicz et al., 2003]. Application of ILs in separation and extraction of various compounds, e.g.

substituted benzene derivatives, organic acids, antibiotics, poly-cyclic aromatic hydrocarbons, amino acids, paints, dyes and sulfur compounds have been reported. Examples of cations (Fig. 1.1) are 1-alkyl-3-alkylimidazolium or 1-alkylpyridinium and examples of anions (Fig. 1.2) are hexafluorophosphate, tetrafluoroborate, aluminium(III) chloride and various organic ions based on fluorinated amides, imides, nitrides and methides.

In recent times SLM technology has gained a lot of attention for the removal of contaminants from wastewater and industrial gases by using ILs as carrier solvents in order to enhance the solute transportation [Danesi, 1984; Parthasarathy et al, 1997; Scovazzo et al., 2004; Matsumoto et al., 2005; Kocherginsky et al., 2007]. This work is first of a kind which attempts to remove EDCs from aqueous phase using supported ionic liquid membrane (SILM). However the selection of right cation and anion is not easy as due to the possibility of limitless combinations of cations and anions. Thus, a computational screening is required to choose the correct cation and anion combination.

### *1.3.2. Computational screening of ionic liquids*

For the effective removal of EDC compounds from water, the structural and theoretical information from micro to macro level is required for IL and its mixture with EDC and water. This can be helpful in reducing the operating and investment cost of the simultaneous EDC removal. To study chemical process involving IL with other compounds it is necessary to understand reactivity and stability of the interacting system *via Ab initio method*. The Higher Occupied Molecular Orbital (HOMO) and Lower Unoccupied Molecular Orbital (LUMO) energies with its energy gap can define the scalar properties of

the mixture of IL and EDC at molecular level. The detailed examination of relative energies (LUMO/HOMO) and structural interaction can therefore be used to build up a picture of interactions occurring in ionic liquid and its complexes.

The COSMO (**CO**nductor like **S**creening **Mo**del) [Klamt et al., 1993, 1995, 2005] in combination with **R**eal **S**olvents i.e. *COSMO-RS* can also be used to compute the chemical potential and activity coefficient of any component in a mixture. Thus, COSMO–RS is an effective way to screen the potential cations and anions for the removal of EDC from waste water. This is essential considering the fact that experimental screening of ILs with various cations and anions combinations is not only time consuming, but also expensive. In such a scenario pseudo mixture of IL, EDC and water is first made computationally and then the activity coefficient at infinite dilution of EDC in IL and water is generated from quantum chemical calculations. The values of activity coefficient give us an indication to the limit of extraction. For example, the value of activity coefficient less than one indicates higher solubility. Likewise a higher value indicates immiscibility. With these values in hand, we can then choose the appropriate IL as a supporting medium to perform experiments. To our best knowledge, no systematic study was made towards the COSMO–RS screening of RTILS followed by SILM and LLE experiments for the removal EDCs such as PCP, DDT, PA, endosulfan and BPA from aqueous phase.

## 1.4 Objectives of the Thesis

Thus, based on the above brief discussion, it is obvious that there is enough scope to carry out further work on the removal of EDCs from aqueous solution using IL's by extraction. To achieve this, the present work was carried out with the following objectives :

(1) Perform a judicious screening of various ILs using quantum chemical based COSMO-RS methodology so as to find out the best IL for the extraction of EDCs such as PCP, DDT, and Endosulfan.

(2) Using the potential IL from (1), predict the HOMO–LUMO energy interactions between PCP, PA and IL's using Density Functional Theory.

(3) Carry out the Liquid–Liquid Extraction experiments on the favorable IL's (as per (1)) in ternary mixtures of IL+[PCP]+[water] and IL+[PA]+[water] at $T$ = 298.15 K and $P$ = 1 atm.

(4) Demonstrate the removal of Phenol, Endosulfan and PCP from wastewater using SILM technique where the IL was chosen as per (1).

## 1.5 Structure of the Thesis

The thesis is organized into the following chapters as discussed below:

*Chapter 1* represents an introductory discussion and literature on wastewater contamination and removal strategies. It additionally discusses regarding major sources of pollutants like Endocrine–Disrupting Compounds like PCP, DDT, Endosulfan, Phthalic acid, BPA, heavy

metals and phenolic derivatives moreover as their impacts on aquatic, animal and human life. It emphasize on the features of various presently available wastewater treatment techniques and therefore the requirement of the alternative technique using ionic liquids based on the detailed review of the literatures. It additionally discusses the importance of membrane technology and ionic liquids as green solvents in membrane based technologies. This chapter also introduces the computational screening of ionic liquids for the extraction of Endocrine–Disrupting Compounds from aqueous phase. It's also focus on interaction energies of ionic liquids with Endocrine–Disrupting Compounds via *ab initio* method. The end of this chapter, the importance and objectives of this work has been made and explained according to the current demand within the field of wastewater treatment technologies. Organization of this thesis is highlighted in simple form in this chapter as well.

*Chapter 2* discusses the Computational Methodology (COSMO–RS and HOMO–LUMO energy studies). This chapter introduces several widely used computational chemistry methodologies to predict thermodynamic properties using quantum chemical calculation such as Gaussian, GAMESS, and NWChem. Thereafter, statistical mechanics was used to furnish the link between quantum mechanics of individual molecules and thermodynamic properties. This chapter also describes fundamentals of COSMO–RS theory, COSMO file generation and its application. The effect of level of theories such as Hartree–Fock, B3LYP and PM3 along with different basis sets used for initial geometry optimization on isolated cations and anions were also studied. The background theory of HOMO/LUMO energy, HOMO–LUMO energy gap and the global hardness and softness, chemical potential, electronegativity and electrophilicity index, were explained thoroughly.

*Chapter 3* explains the Material and Experimental methods**.** This chapter also outlines the experimental details, such as materials and methods adopted, chemicals used and their make and analytical equipments used in this study for both LLE and SILM experiments.

*Chapter 4* reports the results and discussions for both quantum chemical and experimental studies. Initially the values of Infinite Dilution Activity Coefficients (IDAC) using COSMO–RS model was reported. Here the selectivity, performance index and capacity of PCP, DDT, and Endosulfan species at infinite dilution are predicted. These screening results were used for the application of LLE and SILM processes. This chapter also gives emphasis on the experimental and COSMO-RS validation of the octanol-water partition coefficients ($K_{ow}$) of EDC's. Further, the parameters like global hardness and softness, chemical potential, electronegativity and electrophilicity index, HOMO/LUMO energy, HOMO–LUMO energy gap were obtained for individual species and mixtures namely: [PCP]+[$C_4$DMIM][$PF_6$] and [PA]+[$C_4$DMIM][$PF_6$]. In addition to this, the experimental and theoretical $^1$H NMR chemical shifts of [PCP]+[$C_4$DMIM][$PF_6$] and [PA]+[$C_4$DMIM][$PF_6$] was compared and validated.

*Chapter 5* describes the experimental investigation of Liquid–Liquid Equilibrium (LLE) behavior of [$C_4$DMIM][$PF_6$] (1)+PCP(2)+water(3) and [$C_4$DMIM][$PF_6$](1) +PA (2)+water(3) was carried out at $T$ = 298.15 K and $p$ = 1 bar. The concluding part of the work demonstrated the removal of PCP and ES using SILM. Here [$C_4$DMIM][$PF_6$], Tetrabutyl–phosphonium hexaflourophosphate [TBP][$PF_6$] ILs were immobilized with polyvinylidene fluoride membrane (PVDF) membranes for separation of Endosulfan, PCP and phenol from aqueous

phase using SILM. Effect of operating parameters such as pH and feed concentration along with flux calculation and mechanism of separation were presented. The transport mechanism of Endosulfan, PCP and phenol through SILM was explained by hydrogen bonding interactions, hydrophobic interactions and carbon–π bonding interactions.

*Chapter 6* summarizes the key results obtained from the present study. The later part of this chapter also focuses on the scope for the future work that can be carried out.

**References**

Akhtar, M., S.M. Hasany, M.I. Bhanger, S. Iqbal, Low cost sorbents for the removal of methyl parathion pesticide from aqueous solutions, *Chemosphere.* 66 (2007) 1829–1838.

Ang, E.L., H. Zhao, P.J. Obbard, Recent advances in the bioremediation of persistent organic pollutants via biomolecular engineering, *Enzyme Microb. Technol.* 37 (2005) 487.

Bartsch, R.A., S. Chun, S.V. Dzyuba, Ionic Liquids as Novel Diluents for Solvent Extraction of Metal Salts by Crown Ethers, ACS Symposium Series 818 (2002) 58–68.

Behar, D., C. Gonzalez, P. Neta, Reaction Kinetics in Ionic Liquids: Pulse Radiolysis Studies of 1-Butyl-3-methylimidazolium Salts, *J. Phys. Chem. A.* 105 (2001) 7607–7614.

Behar, D., P. Neta, C. Schultheisz, Reaction Kinetics in Ionic Liquids as Studied by Pulse Radiolysis: Redox Reactions in the Solvents Methyltributylammonium Bis(trifluorom ethylsulfonyl)imide and *N*-Butylpyridinium Tetrafluoroborate, *J. Phys. Chem. A.* 106 (2002) 3139–3147.

Brennecke, J.F., E.J. Maginn, Ionic Liquids: Innovative Fluids for Chemical Processing, *AIChE J.* 47 (2001) 2384–2389.

Carlson, L.D., I. Basu, R.A. Hites, Annual Variations of Pesticide Concentrations in Great Lakes Precipitation, *Environ. Sci. Technol.* 38 (2004) 5290–5296.

Chang, H.S., K.H. Choo, B. Lee, S.J. Choi Review: The methods of identification, analysis, and removal of endocrine disrupting compounds (EDCs) in water, *J. Hazard. Mater*. 172 (2009) 1–12.

Chowdhari, D.K., A. Nazir, D.K. Saxena, Effect of Three Chlorinated Pesticides on hsromega stress gene in transgenic Drosophila melanogaster. *J. Biochem. Mol. Toxicol.* 15 (2001) 173–186.

Colborn, T, D. Dumanoski, J.P. Meyers, Our Stolen Future: How We Are Threatening Our Fertility. Intelligence and Survival, 1997, Plume.

Comerton, A.M., R.C. Andrews, D.M. Bagley, P. Yang, Membrane adsorption of endocrine disrupting compounds and pharmaceutically active compounds, *J. Memb. Sci.* 303 (2007) 267–277.

Danesi, P.R., Separation of Metal Species by Supported Liquid Membrane, *Sep. Sci. Technol.* 19 (1984) 11–12.

Daniel. V., Access Science, McGraw–Hill Companies, New York, http://www. accessscience.com (accessed online 27.04.11).

Diaz–Flores, P.E., R. Leyva–Ramos, R.M. Guerrero–Coronado, J. Mendoza–Barron, Adsorption of Pentachlorophenol from Aqueous Solution onto Activated Carbon Fiber, *Ind. Eng. Chem. Res.* 45 (2006) 330–336.

Doig, S.D., A.T. Boam, A.G. Livingston, D.C. Stuckey, Mass transfer of hydrophobic solutes in solvent swollen silicone rubber membranes, *J. Memb. Sci.* 154 (1999) 127–140.

Earle, M.J., McCormac, P.B., Seddon, K.R. Diels–Alder Reactions in Ionic Liquids, *Green Chem.* 1 (1999) 23–25.

Earle, M.J., K.R. Seddon, C.J. Adams, G. Roberts, Friedel – Crafts Reactions in Room Temperature Ionic Liquids, *Chem. Commun.* 19 (1998) 7–2098.

Fan, J., Y. Fan, Y. Pei, K. Wu, J. Wang, M. Fan, Solvent extraction of selected endocrine disrupting phenols using ionic liquids, *Sep. Purif. Technol.* 61 (2008) 324–331.

Fukuoka, M., S. Niimi, T. Kobayashi, Y. Zhou, T. Hayakawa, Possible origin of testicular damage by phthalic acid ester, *Jpn. J. Toxicol. Environ. Health.* 43 (1997) 21.

Francisco, J., R., Soledad, P., Dolores Single–drop coacervative microextraction of organic compounds prior to liquid chromatography Theoretical and practical considerations, *J. Chromatogr. A.* 1195 (2008) 25–33.

Fukushima, M., A. Sawada, M. Kawasaki, K. Tatsumi, Removal of pentachlorophenol from contaminated soil by catalytic oxidation with iron(III)-porphyrin complexes and potassium monopersulfate, *Toxicol. Environ. Chem.* 85 (2003) 1–3.

Gomez, A.B., S. Rubio, D. Perez-Bendito, Analytical methods for the determination of bisphenol A in food, *J. Chromato.* A 1216 (2009) 449–469.

http://en.wikipedia.org/wiki/Bisphenol_A, Accessed: 17th June. 2012.

Huddleston, J.G., A.E. Visser, W.M. Reichert, H.D. Willauer, G.A. Broker, J.P. Hallett, T. Welton, Room-Temperature Ionic Liquids: Solvents for Synthesis and Catalysis. 2, *Chem. Rev.* 111 (2011) 3508–3576.

Hu, Z., R.A. Korus, W.E. Levinson, R.L. Crawfords, Adsorption and Biodegradation of Pentachlorophenol by Polyurethane–Immobilized Flavobacterium, *Environ. Sci. Technol.* 28 (1994) 491–496.

Hviid, A., M. Stellfeld, J. Wohlfahrt, M. Melbye, Association between thimerosal containing vaccine and autism, *J. Am. Med. Assoc.* (JAMA) 290 (2003) 1763.

Lin, J., Z. Wu, W. Tseng, Extraction of environmental pollutants using magnetic nanomaterials, *Anal. Methods: Advancing Methods and Applications.* 2 (2010) 1829–2056.

Livingston, A.G., A novel membrane bioreactor for detoxifying industrial wastewater: I. Biodegradation of phenol in a synthetically concocted wastewater, *Biotechnol. Bioeng.* 41 (1993) 915.

Lozano, L.J., C. Godínez, A.P. de los Ríos, F.J. Hernández–Fernández, S. Sánchez–Segado, Alguacil, Recent advances in supported ionic liquid membrane technology, *J. Memb. Sci.* 376 (2011) 1–14.

Luo, L., L. Lou, X. Cui, B. Wu, J.Hou, B. Xun, et al., Sorption and desorption of pentachlorophenol to black carbon of three different origins, *J. Hazard. Mater.* 185 (2011) 639–646.

Keith, L.H., Walters D.B. The National Toxicology Pro gram's Chemical Data Compendium, Vol I – VIII. Boca Raton, FL: Lewis Publishers, Inc, 1992.

Kocherginsky, N.M, Qian Yang, Lalitha Seelam, Recent advances in supported liquid membrane technology, *Sep. Purif. Technol.* 53 (2007) 171–177.

Kumara, Y., K.M. Popat, H. Brahmbhatt, B. Ganguly, A. Bhattacharya, Pentachlorophenol removal from water using surfactant–enhanced filtration through low–pressure thin film composite membranes, Journal of Hazardous Materials *J. Hazard. Mater.* 154 (2008) 426–431.

Magos, L., Neurotoxic character of thimerosal and the allometric extrapolation of adult clearance half – time to infants, *J. Appl. Toxicol.* 23 (1976) 263.

Matsumoto, M., Y. Inomoto, K. Kondo. Selective separation of aromatic hydrocarbons through supported liquid membranes based on ionic liquids, *J. Memb. Sci.* 246 (2005) 77–81.

Medicines and Healthcare products Regulatory Agency (MHRA), Statement from the Committee on Safety of Medicines –Further data support safety of thiomersal in vaccines (2003) ( http://www.mca.gov.uk).

Mazurkiewicz, J.H., P.C. Innis, G.G. Wallace, D.R. MacFarlane, M. Forsyth, Conducting Polymer Electrochemistry in Ionic Liquids, *Synth. Met.* 135–136 (2003) 31–32.

Murthy, H.M.R., H.K. Manonmani, Aerobic degradation of technical Hexachloro–cyclohexane by a defined microbial consortium. *J. Hazard. Mater.* 149 (2007) 18.

Ning, B., N. Graham, Y. Zhang, M. Nakonechny, E.G. Mohamed, Degradation of Endocrine Disrupting Chemicals by Ozone/AOPs, *Ozone Sci. Eng.* 29 (2007) 153–176.

*OJ European Communities*. Nº L 74/49, 84/156/EEC (1986).

Paris, F., P. Balaguer, B. Terouanne, N. Servant, C. Lacoste, J. Cravedi, J. Nicolas, C. Sultan, Phenylphenols, biphenols, bisphenol-A and 4-tert-octylphenol exhibit alpha and beta estrogen activities and antiandrogen activity in reporter cell lines, *Mol. Cell. Endocrinol.* 193 (2002) 43–49.

Park, S., R.J. Kazlauskas, Biocatalysis in Ionic Liquids–Advantages Beyond Green Technology, *Curr. Opin. Biotechnol.* 14 (2003) 432–437.

Parmar. D., S.P. Srivastava, G.B. Singh, P.K. Seth, Testicular toxicity of di(Z-ethylhexyl) phthalate in developing rats, *Vet. Human Toxicol.* 37 (1995) 310–313.

Parthasarathy, N., M. Pelletier, J. Buffle, Hollow fiber based supported liquid membrane: a novel analytical system for trace metal analysis, Anal. Chim. Acta 350 (1997) 183–195.

Paulson, D.J., R.L. Wilson, D.D. Spatz, Cross flow membrane technology and its applications, *Food Technol.* 38 (1984) 77–87.

Pesticide Action Network North America, Speaking the Truth Saves Lives in the Philippines and India, PAN Magazine, Fall 2006.

Pichichero, M.E., E. Cernichiari, J. Lopreiato, J. Treanor, Mercury concentrations and metabolism in infants receiving vaccines containing thiomersal: a descriptive study, *Lancet.* 360 (2002) 1737.

Pilli, S.R., V.V. Goud, K. Mohanty, Biosorption of Cr(Vi) from aqueous Solutions onto Hydrilla Verticillata Weed: Equilibrium, Kinetics and Thermodynamic Studies, *Environ. Eng. Manag. J.* 9 (2010) 1715.

Pilli, S. R., T. Banerjee, K. Mohanty, Performance of different ionic liquids to remove phenol from aqueous solutions using supported liquid membrane, Desalination and Water Treatment, (2014a) 1–11 (doi: 10.1080/19443994.2014.907750).

Pilli, S. R., T. Banerjee, K. Mohanty, 1-Butyl-2,3-dimethylimidazolium hexaflourophosphate as a Green Solvent for the Extraction of Endosulfan from Aqueous Solution Using Supported Liquid Membrane, Chemical Engineering Journal, 257 (2014b) 56–65.

Pham, T.T.H., S.K. Brar, R.D. Tyagi, R.Y. Surampalli, Ultrasonication of WWS-Consequences on biodegradability and flowbility, *J. Hazard. Mater.*, 163 (2009) 2–13.

Potdar, S., R. Anantharaj, T. Banerjee, Aromatic Extraction Using Mixed Ionic Liquids: Experiments and COSMO–RS Predictions, *J. Chem. Eng. Data.* 57 (2012) 1026–1035.

Qiaolin, Y., D.D. Dionysiou, Photolytic degradation of chlorinated phenols in room temperature ionic liquids, *J. Photochem. Photobiol. A: Chemistry*. 165 (2004) 229–240.

Rogers, R.D., K.R. Seddon, Ionic liquids: Industrial applications for green chemistry, A.C.S: Washington DC, 2003.

Romeo, F., M.D. Quijano, Endosulfan Poisoning in Kasargod, Kerala, India, Report of a \Fact Finding Mission, Manila, Philippines (Unpublished Report, 2002).

Rudel. R., L. Perovich, Endocrine disrupting chemicals in indoor and outdoor air, *Atmos. Environ.* 43(17) (2009) 170–181.

Rudolph. J., J.R. Robert, Plasticizers from Plastic Devices: Extraction, Metabolism, and Accumulation by Biological Systems, *Science.* 170 (1970) 460–462.

Saritha, P., C. Aparna, V. Himabindu, Y. Anjaneyulu, Compar–ison of various advanced oxidation processes for the degradation of 4-chloro-2 nitrophenol. *J. Hazard. Mater*. 149 (2007) 609.

Sato, S., A. Matsumura, Extraction of Phenol in Water Phase using Liquefied Dimethyl Ether, *J. Jpn. Pet. Inst.* 46 (2003) 375–378.

Scovazzo, P., J. Kieft, D.A. Finan, C. Koval, D. DuBois, R. Noble, Gas separations using non–hexafluorophosphate $[PF_6]^-$ anion supported ionic liquid membranes, *J. Memb. Sci.* 238 (2004) 57–63.

Subramanian, B., Y. Qiaolin,, Y. Qiujing, A.P. Khodadoust, D.D. Dionysiou, Photodegradation of pentachlorophenol in room temperature ionic liquids, *J. Photochem. Photobiol., A: Chemistry*. 192 (2007) 114–121.

Susan, C., K. Wilson, C. Jones, Bioremediation of Soil Contaminated With Polynuclear Aromatic Hydrocarbons (PAHs): A Review, *Environ. Pollut.* 81 (1993) 229–249.

Ternes, T.A., M. Meisenheimer, D. McDowell, F. Sacher, H.J. Brauch, B.H. Gulde, G. Preuss, U. Wilme, N. Z. Seibert, Removal of pharmaceuticals during drinking water treatment, *Environ. Sci. Technol.* 36 (2002) 3855–3863.

The European Agency for the evaluation of medical products–Committee for proprietary medicinal products, Points to consider on the reduction, eliminati on or substitution of thiomersal in vaccines (2001) ( http://www.emea.eu.int).

Topalov, A., B. Abramovic, D. Molnar–Gabor, J. Csanadi, Arcson, O. Photocatalytic oxidation of the herbicide (4-chloro-2-methylphenoxy) acetic acid (MCPA) over $TiO_2$, *J. Photochem. Photobiol. A: Chem.* 140 (2001) 249–253.

Toppari, J., J.C. Larsen, P. Christiansen et al., Male reproductive health and environmental chemicals with estrogenic effect. Copenhagen: Danish Environmental Protection Agency, (1995) 50.

Valsaraj, K.T., C. Springer, Removal of Traces of Pentachlorophenol from Aqueous Acidic Solutions by Solvent Extraction and Solvent Sublation, *Sep. Sci. Technol.* 21 (1986) 789–807.

Weber. J.B., H.D. Coble, Microbial decomposition of diquat adsorbed on montmorillonite and kaolinite clays, *J. Agric. Food Chem.* 16 (1968) 475–478.

Wurl, O., R.P. John, P.O. Jeffrey, C. Durville, Persistent Organic Pollutants in the Equatorial Atmosphere over the Open Indian Ocean, *Environ. Sci. Technol.* 40 (2006) 1454–1461.

Xiao, Y., S.V. Malhotra, Diels–Alder Reactions in Pyridinium Based Ionic Liquids, *Tetrahedron Lett.* 45 (2004) 8339–8342.

Zhang, H., L. Bu, M., Li, K. Hong, J.W. Mays, A.E. Visser, R.D. Rogers, Homopolymerization and Block Copolymer Formation in Room Temperature Ionic Liquids using Conventional Free Radical Initiators, ACS Symposium Series Vol. 818, Ionic Liquids, Industrial Applications for Green Chemistry, R. Rogers, K. Seddon, Eds., ACS Press, Washington, pp. 114–124 (2002).

Zhang, T.C., S.C. Emary, Jar tests for evaluation of atrazine removal at drinking water treatment plants, *Environ. Eng. Sci.* 16 (1999) 417–432.

Zhao, H., S. V. Malhotra, Applications of ionic liquids in organic synthesis, *Aldrichim. Acta*. 35 (2002) 75–83.

Zhou, Y., J.H. Schattka, and M. Antonietti, Room–Temperature Ionic Liquids as Template to Monolithic Mesoporous Silica with Wormlike Pores via a Sol–Gel Nanocasting Technique, *Nano Lett.* 4 (2004) 477–481.

Zwiener, C., L. Weil, R. Niessner, Production and kinetics of the OH radical induced dealkylation of atrazine, *Int. J. Anal. Chem.* 58 (1995) 247–264.

## TABLES AND FIGURES OF CHAPTER 1

**Table 1.1.** Common organic compound found in the environment those have been associated with endocrine disruption.

| *Compound* | *Endocrine effect* | *Potential source* |
|---|---|---|
| 2,2′,3,4′,5,5′–Hexachloro–4–biphenylol and other chlorinated biphenylols | Antiestrogenic | Degradation of PCBs released into the environment |
| 4′,7-Dihydroxy daidzein and other isoflavones, flavones, and flavonals | Estrogenic | Natural flora |
| Aldrin | Estrogenic | Insecticide |
| Alkylphenols | Estrogenic | Industrial uses, surfactants |
| Bisphenol A and phenolics | Estrogenic | Plastics manufacturing |
| DDE (1,1-dichoro–2,2bis(p–chlorophenyl)ethylene) | Antiandrogenic | DDT metabolite |
| *DDT and metabolites* | Estrogenic | Insecticide |
| Dicofol | Estrogenic or antiandrogenic in top predator wildlife | Insecticide |
| Dieldrin | Estrogenic | Insecticide |
| Diethylstilbestrol (DES) | Estrogenic | Pharmaceutical |
| *Endosulfan* | Estrogenic | Insecticide |
| Hydroxy-PCB congeners | Antiestrogenic (competitive binding at estrogen receptor) | Dielectric fluids |
| Kepone (Chlorodecone) | Estrogenic | Insecticide |
| Lindane (γ–hexachlorocyclohexane) and other HCH isomers | Estrogenic and thyroid agonistic | Miticide, insecticide |
| Lutolin, quercetin, and naringen | Antiestrogenic (as in uterine hyperplasia) | Natural dietary compounds |
| Malathion | Thryroid antagonist | Insecticide |
| Methoxychlor | Estrogenic | Insecticide |
| Octachlorostyrene | Thryroid agonist | Electrolyte production |
| Pentachloronitrobenzene | Thyroid antagonist | Fungicide, herbicide |
| *Pentachlorophenol* | Antiestrogenic (competitive binding at estrogen receptor) | Preservative |
| Phthalates and their ester compounds | Estrogenic | Plasticizers, emulsifiers |
| Polychlorinated biphenyls (PCBs) | Estrogenic | Dielectric fluid |
| Polybrominated diphenyl ethers (PDBEs) | Estrogenic | Fire retardants, including in–utero exposures |
| Polycyclic aromatic hydrocarbons (PAHs) | Antiandrogenic (aryl hydrocarbon receptor agonist) | Combustion by–products |
| Tetrachlorodibenzo–para–dioxin and other halogenated dioxins and furans | Antiandrogenic (aryl hydrocarbon receptor agonist) | Combustion and manufacturing (such as halogenation) by–product |
| Toxaphene | Estrogenic | Animal pesticide dip |
| Tributyl tin and tin organometallic compounds | Sexual development of gastropods and other aquatic species | Paints and coatings |
| Vinclozolin and metabolites | Antiandrogenic | Fungicide |
| Zineb | Thyroid antagonist | Fungicide, insecticide |
| Ziram | Thyroid antagonist | Fungicide, insecticide |

Tetrabutylphosphonium $[TBP]^+$

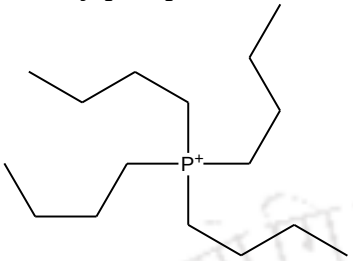

Octyldiethylmethylphosphonium $[ODEMP]^+$

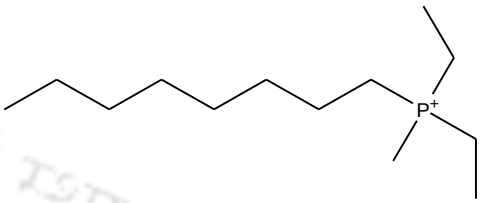

1-Hexyl-1-methyl-pyrrolidinium $[HMPYR]^+$

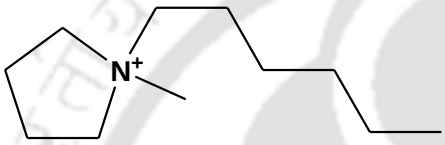

1-Octyl-1-methyl- pyrrolidinium $[OMPYR]^+$

1-Octyl-3-methylimidazolium $[C_8MIM]^+$

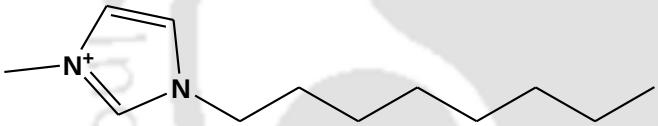

1-Butyl-2,3-dimethylimidazolium $[C_4DMIM]^+$

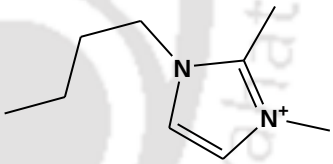

1-Hexyl-4-methylpyridinium $[C_6MPY]^+$

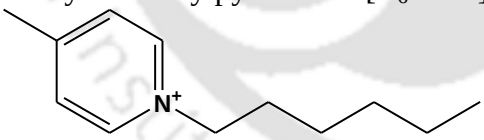

1-Octyl-4-methylpyridinium $[C_8MPY]^+$

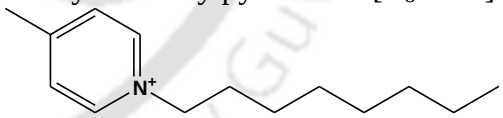

**Figure 1.1.** Structures of cations in Ionic Liquids.

Decanoate $[DEC]^-$

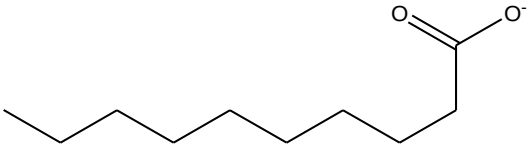

bis(methylsulfonyl)amide $[BMA]^-$

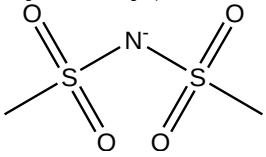

Trifluoromethylsulfonate $[CF_3SO_3]^-$

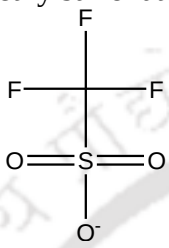

Tetrafluoroborate $[BF_4]^-$

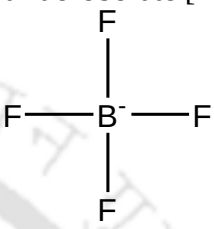

bis(oxalato (2-))borate $[BOB]^-$

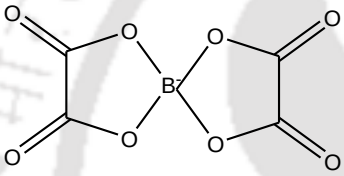

Hexafluoro phosphate $[PF_6]^-$

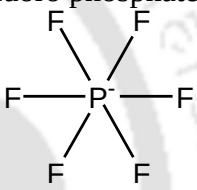

**Figure 1.2**. Structures of anions in Ionic Liquids.

# CHAPTER 2

## COMPUTATIONAL METHODOLOGY

## 2.1. COSMO–RS based methodology

### *2.1.1. Quantum mechanics*

The starting point for the calculation of thermodynamic properties using continuum solvation models are the theories of quantum chemistry where molecular properties of isolated molecules in vacuum are studied. The final aim of majority quantum chemical approaches is to find a solution of the time–independent, non–relativistic Schrödinger equation. This differential equation cannot be solved analytically for more than one–electron systems. Furthermore, the direct numerical integration is not tractable. As an outcome, a large number of approximate methods have been developed to solve the Schrödinger equation, for example electronic structure methods, electron correlation methods and density functional theory.

One of the most fundamental theories is the Hartree–Fock (HF) theory, [Bobrowicz et al., 1977; Szabo and Ostlund, 1996] an electronic structure method where electron correlation is neglected. This approximation is the basis of almost all conventional orbital based quantum chemical methods. A further development is the electron correlation methods that consequently led to more accurate results, usually at higher computational costs. Here, most widely used electron correlation methods are the Møller–Plesset perturbation theory of $n^{th}$ order (MP$n$ ), [Møller and Plesset, 1934] and the coupled cluster theory (CC) [Cížek 1969, Pople et al., 1987]. In the MP$n$ theory, the perturbation theory is applied to the calculation of the correlation energy. The most frequently used variations are MP2 [Head–Gordon et al., 1988, Frisch et al., 1990a,b] and MP4 [Krishnan and Pople, 1978]. Perturbation methods add

all types of corrections to a specified order, whereas coupled cluster (CC) methods include all corrections of a given type to infinite order [Bartlett, 1989]. An important variation is CCSD (T) (coupled cluster with single and double excitations and perturbative triple excitations) [Pople et al., 1978; Bartlett and Purvis, 1978]. A completely different approach to quantum chemistry in comparison to the mentioned orbital based methods with or without electron correlation is the density functional theory (DFT) [Kohn and Sham, 1965; Hohenberg and Kohn, 1964]. Instead of working with wave functions, DFT makes use of the electron density as fundamental variable because Hohenberg and Kohn could prove that the ground–state electronic energy is can be entirely obtained by the electron density [Hohenberg and Kohn, 1964]. Hence, DFT methods utilize empirical functionals connecting electron density and energy. DFT is a ground state theory that comprises both exchange and correlation effects. Among the different methods that exist within DFT, hybrid methods such as B3LYP (Becke three parameter hybrid functional) are commonly used due to its good correctness and computational economy. Quantum chemical methods also allow the calculation of thermodynamic properties of molecules in the gas phase, depending on the method of selection with more or less accurate results. To move from the quantum mechanic prediction of gas phase properties to fluid phase properties, continuum solvation models are useful tools.

### *2.1.2. COSMO*

Among continuum solvation models in literature, one is of particular practical usefulness, namely COSMO (conductor–like screening model). In this model, a continuum is

chosen to represent the solvent in an infinitely extended electrical conductor with $\varepsilon \rightarrow \infty$ [Klamt and Schüürmann, 1993]. This selection leads to a really simple expression for the screening charges and the screening energy, because the resulting electrostatic potential $\Phi$ is zero for every point $r$ (distance from point charge) on the surface of the cavity in the conductor:

$$\Phi(r) = 0 \tag{2.1}$$

Since the electrical conductor screens the charges perfectly, it is intuitively clear that all electrostatic effects vanish behind the electrically conducting surface, including the electrostatic potential. The disadvantage using this assumption is that, it is only exact for a molecule in a conductor, not for a solvent with a finite dielectric constant ($\varepsilon$). An approximate correction for non–conducting media offers the approach to scale the ideal screening charge densities $\sigma^*$:

$$\sigma = f(\varepsilon)\sigma^* = \frac{\varepsilon - 1}{\varepsilon + x}\sigma^* \ . \tag{2.2}$$

For many problems, $x$ can be calculated exactly for $0 \leq x \leq 2$. For when COSMO $x$ =½ was chosen, the relative error is less than *(½)ε*. Some concerns were raised initially that this *post facto* correction for the dielectric behavior is only appropriate for media having reasonably high dielectric constants (such as water), but a systematic study indicated non–polar solvents to be equally amenable to a treatment by the COSMO model [Dolney et al., 2000; Cramer, 2004]. Since its original description at semi–empirical level, COSMO has been generalized to *ab–initio* and density functional levels of theory as well [Klamt et al., 1998].

An important step is the construction of the cavity around the solute. In COSMO, the cavities are constructed by modeling a solute molecule by fused sphere geometry and choosing the radii as the spheres representing the atoms by fitting to experimental data. Here as a thumb rule, the use of 1.2 times the corresponding van der Waals radii [Schäfer et al., 2000] is made. Furthermore, the segmentation of the cavity surface must be done properly for reliable results. In a practical COSMO calculation the number of surface segments typically ranges from about one hundred for diatomic molecules to a few thousand for drug molecules. COSMO calculations have been incorporated into various quantum–chemical computer packages, so that the results can be generated without bothering about every detail of their production [Schäfer et al., 2000]. The thermodynamic energy of solvation obtained from COSMO will in general be no more than a crude approximation of the true experimental value. This is to be expected because the macroscopic dielectric constant cannot accurately reproduce the local electrostatic interactions between solute and solvent molecule. Results of a COSMO calculation are the charge density distribution over the surface of the cavity and the energy of the solute in the conductor, including the back–polarization effect. The difference between the energy of the solute in the conductor and in the gas phase reflects the electrostatic intermolecular interactions. It is not a molecular potential energy, but rather has been shown to be approximate to the electrostatic part of the thermodynamic free energy of solvation. Fig. 2.1.1(a) shows the molecular structure of water and Fig. 2.1.1(b) shows a qualitative picture of the screening charge density distribution on the inner surface of a cavity for a $H_2O$ molecule in an electrical conductor. There is an accumulation of negative

screening charges (blue) around the positively charged hydrogen atoms, whereas the negatively charged oxygen atom is screened by positive charges (red).

Thus COSMO denotes the first realistic approximation to electrostatic solvation effects. Although not generally reliable or sufficiently accurate, it is a good starting point for a realistic semi–empirical model of the molecular potential energy in liquid mixtures beyond the continuum solvation approximation. Hence, surface charge interaction models are an alternative approach to the intermolecular potential energy in liquids.

*2.1.3. Basics of excess function models*

Any molecular model for the excess free energy $A^E$ is made up of two separate contributions, a repulsive $A^E_{rep}$ and an attractive $A^E_{att}$:

$$A^E = A^E_{rep} + A^E_{att} \tag{2.3}$$

The repulsive term accounts for molecular size and shape effects, hence it introduces the molecular geometry. The attractive part is associated with attractive intermolecular forces. Since mixing effects of industrially relevant systems generally occur at high densities, a reasonable approximation is that the molecular system is represented by a space–filling arrangement of molecules interacting via surface contacts. This crude approximation implies that pressure–dependent effects cannot be calculated using these simplified liquids models. In addition, a distance dependency is suppressed which means that only temperature dependencies can be taken into consideration. Because the intermolecular interactions are

formulated in terms of pair contacts, they will depend on the local structure in the liquid. Thus, an essential part of any molecular model for the excess functions in liquid mixtures is a model for the relation between the unknown local compositions and the known bulk compositions in terms of the intermolecular potential energy, hence the short–range non–randomness (Fig. 2.1.2).

Nevertheless, simplified liquid models are useful representations of the intermolecular potential energy of fluid phases. Two different approaches will be presented (Fig. 2.1.3), group interaction models based on the lattice picture (Fig. 2.1.3 (a)) and surface charge interaction models based on the polyhedral surface picture (Fig. 2.1.3 (b)).

*2.1.4. COSMO–RS theory*

The results of COSMO calculations are used to model real solvents. The screening charges obtained from COSMO calculations can be used as a basis to establish the intermolecular potential model due to electrostatic effects in real solvents. This generalization of COSMO is referred to as COSMO for realistic solvation, also called as "**C**onductor–like **S**creening **MO**del for **R**eal **S**olvents" (COSMO–RS). In COSMO–RS, the interactions between molecules are visualized to occur between surface segments of polyhedral surfaces contacting each other in a space–filling manner according to the polyhedral surface picture (Fig. 2.1.3(b)). Each surface segment is associated with a characteristic electrostatic surface charge density.

This section reports the background theory which describes the judicious screening of various IL's used in this study for the extraction of PCP, DDT, Endosulfan, PA and BPA from aqueous solutions as explained in chapter 1. A quantum chemical based COSMO–RS model was used for the prediction of selectivity of these compounds in aqueous medium at infinite dilution. Computational–based screening methods like the COSMO–RS model is less time taken and more efficient when compared to other computational methods. Moreover, experimental screening takes lot of time and is very costly. Thus in this study, continuum solvation model such as COSMO [Klamt and Schüürmann, 1993] and its extension to real solvents COSMO–RS [Klamt, 1995] was adopted.The selectivity at infinite dilution is important since PCP, DDT, Endosulfan, PA and BPA are present in trace amounts in water. This model a–priori predicts the activity coefficient of a solute such as PCP, DDT, Endosulfan, PA and BPA in IL and water using the molecular structure as the only tool. A combination of 35 cations and 29 anions was used to determine the best extractant for the removal of EDCs from aqueous solution.

The initial structure of the chosen cations, anions and water along with EDCs were drawn using visualization freeware MOLDEN [Schaftenaar and Noordik, 2000]. The MOLDEN is a graphical interface for Gaussian and other programs to setup *Gaussian03* input files and graphically examine results. *Gaussian03* package was used to generate the COSMO file [Frisch et al., 2003]. The Hartree–Fock [Fock, 1930] level of theory with 6–31G* basis set was used for initial geometry optimization on isolated cations and anions. To detect the presence of any negative or imaginary frequencies, a frequency optimization was done using the *freq* keyword in *Gaussian03* [Frisch et al., 2003]. The COSMO file was

generated using *Gaussian03* on the final frequency and geometry–optimized molecule via PBV 86 density functional theory. The triple zeta valence potential (TZVP) [Schaefer et al., 1994] and the density fitting basis set DGA1 [Sosa et al., 1992] has been used for the COSMO file generation.

For the prediction, a complete dissociation of IL's into cations and anions was assumed elsewhere [Banerjee et al., 2008]. For this reason; the sigma profile i.e. the distribution of screening charge densities is simply the linear addition of the sigma profiles of the cation and anion.

$$p^{IL}(\sigma) = p^{cation}(\sigma) + p^{anion}(\sigma) \tag{2.4}$$

where $p^{Cation}(\sigma)$ and $p^{Anion}(\sigma)$ are the sigma profiles for cation and anion respectively. The sigma profile of cation and anion are obtained separately and then added via simple algebraic addition followed by normalization. Thus this sigma profile will behave as a profile of a single molecule. This is equivalent in calculating the sigma profile of a mixture of both cation and anion. The COSMO volume and COSMO area also get added linearly along with the sigma profile. COSMO volume cavity and COSMO area cavity were found to increase with carbon chain length of all the cations.

COSMO–RS assumes the interaction energy between two segments to be composed of two terms, *misfit energy* and the *hydrogen bonding energy*. The physical parameters such as $a_{eff}$=6.25 Å$^2$ (surface area of a standard segment), α′= 8896 (kcal Å$^4$)/ (mol e$^2$) (misfit constant for misfit energy interaction), $c_{hb}$=54874(kcal Å$^4$)/ (mol e$^2$) (constant for hydrogen–

bonding interaction) and $\sigma_{hb}$ =0.0085e/ Å$^2$ (the cut off value for hydrogen–bonding interactions) were taken from literature [Banerjee et al., 2007]. Hydrogen bonding is always assumed to be within two segments such that the hydrogen bond acceptor type has $\sigma_{hb}$ > 0.0085 e/ Å$^2$and the hydrogen bond donor type has $\sigma_{hb}$ < -0.0085 e/ Å$^2$. The equations for *misfit energy* (Eq. 2.5) and *hydrogen bonding* energy (Eq. 2.6) are given below.

*Misfit energy*:

$$E_{misfit}\left(\sigma,\sigma^{'}\right)=\frac{a_{eff}\alpha^{'}\left(\sigma+\sigma^{'}\right)^{2}}{2} \tag{2.5}$$

$$\text{where}\quad \alpha^{1}=\frac{\left(0.64*0.3*a_{eff}^{\frac{3}{2}}\right)}{\varepsilon_{0}},$$

and $\varepsilon_0$=2.395 × 10$^{-4}$ (e$^2$ mol)/ (kcal Å) is the permittivity in free space.

*Hydrogen bond interaction energy*:

$$E_{hb}\left(\sigma,\sigma'\right)=a_{eff}c_{hb}\left(\sigma,\sigma'\right)=a_{eff}c_{hb}\min\left\{0,\min\left(0,\sigma_{don}+\sigma_{hb}\right)\max\left(0,\sigma_{acc}-\sigma_{hb}\right)\right\} \tag{2.6}$$

The activity coefficient of any component in the mixture is then given by [Mukhopadhyay and Rao et al., 1987].

$$\ln\gamma_{\text{ilS}}=n_i\sum_{\sigma}p_i\left(\sigma\right)\left[\ln\Gamma\left(\sigma\right)-\Gamma_i\left(\sigma\right)\right]+\ln\gamma_{ilS}^{SG} \tag{2.7}$$

$$\ln \gamma_{ilS}^{SG} = \ln \frac{\phi_i}{x_i} + \frac{z}{2} q_i \ln \frac{\theta_i}{\phi_i} + l_i - \frac{\phi_i}{x_i} \sum_j x_j l_j \tag{2.8}$$

$$\text{where, } \theta_i = \frac{x_i q_i}{\sum_j x_j q_j}, \phi_i = \frac{x_i r_i}{\sum_j x_j r_j} \text{ and } l_i = \frac{z}{2}\left[\left(r_i - q_i\right) - \left(r_i - l\right)\right] \tag{2.9}$$

Here, $r_i$ and $q_i$ are normalized using the volume and surface area of a functional group [Mukhopadhyay and Rao, 1987] and $ln\ \Gamma(\sigma)$ and $ln\ \Gamma_i(\sigma)$ are activity coefficients of the segment in the mixture and the compound respectively. The details of COSMO–RS methodology are given by Sandler and Lin [Lin and Sandler, 2002] and Klamt [Klamt, 1995]. We have re–implemented the COSMO–SAC model as given by Sandler and Lin [Lin and Sandler, 2002]. The applications of our model are given in our earlier work [Banerjee et al., 2007; Ananthraj and Banerjee 2011]. The prediction of activity coefficients at infinite dilution was carried since solvent effects were observed maximum when the concentration of solute (EDCs in this case) is infinitely small. However, infinite dilution also applies to the situation where the presence of a trace amount of EDCs poses the biggest problem.

The selectivity *(S)* is defined as the ratio of the water species in IL rich phase (extract) and to the composition of EDC (effluent) in ionic liquid rich phase [Maduro and Aznar, 2008]. The operational expression mathematically can be written as:

$$S_{12,max} = S_{12}^{\infty} = \left(\frac{\gamma_2^{\infty}}{\gamma_1^{\infty}}\right)^{IL\ phase} \left(\frac{\gamma_1^{\infty}}{\gamma_2^{\infty}}\right)^{Water\ phase} \approx \left(\frac{\gamma_2^{\infty}}{\gamma_1^{\infty}}\right)^{IL\ phase} \tag{2.10}$$

where IL stands for Ionic Liquid, $\gamma_1^\infty$ is the activity coefficient of EDC species at infinite dilution and $\gamma_2^\infty$ activity coefficient of water component at infinite dilution, usually $\gamma_1^\infty$ or $\gamma_2^\infty$ is defined as:

$$\gamma_1^\infty or\ \gamma_2^\infty = \lim_{x \to 0} \ \gamma_i^\infty . \tag{2.11}$$

The capacity is directly used for evaluating the amount of ionic liquids needed for the removal of EDC species [Banerjee et al., 2007]. It signifies, the ability to dissolve maximum amount of EDC species in the solvent. The capacity *(C)* can be expressed in terms of activity at infinite dilution:

$$C_{12}^\infty = \left( \frac{1}{\gamma_1^\infty} \right)^{IL\ Phase} . \tag{2.12}$$

The subscripts *'1'* and *'2'* indicates EDC species in ionic liquid phase and ionic liquid respectively. The performance index is defined as the product of selectivity at infinite dilution and capacity at infinite dilution for any solvent. This is represented by:

$$PI = C_{12}^\infty \times S_{12,\max} = \left( \frac{1}{\gamma_1^\infty} \right)^{\text{IL phase}} \times \left( \frac{\gamma_2^\infty}{\gamma_1^\infty} \right) = \left( \frac{\gamma_2^\infty}{\left( \gamma_1^\infty \right)^2} \right)^{\text{IL phase}} . \tag{2.13}$$

The selectivity and capacity strongly depends on solvent–solute interaction effect [Pereiro and Rodriguez, 2008]. In general, the extraction capacity depends on anion volume and interaction energy between cation and anion.

All activity coefficients calculated in the present study are at infinite dilution. The interaction becomes stronger between the solute and the IL when the value of the activity

coefficient is less than unity. The selectivity values computed using COSMO–RS provide an efficient method for the screening of ILs. A total of 35 cations are used in combination with 29 anions. Table 2.1 and 2.2 describe the list of cations and anions studied in this work respectively. It is also denotes the chemical structure, chemical formulae, molecular weight, COSMO area and COSMO volume. Sections 2.1.5 to 2.1.15 describe the procedure for COSMO file generation using *Gaussian03* package in a systematic way.

### *2.1.5. Working with Gaussian03 program*

*Gaussian* is an electronic structure package capable of predicting properties of atoms, molecules and reactive systems such as: molecular energies, structures, vibrational frequencies and electron densities along with numerous molecular properties derived from these basic computation types. It utilizes *ab initio*, density functional theory, semi–empirical, molecular mechanics, and various hybrid methods. It can be used to study molecules and computation types. It also can be used to study molecules and reactions, including both stable species and unstable or non–observable such as short–lived intermediates and transition structures.

The first task is to decide the type of calculation needed. The *Gaussian* program [Frisch et al., 2004] is usually controlled by different specific *keywords*, which is applied for certain types of calculation. If the keywords are used, the program converts them to internal parameters, which then control the execution.

The different step by step procedures are summarized below:

1. Initial step is to read in a title for the job plus molecular charge, multiplicity (singlet, triplet, etc.), molecular geometry in the form of a *Z–matrix*. This consists of atomic numbers, bond lengths, bond angles, dihedral angles from which the Cartesian [*x*, *y*, *z*] coordinates are calculated. The information from the Z–*matrix* is then used to work out electronic configuration and the orbital occupancies.
2. In second step the nuclear repulsion energy which depends on the atomic numbers and the molecular geometry is calculated.
3. The atomic orbitals or basis sets are then assigned to each nucleus. *Ab–initio* programs uses an internally stored standard set of coefficients and exponents that define the orbitals (the *basis set*).
4. An *ab–initio* program next calculates the various one and two–electron integrals required later in the calculation.
5. *ab–initio* programs then produce an *initial guess* of molecular orbitals used as a starting point for the SCF calculations. The usual form of initial guess for *ab–initio* programs is that obtained from an extended Hückel calculation [Wolfsberg and Helmholz, 1952] on the molecule in question.
6. The solution to the SCF equations is iterated cycle by cycle until the electronic energy is at a minimum and the density matrix does not change. At this stage the calculation is said to be converged, or to have reached self consistency, and the program proceeds to the next step.

7. For a geometry optimization the atomic forces are then determined analytically and used to estimate the minimum–energy geometry for the molecular species being calculated.
8. The above process is repeated for each new geometry, until the atomic forces are close to zero and the total energy does not change significantly from cycle to cycle.
9. The next stage of the calculation depends on the type of job to be performed. For a single point, the program may either move directly to the *population analysis*, which calculates the atomic charges, overlaps, dipole and higher moments. The correlation energy for DFT is then calculated.

At this stage the optimization is complete and the program moves on to a population analysis of the optimized species. Fig. 2.1.4 shows the flow chart for the typical *ab–initio* job.

### *2.1.6. Geometry optimization*

Quantum chemical computation starts with an optimized structure of the molecule. Structural changes within a molecule develop differences in its energy and other properties. The way the energy of a molecular system varies with small changes in its structure is specified by its *potential energy surface*. Geometry optimization locates the minima on the potential energy surface, thereby predicting equilibrium structures. At both minima and saddle points, the gradient of the energy is zero. Since the gradient is the negative of the forces, the forces are zero at such a *stationary point*. At a minimum, any alteration of the geometry increases the energy and hence, all normal vibrations are *positive*. At a saddle

point, displacement along a particular normal vibration decreases the energy and hence the vibration has a *negative frequency*, but all other displacements result in an energy increase. All optimizations can locate a stationary point, although not always a global minima.

### *2.1.7. Geometry optimization using Gaussian03*

The structure of the molecule can be optimized using one of the several quantum chemistry packages. The most popular among them is *Gaussian03* [Frisch et al., 2003]. The next section discusses the steps, as shown in the form of a flowchart in Fig. 2.1.5 to be followed for carrying out geometry optimization in *Gaussian03*.

### *2.1.8. Input specification*

For doing a calculation in *Gaussian03*, an input file is required. The input file contains the *route section*, information about the molecular *charge* and *multiplicity*, and definitions of the molecular structure given in *Z–matrix*. All this information is used to calculate the total number of electrons and the orbital occupancies. Fig. 2.1.6 shows the sample input file for geometry optimization of water molecule.

### *2.1.9. Route section*

The route section of a *Gaussian03* input file specifies the type of calculation to be performed. According to the *Gaussian03* User's Guide and Programmer's Reference [Frisch et al., 1999] there are three key components to this specification: i) the job type, ii) the method and iii) the basis set. Optimization (**opt** keyword) and frequency calculation (**freq** keyword) are examples of job types. The combination of method and basis set specifies a

model chemistry to *Gaussian03*, specifying a level of theory. HF (Hartree Fock), MPn (Moller Plesset Perturbation Theory), DFT (Density Functional Theory) are examples of methods. If no method keyword is specified, HF is assumed as a default. Most methods require a basis set. If no basis set keyword is specified then STO-3G basis will be used. STO-3G, 3-21G, 6-21G, and 6-31G are examples of basis sets. Single first polarization functions can also be requested using the usual * or ** notation. 6-31G* (or 6-31G(d)) is 6-31G with added d polarization functions on non–hydrogen atoms; 6-31G** (or 6-31G(d,p)) is 6-31G* plus p polarization functions for hydrogen. The + and ++ diffuse functions are available with some basis sets. 6-31+G is 6-31G plus diffuse *s* and *p* functions for non–hydrogen atoms; 6-31++G has diffuse functions for hydrogen also. For example, 6-31G(3df, 2p) designates the 6-31G basis set supplemented by diffuse functions, three sets of *d* functions and one set of *f* functions on heavy atoms, and supplemented by two sets of p functions on hydrogens. The basis set selection is related to the objective of the calculation and the molecules to be studied. Even a large basis set does not guarantee an agreement for experimental data. Examples of the *ab–initio* keywords which are listed in the Gaussian User's Guide and Programmer's Reference are as follows [Frisch et al., 1999]:

- **HF**– Hartree Fock (uses RHF for singlets and UHF for others)
- **RHF**– restricted Hartree Fock
- **UHF**– unrestricted Hartree Fock
- **ROHF**– spin–restricted open–shell Hartree Fock
- **OSS** – two open shell singlet wave function
- **GVB** – generalized valence bond

- **CASSCF** – complete active space MCSCF
- **MP2** – Moller–Plesset second order correlation energy correction
- **MP3** – Moller–Plesset third order correlation energy correction
- **MP4** – same as MP4SDTQ
- **MP4DQ** – Moller–Plesset fourth order correlation energy correction with double and quadruple substitutions.
- **MP4SDQ** – Moller–Plesset fourth order correlation energy correction with single, double and quadruple substitutions.
- **MP4SDTQ** – Moller–Plesset fourth order correlation energy correction with single, double, triple and quaduple substitutions.
- **CI** – same as CISD
- **CIS** – configuration interaction with single excitations
- **CID** – configuration interaction with double excitations
- **CISD** – configuration interaction with single and double excitations
- **QCISD** – quadratic configuration interaction with single and double excitations
- **QCISD(T)** – quadratic configuration interaction with single and double excitations and triples contribution to the energy.

*2.1.10. Z–matrix*

The *molecular structure* given by *Z–matrix* definition contains information on the type of atoms used and their geometrical positions. *Z–matrix*, defines a molecule atom by atom in terms of *bond lengths*, *bond angles*, and *dihedral angles*. *Z–matrix* neither defines

the bonds to be formed in the calculation nor represents a given electronic state. [Clark et al., 1985] discusses ways of efficiently writing the *Z–matrix*, the use of *symmetries* in the molecule and the use of *dummy atoms*. The text also contains an excellent explanation of how quantum chemical computational programs work.

For visualizing as well as specifying the *Z–matrix* in MOLDEN [Schaftenaar 2000] visualization package can be used. It automatically assigns initial values to the bond lengths, bond angles, and dihedral angles.

*2.1.11. Charge and multiplicity*

The charge is the *overall charge* (in atomic units) on the system specified in the *Z–matrix*. The individual *electronic spins add vectorially* to give a total electronic spin **S** whose magnitude has the possible values $[S(S+1)]^{½}\hbar$ with $S = 0, ½, 1, ...$ The quantity $2S+1$ is called the multiplicity. The multiplicity is a measure of the number of unpaired electrons in the system. It is generally computed using the following thumb rule:

$$multiplicity = n_u + 1 \tag{2.14}$$

where, $n_u$ is the number of unpaired electrons.

*2.1.12. Submission of job and convergence criteria*

*Gaussian03* may be run using the ***g03*** command. The *ab–initio* calculations are very time consuming and *Gaussian03* jobs may run for several hours or longer. So these jobs are

forced to run in the background using **&**. An optimization is complete when it has converged. *Gaussian03* uses the following criteria for convergence:

i. The forces must be 0. Specifically the maximum component of the force must be below the cutoff value of 0.00045 Hartree/Bohr.
ii. The root mean square of the forces must be below the defined tolerance of 0.0003 Hartree/Bohr.
iii. The calculated displacement for the next step must be smaller than the defined cutoff value of 0.0018 Bohr.
iv. The root mean square of the displacement for the next step must also be below the cutoff value of 0.0012 Bohr.

The presence of four distinct convergence criteria prevents a premature identification of the minimum. If all the above criteria are satisfied, a stationary point has been found and the program terminates normally. This is also indicated by the presence of a quotation at the end of the output file. At this point, one should proceed to carry out a vibrational analysis (Step 5 of Fig 2.1.5). If the program termination is not normal, the user should analyze the output files and look for the errors.

*2.1.13. Vibrational analysis*

After successful completion of an optimization job, *vibrational analysis* (frequency calculation) is used in order to determine the nature of stationary points found by a geometry optimization as explained by [Foresman and Frisch 1996]. Geometry optimizations converge

to a structure on the potential energy surface where the forces on the system are essentially zero. The final structure may correspond to a *minimum* on the potential energy surface, or it may represent a *saddle point*, which is a minimum with respect to some directions on the surface and a maximum in one or more others.

To carry out frequency calculation, ***freq*** keyword is used in place of ***opt***. The rest of the specifications are the same as discussed in Step 1.There are two pieces of information from the output which are critical for characterizing a stationary point (i) the number of imaginary frequencies and (ii) the normal mode corresponding to the imaginary frequency. Imaginary frequencies are listed in the output of a frequency calculation as negative numbers. By definition, a structure which has *n* imaginary frequencies is an $n^{th}$ order saddle point. So if the frequency calculation found zero imaginary frequencies the structure is a minimum, else the structure is a saddle point. A point to note is that the frequency calculations should be done using same method and basis set as were used in the optimization calculations.

*2.1.14. Revised Z–matrix*

Geometry optimization is easy for smaller molecules; larger molecules are usually difficult to optimize. For larger molecules [Hans-Dieter and Folkerts et al., 1996] suggests a *stepping stone approach* start with a lower level of theory and smaller basis set and sequentially optimize the geometry using the optimized geometry from the previous step as the initial geometry for the next step. Information from crystallographic databases can also be used to arrive at a better guess for *Z–matrix.*

*2.1.15. Locating and identifying error(s)*

If the program terminates abruptly, it writes the error messages in the output file. The crash could be attributed to errors in the input file. Some of the errors are – wrongly specified multiplicity (inconsistency with the charge), typographical errors in the route section, and use of integers in place of floating point numbers. Run–time errors can also occur, for example, when a bond angle reaches 180° during the optimization. To avoid such a runtime error use of *dummy atom(s)* is suggested. Dummy atoms are particularly useful for the study of ionic IL's where the cation and anion are initially connected together using a dummy atom. Then the molecule is geometrically optimized; in the final result the structure is without the dummy atom. This concept has been used by earlier work of Meng *et al.,* and Turner *et al.,* [Meng et al., 2002; Turner et al., 2003] for *ab–initio* calculations on IL's.

## 2.2. Interaction Energies and HOMO–LUMO Methodology

*2.2.1. Quantum chemical calculations*

The aim of this section is to investigate in detail the conformational stability and vibrational spectra of molecule: [PCP], [PA], cations, anions and complexes using DFT method, which can most probably help in understanding its interacting behavior. The present study determines the vibrational spectra of molecules and the interaction energies between [PCP]\[PA] with IL using density functional theory (B3LYP) in order to find the thermodynamic stabilities and bonding nature. The 6-31G* basis set was implemented in the *Gaussian03* program suite [Frisch et al., 2003]. Geometries obtained from DFT calculation

were then used to perform NBO analysis to determine the presence of hyper conjugative interactions. The detailed vibrational spectral analysis of the [PCP], [PA] and IL complexes were performed by combining the experimental and theoretical information using DFT theory to derive information about electronic effects and intramolecular charge transfer responsible for thermodynamic activity. Investigations have also been carried out to identify the HOMO–LUMO energies of the optimized molecular structure. Finally, $^{1}$H NMR spectra were measured for [PCP], [PA] and ionic liquid complexes.

Initially the molecular structure of [PCP], [PA], cations, anions and complexes were drawn by MOLDEN freeware. Previous work suggests DFT method for the prediction of complexes consisting of IL's; hence the same has been used in this work [Wang et al., 2006; Chiappe et al., 2006; Zhang et al., 2007]. DFT is based on the time–dependent Kohn–Sham (KS) equations, derived from the time–dependent Schrödinger equation [Casida, 1996]. The ground state molecular energy, wave function, and all other molecular electronic properties are uniquely determined by the ground state electron probability density $\rho$(x, y, z), a function of only three variables. The Hohenberg-Kohn theorem indicates that it is possible to calculate all the ground–state molecular properties from $\rho$. The ground state energy of a n-electron molecule is given by

$$\sum_{i=1}^{n}\left\langle \Psi_i(1) \mid \nabla_1^2 \mid \Psi_i(1)\right\rangle - \sum_{\alpha}\int \frac{Z_\alpha \rho(1)}{r_{1\alpha}} dv_1 + \frac{1}{2}\int\int \frac{\rho(1)\rho(2)}{r_{12}} dv_1 dv_2 + E_{xc}[\rho] \qquad (2.15)$$

where $\Psi_i(1)$, $i$ = 1, 2, …, $n$ are the *Kohn-Sham orbitals*, and $E_{xc}[\rho]$ is the *exchange-correlation energy* which is a functional of $\rho$. The Kohn-Sham orbitals are found by solving the one-electron Eqs.:

$$\hat{F}_{KS}(1)\psi_i(1) = \varepsilon_{i,KS}\psi_i(1)\,. \tag{2.16}$$

where the Kohn-Sham operator $\hat{F}_{KS}$ is

$$\hat{F}_{KS} \equiv -\frac{1}{2}\nabla_1^2 - \sum_{\alpha}\frac{Z_\alpha}{r_{1\alpha}} + \sum_{j=1}^{n}\hat{J}_j(1) + V_{xc}(1)\,. \tag{2.17}$$

where the Coulomb operator $\hat{J}_j(1)$ is defined by:

$$\hat{J}_j(1)f(1) = f(1)\int|\psi_j(2)|^2\frac{1}{r_{12}}dv_2$$

where $\hat{J}_j$ and $\hat{K}_j$ are the *Coulomb operator* and the *exchange operator* respectively. The *exchange-correlation potential* $V_{xc}$ is found as the functional derivative of $E_{xc}$

$$V_{xc} = \frac{dE_{xc}[\rho]}{d\rho} \tag{2.18}$$

If $E_{xc}[\rho]$ is known, its functional derivative is readily found, and $V_{xc}$ is known. $\hat{F}_{KS}$ is like the Hartree–Fock operator, except that the exchange operators $-\sum_{j=1}^{n}\hat{K}_j$ are replaced by $V_{xc}$, which handles the effects of both exchange (antisymmetry) and electron correlation. Various approximate functionals $E_{xc}[\rho]$ have been used in molecular density out of which we have

used the Becke three-parameter Lee–Yang–Parr (B3LYP) in our study. This level was thus used for the complex molecules [PCP]+[IL], [PA]+[IL] and for individual molecules. The molecules were first optimized using the B3LYP with 6-31G* basis set in Gaussian 03 [Frisch et al., 2003]. Thereafter a molecular visualization program, *Gaussview 5.0.8* [Frisch et al., 2000] was used to study the electronic properties, such as HOMO–LUMO energies and HOMO–LUMO energy visualization contours. Gaussview package is a graphical interface for Gaussian 03. It can be used to sketch molecules, setup Gaussian 03 input file and also graphically examine results.

DFT/B3LYP method is also one of the most common approaches for providing accurate magnetic shielding. The DFT method is extensively used for finding the energetic and geometric properties of atoms or molecules at very much lower costs than conventional *ab* initio wave function methods. It performs very well, gives no precision loss and contributes more authentic results for hydrogen bond molecular systems as compared to Hartree–Fock (HF) and MP2 methods [Geerlings et al., 2003; Yang, 2011; Li, 2003]. In our work the DFT/B3LYP method was used to approximate harmonic magnetic shielding with the 6-31G* basis set. Additionally, molecular electrostatic potentials and Mulliken atomic charges were also carried out. Furthermore, the thermodynamic properties such as vibrational and zero-–point vibrational energy, nuclear repulsion energy, triplet energy (SCF), thermal energy, specific heat capacity, rotational constants, entropy, and dipole moment of the selected compound were also calculated.

In the final step, the optimized structure of [PCP]+[$C_4$DMIM][$PF_6$] and [PA]+[$C_4$DMIM][$PF_6$] were used to compute the $^1$H NMR chemical shifts using the GIAO method [Wolinsk et al., 1990] in DMSO at DFT/B3LYP method with 6-311++G(d,p) basis set. The GIAO method is one of the most common approaches for calculating nuclear magnetic shielding tensors as reported by Karabacak *et al.*, [Karabacak et al., 2013]. Proportional chemical shifts were figured using the corresponding TMS shielding at the same theoretical level as the reference.

### *2.2.2. HOMO–LUMO theory*

The HOMO and LUMO energy values are related to the ionization potential (IP) and electron affinities (EA) [Gázquez, 1993] as per Eq. (2.19) and (2.20).

$$IP = -E_{HOMO} \tag{2.19}$$

$$EA = -E_{LUMO} \tag{2.20}$$

The difference between HOMO and LUMO energy values gives the HOMO–LUMO energy gap. By using these HOMO–LUMO energy values, important properties like global hardness ($\eta$), global softness ($\sigma$), electronegativity ($\chi$), chemical potential ($\mu$) and electrophilicity index ($\omega$) were calculated. The sections below describe the theoretical backgrounds of above said properties.

### *2.2.3. Global hardness and softness*

In the simplest terms, the hardness of a species (atom, ion, or molecule) is a qualitative indication of how polarizable it is, in another way how much its electron cloud is distorted in an electric field. The hardness and softness were suggested in literature [Pearson, 1963a,b] to denote resistance to deformation by mechanical force. This explains the changes in the energy linked with the transition state to ground–state using different descriptors. The softness is simply the reciprocal of the hardness. The global hardness (η) and softness ($\sigma$) of chosen molecule calculates the energy gap between the HOMO and LUMO orbitals. The mathematical expression of ($\eta$) and ($\sigma$) can be written as:

$$\eta = E_{LUMO} - E_{HOMO} = \left( \frac{IP - EA}{2} \right) \tag{2.21}$$

$$\sigma = \left( \frac{1}{\eta} \right) = \left( \frac{2}{E_{LUMO} - E_{HOMO}} \right) = \left( \frac{2}{IP - EA} \right) \tag{2.22}$$

Molecules with large HOMO–LUMO gap are hard which implies higher stability and opposing charge transfer, since they oppose changes in their electron density and distribution. On the contrary, molecules having a smaller gap require very small amount of energies to acquire them to the excited states are known called soft molecules. Hence they are highly polarisable in nature. In terms of chemical change, soft molecules are more reactive than hard molecules.

### 2.2.4. *Electronegativity*

Electronegativity is the tendency of molecules to attract electrons [Pearson, 1986]. Parr and Yang attempted to quantify this very descriptor [Parr and Yang, 1989]. This is found by the average of HOMO and LUMO energy values, as represented by Mulliken [Pearson, 1986]. It can be expressed in terms of orbital energies:

$$\chi = -\left(\frac{E_{HOMO} - E_{LUMO}}{2}\right) = \left(\frac{IP + EA}{2}\right) \tag{2.23}$$

From this point of view the electronegativity of a molecule is the drop in energy when an infinitesimal amount of electronic charge is added to the system. It is a measure of resistance of an atom or ion, or a group or atoms in a molecule for an entering electronic charge.

### 2.2.5. *Chemical potential*

Chemical potential denotes the affinity of an electron to flee and is defined as the first derivative of the total energy with respect to the number of electrons in a molecule [Kavita et al., 2010]. By the expression of MO theory, $\mu$ is simply the negative of electronegativity value. It is given as:

$$\mu = \left(\frac{E_{HOMO} - E_{LUMO}}{2}\right) = -\left(\frac{IP + EA}{2}\right) \tag{2.24}$$

### 2.2.6. *Electrophilicity index*

The capability of a substance to accept electrons is quantified as electrophilicity index ($\omega$). Parr *et al.*, defined the electron affinity as the capability of a substance to have only one electron from the surroundings [Parr et al., 1999]. This index measures the energy lowering of a substance due to the electron flow between donor and acceptor. Parr and co–workers [Parr et al., 1999] suggested that $\omega$ can be measured through the below Eq.:

$$\omega = \left(\frac{\mu^2}{2\eta}\right) = \left\{\frac{\left(\frac{E_{HOMO} - E_{LUMO}}{2}\right)^2}{E_{LUMO} - E_{HOMO}}\right\} = \left\{\frac{\left(\frac{IP + EA}{2}\right)^2}{IP - EA}\right\} \tag{2.25}$$

### 2.2.7. *Interaction energy*

$\Delta E_{int}$ or the interaction energy [Kavita et al., 2010; Lü et al., 2013] can be quantified and approximated by the difference between the energy of the system or complex and the energies of individual molecules. The expression for interaction energy is given below.

$$\Delta E_{\text{int.}} = E_{Solute-CAT-AN} - \left(E_{solute} + E_{CAT} + E_{AN}\right) \tag{2.26}$$

where $E_{solute}$, $E_{CAT}$ and $E_{AN}$ are the total energy of [PCP] or [PA], cation and anion respectively.

## References

Anantharaj, R., T. Banerjee, COSMO–RS based predictions for the desulphurization of diesel oil using ionic liquids: Effect of cation and anion combination, *Fuel Process. Technol.* 92 (2011) 39–52.

Banerjee, T., K.K. Verma, A. Khanna, Liquid–Liquid Equilibrium for Ionic Liquid Systems using COSMO–RS: Effect of Cation and Anion Dissociation, *AIChE J.* 54 (2008) 1874–1885.

Banerjee, T., R.K. Sahoo, A. Khanna, Multi–component liquid–liquid equilibria prediction for aromatic extraction systems using COSMO–RS, *Ind. Eng. Chem. Res.* 46 (2007) 1292–1304.

Bartlett, R.J., Coupled-Cluster Approach to Molecular Structure and Spectra: A Step toward Predictive Quantum Chemistry, *J. Phys. Chem.* 93 (1989) 1697–1708.

Bartlett, R.J., Purvis, G.D., Many-body perturbation theory, coupled-pair many-electron theory, and the importance of quadruple excitations for the correlation problem, *Int. J. Quant. Chem.* 14 (1978) 561–581.

Bobrowicz, W., W. Goddard, H.F. Schaefer, Methods of Electronic Structure Theory, Vol. III, Modern Theoretical Chemistry Plenum, New York, Chap. The Self–Consistent Field Equation for Generalized Valence Bond and Open–Shell Hartree–Fock Wave Functions, 1977, pp. 79–126.

Casida, M.E., Recent Developments and Applications of Modern Density Functional Theory, J. M. Seminario, 1996, Ed., Elsevier, Amsterdam.

Chiappe, C., F. Signori, G. Valentini, L. Marchetti, C.S. Pomelli, F. Bellina, Novel (Glycerol) borate-based ionic liquids: An experimental and theoretical study, *Phys. Chem. B.* 114 (2010) 5082–5088.

Cížek, J., On the Use of the Cluster Expansion and the Technique of Diagrams in Calculations of Correlation Effects in Atoms and Molecules, *Adv. Chem. Phys.* 14 (1969) 35–88.

Clark, T. A., Handbook of Computational Chemistry, John Wiley and Sons, New York, 1985.

Cramer, C.J., Essentials of Computational Chemistry–Theories and Models, John Wiley and Sons Ltd., 2004, 2nd ed.

Dolney, D.M., G.D. Hawkins, D.A. Truhlar, Winget, D.G. PLiotard, C.J. CramerUniversal solvation model based on conductor-like screening model, *J. Comput. Chem.* 21 (2000) 340–366.

Fock, V.Z., Näherungsmethode zurLösung des quantenmechanischen Mehrkörper problems, *Physik*. 61 (1930) 126–148.

Frisch, A., A.B. Nielson, A.J. Holder, Gaussview Users Manual Gaussian Inc., 2000, Pittsburgh, PA.

Frisch, E., M.J. Frisch, Gaussian 98 User's Reference, 2nd edition, 1999, Gaussian Inc. Pittsburgh.

Frisch, M.J., G.W. Trucks, H.B. Schlegel, G.E. Scuseria, M.A. Robb, J.R. et al. Cheeseman, Gaussian 03, revision C.02. 2003, Pittsburgh, PA: Gaussian, Inc.

Frisch, M.J., G.W. Trucks, H.B. Schlegel, G.E. Scuseria, M.A. Robb, J.R. Cheeseman, J.A. Montgomery, Jr., T. Vreven, K.N. Kudin, J.C. Burant, J.M. Millam, S.S. Iyengar, J. Tomasi,V. Barone, B. Mennucci, M. Cossi, G. Scalmani, N. Rega,G. A. Petersson, H. Nakatsuji, M. Hada, M. Ehara, K. Toyota, R. Fukuda, J. Hasegawa, M. Ishida, T. Nakajima, Y. Honda, O. Kitao, H. Nakai, M. Klene, X. Li, J. E. Knox, H.P. Hratchian, J.B. Cross, C. Adamo, J. Jaramillo, R. Gomperts, R.E. Stratmann, O. Yazyev, A.J. Austin, R. Cammi, C. Pomelli, J.W. Ochterski, P.Y. Ayala, K. Morokuma, G.A. Voth, P. Salvador, J.J.

Dannenberg, V.G. Zakrzewski, S. Dapprich, A.D. Daniels, M.C. Strain, O. Farkas, D.K. Malick, A.D. Rabuck, K. Raghavachari, J.B. Foresman, J.V. Ortiz, Q. Cui, A.G. Baboul, S. Clifford, J. Cioslowski, B.B. Stefanov, G. Liu, A. Liashenko, P. Piskorz, I. Komaromi, R.L. Martin, D.J. Fox, T. Keith, M.A. Al-Laham, C.Y. Peng, A. Nanayakkara, M. Challacombe, P.M. W. Gill, B. Johnson, W. Chen, M.W. Wong, C. Gonzalez, J.A. Pople, Gaussian, Inc., Wallingford CT, Gaussian 03, Revision C.02, 2004.

Frisch, M.J., Head–Gordon, M., Pople, J.A., 1990a, A direct MP2 gradient method, *Chem. Phys. Lett.* 166, 275–280.

Frisch, M.J., M. Head–Gordon, J.A. Pople, A direct MP2 gradient method, *Chem. Phys. Lett.* 166 (1990a) 275–280.

Frisch, M.J., M. Head–Gordon, J.A. Pople, Semi-direct algorithms for the MP2 energy and gradient, *Chem. Phys. Lett.* 166 (1990b) 281–289.

Foresman, J.B., E. Frisch, Exploring Chemistry with Electronic Structure Methods, 2nd edition. 1996, Gaussian Inc., Pittsburgh.

Gázquez, J.L., Structure and bonding: Hardness and softness in DFT theory, Vol. 80, 1993, Springer–Verlag Berlin Heidelberg.

Geerlings, P., F. De Proft, F.W. Langenaeker, Conceptual Density Functional Theory, *Chem. Rev.* 103 (2003) 1793–1873.

Hans-Dieter, H., G. Folkerts, Molecular Modeling: Basic Principles and Applications, VCH, 1996.

Head–Gordon, M., J.A. Pople, M.J. Frisch, MP2 energy evaluation by direct methods, *Chem. Phys. Lett.* 153 (1988) 503–506.

Hohenberg, P., W. Kohn, Inhomogeneous Electron Gas, *Phys. Rev.* 136 (1964) B864–B871.

Karabacak, M., S. Bilgili, T. Mavis, M. Eskici, A. Atac, Molecular structure, spectroscopic characterization (FT-IR, FT-Raman,UV and MR), HOMO and LUMO analysis of 3-ethynylthiophenen with DFT quantum chemical alculations, *Spectrochim. Acta. A Mol Biomol. Spectrosc.* 115 (2013) 709–718.

Kavitha, E., N. Sundaranganesan, S. Sebastian, Molecular structure, vibrational spectroscopic and HOMO, LUMO studies of 4–nitroaniline by density functional method, *Indian J. Pure. Appl. Phys.* 48 (2010) 20–30.

Klamt, A., Conductor like Screening Model for Real Solvents: A New Approach to the Quantitative Calculation of Solvation Phenomena, *J. Phys. Chem.* 99 (1995) 2224–2235.

Klamt. A., G. Schüürmann, COSMO: a new approach to dielectric screening in solvents with explicit expressions for the screening energy and its gradient, *J. Chem. Soc. Perk.* T. 2 (1993) 799–805.

Klamt, A., V. Jonas, T. B¨urger, J. C. W. Lohrenz, Refinement and Parametrization of COSMO-RS, *J. Phys. Chem. A.* 102 (1998) 5074–5085.

Kohn, W., L.J. Sham, Self-Consistent Equations Including Exchange and Correlation Effects, *Phys. Rev.* 140 (1965) A1133–A1138.

Krishnan. R., J. A. Pople, Approximate fourth-order perturbation theory of the electron correlation energy, *Int. J. Quant. Chem.* 14 (1978) 91–100.

Lin, S., S.I. Sandler, A priori phase equilibrium prediction from a segment contribution solvation model, *Ind. Eng. Chem. Res.* 41 (2002) 899–913.

Li, X., M.D. Sevilla, L. Sanche, DFT investigation of dehalogenation of adenine-halouracil base pairs upon low-energy electron attachment, *J. Am. Chem. Soc.* 125 (2003) 8916–8920.

Lü, R., Z. Qu, J. Lin, Comparative study of interactions between thiophene-\pyridine\benzene \heptane and 1-butyl-3-methylimidazolium trifluoro–methanesulfonate by density functional theory, *J. Mol. Liq.* 180 (2013) 207–214.

Maduro, R.M., M. Aznar, Liquid–liquid equilibrium of ternary systems 1-butyl-3-methyl–imidazolium hexafluorophosphate + aromatic + aliphatic, *Fluid Phase Equilib.* 265 (2008) 129–138.

Meng, J., A. Dolle, R.W. Carper, Gas Phase Model of an Ionic Liquid: semi-empirical and ab-initio bonding and molecular structure, *J. Mol. Struct. (Theochem)* 585 (2002) 119–125.

Møller, C., M.S. Plesset, Note on an Approximation Treatment for Many-Electron Systems, *Phys. Rev.* 46 (1934) 618–622.

Mukhopadhyay, M., B.D.M. Rao, Studies on Selectivities of Solvent for Liquid–Liquid Extraction of C7–C10 Aromatics, *Ind. Eng. Chem. Res.* XXIX (1987) T89.

Parr, R.G., L.v. Szentpály, Electrophilicity Index, S. Liu, *J. Am. Chem. Soc.* (1999) 1922–1924.

Parr, R.G., W. Yang, Density-Functional Theory of Atoms and Molecules, Oxford University Press, 1989, New York,

Pearson, R.G., Absolute electronegativity and hardness correlated with molecular orbital theory, *Proc. Natl. Acad. Sci.* U. S. A. (1986) 8440–8441.

Pearson, R.G., Acids and Bases, *Science.* 151 (1963b) 172.

Pearson, R.G., Hard and Soft Acids and Bases, *J. Am. Chem. Soc.* 85 (1963a) 3533.

Pereiro, A.B., A. Rodriguez, A study on the liquid–liquid equilibria of 1-alkyl-3 ethylimidazolium hexafluorophosphate with ethanol and alkanes, *Fluid Phase Equilib.* 270 (2008) 23–29.

Pople, J.A., M. Head–Gordon, K. Raghavachari, Quadratic Configuration Interaction. A General Technique for Determining Electron Correlation Energies, *J. Chem. Phys.* 87 (1987) 5968–5975.

Pople, J.A., R. Krishnan, H.B. Schlegel, J.S. Binkley, Electron correlation theories and their application to the study of simple reaction potential surfaces, *Int. J. Quant. Chem.* 14 (1978) 545–560.

Schäfer, A., A. Klamt, D. Sattel, J.C. W. Lohrenz, F. Eck ert, COSMO Implementation in TURBOMOLE: Extension of an efficient quantum chemical code towards liquid systems, *Phys. Chem. Chem. Phys.* 2 (2000) 2187–2193.

Schäfer, A., C. Huber, R. Ahlrichs, Fully Optimized Contracted Gaussian Basis Sets of Triple Zeta Valence Quality for Atoms Li to Kr, *J. Chem. Phy.* 100 (1994) 5829–5835.

Schaftenaar, G., J.H. Noordik, A Pre–and Post–processing Program for Molecular and Electronic Structures, *J. Comput. Aided Mol. Des.* 14 (2000) 123–134.

Sosa, C., J. Andzelm, B.C. Elkin, E. Wimmer, K.D. Dobbs, D.A. Dixon, A local density functional study of the structure and vibrational frequencies of molecular transition–metal compounds, *J. Phys. Chem. A.* 96 (1992) 6630–6636.

Szabo, A., N.S. Ostlund, Modern Quantum Chemistry, Dover Publ. Inc., New York, 1996.

Turner, A.E., C.C. Pye, D.R. Singer, Use of ab initio Calculations toward the Rational Design of Room Temperature Ionic Liquids, *J. Phys. Chem. A*, 107 (2003) 2277–2288.

Wang, Y., H. Li, S. Han, A theoretical investigation of the interactions between water molecules and ionic liquids, *J. Phys. Chem. B.* 2006, 110, 24646– 24651.

Wolfsberg, M., L. Helmholz, The spectra and electronic structure of the tetrahedral ions $MnO_{4-}$, $CrO_{4--}$, and $ClO_{4-}$, *J.Chem.Phys*. 20 (1952) 837-843.

Wolinski, K., J.F. Hinton, P. Pulay, Efficient implementation of the gauge-independent atomic orbital method for NMR chemical shift calculations, *J. Am. Chem. Soc.* 112 (1990) 8251–8260.

Yang, X.Z., Unexpected direct reduction mechanism for hydrogenation of ketones catalyzed by iron PNP pincer complexes, *Inorg. Chem.* 50 (2011) 12836.

Zhang, L., H. Li, Y. Wang and X. Hu, Characterizing the structural properties of N, N-dimethyl formamide-based ionic liquid: A density-functional study, *J. Phys. Chem. B.* 111 (2007) 11016–11020.

# TABLES AND FIGURES OF CHAPTER 2

**Table 2.1.1.** List of cations studied in this work.

| S. No. | Name of Cation | Acronym | Chemical Formulae/ Mol. Wt. | COSMO Area ($Å^2$) | COSMO Volume ($Å^3$) |
|---|---|---|---|---|---|
| 1 | 1-octylquinolinium | $[C_8CHIN]^+$ | $C_{51}H_{61}ClNO_2$/897.3 | 1150.38 | 2165.47 |
| 2 | 1-ethtyl-3-methylimidazolium | $[C_2MIM]^+$ | $C_6H_{11}N_2$+/111.164 | 599.80 | 1006.59 |
| 3 | 1-butyl-3-methylimidazolium | $[C_4MIM]^+$ | $C_8H_{17}N_2$+/139.218 | 746.01 | 1279.15 |
| 4 | 1-methyl-3-pentylimidazolium | $[C_5MIM]^+$ | $C_9H_{17}N_2$+/153.244 | 821.23 | 1414.94 |
| 5 | 1-hexyl-3-methylimidazolium | $[C_6MIM]^+$ | $C_{10}H_{19}N_2$+/167.271 | 892.55 | 1549.42 |
| 6 | 1-octyl-3-methylimidazolium | $[C_8MIM]^+$ | $C_{12}H_{23}N_2$+/195.186 | 1038.47 | 1822.07 |
| 7 | 1,3-dimethylimidazolium | $[C_1MIM]^+$ | $C_5H_9N_2$+/97.138 | 525.12 | 871.17 |
| 8 | Methyl-methyl-methyl-imidazolium | $[C_1DMIM]^+$ | $C_6H_{11}N_2$+/111.164 | 517.23 | 860.52 |
| 9 | 1-ethyl-2,3-dimethylimidazolium | $[C_2DMIM]^+$ | $C_7H_{13}N_2$+/125.191 | 652.90 | 1131.94 |
| 10 | 1-butyl-2,3-dimethylimidazolium | $[C_4DMIM]^+$ | $C_9H_{17}N_2$+/153.244 | 802.99 | 1403.62 |
| 11 | 1-ethyl-4-methylpyridinium | $[C_2MPY]^+$ | $C_8H_{12}N_2$+/122.187 | 649.44 | 1123.80 |
| 12 | 1-butyl-4-methylpyridinium | $[C_4MPY]^+$ | $C_{10}H_{16}N$+/150.24 | 799.65 | 1395.80 |
| 13 | 1-hexyl-4-methylpyridinium | $[C_6MPY]^+$ | $C_{12}H_{20}N$+/178.293 | 951.50 | 1669.13 |
| 14 | 1-octyl-4-methylpyridinium | $[C_8MPY]^+$ | $C_{14}H_{24}N$+/206.347 | 1102.38 | 1941.82 |
| 15 | 1,1-dimethyl-pyrrolidinium | $[DMPYR]^+$ | $C_6H_{14}N$+/100.182 | 554.00 | 948.93 |
| 16 | 1-1-dipropyl-pyrrolidinium | $[DPPYR]^+$ | $C_{10}H_{22}N$+/156.288 | 821.65 | 1492.03 |
| 17 | 1-butyl-1-ethyl-pyrrolidinium | $[BEPYR]^+$ | $C_{10}H_{22}N$+/156.288 | 822.70 | 1491.18 |
| 18 | 1-butyl-1-methyl-pyrrolidinium | $[BMPYR]^+$ | $C_9H_{20}N$+/142.261 | 723.57 | 1299.08 |
| 19 | 1-hexyl-1-methyl-pyrrolidinium | $[HMPYR]^+$ | $C_{11}H_{24}N$+/170.314 | 858.05 | 1547.25 |
| 20 | 1-octyl-1-methyl-pyrrolidinium | $[OMPYR]^+$ | $C_{13}H_{28}N$+/198.368 | 1025.58 | 1817.48 |
| 21 | Benzyltrimethyl-ammonium | $[BETNH]^+$ | $C_{10}H_{10}N$+/150.24 | 758.61 | 1380.66 |
| 22 | Butyltrimethyl-ammonium | $[BTNH]^+$ | $C_7H_{18}N$+/116.143 | 692.16 | 1182.72 |

**Table 2.1.1.** Continued

| S. No. | Name of Cation | Acronym | Chemical Formulae/ Mol. Wt. | COSMO Area ($Å^2$) | COSMO Volume ($Å^3$) |
|---|---|---|---|---|---|
| 23 | Dimethyl-ammonium | $[DMNH]^+$ | $C_2H_8N$+/46.091 | 348.10 | 511.33 |
| 24 | 2-Hydroxyethyl-trimethylammonium | $[HeTNH]^+$ | $C_5H_{14}NO$+/104.17 | 581.00 | 974.99 |
| 25 | Methyl-ammonium | $[MNH]^+$ | $CH_6N$+/32.064 | 268.88 | 366.56 |
| 26 | Ethyl-ammonium | $[ENH]^+$ | $C_2H_8N$+/46.091 | 345.02 | 503.84 |
| 27 | Propyll-ammonium | $[PNH]^+$ | $C_3H_{10}N$+/60.118 | 420.11 | 640.29 |
| 28 | Hexyldiethylmethylphosphonium | $[HDEMP]^+$ | $C_{11}H_{26}P^+$/189.3 | 1050.89 | 1831.43 |
| 29 | Hexyltrimethylphosphonium | $[HTMP]^+$ | $C_9H_{22}P^+$/161.24 | 914.95 | 1561.10 |
| 30 | Octyltrimethylphosphonium | $[OTMP]^+$ | $C_{12}H_{22}P^+$/204.33 | 1061.34 | 1832.54 |
| 31 | Octyldiethylmethylphosphonium | $[ODEMP]^+$ | $C_{13}H_{30}P^+$/217.35 | 1197.27 | 2103.81 |
| 32 | Diethyldimethylpropylphosphonium | $[DEDMPP]^+$ | $C_9H_{22}P^+$/161.24 | 876.01 | 1553.30 |
| 33 | Tributylmethylphosphonium | $[TBMP]^+$ | $C_{13}H_{30}P^+$/217.35 | 1195.22 | 2102.03 |
| 34 | Tetrabutylphosphonium | $[TBP]^+$ | $C_{16}H_{36}P^+$/259.43 | 1413.94 | 2514.52 |
| 35 | Triisobutylmethylphosphonium | $[TIBMP]^+$ | $C_{13}H_{30}P^+$/217.35 | 1138.84 | 2087.54 |

**Table 2.1.2.** List of anions studied in this work.

| S. No. | Name of Anion | Acronym | Chemical Formulae/ Mol. Wt. (g/mol) | COSMO Area ($Å^2$) | COSMO Volume ($Å^3$) |
|---|---|---|---|---|---|
| 1 | Acetate | [OAc]- | $C_2H_3O_2^-$/59.014 | 324.56 | 475.39 |
| 2 | Tetracyanoborate | $[B(CN)_4]$- | $C_4BN_4^-$/114.881 | 584.76 | 975.27 |
| 3 | Tetrafluoroborate | $[BF_4]$- | $BF_4^-$/86.805 | 384.80 | 567.46 |
| 4 | Bis(methylsulfonyl)amide | [BMA]- | $C_2H_6NO_4S_2^-$ /172.204 | 605.84 | 1036.03 |
| 5 | Bis(oxalato (2-))borate | [BOB]- | $C_8H_{14}BO_4^-$/249.004 | 619.64 | 1056.41 |
| 6 | Bis(trifluoromethylsulfonyl)amide | [BTA]- | $C_2F_6NO_4S_2^-$ /280.147 | 771.89 | 1328.92 |
| 7 | Trifluoro-methylsulfonate | $[CF_3SO_3]$- | $CF_3O_3S^-$/148.953 | 462.25 | 734.16 |
| 8 | Methylsulfonate | $[CH_3SO_3]$- | $CH_3O_3S^-$/95.098 | 383.90 | 588.65 |
| 9 | Methyl sulfate | $[CH_3SO_4]$- | $CH_4O_4S^-$/112.105 | 420.3 | 658.09 |
| 10 | Ethylsulfate | $[C_2H_5SO_4]$- | $C_2H_6O_4S^-$/126.132 | 491.58 | 793.51 |
| 11 | Octylsulfate | $[C_8H_{17}SO_4]$- | $C_8H_{18}O_4S^-$/210.291 | 945.45 | 1610.46 |
| 12 | Chloride | [Cl]- | $Cl^-$/35.454 | 188.59 | 243.53 |
| 13 | Dimethylphosphate | $[DMPO_4]$- | $C_2H_7O_4P$/12126.048 | 516.63 | 827.84 |
| 14 | Hydrogensulfate | $[HSO_4]$- | $H_2O_4S^-$/98.078 | 346.73 | 514.95 |
| 15 | N-methylsulfonylacetamide | [MAcA]- | $C_3H_7NO_3S$/137.158 | 557.06 | 923.20 |
| 16 | 2-(2-methoxyethoxy)ethylsulfate | [MDEGSO]- | $C_5H_{12}O_6S$/200.210 | 765.83 | 1340.19 |
| 17 | Dicyanamide | $[N(CN)_2]$- | $C_2N_3$/60.8 | 359.89 | 545.93 |
| 18 | Hexafluorophosphate | $[PF_6]$- | $F_6P$/144.965 | 430.83 | 674.69 |
| 19 | Thiocyanate | [SCN]- | CNS/58.083 | 309.73 | 465.90 |
| 20 | p-toluenesulfonate | [TOS]- | $C_7H_7O_3S$/171.194 | 678.49 | 1197.19 |
| 21 | Salicylate | [Sal]- | $C_7H_5O_3$/137.113 | 564.18 | 995.26 |
| 22 | Nitrate | $[NO_3]$- | $NO_3$/62.01 | 269.87 | 366.72 |
| 23 | Trifluoroacetate | $[CF_3COO]$- | $C_2F_3O_2$/113.016 | 403.68 | 621.01 |
| 24 | Diethyl phosphate | [DEP]- | $C_4H_{11}O_4P$/154.102 | 664.86 | 1101.36 |
| 25 | Decanoate | [DEC]- | $C_{10}H_{19}O_2$/171.257 | 925.51 | 1565.97 |
| 26 | Dibutyl phosphate | [DBP]- | $C_{18}H_{19}O_4P$/210.208 | 962.02 | 1644.95 |
| 27 | Bromide | [Br]- | $Br^-$/79.905 | 209.37 | 284.87 |
| 28 | Dihydrogen phosphate | $[DHPO_4]$- | $H_3O_4P$/97.995 | 365.02 | 539.57 |
| 29 | Perchlorate | $[ClO_4]$- | $ClO_4$/99.451 | 334.60 | 485.12 |

**Table 2.3.** Examples of list of basis sets available and used in *Gaussion03* for different atoms.

| S.No. | Basis | Options | Atoms |
|---|---|---|---|
| 1 | STO-3G | * | H-Xe |
| 2 | 3-21G | * ** | H-Cl |
| 3 | 4-21G | * ** | |
| 4 | 4-21G | * ** | H-Ne |
| 5 | 6-21G | * ** | |
| 6 | 6-21G | + ++ * ** | H-Cl |
| 7 | LP-31G | * ** | |
| 8 | LP-41G | * ** | |
| 9 | 6-311G | + ++ * ** | H-Ar |
| 10 | MC-311G | None | H-Ar |
| 11 | D95 | + ++ * ** | H-Cl |
| 12 | D95V | + ++ * ** | H-Ne |
| 13 | SEC | + ++ * ** | H-Cl (same as SHC) |
| 14 | CEP-4G | + ++ * ** | H-Cl |
| 15 | CEP-31G | + ++ * ** | H-Cl |
| 16 | CEP-121G | + ++ * ** | H-Cl |
| 17 | LANLIMB | None | H-Bi (except lanthanides) |
| 18 | LANLIDZ | None | H-Bi (except lanthanides) |

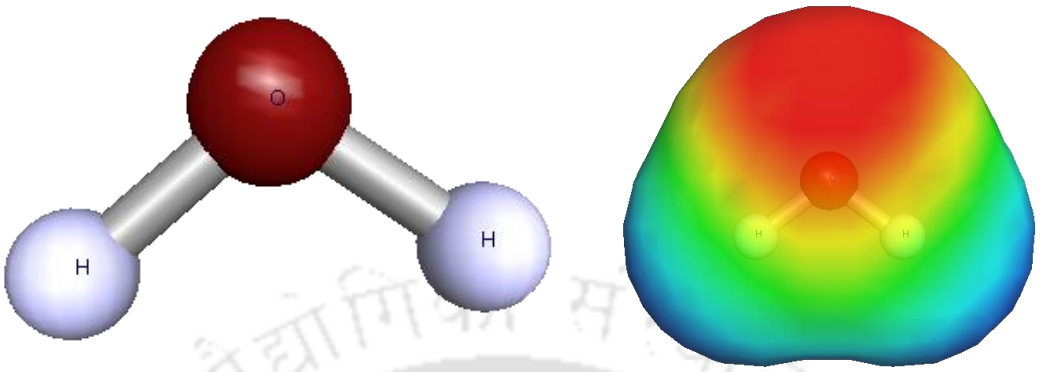


(a) Molecular structure (b) Screening charge distribution

**Figure 2.1.1(a).** Molecular structure and (b): screening charge distribution of $H_2O$ with red: positive surface charge, blue: negative surface charge, yellow and green: almost neutral surface charges.

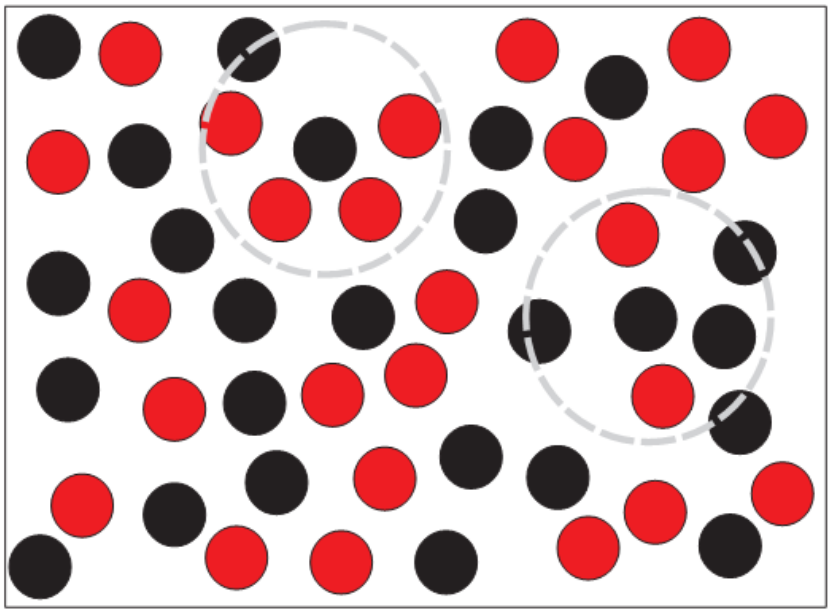

**Figure 2.1.2.** The concept of local composition: Although the bulk composition of red and black balls is 1:1, the local compositions, exemplary accentuated by gray circles, differ [Klamt et al., 1998].

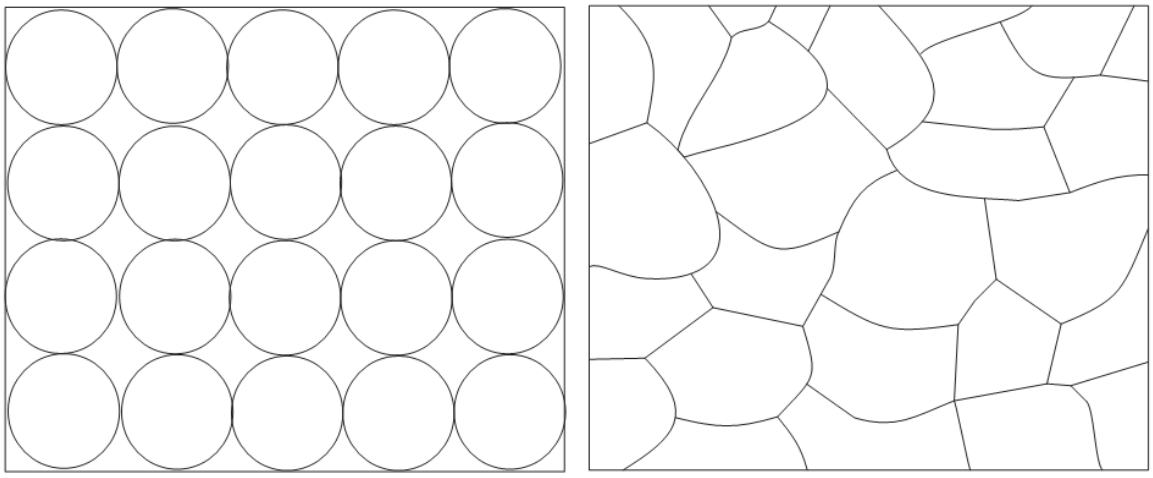

(a) Lattice picture (b) Polyhedral surface picture

**Figure 2.1.3(a).** Liquid model in the lattice and (b): the polyhedral surface picture; circles and polyhedrons represent molecules in the liquid phase [Klamt et al., 1998].

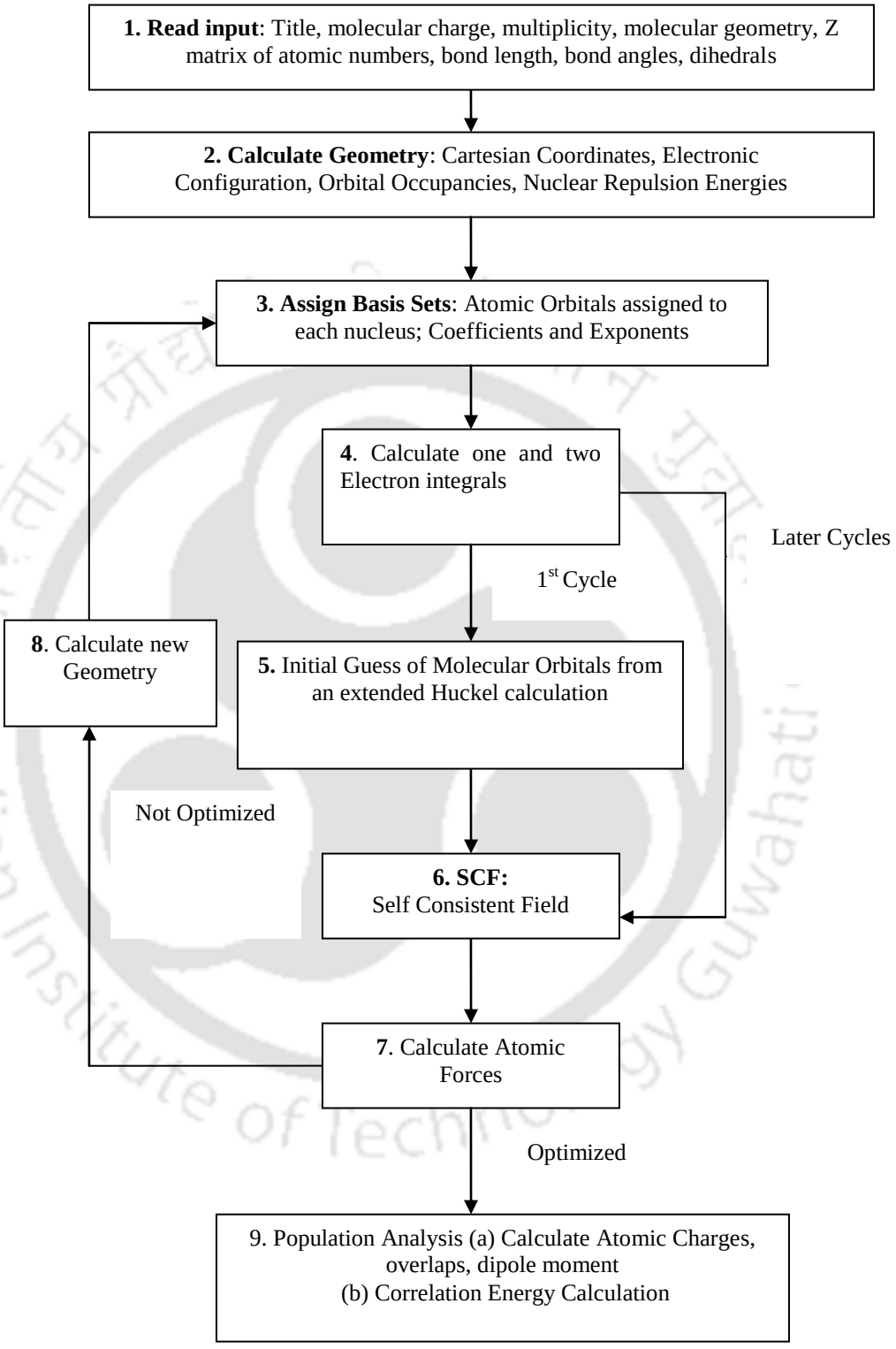


**Figure 2.1.4.**Typical flow chart for an *ab–initio* optimization.

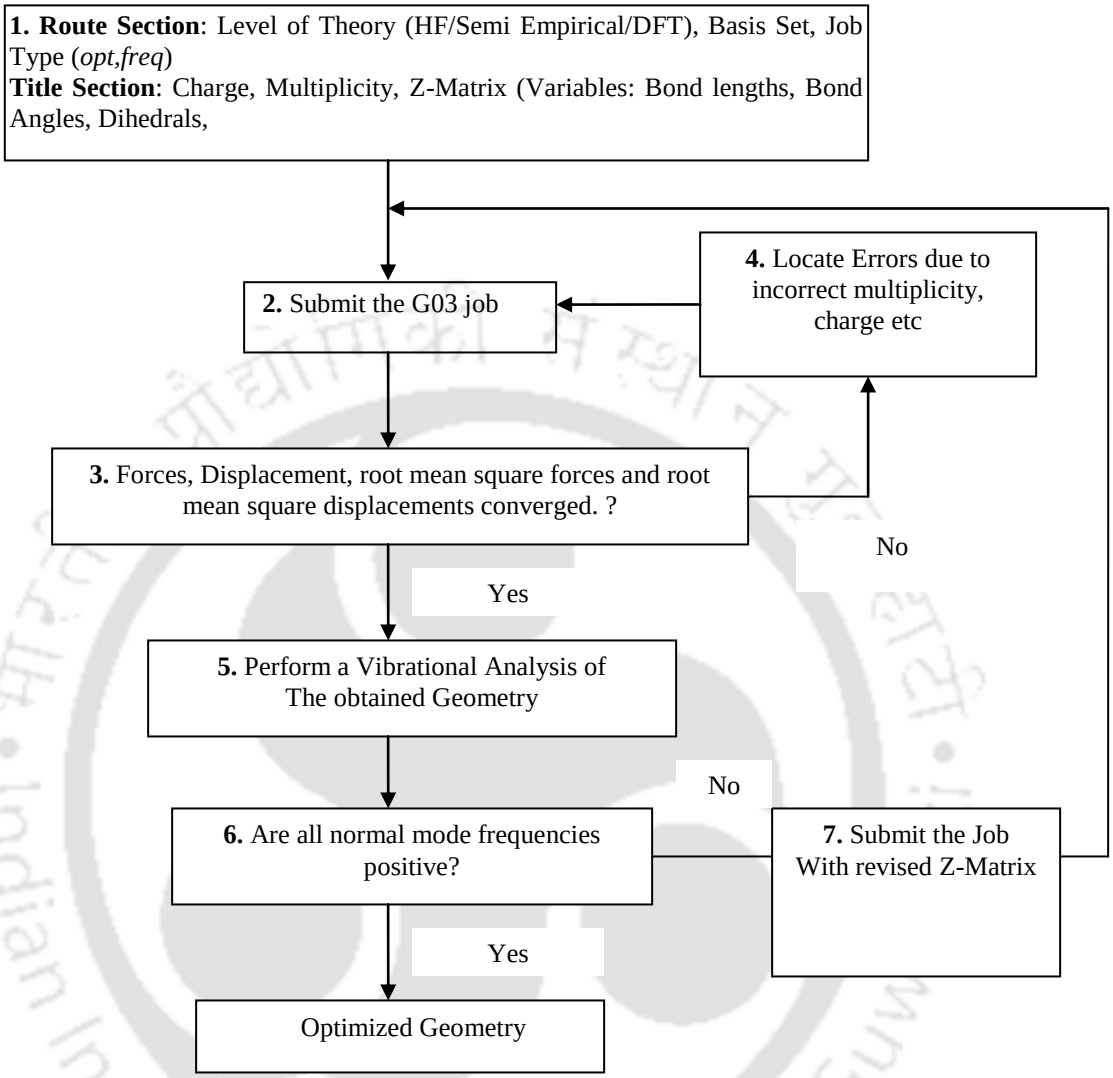


**Figure 2.1.5.** Flow chart for geometry optimization.

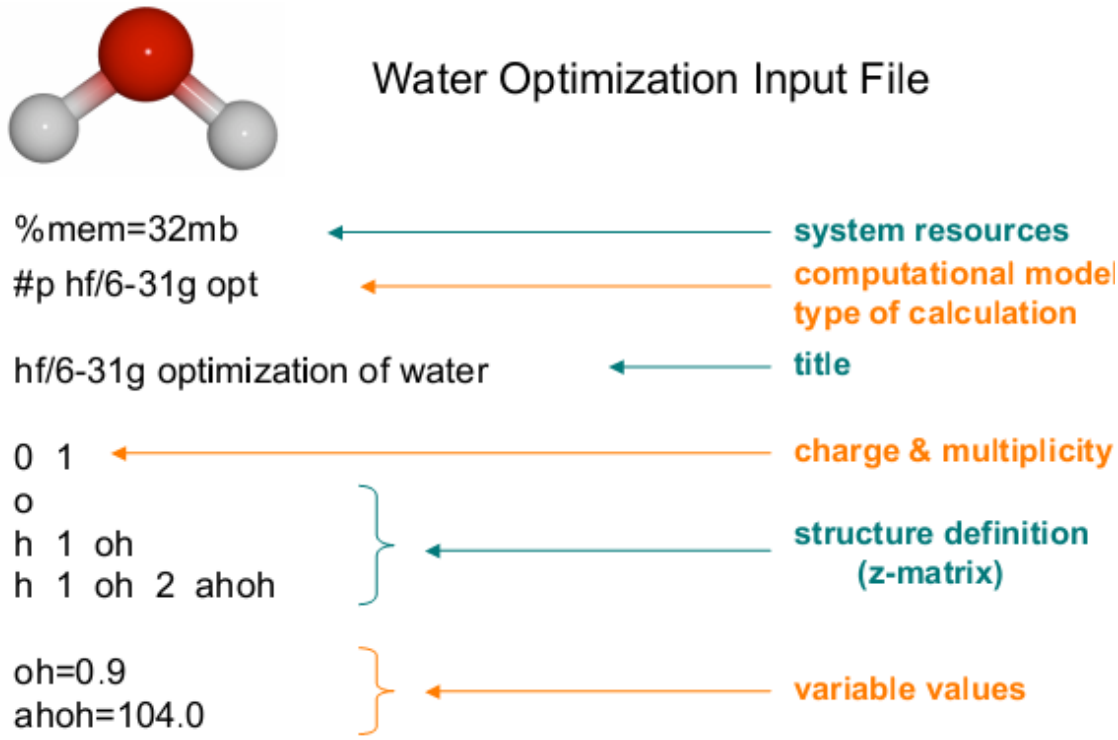


**Figure 2.1.6.** Sample input file for geometry optimization of water molecule.

# CHAPTER 3

## MATERIALS AND EXPERIMENTAL METHODS

### 3.1. Reagents used in LLE experiments

All major commercial chemicals used were of analytical reagent grade and used without further purification. Ionic liquid [$C_4$DMIM][$PF_6$] (assay–98%, Fluka, Germany, CAS: 227617–70–1) was obtained from Sigma Aldrich (Germany). The ionic liquid was dried under vacuum of 500 mmHg at 25 °C for 24 h to remove volatile impurities prior to use. PCP (assay–90%) and PA (99.5% Pure) were purchased from National Chemicals Ltd., and Sigma Aldrich respectively. Acetone was purchased from Spectrochem Pvt. Ltd. (India). Dimethyl sulfone oxide–D6 (DMSO–$D_6$) used as NMR solvent and was supplied by Merck, Germany.

### 3.2. Liquid-liquid extraction experiments

LLE experiments were carried out in such a way that the concentration of PA, PCP, ionic liquid and water forms two different layers. Glass vials (Merck, Germany) of 15 mL size were used to prepare samples. 5 mL of each sample was prepared and the glass vials were sealed using parafilm tape. The ternary system of known composition was prepared in these sealed glass vials using an analytical balance (Shimadzu Model: *TX323L*) with an accuracy of 0.1 mg. These sealed glass vials were then transferred to a thermostatic shaker bath (Dailhan Lab, China) which was operated at 150 rpm with an uncertainty of ± 0.01 K. All samples were continuously stirred for 6 h and then allowed to settle for 12 h to reach the equilibrium state. Then, samples of each phase were separated using a micropipette for further compositional analysis. The procedure followed for all the experiments is as reported in literature [Potdar et al., 2012]. $^1$H NMR spectroscopy (Make: Varian, Model: Mercury

plus) technique was used to measure the concentration of both equilibrated extract and raffinate phase samples. DMSO–$D_6$ (Merck, Germany, 99.8%) was used as a NMR reference solvent to characterize each sample. 0.1 mL of each experimental sample in equilibrium was dissolved with 0.4 mL of DMSO–$D_6$ and transferred to a NMR tube (thrift grade) and the tube was sealed with paraffin tape. Then these tubes were placed in a NMR spectrophotometer for $^1$H analysis. The NMR spectrometer of 11.74 T (400 MHz response of $^1$H) was used to carry out the $^1$H NMR spectral analysis for the measurement of the peak areas of the hydrogen molecule of each component. The peak areas corresponding to hydrogen moles in each phase were noted down for the estimate of mole fraction of each component.

$^1$H NMR (400 MHz, DMSO–$D_6$) δ: 1.74–1.99 (2H, m) was considered to quantify the ionic liquid [Itoh et al., 2003]. The water peak in DMSO–$D_6$ showed a peak at 3.67 ppm. Similarly, peak at 7.3 and 7.5 ppm were considered to calculate the 2 acidic hydrogen atoms of ionic liquid and 4 hydrogen atoms of PA. In case of PCP, peak at 2 ppm (1H) and peak at 7.3 and 7.5 ppm were considered for 17H of ionic liquid. Suitable equations were formed in order to solve the contribution of individual Hydrogen atom of each component. The final composition quantification for all compounds through NMR spectrum was carried out using the Eq. 3.1 given below.

$$x_i = \frac{H_i}{\sum_{i=1}^{n} H_i} \tag{3.1}$$

Where, $H_i$ denotes the peak area of single hydrogen for sample and $x_i$ is the mole fraction of samples.

### 3.3. Reagents used in PCP and phenol removal by SILM

1-Butyl-2,3-dimethylimidazolium hexaflourophosphate [$C_4$DMIM][$PF_6$], Tetrabutyl–phosphonium hexaflourophosphate [TBP][$PF_6$] (Fluka, Germany, CAS: 227617-70-1) was used as the membrane carrier. Chemicals such as HCl, KOH and NaOH were purchased from Merck India. PVDF (Durapore® Membrane filters) membranes (porous hydrophilic) were obtained from Millipore, India. HPLC grade Acetonitrile was supplied by Rankhem, India. Acetone was purchased from Spectrochem Pvt. Ltd., (India). PCP was purchased from National fertilizers Ltd., India. Phenol ($C_6H_5OH$) was procured from Merck, Germany. ILs used in this study was purchased from Sigma Aldrich (Germany) until unless stated. All major chemicals were used of analytical reagent grade and used as received without further treatment.

A 1000 mg $L^{-1}$ of standard aqueous solution of PCP was prepared in 1 L of deionized (Millipore, India) water by dissolving appropriate PCP in acetone to obtain a standard stock solution. Working solutions were prepared by dilution of standard stock in deionized (Millipore, India) water for further use. All the solution samples were kept in refrigerator at 4°C. In order to avoid the influence on the results from the feasible degradation of the PCP, the working solutions were prepared every day by diluting the stock solutions to appropriate volumes with deionized water. While storing stock and samples photolysis free coloured bottles/flasks were used to avoid the photodegradation of PCP.

### 3.4. PCP analysis

The concentration of PCP in feed phase and strip phase was found out by HPLC (Prominence UFLC, Shimadzu, with LC-20AD liquid chromatography and SPD–20A UV/Visible detector). Oyster BDS premium C18 HPLC column (250×4.6mm, 5 μm) was used from Merck Millipore, India. The operating conditions used during analysis as follows: mobile phase: Acetonitrile: water (70:30 V/V), flow rate: 1 mL $min^{-1}$, injection volume: 20 μL, retention time: 1.8 min, wave length of PCP: 332 nm and mode of operation: through UV detector. Solution pH was measured with digital pH meter (pH spear, Eutech Instruments, India). The wave length of PCP solution was measured with UV/Visible spectrophotometer (Thermo Scientific Spectra scan UV 2700 with a double beam, India) prior to HPLC analysis. Glass diffusion cells which were used in this study was fabricated by local vendor (M/S ab Chemicals, Guwahati, India). Fig. 3.1 represents the SILM **e**xperimental setup used in this study.

The experimental studies were carried out at 25±2 °C using glass diffusion cell with two independent compartments, each volume of 100 mL and placed on a magnetic stirrer. The prepared SILM was inserted between the two cells by applying vacuum grease to the glass cells to prevent slipping of glass cells and leakage of feed and permeate solutions. The whole setup was tightened by a stainless steel screw connector carefully. The effective membrane contact area (A) between the glass cells is 12.0 $cm^2$.

### 3.5. Experimental details of PCP and phenol removal

The transport experiments of PCP from feed phase to strip phase via SILM was conducted for 30 h each. The samples from the feed and receiving solutions were drawn at chosen time intervals to measure PCP concentration. Samples were analyzed in HPLC at a wavelength of 332 nm. The precision of various readings of the same sample was observed within 3 to 5%. All experiments were carried at concentration between 10–50 mg $L^{-1}$, HPLC calibration was carried from 1 to 10 mg $L^{-1}$, and experimental samples were diluted to calibration range and analyzed. During the experiment stirring was carried at 100–300 rpm. Fig. 3.2 shows the HPLC chromatogram of standard 4 mg $L^{-1}$ and 8 mg $L^{-1}$ of PCP at feed pH=6.5. Similar procedure was carried for phenol removal by SILM experiments. The analysis of phenol was done by UV–vis Spectrophotometer (Varian, Model Cary 50 Bio) at the wavelength of 500 nm using 4–aminoantipyrine method.

### 3.6. Reagents used in Endosulfan removal by SILM

All major chemicals used were of analytical reagent grade. 1-Butyl-2,3-dimethylimidazolium hexaflourophosphate [$C_4$DMIM][$PF_6$] (Fluka, Germany, CAS: 227617-70-1) was used as the membrane phase. The α–endosulfan was procured from Sigma-Aldrich, India. Chemicals such as HCl, $H_2SO_4$, NaOH, KOH, and $NH_4OH$ were supplied by Merck, India. Porous hydrophilic PVDF (Durapore® Membrane filters) membranes were obtained from Millipore, India. Acetonitrile (HPLC grade) was supplied by Rankem, India. Acetone was purchased from Spectrochem Pvt. Ltd., (India).

Desired amount of α–endosulfan was dissolved in acetone to obtain a standard stock solution with a concentration of 1000 mg $L^{-1}$. Working solutions were prepared by dilution of standard stock in deionized (Millipore, India) water for further use. Stored stock solutions were diluted into required working solutions. All the solution samples were then stored in refrigerator (4 °C).

### 3.7. Endosulfan analysis

The transport of endosulfan from feed phase to strip phase was determined by analyzing the endosulfan ion concentration using HPLC (Prominence UFLC, Shimadzu, with LC-20AD liquid chromatography and SPD–20A UV/Visible detector) with Oyster BDS premium C18 HPLC column (250×4.6 mm, 5 μm) from Merck Millipore, India. The operating conditions used were as follows: mobile phase, Acetonitrile: water (70:30 V/V), flow rate: 1 mL $min^{-1}$, injection volume: 20 μL, retention time: 3.2 min, wave length of endosulfan: 265 nm and mode of operation: UV/Visible detector mode. Solution pH was measured with digital pH meter (pH spear, Eutech Instruments, India). Prior to the HPLC analysis, endosulfan solution wave length was measured with UV–Visible spectrophotometer (Thermo Scientific Spectra scan UV 2700 with a double beam, India). Glass diffusion cells (Fig. 3.1) each having a volume of 100 mL was fabricated and supplied by local vendor (M/.s a.b Chemicals & Instruments, Guwahati, India). The glass diffusion cells were enclosed to prevent possible solution evaporation. Entire experimental work was carried out at ambient temperature 25 ± 2 °C.

### 3.8. Experimental details of Endosulfan removal

The endosulfan transport experiment studies were carried out at 25 ± 2 °C using a glass diffusion cell with two independent compartments of 100 mL volume each and placed on a magnetic stirrer as shown in Fig. 3.1 The prepared SILM was inserted between the two cells by applying vacuum grease to avoid slipping of glass diffusion cells and leakage of feed and permeate solutions. The whole setup was tightened with the help of stainless steel screw connector. The effective membrane contact area (A) between the glass cells was approximately 12.5 $cm^2$.

The transport experiments of endosulfan from feed phase to strip phase through SILM was conducted for 30 h each. The endosulfan concentration was measured by taking samples from the feed and receiving solutions at chosen time intervals. Endosulfan samples were analyzed in HPLC at a wavelength of 265 nm. The accuracy of multiple readings of the same sample was observed within 3 to 6%. Fig. 3.3(a–d) shows the HPLC chromatogram of standard 10 mg $L^{-1}$ of ES (a) at feed pH=6.5 (without changing the solution pH) , (b) 0.1 M NaOH phase, (c) 0.1 M KOH phase and (d) 0.1 M $NH_4OH$ phase.

### 3.9. Flux measurement and membrane liquid loss

The prepared SILM was placed between the two glass chambers and then the feed chamber was simultaneously filled with endosulfan solution and the other side with stripping solution. Immediately, after transferring the feed and stripping solutions, the magnetic stirrers were operated with a rpm of 100–300. The flux ($J$ mol $m^{-2}$ $s^{-1}$) measures the number of moles

or amount of substance diffusing per unit time and unit effective contact area and is given by the following Eq.

$$J = -\left(\frac{V}{A}\right)\times\left(\frac{dC}{dt}\right) \tag{3.2}$$

where $V$ is the volume of the stripping phase in $m^3$; $A$ is the effective contact area of the membrane in $m^2$; $C$ is the concentration of ES in the receiving phase in mol $L^{-1}$ and $t$ is the time elapsed in s. The membrane fluxes were measured with fresh feed and stripping solutions. New membrane was used for each flux measurement experiment; which provided the same driving force for each experiment. Similarly, the membrane liquid (IL) loss was measured by the weighing i.e. by weighing the membrane before and after the transport experiment. The percentage weight loss of the membrane was calculated by the following equation:

$$\text{Membrane Wt. loss (\%)} = \left(\frac{\text{Initial wt. before expt.-Final wt. after expt.}}{\text{Initial wt. before expt.}}\right)\times 100 \tag{3.3}$$

The ES separation process was checked through change of solute concentration in the feed and permeate phase. The permeation rate was calculated as per the following formula,

$$\text{Rate of permeation (\%)} = \frac{C_{R,24h}}{C_{F,0}}\times 100 \tag{3.4}$$

where $C_{R,24h}$ is concentration of ES in receiving phase after 24 h, $C_{F,0}$ is initial concentration of ES in feed phase.

Multiple transport experiments through SILM were carried out with and without pH control on the feed phase. Different stripping phase solutions such as 0.1M NaOH (~pH = 13 ± 0.1), 0.1M KOH (~pH = 13 ± 0.1) and 0.1M $NH_4OH$ (~pH = 11 ± 0.1) were tested and 0.1 M NaOH was found to be the best among all the stripping phase solutions. All the further experiments were carried out by using 0.1M NaOH as stripping phase solution unless until stated. The endosulfan working solution concentration (aq.) consisted of 50 mg $L^{-1}$. The transport experiments for the SILM were started by adding 100 mL of 50 mg $L^{-1}$ solution into their feed and 100 mL of respective strip solution in glass cell compartments. In case of pH control experiments NaOH/HCl was used to maintain the initial feed pH whenever required.

### 3.10. Preparation of SILM

The SILM were prepared using porous PVDF hydrophilic membrane for both PCP/endosulfan experiments. PVDF membrane was act as support and the ionic liquid served as a carrier. Properties and specifications of PVDF membrane is shown in Table 3.1. The preparation of SILM comprises of following steps: (i) the membrane filter paper was soaked in required amount of ionic liquid in a petridish. The petridish was covered with a lid and was rolled with paraffin tape to avoid exposing to air. Soaking was carried out for 24 h and then the membrane was taken out, gently wiped with tissue paper, (ii) the membrane was kept in a vacuum desiccator (~500 mm Hg) about 24 h to dry off the excess ionic liquid remaining on the surface. Dried membranes were taken out after 24 h, and (iii) weighed on an analytical balance. The weights of the membranes were noted for further calculation. Alike practice was repeated for each experiment. A new membrane filter paper was used

every time. The surface morphological study of membrane paper before and after the immobilization was carried out through scanning electron microscope (SEM). The elemental analysis membrane was carried out using energy dispersive X–ray spectroscopy (EDX). Detailed explanation of SEM and EDX characterization was given in chapter 5.

### 3.11. Selection of ionic liquid

Prior to the experiment, the selection of ionic liquid was carried by judicious screening of ionic liquids using a well–known quantum chemical based theoretical model called COSMO–RS (COnductor like Screening MOdel for Real Solvents). The detailed methodology and approaches followed in COSMO–RS model was systematically explained in chapter 2. In addition the selection ionic liquid was also considered based on hydrophobicity and commercial availability after successful screening. Previously, Seddon and his co–workers (Seddon et al., 2000) furnished a selection process on the choice of anion on the miscibility of ionic liquid and water.

### References

Itoh, T., Y. Nishimura, N. Ouchi, S. Hayase, 1-Butyl-2,3-dimethylimidazolium tetra–fluoroborate: the most desirable ionic liquid solvent for `recycling use of enzyme in lipase-catalyzed transesterification using vinyl acetate as acyl donor, *J. Mol. Catal. B: Enzym.* 26 (2003) 41–45.

Potdar, S., R. Anantharaj, T. Banerjee, Aromatic extraction using mixed ionic liquids: experiments and COSMO–RS predictions, *J. Chem. Eng. Data.* 57 (2012) 1026−1035.

Seddon, K.R., A. Stark, M.J. Torres, Influence of Chloride, Water, and Organic Solvents on the Physical Properties of Ionic Liquids, *Pure Appl. Chem.*72 (2000) 2275–2287.

## TABLES AND FIGURES OF CHAPTER 3

**Table 3.1.** Specifications and properties of PVDF membrane by the supplier

| Description | Specification | Description | Specification |
|---|---|---|---|
| Refractive Index: | 1.42 | Maximum Operating Temperature, °C: | 85 |
| Pore Size (µm): | 0.45 | Porosity %: | 70 |
| Filter Diameter (mm): | 90 | Wettability: | Hydrophilic |
| Thickness, µm: | 125 | Filter Color: | White |
| Water Flow Rate, mL/min x cm²: | 29 | Filter Surface: | Plain |
| Gravimetric Extractables, %: | 0.5 | Bubble Point at 23 °C: | ≥1.55 bar, Air-with water |
| Air Flow Rate, L/min x cm²: | 4 | Filter Type: | Screen filter |
| Chemistry: | Hydrophilic PVDF | Trade Name: | Durapore |

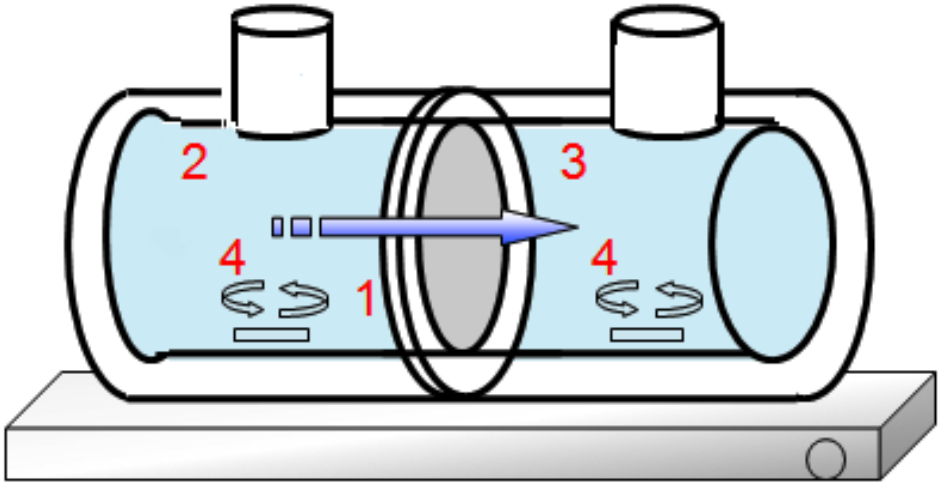


**Figure 3.1.** SILM **e**xperimental setup, 1). PVDF membrane immobilized with IL (SILM), 2). Feed phase of glass diffusion cell, 3). Strip phase of glass diffusion cell, 4) magnetic spin bars.

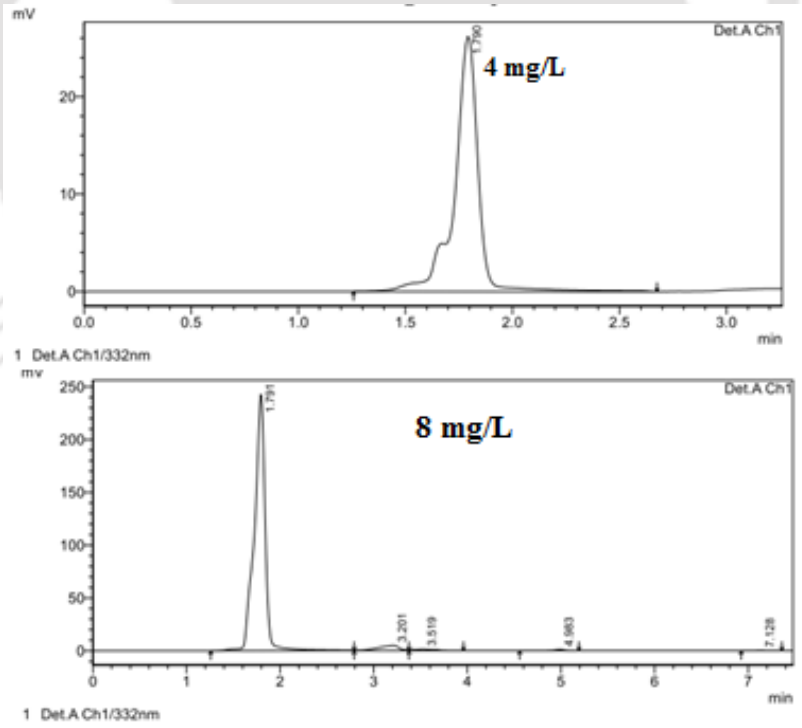


**Figure 3.2.** HPLC chromatogram of standard 4 and 8 mg $L^{-1}$ of PCP at feed pH=6.5.

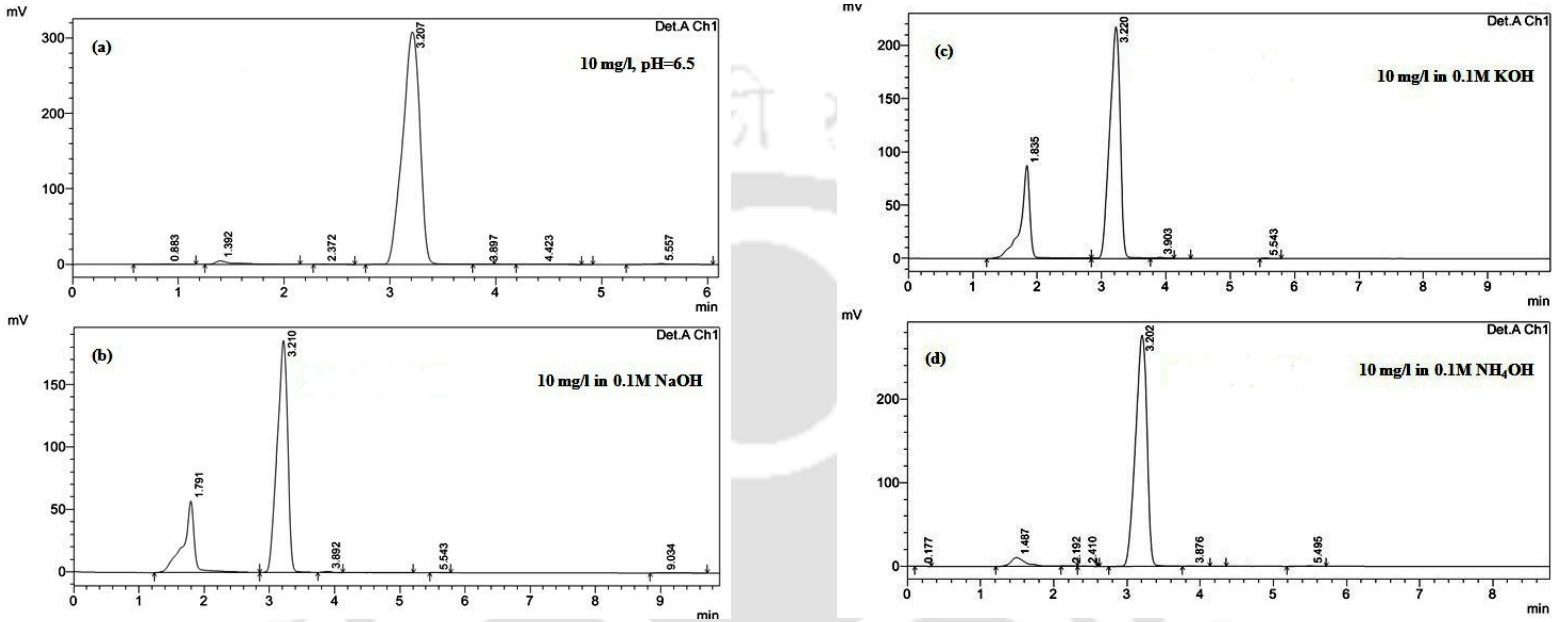


**Figure 3.3.** HPLC chromatograms of 10 mg $L^{-1}$ α–endosulfan (a) at pH=6.5 (without changing work solution pH) and (b) in 0.1 M NaOH phase, (c) in 0.1 M KOH phase and (d) in 0.1 M $NH_4OH$ phase.

# CHAPTER 4

## COMPUTATIONAL SCREENING AND HOMO-LUMO INTERACTION OF ILS FOR ENDOCRINE DISRUPTING CHEMICALS

The first step for extraction of EDC involving ILs is the choice of cations and anion. This is a cumbersome process as the combinations are infinite. Further the physical state of the Ionic Liquid with respect to the density, viscosity and melting point also needs to be considered. For the very reason we have selected the potential ILs from the well known worldwide supplier Sigma Aldrich. Looking at the Material Safety Data Sheet (MSDS) we have selected the ILs which are liquid at room temperature. A combination of 35 cations and 29 anions, which resulted in 1015 possible ILs, was used to determine the best extractant for the removal of the selected EDCs from aqueous solution. Once the ILs or the potential cation and anion is selected, we have proceeded with the computational screening using the conventional COSMO–RS model where the model Eq.s and the expression for Infinite Dilution Activity Coefficient (IDAC) are explained in chapter 2.

The descriptors namely selectivity (Eq.2.10), capacity (Eq. 2.12) and performance index (Eq. 2.13) at infinite dilution will be used to the rank the IL's based on their effectiveness. We will apply the screening studies on Pentachlorophenol (PCP), Dichlorodiphenyltrichloroethane (DDT), and Endosulfan (ES). Here we are concerned with the two phases namely one aqueous rich phase containing trace amounts of EDC and the other solvent or IL rich phase. Thus the EDC will get transferred from the aqueous rich phase to solvent rich phase. The chapter reports the judicious screening of 1015 cation and anion combination for the extraction of PCP, DDT, and Endosulfan species from aqueous solutions. The selectivity at infinite dilution is important since EDCs such as PCP, DDT, Endosulfan, PA and BPA are present in trace amounts in water. Section 4.1 discusses the

COSMO-RS screening of PCP and DDT, while section 4.2 illustrates the values of selectivities of endosulfan.

In the concluding section (4.3) of the chapter we will also focus our attention to the other important descriptors namely HOMO and LUMO orbitals of the complexes which include IL-EDC. This was attempted so that we can have a thermodynamic insight into the interaction occurring between EDC and IL. The parameters like global hardness and softness, chemical potential, electronegativity and electrophilicity index, HOMO/LUMO energy, HOMO–LUMO energy gap were predicted for systems such as: [PCP]+[$C_4$DMIM][$PF_6$] and [PA]+[$C_4$DMIM][$PF_6$] and individual species. In addition, the experimental and theoretical $^1$H NMR chemical shifts of [PCP]+[$C_4$DMIM][$PF_6$] and [PA]+[$C_4$DMIM][$PF_6$] were also carried out to benchmark our predictions.

## 4.1. COSMO–RS Based Screening of Pentachlorophenol and Dichlorodiphenyl–trichloroethane from Aqueous Solutions using ILs

The selectivity at infinite dilution is important since PCP and DDT are present in trace amounts in water. COSMO-RS model a–priori predicts the activity coefficient of a solute such as PCP and DDT in IL using the molecular structure as the only tool. A combination of 35 cations and 29 anions, which resulted in 1015 possible ILs, was used to determine the best extractant for the removal of these selected EDCs from aqueous solution. Sections (4.1.1 to 4.1.10) describe the COSMO–RS screening of PCP and DDT species in aqueous solutions using ILs.

*4.1.1. Experimental Validation*

Before proceeding for prediction of selectivity values, we have benchmarked the COSMO-RS model with known octanol–water partition coefficients as reported in literature [Mackay, 1982; Veith et al., 1979]. Primary benchmarking studies have been carried out for PCP and DDT by comparing our predictions with the experimental (Table 4.1). Theoretical partition coefficients were calculated by the following Eq.:

$$K_{OW,i} = \frac{C_i^{OR}}{C_i^{WR}} = \frac{C_{tot}^{OR} x_i^{OR}}{C_{tot}^{WR} x_i^{WR}} = \frac{C_{tot}^{OR} \gamma_{i,WR}^{\infty}}{C_{tot}^{WR} \gamma_{i,OR}^{\infty}} = 0.148 \frac{\gamma_{i,WR}^{\infty}}{\gamma_{i,OR}^{\infty}} \quad (4.1)$$

Results from the Table 4.1 shows that the $\log(K_{ow})_{pred}$ and $\log(K_{ow})_{exp}$ values of PCP very close to each other and were 4.48 and 5.01 respectively. In case of DDT similar trend was observed but $\log(K_{ow})_{pred}$ value was little higher than $\log(K_{ow})_{exp}$ i.e. 10.85 and 6.91 respectively (Table 4.1) [Shiu et al., 1994; Wightman and Fein, 1999; Park and Bielefeldt, 2003; Gunther, 1945].

Benchmarking studies have also been carried out for 13 other Polychlorinated Biphenyls (PCBs) by comparing our predictions with the experimental octanol–water partition coefficients as reported by Darryl and Des [Darryl and Des, 1988]. The PCB's were chosen since it represents a similar structure as that of DDT and PCP. Thus it served as another evidential basis for our comparison. Table 4.2 describes the infinite dilution activity coefficient of different PCBs in water rich phase and activity coefficient of different Polychlorinated PCBs in octanol rich phase respectively. It also describes theoretical and experimental logarithms of octanol–water partition coefficient of different PCBs.

The predictions agree well but a higher trend was observed with the experimental findings for PCBs. Similar higher values of deviation was observed from the work of Gerber and Rafael de [Gerber and Rafael de, 2010]. In their work they obtained a ln AAD (logarithmic Absolute Average Deviation) of 81% using optimized COSMO–RS parameters for 748 aqueous system data points. In another work by Putnam *et al.,* [Putnam and Taylor, 2003] a 44% AAD (Absolute Average Deviation) was reported for 106 aqueous system consisting of water with alcohol, aldehyde, alkane and aromatics respectively. Nevertheless, the benchmarking study clearly shows that similar trend was observed when compared predicted partition coefficient log $(K_{ow})_{pred}$ with experimental partition coefficient log $(K_{ow})_{exp}$.

After successful benchmarking, five different groups namely imidazolium, pyridinium, pyrrolidinium, ammonium and phosphonium based cations were combined with 29 different anions and were then investigated using COSMO–RS based model for screening. It should be noted that the selectivity and capacity are functions of infinite dilution activity coefficients (IDAC).

### *4.1.2. Imidazolium based cations*

Fig. 4.1.1 shows the selectivity values of all imidazolium cations for PCP and DDT. During the screening process, $[C_8MIM][Sal]$, $[C_4DMIM][C_8H_{17}SO_4]$, $[C_4DMIM][BTA]$ gave the highest selectivity of 530.5, 512.8 and 355.1 respectively for the removal of PCP (Fig. 4.1.1 (a)). Favorable anions are $[PF_6]$, [BTA], [BOB] and $[B(CN)_4]$ for all cations except for the cation $[C_1DMIM)$ (where its IDAC value was < 1) due to their higher activity coefficient

(between 4 to 36) of water component at infinite dilution for PCP and DDT. In case of DDT (Fig. 4.1.1 (b)), selectivity pattern follows: [$C_4$DMIM][$PF_6$] (6.7) and [$C_4$DMIM] [BTA**]** (6.407). Among all the cations [$C_8$MIM] gave high selective value (530.5) because of its higher carbon chain length. It can be seen that irrespective of pollutant, the selectivity increases with an increase in the carbon chain length on imidazolium cation. This was due to the increasing van der Waals volumes which lead to increasing entrapment of the pollutant in the cation structure. However the selectivity of DDT is low as compared to PCP.

It was observed that the higher activity coefficient of water component at infinite dilution for anion [$PF_6$] with [$C_4$DMIM] and [$C_2$DMIM] as 181.7 and 145.9 respectively. Anions [OAc], [Cl], [DEC] and [$ClO_4$] were not suitable for imidazolium based cation for PCP extraction. Similarly ILs [$C_2$DMIM][DEP], [$C_4$DMIM][DEP], [$C_6$MIM] [DBP], [$C_8$MIM][DBP], [$C_2$DMIM][DBP], [$C_4$DMIM][DBP], [$C_2$DMIM][DMPO4] and [$C_2$DMIM] [Br] also not suitable because of their IDAC values with PCP were found to be zero. In case of DDT extraction, anion [$ClO_4$] was not suited as its IDAC values was zero.

*4.1.3.Pyridinium based cations*

Figure 4.1.2 shows the selectivity values for the pyridinium based cation with PCP and DDT. For pyridinium based cations, [$C_8$MPY][MAcA] (731) (Figure 4.1.2 (a)), gave higher selectivity and the second highest selectivity values obtained in this group of IL were [$C_8$MPY][Sal] (584), [$C_8$MPY][$C_8H_{17}SO_4$] (582.7), [$C_4$MPY][Sal] (584) and [$C_6$MPY] [Sal] (533) for the removal of PCP. Anions [OAc], [Cl], [DEC], [DBP] and [$ClO_4$] were not

suitable for pyridinium based cation for PCP removal. Similarly except cation [$C_8$MPY], anion [DEP] was also not suitable for the extraction of PCP. In case of DDT

(Figure 4.1.2 (b)), selectivity of [$C_8$MPY][$PF_6$] was 9.0 followed by [$C_8$MPY][BTA] where the selectivity value was 5.454. Other ILs with moderate selectivities in this case were [$C_6$MPY][PF6] and [$C_6$MPY][BTA] respectively and its selectivity values were 3.4 and 3.4. The cation [$C_8$MPY] has higher selectivity (731) because of its higher carbon chain length. As compared to imidazolium cations, the pyridinium cations have higher selectivity for PCP. However the increasing trend with size of cation was also observed for pyridinium cations.

*4.1.4.Pyrrolidinium based cations*

In the pyrrolidinium based ILs: [DPPYR][$C_8H_{17}SO_4$] and [BEPYR][$C_8H_{17}SO_4$] gave highest selectivity of 984.6 and 980.3 respectively for PCP as shown in Figure 4.1.3 (a). The selectivity values of DDT were very poor when compared with PCP. Among them the highest were: [BEPYR][BTA] (5.4) and [DPPYR][BTA] (4.9) as shown in Figure 4.1.3 (b). Out of imidazolium, pyridinium and pyrrolidinium cations, the pyrrolidinium based cations gave the highest selectivity. Anions [Cl], [DEC] and [$ClO_4$] were not suitable for pyrrolidinium based cation for the extraction of PCP. Similarly cations [DPPYR] and [BEPYR] combined with anions [DMPO4], [MAcA], [Sal], [DEP], [DBP], [Br] and [DHPO4] were also undesirable for PCP extraction. Except cation [DMPYR], anion [OAc] was undesirable in this group. However as observed earlier, DDT gave poor selectivity for most cations. Except cation [DMPYR], all pyridinium based cations gave higher IDAC

values for water component and the favourable anions were [$PF_6$], [BTA], [BOB] and [$B(CN)_4$].

*4.1.5.Ammonium based cations*

Figure 4.1.4 shows the selectivity values of different combinations of anions and cations of ammonium group. In case of ammonium based ILs the highest selectivity values of PCP (Figure 4.1.4 (a)) were observed as [$C_8$CHIN][MAcA] (856) and [$C_8$CHIN][CF3COO] (823). Similarly other than cation [$C_8$CHIN], selectivity order followed: [BTNH][Sal] (342), [BTNH][$B(CN)_4$] (20.5) and [BTNH][Sal] (17.6). In case of DDT (Figure 4.1.4 (b)), [$C_8$CHIN][BTA] (4.0) gave highest selectivity followed by [$C_8$CHIN][$B(CN)_4$] (2.6) and [BTNH][BTA] (0.2) and [BTNH][$B(CN)_4$] (0.12). It can be seen that the selectivity values for DDT are less than unity in most of the cases, which is undesirable. Thus ammonium based cations having selectivity of < 1 are not recommended for extraction of DDT from aqueous phase. Among imidazolium, pyridinium, pyrrolidinium and ammonium based cations, pyrrolidinium based cations gave the high selectivity followed by the ammonium based cations for extraction of PCP and for DDT, pyridinium based cations gave the high selectivity followed by the pyrrolidinium based cations.

*4.1.6.Phosphonium based cations*

Figure 4.1.5 shows the selectivity values of different combinations of anions and cations of phosphonium based group. In this case [TBP][$PF_6$], gave the highest selectivity among the all ILs for the removal of PCP and having selectivity of 243239 which is a very high value when compared to imidazolium, pyridinium, pyrrolidinium and ammonium based

ILs and is shown in Figure 4.1.5 (a). Second high selective IL in this same group was found to be [TBP][BOB] and its selectivity was (69252). Similarly, the favourable anions for this case were [$B(CN)_4$], [$C_8H_{17}SO_4$], [$MDEGSO_4$], [N(CN)2], [TOS] and [$NO_3$]. In case of DDT (Figure 4.1.5 (b)), order of high selective ILs were [TBP][$PF_6$] (26.1), [TBP][BTA] (24.8), [TBP][$B(CN)_4$] (13.8) and [ODEMP][BTA] (11.1) for the extraction of PCP. It was observed that the higher activity coefficient of water component at infinite dilution for anion [$PF_6$] with [TBP] and [ODEMP] are 48.6 and 31.1 respectively. Among of imidazolium, pyridinium, pyrrolidinium, ammonium and phosphonium based cations, phosphonium based cations gave the highest selectivity for both PCP and DDT extraction. From the section 4.1.2–4.1.6, the highest selective pattern of different cations groups for the removal of PCP followed the order: phosphonium > pyrrolidinium > ammonium > Pyridinium > imidazolium.

Fan *et al.*, [Fan al., 2008] and Blanchard *et al.*, [Blanchard et al., 1999] described the hydrophobic nature ILs which are. Th suitable for liquid–liquid extraction of organic chemicals from their aqueous solutione hydrophobic nature of any component depends on the activity coefficient of the extractant. Even though selectivity values were very high their corresponding activity coefficients at infinite dilution (IDAC) were very less and most of the cases they were less than one indicating high miscibility with water. This may cause the solubility of the ionic liquid to increase in aqueous phase. Table 4.3 summarizes the results obtained in sections 4.1.2 to 4.1.6.

The ILs having higher selectivity values were chosen and the corresponding $\gamma_i^{\infty}$ of IL in water is also indicated. This helps as a guide in the selection of the proper IL i.e. higher values of selectivity as well as high values of $\gamma_i^{\infty}$ water as the requirements.

*4.1.7. Capacity at Infinite Dilution*

The capacities of ILs at infinite dilution were predicted using COSMO–RS model for the extraction of EDCs from the Eq. 2.12. Five group of cations, imidazolium, pyridinium, pyrrolidinium, ammonium and phosphonium based were predicted using COSMO–RS model. Fig. 4.1.6 shows the imidazolium based cations with 29 anion combinations for the PCP species which gave high capacity. The maximum extraction capacity was as high as 10000 for PCP. Similar values were observed for phosphonium and pyrrolidinium based cations. Cations, from phosphonium group [TBP], [TBMP], [OTMP], [TIBMP], [OTMP] and [DEDMPP], from pyrrolidinium group [DPPYR], [OMPYR] and [HMPYR] and from imidazolium [$C_4$DMIM], [$C_2$DMIM], [$C_1$DMIM] and [$C_4$DMIM] gave high capacity of 10000. These cations possess more capacity for the extraction of six membered compounds like PCP and DDT. Fig. 4.1.7 shows the capacity of phosphonium based ILs at infinite dilution for DDT which was very poor when compared to PCP. In case of DDT, the maximum extraction capacity was 7.4 for [TBP] with anion [Cl] (Fig. 4.1.7). On the contrary the lowest value was encountered for pyridinium based cations on account of DDT.

*4.1.8.Performance index at infinite dilution*

Fig. 4.1.8 and Fig. 4.1.9 shows the performance index of the PCP and DDT and was predicted using COSMO–RS model for all the five group of cations. By using Eq. 2.13 we can calculate the performance index at infinite dilution. It can be seen that PI values of cations having higher carbon chain length gave the high performance index values for PCP (Fig. 4.1.8 (a)) and the corresponding order followed: [TBP][$PF_6$] (1216195000**)** > [$C_8$CHIN] (8560000) > [$C_8$MPY] (7310000) > [DPPYR] (4680000) > [C4DMIM] (3530000). Similarly, for Fig. 4.1.8 (b), very higher values PI were observed by ammonium based ILs. As observed in case of capacity, the performance index also followed the similar trend. Where as in case of DDT (Fig. 4.1.9), very smaller (< 2 ) values of PI was observed (Fig. 4.1.9 (a)) for pyridinium based ILs. In case of Fig. 4.1.9 (b), it was observed that performance index values obtained with anion [BTA] i.e.: [TBP] (23.08865) > [BEPYR] (1.8) > [$C_8$CHIN] (1.4) > [$C_8$MPY] (1.35744472) > [$C_4$DMIM] (1.2). It can be seen that the [TBP], [$C_8$CHIN], [BEPYR], [$C_4$DMIM] and [$C_8$MPY] have higher PI values for long carbon chain structure of EDCs. This result leads to the fact that the structural characteristics of ILs play a vital role in the extraction of both PCP and DDT. It can be seen that [TBP] cation is the most effective cation for the removal PCP and DDT. It provides an awesome indicator in the judicious choice of cations and anions.

*4.1.9. Sigma Profile*

In the COSMO system, sigma profile is the only descriptor which describes the local polarity of molecular surface and determines the interaction energies between the IL and

extractant. For the choice of the ILs based on their selectivity values it is necessary to study the effect of hydrogen bonding on the extraction process. Among the imidazolium group ILs: $[C_8MIM][PF_6]$ and $[C_4DMIM][PF_6]$ were chosen for sigma profile calculations**.** Fig. 4.1.10 shows the sigma profiles of the ILs along with the sigma profile of DDT and PCP with water respectively. From Fig. 4.1.10 (a) it was found that the sigma profile for $[C_4DMIM]$

$[PF_6]$ and [C8MPY][PF6] were complimentary with the sigma profile of DDT. It should be noted that complementary sigma profile indicates higher solubility with each other. Thus DDT is highly soluble in both the ILs. The same phenomena is observed in Fig. 4.1.10(b) with profiles of $[C_8MIM][PF_6]$ and $[C_4DMIM][PF_6]$ with PCP. This again confirmed that the ILs soluble in PCP. Both the compounds viz. effluent and IL have a higher fraction of donor as well as acceptor segments, thus the hydrogen bond is strong between compounds. CH–π interaction will mainly occur within segments, that are lying in between the region, i.e., $\sigma_{hb}$ (-0.0082 e/Å$^2$) > σ > + $\sigma_{hb}$ (0.0082 e/ Å$^2$). These regions will be non– polar in nature and thus,

contribute mainly to CH–π interaction. In the sigma profiles of both DDT and ionic liquid, it is clear that both donor and acceptor segments are very small; thus, hydrogen bonding is less in comparison to PCP. The sigma profiles of PCP and DDT has a small fraction of hydrogen bond donor segments, which is a bit greater than hydrogen bond acceptor segments.

## 4.2. COSMO–RS Based Screening of Endosulfan from Aqueous Solutions using Ionic Liquids

For endosulfan, benchmarking was done by comparing the known octanol–water partition coefficients as reported in literature (Soasa *et al.*, 1992). The validation of COSMO–RS model with experimental data has been done by using Eq. 4.1 for octanol–water partitioning coefficient.

Primary benchmarking studies have been carried out for α–Endosulfan, β–Endosulfan, Endosulfan sulfate and Endosulfan–alcohol, Endosulfan lactone and Endosulfan ether by comparing our predictions with the experimental values (Table 4.4). Fig. 4.2.1 represents the list of Endosulfan metabolites studied in this work. From the Table 4.4 it was observed that $\log(K_{ow})_{exp}$ values for α–Endosulfan and β–Endosulfan are close to each other (4.74 and 4.79 respectively) with their corresponding $\log(K_{ow})_{pred}$ values to be 5.18 and 5.48 respectively. In case of other metabolites of Endosulfan, a similar trend was observed but $\log(K_{ow})_{pred}$ value was little higher than $\log(K_{ow})_{exp}$ (Table 4.4). Gerber and Rafael de [Gerber and Rafael de, 2010] observed a similar kind of higher values of deviation. According to their work, they obtained a logarithmic AAD (A COSMO–RS parameters for 748 aqueous system data points. In addition to this, Putnam *et al.*, [Putnam *et al.*, 2003] obtained 44% AAD for 106 aqueous systems containing of water with alcohol, aldehyde, alkane and aromatic compounds respectively. However, our validation study clearly shows the good agreement with experimental partition coefficient ($\log (K_{ow})_{pred}$ ). It should be noted that the data set for $K_{ow}$ is very small. So the COSMO–RS prediction in this work does not provide

statistical analysis. Also the $K_{ow}$ values are functions of activity coefficient which can also be obtained via NRTL or UNIQUAC models [Jaime–Leal and Bonilla–Petriciolet, 2008]. But both these methods regress experimental data to absolute Average Deviation) of 81% using optimized determine interaction parameters. Similarly functional groups are not available for UNIFAC, so the activity coefficients in COSMO–RS are predicted via screening charge densities which in turn are obtained via quantum chemical calculations (which are in vacuum). Thus uncertainty values do not have any significance in quantum chemical predictions.

Present study describes five different groups of ILs i.e. imidazolium, pyridinium, pyrrolidinium, ammonium and phosphonium based cations (total of 34) combined with 29 different anions (total of 986). No comparison with industrial solvents was possible due to lack of experimental data in literature.

*4.2.1. Selectivity of imidazolium based ILs*

Imidazolium group cations are the five membered ring structures with two nitrogen atoms on two sides. Fig. 4.2.2(a) shows the selectivity values of all imidazolium ILs for Endosulfan. Ionic liquid [$C_2$DMIM][Br] gave a high selectivity of 101 and was highest within the imidazolium cations. Second highest selectivity was recorded with [$C_4$DMIM][MDEGSO$_4$] (43.009) followed by [$C_4$DMIM[DBP] (42.5) for the removal of Endosulfan from aqueous phase. Within the imidazolium cation, IDAC of Endosulfan rich phase for anion [$PF_6$] were very less (< 1) for all cations except for [$C_4$DMIM] (7.0). Similarly ILs [$C_4$DMIM][OAc], [$C_2$DMIM][OAc], [$C_4$DMIM][Cl], [$C_2$DMIM][Cl],

[$C_1$DMIM][Cl], [$C_2$DMIM][DEC] and [$C_4$DMIM][DEC] were having low selectivity and thus are not potential candidates for Endosulfan removal. From the results it was observed that anion $[ClO_4]^-$ gave undesirable values with all cations. From Fig. 4.2.2(a) it is evident that imidazolium based ILs with low selectivity are the ones containing anions such as $[Cl]^-$, $[OAc]^-$, and $[DEC]^-$. However in a recent work [Pinter *et al.*, 201] it is concluded that the selectivities are attributed to two phenomena: namely steric strain and sterical hindrance. In that study a quantitative analysis of the steric effect of open chain carbon (aliphatic) groups was expressed out from first principles. Such a work has not been performed in this text, hence one cannot conclude in principle whether the selectivities vary with sterical hindrance. The selectivity of the IL was observed to reduce with increase of the number of alkyl side group within the ring (Fig. 4.2.2(a)). This increases the amount of free volume within the IL molecule, which leads to the entrapment of water molecules thereby lowering selectivity. However it should be noted that the free volume concept is independent of COSMO–RS predictions as the model only incorporates screening charge densities via quantum chemical calculations.

### *4.2.2. Selectivity of pyridinium based ILs*

The selectivity values of all pyridinium based ILs for Endosulfan extraction are shown in Fig. 4.2.2(b) at $T$=298.15 K. During the screening process, [$C_8$MPY][$C_8H_{17}SO_4$] (31.6) gave the highest selectivity value followed by [$C_8$MPY][MDEGS$O_4$] (31.3) for the extraction of Endosulfan. Overall the values are smaller as compared to imidazolium cations as seen above. It was observed that irrespective of the nature of pollutant, the selectivity

increased with an increase in the carbon chain length on pyridinium cation. As observed in case of imidazolium based ILs, anion $[ClO_4]^-$ was undesirable and not suitable for the extraction of Endosulfan.

*4.2.3. Selectivity of pyrrolidinium based ILs*

Fig. 4.2.2(c) shows the selectivity values of the pyrrolidinium group ILs for Endosulfan. For the same cation, selectivity of pyrrolidinium based ILs reduced when the anion size increased (Fig. 4.2.2(c)), whereas limiting capacity followed the opposite trend.

For the same anion, the longer the alkylchain of the ionic liquid cation, the smaller the selectivity and higher the capacity was observed. From the screening results it was observed that cations [DPPYR] and [BEPYR] gave higher selectivity values with most of the anions except anion $[ClO_4]^-$, $[Cl]^-$, $[OAc]^-$ and [DEC]. Higher selectivity values of 107 and 106 were obtained by [DPPYR][Br] and [BEPYR][Br] respectively. This was followed by [BEPYR][$MDEGSO_4$] (99.0) and [DPPYR][$MDEGSO_4$] (96.8). From the Fig. 4.2.2(C) it was observed that cations other than [DPPYR] and [BEPYR], gave very low selectivity values (< 11) for all the anion and cation combinations. Smaller anions lead to higher selectivities.

*4.2.4. Selectivity of ammonium and phosphonium based ILs*

Within ammonium group (Fig. 4.2.2(d), the selectivity values followed higher order: [BTNH][Br] (27.2), [BTNH][$C_8H_{17}SO_4$] and [BETNH][Br] (23.4). ILs [BTNH][OAc], [BTNH][DEC], [BTNH][Cl], [BETNH][Cl] and [HETNH][Cl] were found to be not suitable

for the extraction of Endosulfan. Similarly anion $[ClO_4]^-$ was also found undesirable. Among all the above groups viz. imidazolium, pyridinium, pyrrolidinium and ammonium based cations, lowest selectivity was obtained by ammonium based cations.

Within the phosphonium based ILs, [TBP][TOS] gave the highest selectivity of 212.5 as shown in Fig. 4.2.2(e). [TBP][$MDEGSO_4$] (209.5) and [TBP][$C_8H_{17}SO_4$] (202.3) gave second and third highest selectivity and are found to be the best solvents for this separation problem among all the ILs screened in this work. From Fig. 4.2.2(e) it can be seen that the cation [TBP] possessed higher selectivity values with most of the anions. Anions [OAc], [Cl], [DEC] and [$ClO_4$] were not suitable for the extraction of Endosulfan from aqueous phase. Similarly ILs [TIBMP][DEP], [TIBMP][$DMPO_4$], [TBP][$DMPO_4$] [TBP][DEP], [TBP][DBP] and [TBP][$DMPO_4$] were also found to be undesirable. Cations [HTMP] and [OTMP] gave low selectivity values with most of the anions within this group.

The overall selectivity among all the above groups ILs: imidazolium, pyridinium, pyrrolidinium, phosphonium and ammonium based ILs preferably depends on the IDAC value, which was related to the solubility data. Since the aqueous phase IDAC value is also a very important parameter, the aqueous phase IDAC value < 1 are soluble in water, so by keeping in mind for real life application we need to choose the aqueous phase IDAC value of IL > 1. The entry of water molecule can be restricted by chosen anions such that mostly they are hydrophobic in nature. It should be noted that the water solubility is governed by the anions only. Alternatively, all ILs from the Table 4.2.2 which are having IDAC value of water > 1 such as [TBP][$CF_3SO_3$] (108.4), [TIBMP][$CF_3SO_3$] (60.7), [TBP][BTA] (59.5)

from phosphonium group, [BEPYR] [$CF_3SO_3$] (30.43), [BEPYR][BTA] (25.8), [DPPYR][BTA] (23.74), [BEPYR][$B(CN)_4$] (20.0), [DPPYR][$B(CN)_4$] (18.5) from pyrrolidinium group, [$C_8$MPY][BTA] (21.4), [$C_6$MPY][BTA] (15.8), [$C_8$MPY][$B(CN)_4$] (13.9), [$C_8$MPY][$PF_6$] (7.9) from pyridinium group, [$C_4$DMIM][BTA] (32.8), [$C_2$DMIM][BTA] (19.1), [$C_4$DMIM][$B(CN)_4$] (14.8), [$C_4$DMIM][BOB] (8.9), [$C_4$DMIM][$PF_6$] (7.0) from imidazolium group, [BTNH][BTA] (1.5) and [BETNH][BTA] (1.18) from ammonium group are applicable for the for real life application for the extraction of endosulfan from water. The ILs having IDAC values of water lesser than unity are may not be useful for the experimentation.

The hydrophobic ILs are generally suitable for the liquid–liquid extraction, membrane separation process of organic effluents from aqueous phase [Fan et al., 2008] and for the separation of industrial gases [Blanchard et al., 1999; Luisa et al., 2009; Shiflett and Yokozeki, 2010; Anantharaj and Banerjee, 2010]. The hydrophobic nature of any component depends on the activity coefficient of the extracting compound (Endosulfan). Lower activity coefficients of water at infinite dilution (IDAC) combined with high selectivity values indicates a high miscibility of IL with water. This may cause the solubility of the ionic liquid to increase in aqueous phase. Thus a guide in the selection of the proper IL i.e. higher values of selectivity as well as high values of IDAC in water is required. Table 4.5 describes the best selective ILs and their corresponding aqueous phase activity coefficients at infinite dilution.

### *4.2.5. Capacity at infinite dilution*

It can be seen that a longer alkyl chain length of the cation contributes to an increase in the extraction capacity (Fig. 4.2.3(a–e)) for the ionic liquid. A similar phenomenon was observed by Putnam *et al.,* [Putnam *et al.,* 2003] for IL mixtures. The capacities of ILs at infinite dilution were predicted using COSMO–RS model for the extraction of Endosulfan using Eq. (2.12). Fig. 4.2.4(a–e) shows capacity values of the imidazolium, pyridinium, pyrrolidinium, ammonium and phosphonium based cations with 29 anion combinations. The maximum extraction capacity was observed as high as 10000 for various ionic liquid combinations. Among the imidazolium based ILs, [$C_1$DMIM][Cl], [$C_2$DMIM][Br] and [$C_2$MIM][Cl] gave high capacity of 10000 as observed from Fig. 4.2.3(a). Except [$C_2$MIM][Cl], all other ILs gave high capacity as from imidazolium based ILs. From Fig. 4.2.3 (b) high capacity values for the pyridinium based ILs were: [$C_2$MPY][DEC], [$C_4$MPY][DEC], [$C_6$MPY][DEC], [$C_8$MPY] [DEC], [$C_4$MPY][Cl], [$C_6$MPY][Cl] and [$C_8$MPY][Cl]. It is interesting to note that the order of selectivity among cations is exactly the opposite of the one observed with capacity. However, cation [$C_8$MPY] was commonly observed the best cation for both selectivity and capacity. In case of pyrrolidinium based cation, [DEPYR] and [DPPYR] combined with anions [$DMPO_4$], [DEP], [DBP] and [Br] gave high capacity values of 10000 as seen from Fig. 4.2.3 (c). [DEPYR][Br] is another IL from the pyrrolidinium group which possessed high selectivity and capacity. For the ammonium based group high capacity values were obtained for [BETNH][OAc] and [BETNH][DEC] with its value as high as 10000 (Fig. 4.2.3(d)). Thus longer alkyl chain of the ionic liquid leads to lower selectivities and higher capacities. In case of phosphonium

based ILs (Fig. 4.2.3(e)) most combinations gave high capacity values but lower selectivities as evident from Fig. 4.2.3(e). Cations, [HDEMP], [ODEMP], [DEDMPP], [TBMP] with anions [$DMPO_4$], [DEP], [DBP] and [Br] gave high capacity of 10000. Similarly cation [TBP] with anions [Sal], [Br] and [$DHPO_4$] gave high capacity value of 10000 within the same group. Cation [TIBMP] also gave higher capacity values of 10000 with anions [DBP] and [Br].

### *4.2.6. Performance index at infinite dilution*

In order to compare all the ILs studied we have compared the values of performance index (PI) for the different combinations. Eq. (2.13) was used to calculate the PI. Fig. 4.2.4 (a–e) shows the predicted values of PI of Endosulfan for five different groups of cations: imidazolium, pyridinium, pyrrolidinium, ammonium and phosphonium. It was observed that the [TBP], [DPPYR], [BEPYR], [$C_4$DMIM] and [$C_8$MPY] have higher PI values for the extraction of Endosulfan. In terms of good compromise between selectivity and capacity, ILs are arranged in decreasing order of limiting performance index values which are as follows: [TBP][Sal] (1.71+E5) > [DPPYR][Br] (1.07+E6) > [$C_2$DMIM] (1.01+E6) > [$C_8$MPY][Cl] (1.6+E5) > [BETNH][DEC] (1.2+E5). The best selectivity and the performance index were obtained with the cation [TBP]. It can be seen that (Fig. 4.2.4(a)) for imidazolium based ILs, [$C_2$DMIM][Br] (1.01+E6) gave highest PI followed by [$C_4$DMIM][DBP] (2.125+E5). For pyridinium based ILs,

PI followed the order (Fig. 4.2.4(b)): [$C_8$MPY][Cl] (1.6+E5) > [$C_6$MPY][Cl] (1.4+E5). Similarly for pyrrolidinium group (Fig. 4.2.4(c)), [DPPYR][Br] (1.07+E6) and

[BEPYR][Br] (1.06+E6) gave the best and second best PI respectively. In case of ammonium group ILs, [BETNH][DEC] (1.2+E5) and [BETNH][OAc] (8+E4) gave higher PI values (Fig. 4.2.4(d)). Lastly for the phosphonium based ILs the PI trend followed: [TBP][Sal] (1.71+E6) > [TIBMP][Br] (1.32+E6) > [TBP][Br] (1.32+E6) > [ODEMP][Br] (1.28+E5) (Fig. 4.2.4(e)). Among the all ILs studied in this work [TBP][Sal] (1.71+E6) and [DPPYR][Br] (1.07+E6) stands out with the best performance index. This shows that a larger cation combination with a small bromide anion gives the highest value of PI.

## 4.3. HOMO–LUMO Energy Interactions between PCP\PA and ILs

Initially geometry optimization was carried using DFT based B3LYP/6-31G*method for individual molecules of [PCP], [PA], cations, anions and [PCP]\[PA]+ILs complexes. Fig. 4.3.1 represents the structures of cations and anions were studied in this work. Thus, after discussions of various quantum chemical descriptors in chapter 2, the effect of these quantities on individual molecules as well as on complex systems is reported in this section.

### *4.3.1. HOMO–LUMO band gap*

This represents the electronic absorption from ground state to transition state of a molecule or complex [Kavitha et al., 2010; Prasad et al., 2010]. Fig. 4.3.2(a) represents the HOMO and LUMO energies projected on the van der Waals surface for [PCP] and [PA] using

B3LYP/6-31G* method. Similarly Fig. 4.3.2(b) shows the HOMO–LUMO energies projected on the van der Waals surface for [PCP] and [PA] using PM3/6-31G* method. In

both the figures green and dark red isosurfaces of HOMO and LUMO indicates positive and negative values, respectively. The optimized geometries of [PCP], [PA], cations and anions are also shown in Fig. 4.3.2(a,b). The molecular orbital energy diagram projected on the van der Waals surface for HOMO and LUMO of [PCP]+[$C_4$DMIM][$PF_6$] and [PA]+[$C_4$DMIM][$PF_6$] complex molecule using B3LYP/6-31G* method are also shown in Fig. 4.3.3(a,b) respectively. For [PCP]+[$C_4$DMIM][$PF_6$] the HOMO–LUMO band gap ($\Delta(E_{LUMO}$-$E_{HOMO}$)) is 0.1465 eV as shown in Fig. 4.3.3(a), Table 4.6 and Fig 4.3.4(a). In case of [PA]+[$C_4$DMIM][$PF_6$] complex molecule, the $\Delta(E_{LUMO}$-$E_{HOMO}$) value was 0.0597 eV, which is lower than [PCP]+[$C_4$DMIM][$PF_6$] as shown in Fig. 4.3.3(b) and Fig 4.3.4(a). Thus implies that [PA]+ [$C_4$DMIM][$PF_6$] is easier to polarize and hence higher separation can be achieved. Fig. 4.3.4(b) represents the energy level bar diagram of HOMO and LUMO energies and HOMO–LUMO energy gaps of individual molecules used in this study. From Fig. 4.3.4(b) it was observed that the anion [$PF_6$] gave highest HOMO–LUMO band gap of 0.4376 eV among all individual molecules studied indicating its higher resistance to polarization. The HOMO-LUMO gap for all the binary systems decreases in the following order: [PCP]+[$C_4$DMIM][$PF_6$]> [PCP]+[$C_4$DMIM][BTA]> [PA]+[$C_4$DMIM] [BTA]> [PA]+[$C_4$DMIM][$PF_6$]. This implies that [PA]+[$C_4$DMIM][$PF_6$] is the easiest to polarize, while [PCP]+[$C_4$DMIM][$PF_6$] provides the maximum resistance for polarization.

The predictions were tested with the semi empirical formalism PM3 theory. Table 4.7 shows the correlation of calculated $E_{LUMO}$ of several cations and anions by B3LYP and PM3 calculations. The observed correlation coefficient obtained was 0.859. From this, it can be

concluded that both B3LYP and PM3 methods are favorable theories for HOMO–LUMO studies of selected cations and anions used in this study.

The values of zero-point vibrational energy, rotational constants, self–consistent fields (SCF) energy and dipole moment of four different systems [PA]+[$C_4$DMIM]+[$PF_6$], [PCP]+[$C_4$DMIM]+[$PF_6$], [PA]+[$C_4$DMIM]+[BTA] and [PCP]+ [$C_4$DMIM]+[BTA] by B3LYP with 6-31G* method at 298.15 K in ground state were calculated and presented in Table 4.8. The maximum dipole moment has been found to be 16.996 Debye for [PCP]+[$C_4$DMIM]+[$PF_6$] system, which is measure of polarity of a chemical bond. The dipole moment for all the binary systems decreases in the following order: [PCP]+[$C_4$DMIM][$PF_6$]> [PCP]+[$C_4$DMIM][BTA]> [PA]+[$C_4$DMIM][BTA]> [PA] +[$C_4$DMIM][$PF_6$]. This order is exactly the same as obtained from HOMO-LUMO energy gap. Thus both the descriptors point out to the fact that [$PF_6$] containing IL along with [PCP] is the most polarized and it will resist any additional deformation. Similarly, by B3LYP/6-31G* level theory on the basis of vibrational analysis, the standard statistical thermodynamic functions such as heat capacity ($C_v$), entropy ($S$) and enthalpy ($H$) for the studied compound were obtained from the theoretical harmonic frequencies and given in Table 4.8.

### *4.3.2. Global hardness and global softness*

The hardness is a measure of a molecule's ability to be polarised, as softness is indicative of its ability to accept electron. Global hardness and softness of [PA] and [PCP] with [$C_4$DMIM][$PF_6$] used in this study are given in Fig. 4.3.5(a,b). A higher softness indicates an extended molecular interaction through hydrogen bond network or a higher π

density in aromatic compounds as reported by Anantharaj and Banerjee [Anantharaj and Banerjee, 2010]. The highest and lowest softness was recorded for [PA]+[$C_4$DMIM][$PF_6$] (33.5 Ha and 0.0597 Ha) (Fig. 4.3.5(a)). This perfectly matches with the predictions using HOMO-LUMO energy gap and dipole moment where [PA]+[$C_4$DMIM][$PF_6$] had the highest values. This implies that for this system, there would be an extended molecular interaction through hydrogen bond network [Fumino and Ludwig, 2010].

In case of individual molecules Fig. 4.3.5(b), the highest softness (16.38 Ha) was observed for anion [$C_8H_{17}SO_4$] which was expectedly seen to have the lowest hardness (0.122 Ha). On the contrary, anion [$PF_6$] has the lowest softness (4.5704 Ha) but highest hardness (0.4376 Ha) as reported in Table 4.9. However, it should be noted that the softness of the whole complex molecule is important as it gives an indication of the degree of polarization [Fumino and Ludwig, 2010]. The most favorable ILs for removal of [PA] and [PCP] would be the ones whose complexes show the highest softness value. Based on the global softness values, [$C_4$DMIM][$PF_6$] is considered the most favorable IL for [PA] removal followed by [$C_4$DMIM][BTA]. This is primarily due to the fact that the softness value of the complex is higher than that of individual ion. In case of PCP removal the preferred IL was [$C_4$DMIM][BTA] followed by [$C_4$DMIM][$PF_6$]. This was also confirmed by our previous finding using COSMO-RS based theoretical study for the extraction of PCP from aqueous phase [Pilli et al, 2012].

### *4.3.3. Electronegativity and electrophilicity index*

Fig. 4.3.6(a,b) and Table 4.9 denotes the electrophilicity index vs electronegativity of complex and individual molecules used in this study. It was observed that [PA]+[$C_4$DMIM][$PF_6$] gave high electrophilicity index (1.347) and low electronegativity (-0.283) values followed by [PA]+[$C_4$DMIM][BTA]. This further agrees with the findings as reported in section 3.1 (HOMO-LUMO energy gap and dipole moment) and section 3.2 (softness value), where [PA]+[$C_4$DMIM][$PF_6$] possessed the highest values. In terms of electrophilicity index it implies that it can accept more electrons. The lowest electrophilicity index of 0.3419 was obtained for the [PCP]+[$C_4$DMIM][BTA] complex. It also possessed the highest electronegativity (-0.203) among all four molecules. In case of individual ions, high electrophilicity index was obtained for [$C_2$DMIM] (0.3447) whereas lowest electrophilicity index was given by [BOB] (0.004). In the same way, higher electronegativity was predicted for anions [$PF_6$] (0.0622) and [BTA] (0.0200), followed by cations [TBP] (0.264) and [$C_4$DMIM](0.3447). From Fig. 4.3.6(b), it can be seen that the cations [$C_4$DMIM] and [TBP] have higher electronegativity as compared to the anions i.e. [$PF_6$] and [BTA]. Thus the cations can accept electrons and anions can donate electron although with a lesser intensity as their values are still positive.

### *4.3.4. Interaction energies*

The interaction energy can be expressed as the difference between the energy of [$C_4$DMIM][$PF_6$] or [$C_4$DMIM][BTA] molecule and the addition of the energies of [$C_4$DMIM][$PF_6$] or [$C_4$DMIM][BTA] and isolated molecule [Lü et al., 2013]. The solubility

of organic compounds in ILs are subject to the distance between the cation and anion of the ILs. The interaction energy of [PCP]\[PA]–ionic liquid complex molecules used in this study are shown in Fig. 4.3.7. The Interaction energies were calculated using Eq. (2.8). The highest interaction energy of 5.371 kcal $mol^{-1}$ was observed for [PA]+[$C_4$DMIM][BTA] followed by 4.449 kcal $mol^{-1}$ for [PCP]+[$C_4$DMIM][$PF_6$]. The magnitude of interaction energies are similar to the one obtained earlier [Lü et al., 2012] for the IL: [MMIM][$MeSO_4$] with dibenzothiophene (11.22 kcal/mol), diphenylsulfide (8.91 kcal/mol), diphenyldisulfide (7.63 kcal/mol), tetralin (6.84 kcal/mol), benzene (5.78 kcal/mol). The more positive the values of $\Delta E_{int}$ the stronger the bond is. However, the interaction energy is negative for [PA]+[$C_4$DMIM][$PF_6$] which implies that the bond is weaker and there is probability for adding more molecules of [PA]. Thus, negative values of $\Delta E_{int}$ signify favourable interaction between the molecules in the system [Tsuzuki et al., 2007; Zhou et al, 2008].

### *4.3.5. Charge distribution*

The CHELPG population analysis [Mulliken et al., 1955] is a widely used analysis for estimating partial atomic charges. CHELPG charges were developed from the CHELPG partial charge analysis via *Gaussian 03.* It was employed to characterize the electronic charge distribution in a molecule and the bonding, antibonding, or nonbonding nature of the molecular orbitals for particular pair of atoms. It also estimates the partial atomic charges from calculations through computational chemistry methods. From the Natural Bond Orbital (NBO) analysis [Berzelius et al., 1993], the chemical reactivity can be easily explained and the differences in H–bonding, electrostatic interaction and CH–π interaction are measured.

For positive interaction between [PA] or [PCP] and ILs, solute molecule can form cation–π or H–bond by overcoming the cation–anion interaction. For the formation of effective CH–π interaction, the aromatic π density needs to be increased. Fig. 4.3.8 represents the contours of deformation of electron density of [PA] and [PCP] with [$C_4$DMIM][$PF_6$]. It can seen that the yellow lines in [PA]-[$C_4$DMIM][$PF_6$] is more pronounced than [PCP]-[$C_4$DMIM][$PF_6$], thereby indicating a higher charge difference and more extraction efficiency. Table 4.10(a,b) gives the CHELPG charges using B3LYP/6-31G* method for [PCP]+[$C_4$DMIM][$PF_6$] and [PA]+[$C_4$DMIM][$PF_6$].

Table 4.10(a) describes the partial charge values of N3, N5, C6, C10, C14, C15, C20, C21, F30-35, C36–40, and O44 in [PCP]+[$C_4$DMIM][$PF_6$]. All had negative charges and thus acted as potential electron acceptors. The positively charged atoms were P29 and C4 for [PCP]+[$C_4$DMIM][$PF_6$] complex. For the [PA]+[$C_4$DMIM][$PF_6$] system (Table 4.10(b)) it was also observed that the atomic charge values, N3, N5, C6, C10, C14, C15, C20, C21, F30-35, C36-40, and O44 had negative charges and behaved as potential electron acceptors. It was found that the most positively charged atoms were P29 and C4 which is similar to [PCP]+[$C_4$DMIM][$PF_6$](Table 4.10(a)). It was also noted that there is a prominent accumulation of positive charge on atom P29 and negative charge on O51 for [PA]+[$C_4$DMIM][$PF_6$] complex molecule. Hence, this might had given (P29– O51) bond a greater ionic character for [PA]+[$C_4$DMIM][$PF_6$] followed by for [PCP]+[$C_4$DMIM][$PF_6$] complex (P29– O44). Another experimental evidence pointed out that the selectivity of [$C_4$DMIM][$PF_6$] +[PCP] is higher than [$C_4$DMIM][$PF_6$]+[PA] at ambient conditions [Pilli et al., 2014].

### *4.3.6. Experimental and theoretical NMR spectra*

The isotropic chemical shifts are commonly used as an aid in identification of reactive ionic species. It is known that precise predictions of molecular geometries are vital for consistent calculations of magnetic properties. The isotropic chemical shifts of optimized structures of [PCP]/[PA]+IL complex molecules having minimum energy were calculated and used to predict $^{1}$H NMR chemical shifts using *Gaussian 03* package.

The experimental $^{1}$H NMR analysis was carried in DMSO. Figs. 4.3.9(a) and 4.3.10(a) represents the theoretically calculated and experimental $^{1}$H NMR spectra of [PCP]+[$C_4$DMIM][$PF_6$] respectively. The corresponding peak values of calculated and experimental spectra are presented in Table 4.11. Similarly, Figs. 4.3.9(b) and 10(b) indicates $^{1}$H NMR spectra of theoretically calculated and experimental [PA]+[$C_4$DMIM][$PF_6$] complex. The experimental and theoretical $^{1}$H chemical shifts were calculated by DFT (B3LYP/6-311++G(d,p) method. The correlation graph between the experimental and calculated (B3LYP) chemical shifts of [PCP]+[$C_4$DMIM][$PF_6$] molecule is shown in Fig. 4.3.11(a). The correlation coefficient ($R^2$) obtained was 0.981 which is in good agreement. Fig. 4.3.11(b) presents the correlation graph between experimental and calculated (B3LYP) chemical shifts of [PA]+[$C_4$DMIM][$PF_6$] molecule. Corresponding correlation coefficient $R^2$=0.973 also points a good match with theoretical predictions. The calculated $^{1}$H chemical shifts in DMSO are summarized in Table 6 and compared with experimental data. Similar studies were recently reported by Karabacak *et al.*, [Karabacak et al., 2013].

## 4.4. Conclusions

Results of the present section 4.1 showed that the extraction of endocrine disrupting organic effluents of environmental interest such as PCP and DDT has been screened theoretically. A screening of 35 cations and 29 anions, a total of 1015 possible ILs combinations was investigated via COSMO–RS based model to determine the best extractant for the removal of PCP and DDT from aqueous solution. Five different groups of cations namely imidazolium, pyridinium, pyrrolidinium, ammonium and phosphonium were investigated. All the selectivity calculations were done using infinite dilution activity coefficients as an indicator for the screening potential of ILs. In case of phosphonium based cations [TBP] gave high selectivity with anions [$PF_6$], whereas [BOB] was the highest selective among all cations. Then the pyrrolidinium based ILs [DPPYR][$C_8H_{17}SO_4$] and [BEPYR][$C_8H_{17}SO_4$] gave highest selectivity. In case of ammonium based ILs the highest selectivity values of PCP were observed as [$C_8$CHIN][MAcA] (856) and [$C_8$CHIN][CF3COO] (823) and other than cation [$C_8$CHIN], selectivity order followed: [BTNH][Sal] (342), [BTNH][$B(CN)_4$] (20.5). The selectivity order for the pyridinium based cations followed the order: [DPPYR] > [BEPYR] > [OMPYR] > [BMPYR] and for imidazolium based cations: [$C_8$MIM] > [$C_4$DMIM] > [$C_2$DMIM] > [$C_6$DMIM]. Similar trends were also seen for pyridinium cations. Highest selective pattern of different cations groups for the removal of PCP followed the order: phosphonium > pyrrolidinium > ammonium > Pyridinium > imidazolium. Anions such as [$C_8H_{17}SO_4$], [MAcA], [Sal], [$B(CN)_4$], [$N(CN)_2$], [BTA], [$CF_3SO_3$], [$MDEGSO_4$], [TOS] and [$NO_3$] gave high selectivities because the sterical shielding effect around their charge centres was absent.

Sigma profiles confirmed that the hydrogen bonding effect was weak in comparison to CH–π interaction of the effluent and IL. Benchmarking studies were carried for comparison of experimental data with predicted data for both PCP and DDT where the predictions agree well. Other 13 PCBs were also used for the validation of experimental data with theoretical data. Trends obtained in both the cases were similar to each other. The results of this study are encouraging and suggest that ILs can be a potential substitute for the treatment of organic rich water and wastewater. The accuracy of results obtained by the present method can be useful for further experimental investigations.

Section 4.2. describes the detailed theoretical study of the predicted selectivities via COSMO–RS model for the extraction of Endosulfan from the aqueous solution. Initially benchmarking studies were successfully performed by predicting the octanol–water coefficients with those of the reported Endosulfan. Thereafter different groups of cations such as imidazolium, pyridinium, pyrrolidinium, ammonium and phosphonium were investigated via COSMO–RS model. Total of 984 possible ILs (a combination of 34 cations × 29 anions) were extensively screened to find out the best ILs. All the selectivity calculations were carried out at infinite dilution condition, which was chosen as an indicator for the screening of potential ILs. The selectivity values among the cations decreased in the following manner: [TBP] > [TIBMP] > [TBMP] > [$C_2$DMIM] > [BEPYR] > [DPPYR] > [$C_4$DMIM] > [$C_8$MPY] > [BTNH] > [BETNH]. The best ionic liquid was [TBP][TOS] among all ionic liquid combinations. Anions such as [$C_8H_{17}SO_4$], [Br], [Sal], [TOS], [$MDEGSO_4$] and [DEC] gave high selectivities because the sterical shielding effect around their charge centers was absent. All the ILs from Table 4.5 having IDAC value of water > 1

are applicable for the real life applications commercially to implement the SILM technology for the extraction of endosulfan from aqueous phase. Best performance index values were found to follow: [TBP][Sal] (1.71+E6) > [DPPYR][Br] (1.07+E6) > [$C_2$DMIM] (1.01+E6) > [$C_8$MPY][Cl] (1.6+E5) > [BETNH][DEC] (1.2+E5). The best selectivity and the best PI were obtained with cation [TBP]. High capacity value of the order of ~10000 was obtained for [$C_1$DMIM][Cl], [$C_2$DMIM][Br], [$C_2$MPY][DEC], [$C_4$MPY][DEC], [$C_6$MPY][DEC], [DEPYR][$DMPO_4$], [DEPYR][DBP], [DEPYR][Br], [BETNH][OAc], [BETNH][DEC], [TBP][Sal], [TBP][Br], [TBP][$DHPO_4$], [HDEMP][$DMPO_4$] and [DEDMPP][DBP]. COSMO–RS methodology might be the more suitable theoretical tool for the screening of ILs for removal of EDCs and other industrial pollutants through the liquid–liquid extraction. This process of screening is far less time consuming and less expensive.

Quantum chemical descriptors such as global hardness and softness, chemical potential, electronegativity and electrophilicity index, HOMO/LUMO energy, HOMO–LUMO energy gap were studied in section 4.3 for [PCP]+[$C_4$DMIM][$PF_6$] and [PA]+[$C_4$DMIM][$PF_6$] complex and individual molecules. The highest HOMO–LUMO energy gap was obtained for [PCP]+[$C_4$DMIM][$PF_6$] (0.146 eV) whereas the lowest for [PA]+[$C_4$DMIM][$PF_6$] (0.0597 eV). Based on the global softness values, [$C_4$DMIM][$PF_6$] is considered the most favourable IL for [PA] removal followed by [$C_4$DMIM][BTA]. The cations [$C_4$DMIM] and [TBP] have higher electronegativity as compared to the anions i.e. [$PF_6$] and [BTA]. The decreasing order of HOMO-LUMO energy gap, dipole moment, global softness and electrophilicity index gave an exact matching order of [PCP]+[$C_4$DMIM][$PF_6$]> [PCP]+[$C_4$DMIM][BTA]> [PA]+[$C_4$DMIM][BTA]> [PA]

+[$C_4$DMIM][$PF_6$] which proves that it very difficult to polarize [PCP]+[$C_4$DMIM][$PF_6$]. Theoretical and experimental $^1$H NMR spectra of [PCP]+[$C_4$DMIM][$PF_6$] and [PA]+[$C_4$DMIM][$PF_6$] comparison gave correlation coefficient ~0.95. Using interaction energies, the highest values of 5.371 kcal mol$^{-1}$ was observed for [PA]+[$C_4$DMIM][BTA] followed by 4.449 kcal mol$^{-1}$ for [PCP]+[$C_4$DMIM][$PF_6$].

**References**

Anantharaj, R., T.Banerjee, Evaluation and comparison of global scalar properties for the simultaneous interaction of ILs with thiophene and pyridine, Fluid Phase Equilib. 293 (2010) 22–31.

Banasiak, L, B. Van der Bruggen, A.I. Schäfer, Sorption of pesticide Endosulfan by electrodialysis membranes, *Chem. Eng. J.* (2011) 166, 233–239.

Berzelius, J.J., "Essai sur la théorie des proportions chimiques et sur l' influence chimique del' électricité," 1819; see M. J. Nye, "From Chemical Philosophy to Theoretical Chemistry, University of California Press, Berkeley, CA, 1993, pp. 64.

Blanchard, L.A., Hancu, D., Beckman, E.J., Brennecke, J.F., 1999, Green Processing Using ILs and CO2, *Nature*. 399, 28–29.

Darryl, W.H., W.C. Des, Octanol-water partition coefficients of polychlorinated biphenyl congeners, *Environ. Sci. Technol.* 22 (1988) 382–387.

Fan, J., Fan, Y., Pei, Y., Wu, K., Wang, J., Fan, M., Solvent extraction of selected endocrine disrupting phenols using ILs, *Sep. Purif. Technol.* 61 (2008) 324–331.

Fumino, K., R. Ludwig, Analyzing the interaction energies between cation and anion in ILs: The subtle balance between Coulomb forces and hydrogen bonding, *J. Mol. Liq.* (2013), http://dx.doi.org/10.1016/j.molliq.2013.07.009.

Gerber, R.P., P.S. Rafael de, Prediction of Infinite–Dilution Activity Coefficients Using UNIFAC and COSMO–SAC Variants, *Ind. Eng. Chem. Res.* 49 (2010) 7488–7496.

Gunther, F.A., Solubility of Dichlorodiphenyltrichloroethane, *JACS.* 67 (1945) 180–90.

Jaime–Leal, J.E., A. Bonilla–Petriciolet, Correlation of Activity Coefficients in Aqueous Solutions of Ammonium Salts Using Local Composition Models and Stochastic Optimization Methods, *Chem. Prod. Process Model.* 3 (2008) 1934–2659.

Karabacak, M., S. Bilgili, T. Mavis, M. Eskici, A. Atac, Molecular structure, spectroscopic characterization (FT-IR, FT-Raman,UV and MR), HOMO and LUMO analysis of 3-ethynylthiophenen with DFT quantum chemical alculations, *Spectrochim. Acta. A Mol Biomol. Spectrosc.* 115 (2013) 709–718.

Kavitha, E., N. Sundaranganesan, S. Sebastian, Molecular structure, vibrational spectroscopic and HOMO, LUMO studies of 4–nitroaniline by density functional method, *Indian J. Pure. Appl. Phys.* 48 (2010) 20–30.

Kwon, J.H., H.M. Liljestrand, L.E. Katz, Partitioning of moderately hydrophobic endocrine disrupters between water and synthetic membrane vesicles, *Environ. Toxicol. Chem.* 25 (2006) 1984–1992.

Lide, D.R., CRC *Handbook of Chemistry and Physics*, CRC Press/Taylor and Francis, Boca Raton, USA, 2008.

Lü, R., J. Lin, Z. Qu, Theoretical study on interactions between ILs and organosulfur compounds, *Comput. Theor. Chem.* 1002 (2012) 49–58.

Lü, R., Z. Qu, J. Lin, Comparative study of interactions between thiophene-\pyridine\benzene \heptane and 1-butyl-3-methylimidazolium trifluoromethanesulfonate by density functional theory, *J. Mol. Liq.* 180 (2013) 207–214.

Luisa, P., L.A. Nevesb, C.A.M. Afonsoc, I.M. Coelhosob, J.G. Crespob, A. Gareaa, A. Irabien, Facilitated transport of $CO_2$ and $SO_2$ through Supported Ionic Liquid Membranes (SILMs), *Desalination.* 245 (2009) 485–493.

Mackay, D., Correlation of Bioconcentration Factors, *Environ. Sei. Technol.* 16 (1982) 274–278.

Mühiberger, B. G. Lemke, Endosulfan and metabolites, 1–octanol/water partition coefficient 1–octonal/water partition coefficient (HPLC method). Bayer CropScinece GmbH, Product Technology–Analytics Frankfurt, D–65926, Germany, 2004.

Mulliken, R.S., "Electronic Population Analysis on LCAO-MO Molecular Wave Functions. I", *J. Chem. Phys.* 23 (1955) 1833–1840.

Park, S.K., A.R. Bielefeldt, Equilibrium partitioning of a non–ionic surfactant and pentachlorophenol between water and a non–aqueous phase liquid, Water Res. 37 (2003) 3412–3420.

Pilli, S.R., T. Banerjee, K. Mohanty, Extraction of Pentachlorophenol and Dichlorodiphenyl–trichloroethane from aqueous solutions using ionic liquids, *J. Ind. Eng. Chem.* 18 (2012) 1983–1996.

Pilli, S.R., T. Banerjee, K. Mohanty, Liquid–liquid equilibrium (LLE) data for ternary mixtures of [C4DMIM][PF6]+[PCP]+[water] and [C4DMIM][PF6] +[PA]+[water] at T = 298.15 K and p = 1 atm, *Fluid Phase Equilib.* (2014) (Accepted, DOI: 10.1016/j.fluid.2014.08.004).

Pinter, B., T. Fievez, F.B. Matthias, P. Geerlings, F. De Proft, On the origin of the steric effect, *Phys. Chem. Chem. Phys.*14 (2012) 9846–9854.

Prasad, O., L. Sinha, N. Kumar, Theoretical Raman and IR spectra of tegafur and comparison of molecular electrostatic potential surfaces, polarizability and hyerpolarizability of tegafur with 5-fluoro-uracil by density functional theory, *J. At. Mol. Sci.* 1 (2010) 201–214.

Putnam, R., R. Taylor, A. Klamt, F. Eckert, M. Schiller, Prediction of Infinite Dilution Activity Coefficients Using COSMO-RS, *Ind. Eng. Chem. Res.* 42 (2003) 3635–3641.

Shiflett, M.B., A. Yokozeki, Separation of $CO_2$ and $H_2S$ using room–temperature ionic liquid [bmim][$PF_6$], *Fluid Phase Equilib.* 294 (2010) 105–113.

Shiu, W.Y., K.C. Ma, D. Varhanickova, D. Mackay, Chlorophenols and alkylphenols: areview and correlation of environmentally relevant properties and fate in an evaluative environment, *Chemosphere*. 29 (1994) 1155–224.

Sosa, C., J. Andzelm, B.C. Elkin, E. Wimmer, K.D. Dobbs, D.A. Dixon, A local density functional study of the structure and vibrational frequencies of molecular transition–metal compounds. *J Phys. Chem.* 96 (1992) 6630–6636.

Tsuzuki, S., H. Tokuda, M. Mikami, Theoretical analysis of the hydrogen bond of imidazolium $C_2$–H with anions, *Phys. Chem. Chem. Phys.* 9 (2007) 4780–4784.

Veith, G.D., D.L. De Foe, B.V. Bergstedt, Measuring and estimating the bioconcentration factor of chemicals on fish, *J. Fish Res. Board Can.* 36 (1979) 1040–1048.

Wightman, P.G., J.B. Fein, Experimental study of 2,4,6-trichlorophenol and Pentachloro–phenol solubilities in aqueous solutions: derivation of a speciation–based chlor-ophenol solubility model, *Apipl Geochem*. 14 (1999) 319–31.

Zhou, J., J. Mao, S. Zhang, Ab initio calculations of the interaction between thiophene and ILs, *Fuel Process. Technol.* (2008) 1456–1460.

## TABLES AND FIGURES OF CHAPTER 4

**Table 4.1.** Reported properties and structures of PCP and DDT.

| No. | Name and Chemical Structure | Chemical Formulae/ Mol. Wt. (g/mol) | p*Kd* | Water Solubility @ 25 °C (mg/L) @ Ionic Strength (μM) | $\log(Ko_W)_{pred}$* | $\log(Ko_W)_{exp}$ |
|---|---|---|---|---|---|---|
| 1 | 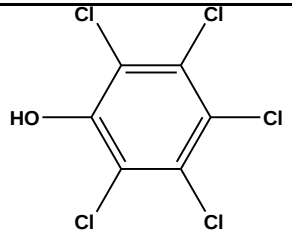 Pentachlorophenol | $C_6Cl_5OH$/ 266.34 | 4.6–5.3 4.5±0.3 | 44 @ 5.8, 0.0003 57 @ 5.6, 0.2 260 @ 6.6, 0.002 273 @ 6.3, 0.2 1275 @ 7.2, 0.01 2789@ 7.2, 0.2 | 4.48 | 5.01 |
| 2 | 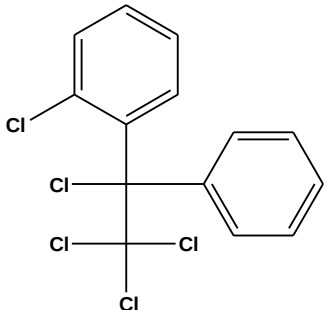 Dichlorodiphenyltrichloroethane | $C14_4H_9Cl_5$/ 354.49 | 0.05 - 0.1 | Highly soluble in organic solvents | 10.85 | 6.91 |

* Predicted using COSMO–RS

**Table 4.2.** Comparison of predicted and experimental Octanol–Water partition coefficients.

| Name of PCB Compound | $\gamma_{water}$ | $\gamma_{octanol}$ | $K_{OW,i} = 0.148\left(\frac{\gamma^{\infty}_{i,WR}}{\gamma^{\infty}_{i,OR}}\right)$ | log $(K_{OW})_{pred}$* | log $(K_{OW})_{exp}$ # |
|---|---|---|---|---|---|
| 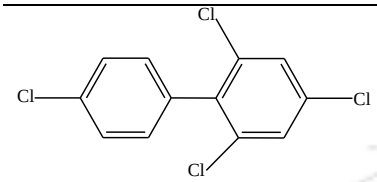 2,2',6'6-tetrachlorobiphenyl | 6.18E+09 | 0.880 | 1039093842 | 9.016 | 5.48 |
| 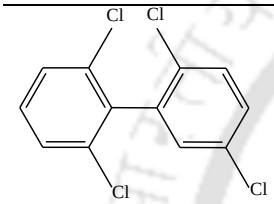 2,2'5,6'-tetrachlorobiphenyl | 3.09E+09 | 0.791 | 578101617.8 | 8.762 | 5.46 |
| 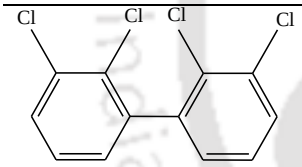 2,2',3,3'-tetrachlorobiphenyl | 8.73E+09 | 1.111 | 1162554776 | 9.065 | 5.55 |
| 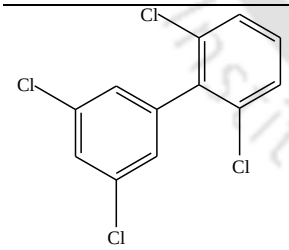 2,3',5,6'-tetrachlorobiphenyl | 6.28E+09 | 0.817 | 1136755936 | 9.055 | 5.94 |
| 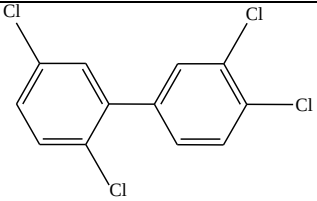 | 6.69E+09 | 0.908 | 1089939661 | 9.037 | 6.18 |

| | | | | | |
|---|---|---|---|---|---|
| 2,3',4,5'-tetrachlorobiphenyl | | | | | |
| 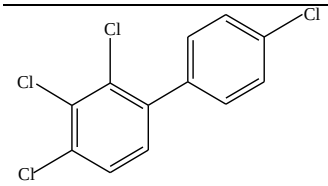 2,3',4,4'-tetrachlorobiphenyl | 5.25E+09 | 0.659 | 1178949189 | 9.071 | 6.31 |
| 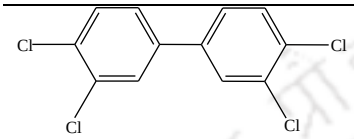 3,3',4,4'-tetrachlorobiphenyl | 2.02E+09 | 0.322 | 927307477.5 | 8.967 | 6.21 |
| 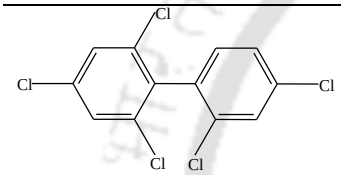 2,2',4,6,6'-pentachlorobiphenyl | 3.69E+10 | 0.807 | 6758355011 | 9.829 | 5.37 |
| 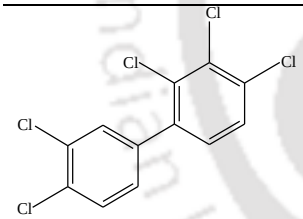 2,3,3',4,4'-pentachlorobiphenyl | 4.84E+10 | 1.061 | 6752447711 | 9.829 | 5.82 |
| 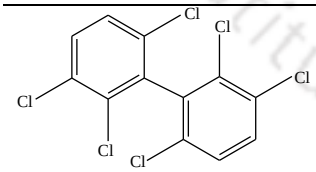 2,2',3,3',6,6'-hexachlorobiphenyl | 2.93E+11 | 1.047 | 41424181697 | 10.617 | 5.76 |

| | | | | | |
|---|---|---|---|---|---|
| 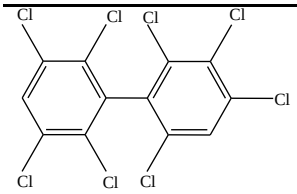 2,2',3,3',4,5',6,6'-octachlorobiphenyl | 1.51E+13 | 1.203 | 1.85387E+12 | 12.268 | 7.21 |
| 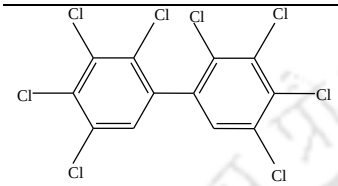 2,2',3,3',4,4',5,5'-octachlorobiphenyl | 1.36E+13 | 1.274 | 1.57591E+12 | 12.197 | 7.67 |
| 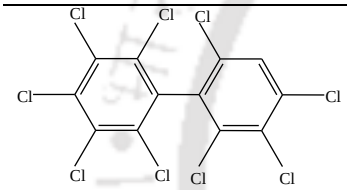 2,2',3,3',4,4',5,6,6'-nonachlorobiphenyl | 1.64E+14 | 2.138 | 1.13182E+13 | 13.053 | 7.52 |

* Predicted using COSMO–RS, # [Darryl and Des, 1988]

**Table 4.3.** Best selective ILs and their corresponding aqueous phase activity coefficient at infinite dilution*.

| Chosen EDCs ⟶ | | PCP | | DDT | |
|---|---|---|---|---|---|
| No. | Name of the selective IL | Selectivity | $\gamma^{\infty}_{water}$ | Selectivity | $\gamma^{\infty}_{water}$ |
| | *Imidazolium based ILs:* | | | | |
| 1 | $[C_8MIM][Sal]$ | 530.5 | 0.106 | - | - |
| 2 | $[C_4DMIM][C_8H_{17}SO_4]$ | 512.833 | 0.307 | - | - |
| 3 | $[C_4DMIM][BTA]$ | 355.124 | 33.559 | 6.407 | 33.559 |
| 4 | $[C_8MIM][BTA]$ | 71.871 | 8.078 | - | - |
| 5 | $[C_4DMIM][PF_6]$ | 17.688 | 181.76 | 6.768 | 181.76 |
| 6 | $[C_8MIM]$ $[PF_6]$ | 3.044 | 7.735 | - | - |
| | *Pyridinium based ILs:* | | | | |
| 1 | $[C_8MPY][MAcA]$ | 731 | 0.073 | - | - |
| 2 | $[C_8MPY][BTA]$ | 282.816 | 21.918 | - | - |
| 3 | $[C_8MPY][B(CN)_4]$ | 250.356 | 13.995 | 2.236 | 13.994 |
| 4 | $[C_6MPY][PF_6]$ | 17.961 | 47.121 | - | - |
| 5 | $[C_6MPY][BTA]$ | 193.438 | 18.686 | - | - |
| 6 | $[C_8MPY][PF_6]$ | - | - | 9.081 | 66.691 |
| 7 | $[C_8MPY][BTA]$ | - | - | 5.454 | 21.918 |
| 8 | $[C_6MPY][B(CN)_4]$ | - | - | - | - |
| | *Pyrrolidinium bases ILs:* | | | | |
| 1 | $[DPPYR][C_8H_{17}SO_4]$ | 984.666 | 0.295 | - | - |
| 2 | $[BEPYR][C_8H_{17}SO_4]$ | 980.333 | 0.294 | - | - |
| 3 | $[BEPYR][CF_3SO_3]$ | 295.552 | 1.123 | - | - |
| 4 | $[BEPYR][B(CN)_4]$ | 262.654 | 12.239 | - | - |
| 5 | $[BEPYR][BTA]$ | 246.954 | 15.780 | 5.417 | 15.780 |
| 6 | $[DPPYR][BTA]$ | 226.160 | 14.474 | 4.961 | 14.474 |
| 7 | $[BEPYR][BOB]$ | 68.228 | 12.547 | | |
| 8 | $[BRPYR][B(CN)_4]$ | - | - | 2.226 | 12.239 |

| | | | | | |
|---|---|---|---|---|---|
| 9 | [DPPYR][BOB] | - | - | - | - |
| | *Ammonium based ILs:* | | | | |
| 1 | [BTNH][Sal] | 342 | 0.034 | - | - |
| 2 | [BTNH] [$B(CN)_4$] | 20.556 | 2.792 | 0.122 | 3.848 |
| 3 | [BTNH] [BTA] | 17.604 | 3.848 | 0.265 | 2.792 |
| 4 | [BETNH] [$B(CN)_4$] | - | - | 0.079 | 3.424 |
| 5 | [BTNH][BOB] | - | - | 0.037 | 2.502 |
| | *Phosphonium based ILs:* | | | | |
| 1 | [TBP][PF6] | 243239 | 48.648 | 26.18 | 48.648 |
| 2 | [TBP][BOB] | 69252 | 20.776 | 12.09 | 20.776 |
| 3 | [TBP][BMA] | 5317 | 0.531 | - | - |
| 4 | [ODEMP][BF4] | 1858 | 0.185 | - | - |
| 5 | [TBP][$C_8H_{17}SO_4$] | 1821 | 0.364 | - | - |
| 6 | [TIBMP][$C_8H_{17}SO_4$] | 1708.5 | 0.341 | - | - |
| 7 | [ODEMP][$CF_3SO_3$] | 713.9 | 1.356 | - | - |
| 8 | [TIBMP][$CF_3SO_3$] | 686.47 | 1.167 | - | - |
| 9 | [TBMP][$CF_3SO_3$] | 663.1 | 1.127 | - | - |
| 10 | [TBP][BTA] | 579.25 | 26.761 | 24.86 | 26.761 |
| 11 | [TBP][B(CN)4] | - | - | 13.88 | 18.486 |
| 12 | [ODEMP][BTA] | - | - | 11.108 | 19.558 |
| 13 | [ODEMP][PF6] | - | - | 8.136 | 31.175 |
| 14 | [HDEMP][BTA] | - | - | 7.481 | 15.978 |
| 15 | [DEDMPP][BTA] | - | - | 5.162 | 13.377 |

* Predicted using COSMO–RS

**Table 4.4.** Comparison of predicted and experimental Log ($K_{o-w}$) with other physical and chemical properties of Endosulfan.

| | α–Endosulfan | β–Endosulfan | Endosulfan sulfate | Endosulfan alcohol | Endosulfan lactone | Endosulfan ether |
|---|---|---|---|---|---|---|
| Formula | $C_9H_6Cl_6O_3S$ | $C_9H_6Cl_6O_3S$ | $C_9H_6Cl_6O_4S$ | $C_9H_8Cl_6O_2$ | $C_9H_4\ Cl_6\ O_2$ | $C_9H_6Cl_6O$ |
| CAS Number: | 959-98-8 | 33213-65-9 | 1031-07-8 | 2157-19-9 | 3868-61-9 | 3369-52-6 |
| Molecular wt. (g/mol) | 406.93 | 406.93 | 422.93 | 360.88 | 356.84 | 342.86 |
| Log $(Kow)_{Exp.}$ | 4.74[a] | 4.79[a] | 3.66[a] | 2.92[b] | 3.4[b] | 4.15[b] |
| Log $(Kow)_{Pred.}$ | 5.18 | 5.48 | 6.61 | 3.35 | 6.09 | 5.34 |
| Solubility in water (mg/L , 20 °C) | 0.51[c] | 0.45[c] | 0.48[c] | 300[c] | - | - |
| Specific gravity at 20 °C | 1.745 | 1.745 | 1.94 | 1.8 | 1.75 | - |
| Henry's Law Constant $Pa.m^3/mol$ at 22 °C | 6.6X10-5 | 6.6X10-5 | 1.60E-01 | - | - | - |
| Vapour Pressure , Pa , at 25 °C | 1.9E-03 | 9.2E-05 | 2.3E-05 | - | - | - |
| Dissociation Constant (pK a) | not readily dissociable groups | not readily dissociable groups | not readily dissociable groups | [d]14.62–15.22 | no acidic protons | no acidic protons |

[a]Banasiak et al. 2011, [b]Mühiberger and Lemke, 2004, [c]Lide, 2008, [d]Kwon and Liljestrand, 2006

**Table 4.5.** Best selective ILs and corresponding aqueous phase activity coefficient of ILs at infinite dilution predicted by COSMO–RS for endosulfan.

| No. | Acronym of IL | Selectivity | $\gamma^{\infty}_{water}$ | No. | Acronym of IL | Selectivity | $\gamma^{\infty}_{water}$ |
|---|---|---|---|---|---|---|---|
| | *Phosphonium based ILs* | | | | *Pyrrolidinium based ILs* | | |
| 1 | [TBP][TOS] | 212.5 | 0.17 | 1 | [DPPYR][Br] | 107 | 0.010 |
| 2 | [TBP][$MDEGSO_4$] | 209.57 | 0.586 | 2 | [BEPYR] [Br] | 106 | 0.010 |
| 3 | [TBP][$C_8H_{17}SO_4$] | 202.33 | 0.364 | 3 | [DPPYR][$MDEGSO_4$] | 96.872 | 0.455 |
| 4 | [TBP][MAcA] | 191 | 0.038 | 4 | [BEPYR] [$CF_3SO_3$] | 30.436 | 1.123 |
| 5 | [TBP][BMA] | 183.34 | 0.537 | 5 | [BEPYR][BTA] | 25.899 | 15.78 |
| 6 | [TIBMP][$C_8H_{17}SO_4$] | 155.32 | 0.341 | 6 | [DPPYR][BTA] | 23.744 | 14.474 |
| 7 | [ODEMP][Br] | 128 | 0.128 | 7 | [BEPYR][$B(CN)_4$] | 20.039 | 12.24 |
| 8 | [TBP][$CF_3SO_3$] | 108.49 | 1.605 | 8 | [DPPYR][$B(CN)_4$] | 18.579 | 11.428 |
| 9 | [TIBMP][$CF_3SO_3$] | 60.781 | 1.167 | | *Pyridinium based ILs* | | |
| 10 | [TBP][BTA] | 59.522 | 26.761 | 1 | [$C_8$MPY][$C_8H_{17}SO_4$] | 31.62 | 0.407 |
| 11 | [BP][$B(CN)_4$] | 57.652 | 18.483 | 2 | [$C_8$MPY][$MDEGSO_4$] | 31.326 | 0.585 |
| | *Imidazolium based ILs* | | | 3 | [$C_6$MPY][$MDEGSO_4$] | 25.355 | 0.535 |
| 1 | [BEPYR][$MDEGSO_4$] | 101 | 0.0001 | 4 | [$C_8$MPY][BTA] | 21.411 | 21.918 |
| 2 | [$C_4$DMIM][$MDEGSO_4$] | 43.009 | 0.464 | 5 | [$C_6$MPY][BTA] | 15.842 | 18.686 |
| 3 | [$C_4$DMIM][DBP] | 42.5 | 0.008 | 6 | [$C_8$MPY][$B(CN)_4$] | 13.939 | 13.995 |
| 4 | [$C_4$DMIM][BTA] | 32.863 | 33.559 | 7 | [$C_8$MPY][$PF_6$] | 7.966 | 66.692 |
| 5 | [$C_2$DMIM][BTA] | 19.172 | 28.343 | | *Ammonium based ILs* | | |
| 6 | [$C_4$DMIM][$B(CN)_4$] | 14.803 | 17.521 | 1 | [BTNH][Br] | 27.25 | 0.010 |
| 7 | [$C_4$DMIM][BOB] | 8.918 | 24.198 | 2 | [BTNH][$C_8H_{17}SO_4$] | 23.508 | 0.016 |
| 8 | [$C_4$DMIM][$PF_6$] | 7.045 | 181.76 | 3 | [BETNH][Br] | 23.429 | 0.016 |
| | | | | 4 | [BTNH][DBP] | 22.5 | 0.009 |
| | | | | 5 | [BTNH][BTA] | 1.599 | 2.792 |
| | | | | 6 | [BETNH][BTA] | 1.188 | 2.209 |

**Table 4.6.** Predicted HOMO, LUMO values using B3LYP/6-31G*.

| Name of compound | $E_{HOMO}$ (eV) | $E_{LUMO}$ (eV) | $E_{HOMO–LUMO}$ gap (eV) |
|---|---|---|---|
| [PA]+[$C_4$DMIM]+[$PF_6$] | -0.3135 | -0.2538 | 0.0597 |
| [PCP]+[$C_4$DMIM]+[$PF_6$] | -0.2892 | -0.1427 | 0.1465 |
| [PA]+[$C_4$DMIM]+[BTA] | -0.3037 | -0.2019 | 0.1018 |
| [PCP]+[$C_4$DMIM]+[BTA] | -0.2635 | -0.1428 | 0.1207 |
| [PCP] | -0.2504 | -0.0531 | 0.1973 |
| [PA] | -0.2632 | -0.0606 | 0.2025 |
| [$C_4$DMIM] | -0.409 | -0.1646 | 0.2444 |
| [$C_2$DMIM] | -0.4122 | -0.1680 | 0.2442 |
| [TBP] | -0.4352 | -0.0938 | 0.3413 |
| [$PF_6$] | -0.1566 | 0.2810 | 0.4376 |
| [BTA] | -0.1353 | 0.1753 | 0.3106 |
| [$C_8H_{17}SO_4$] | -0.0586 | 0.0633 | 0.1220 |
| [BOB] | -0.136 | 0.0737 | 0.2097 |

**Table 4.7.** HOMO–LUMO values of several cations and anions using B3LYP/6-31G* and PM3/6-31G*.

| Name of compound | $E_{HOMO}$ (eV)/B3LYP | $E_{HOMO}$ (eV)/PM3 | $E_{LUMO}$ (eV)/B3LYP | $E_{LUMO}$ (eV)/PM3 |
|---|---|---|---|---|
| [$C_4$DMIM] | -0.409 | -0.32131 | -0.1646 | -0.1242 |
| [$C_2$DMIM] | -0.41229 | -0.5331 | -0.16802 | -0.17872 |
| [TBP] | -0.43522 | -0.53012 | -0.09386 | -0.16568 |
| [$PF_6$] | -0.1566 | -0.39731 | 0.281 | 0.05757 |
| [BTA] | -0.1353 | -0.26401 | 0.1753 | 0.07496 |
| [$C_8H_{17}SO_4$] | -0.05869 | -0.2004 | 0.06335 | 0.18837 |

**Table 4.8.** Thermodynamic parameters and nonlinear optical properties (theoretically computed energies) via B3LYP/6-31G* method.

| Parameters | PA+$C_4$DMIM +$PF_6$ | PCP+$C_4$DMIM +$PF_6$ | PA+$C_4$DMIM+ BTA | PCP+$C_4$DMIM +BTA |
|---|---|---|---|---|
| Total energy E (thermal) (kcal/mol) | 265.579 | 230.099 | 302.986 | 256.067 |
| Heat capacity at const. volume ($C_v$)(cal/mol K) | 116.892 | 118.267 | 144.053 | 149.079 |
| Entropy (S) (cal/mol K) | 211.456 | 224.769 | 262.145 | 294.465 |
| Zero point vibrational energy (kcal/mol) | 245.16 | 209.044 | 277.209 | 228.58 |
| Vibrational energy, $E_{vib}$ (kcal/mol) | 263.801 | 228.322 | 301.208 | 254.289 |
| Triplet energy (SCF) (a.u) | -1936.3 | -4000.9 | -2899.2 | -4895.2 |
| Triplet energy (SCF) (kcal/mol) | -1.22E+06 | -2.51E+07 | -1.82E+06 | -3.07E+06 |
| Rotational constants (GHz) | | | | |
| X | 0.2204 | 0.2269 | 0.1094 | 0.1079 |
| Y | 0.1168 | 0.0531 | 0.0741 | 0.0446 |
| Z | 0.1075 | 0.0464 | 0.0539 | 0.04 |
| Dipole moment (debye) | | | | |
| $l_x$ | -9.5595 | 9.0715 | -14.466 | 12.664 |
| $l_y$ | 2.1959 | -14.051 | 6.3574 | 5.4968 |
| $l_z$ | 2.4011 | 3.0254 | 1.7964 | -3.7108 |
| $l_{tot}$ | 10.098 | 16.9964 | **14.2955** | **15.9027** |

**Table 4.9.** Calculated global scalar properties of compounds and complexes used in this study (B3LYP/6-31G*).

| Name of compound | Global softness | Global hardness | Electronegativity | Chemical potential | Electrophilicity index |
|---|---|---|---|---|---|
| [PA]+[$C_4$DMIM]+[$PF_6$] | 33.5008 | 0.0597 | -0.2837 | 0.2837 | 1.3477 |
| [PCP]+[$C_4$DMIM]+[$PF_6$] | 13.6519 | 0.1465 | -0.2160 | 0.2160 | 0.3183 |
| [PA]+[$C_4$DMIM]+[BTA] | 19.6464 | 0.1018 | -0.2528 | 0.2528 | 0.6278 |
| [PCP]+[$C_4$DMIM]+[BTA] | 16.5700 | 0.1207 | -0.2032 | 0.2032 | 0.3419 |
| [PCP] | 10.1338 | 0.1974 | -0.1518 | 0.1518 | 0.1167 |
| [PA] | 9.8736 | 0.2026 | -0.1619 | 0.1619 | 0.1295 |
| [$C_4$DMIM] | 8.1833 | 0.2444 | -0.2868 | 0.2868 | 0.3366 |
| [$C_2$DMIM] | 8.1877 | 0.2443 | -0.2902 | 0.2902 | 0.3447 |
| [TBP] | 5.8589 | 0.3414 | -0.2645 | 0.2645 | 0.2050 |
| [$PF_6$] | 4.5704 | 0.4376 | 0.0622 | -0.0622 | 0.0088 |
| [BTA] | 6.4392 | 0.3106 | 0.0200 | -0.0200 | 0.0013 |
| [$C_8H_{17}SO_4$] | 16.3881 | 0.1220 | 0.0023 | -0.0023 | 0.0000 |
| [BOB] | 9.5374 | 0.2097 | -0.0312 | 0.0312 | 0.0046 |

**Table 4.10(a).** CHELPG charges of [PCP]+[$C_4$DMIM][$PF_6$] using B3LYP/6-31G*.

| S.No | Atom | Charge | S.No | Atom | Charge |
|---|---|---|---|---|---|
| 1 | C | 0.003111 | 26 | H | 0.148143 |
| 2 | C | 0.048508 | 27 | H | 0.171383 |
| 3 | N | -0.43711 | 28 | H | 0.160918 |
| 4 | C | 0.576051 | 29 | P | 1.483619 |
| 5 | N | -0.46197 | 30 | F | -0.39076 |
| 6 | C | -0.54966 | 31 | F | -0.33839 |
| 7 | H | 0.20191 | 32 | F | -0.35348 |
| 8 | H | 0.233145 | 33 | F | -0.4263 |
| 9 | H | 0.19093 | 34 | F | -0.40234 |
| 10 | C | -0.35935 | 35 | F | -0.3785 |
| 11 | H | 0.166124 | 36 | C | -0.13655 |
| 12 | H | 0.222313 | 37 | C | -0.0904 |
| 13 | H | 0.259987 | 38 | C | -0.08382 |
| 14 | C | -0.13882 | 39 | C | -0.09214 |
| 15 | C | -0.29784 | 40 | C | -0.13084 |
| 16 | H | 0.1811 | 41 | C | 0.393566 |
| 17 | H | 0.187336 | 42 | Cl | 0.045443 |
| 18 | H | 0.202578 | 43 | Cl | 0.021545 |
| 19 | H | 0.251324 | 44 | O | -0.65433 |
| 20 | C | -0.26127 | 45 | H | 0.481372 |
| 21 | C | -0.44696 | 46 | Cl | 0.079961 |
| 22 | H | 0.160009 | 47 | Cl | 0.05894 |
| 23 | H | 0.156695 | 48 | Cl | 0.04857 |
| 24 | H | 0.152306 | - | - | - |
| 25 | H | 0.143952 | - | - | - |

**Table 4.10(b).** CHELPG charges of [PA]+[$C_4$DMIM][$PF_6$] using B3LYP/6-31G*.

| S.No | Atom | Charge | S.No | Atom | Charge |
|---|---|---|---|---|---|
| 1 | C | 0.000 | 26 | H | 0.164 |
| 2 | C | 0.042 | 27 | H | 0.178 |
| 3 | N | -0.430 | 28 | H | 0.138 |
| 4 | C | 0.571 | 29 | P | 1.477 |
| 5 | N | -0.448 | 30 | F | -0.386 |
| 6 | C | -0.575 | 31 | F | -0.346 |
| 7 | H | 0.218 | 32 | F | -0.379 |
| 8 | H | 0.237 | 33 | F | -0.430 |
| 9 | H | 0.178 | 34 | F | -0.392 |
| 10 | C | -0.384 | 35 | F | -0.379 |
| 11 | H | 0.170 | 36 | C | -0.095 |
| 12 | H | 0.243 | 37 | C | -0.076 |
| 13 | H | 0.221 | 38 | C | -0.165 |
| 14 | C | -0.167 | 39 | C | 0.432 |
| 15 | C | -0.268 | 40 | C | 0.355 |
| 16 | H | 0.169 | 41 | C | -0.133 |
| 17 | H | 0.208 | 42 | H | 0.177 |
| 18 | H | 0.194 | 43 | H | 0.189 |
| 19 | H | 0.241 | 44 | H | 0.200 |
| 20 | C | -0.262 | 45 | H | 0.169 |
| 21 | C | -0.446 | 46 | O | -0.184 |
| 22 | H | 0.148 | 47 | O | -0.502 |
| 23 | H | 0.154 | 48 | H | 0.392 |
| 24 | H | 0.144 | 49 | O | -0.306 |
| 25 | H | 0.128 | 50 | H | 0.432 |
| | | | 51 | O | 0.164 |

**Table 4.11.** Experimental and theoretical,$^{1}$H correlation NMR isotropic chemical shifts (with respect to TMS) [PCP]\[PA]+IL by DFT (B3LYP/6-311++G(d,p) method (all values in ppm).

| [PA]+[$C_4$DMIM][$PF_6$] | | | [PCP]+[$C_4$DMIM][$PF_6$] | | |
|---|---|---|---|---|---|
| Hydrogen | B3LYP | Exp. | Hydrogen | B3LYP | Exp. |
| 18-H | 11.23 | NA | 36-H | 23.11 | NA |
| 19-H | 9.12 | NA | 32-H | 18.37 | NA |
| 12-H | 8.21 | NA | 35-H | 7.92 | 7.607 |
| 48-H | 7.87 | 7.614 | 30-H | 7.71 | 7.578 |
| 47-H | 7.81 | 7.584 | 31-H | 5.12 | 4.088 |
| 50-H | 6.73 | NA | 51-H | 3.82 | 4.076 |
| 49-H | 6.10 | NA | 34-H | 3.74 | 4.064 |
| 46-H | 4.98 | 4.077 | 33-H | 3.58 | 3.838 |
| 42-H | 4.96 | 4.065 | 28-H | 2.56 | 2.552 |
| 13-H | 3.69 | 3.717 | 29-H | 2.56 | 2.518 |
| 16-H | 3.47 | 3.35 | 27-H | 2.35 | 2.44 |
| 17-H | 3.42 | 3.317 | 42-H | 1.96 | 1.686 |
| 11-H | 2.91 | 2.551 | 43-H | 1.53 | 1.637 |
| 9-H | 2.64 | 2.482 | 41-H | 1.23 | 1.241 |
| 8-H | 2.61 | 2.48 | 37-H | 1.19 | 1.241 |
| 27-H | 2.04 | 2.77 | 40-H | 1.13 | 1.229 |
| 28-H | 2.01 | 1.662 | 38-H | 0.96 | 0.891 |
| 7-H | 1.97 | 1.65 | 39-H | 0.82 | 0.878 |
| 23-H | 1.16 | 1.26 | | | |
| 24-H | 1.10 | 1.254 | | | |
| 25-H | 0.97 | 0.896 | | | |
| 22-H | 0.97 | 0.884 | | | |
| 26-H | 0.94 | 0.872 | | | |

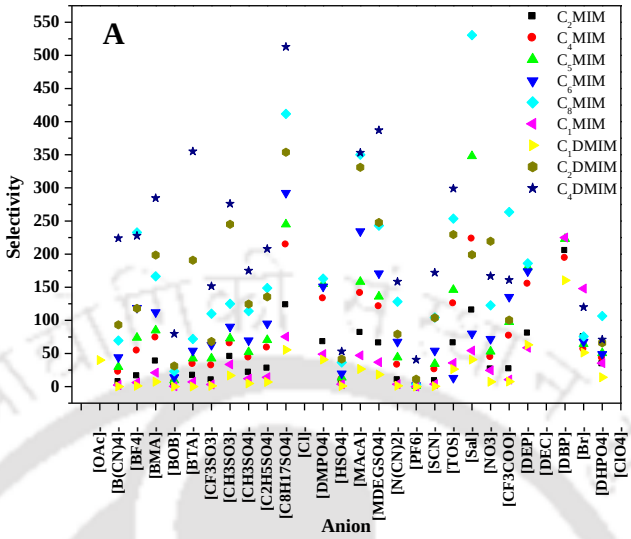


**Figure 4.1.1(a).** Selectivity at infinite dilution and at ambient temperature (T=25 °C) for imidazolium based IL with PCP.

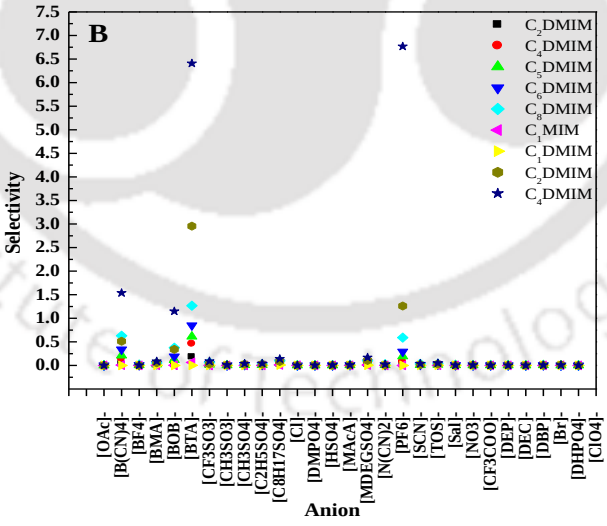


**Figure 4.1.1(b).** Selectivity at infinite dilution and at ambient temperature (T=25 °C) for imidazolium based IL with DDT.

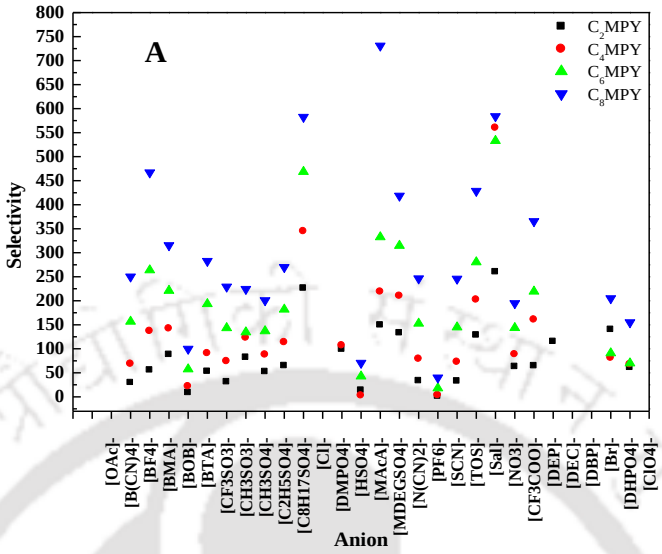


**Figure 4.1.2(a).** Selectivity at infinite dilution and at ambient temperature (T=25 °C) for pyridinium based IL with PCP.

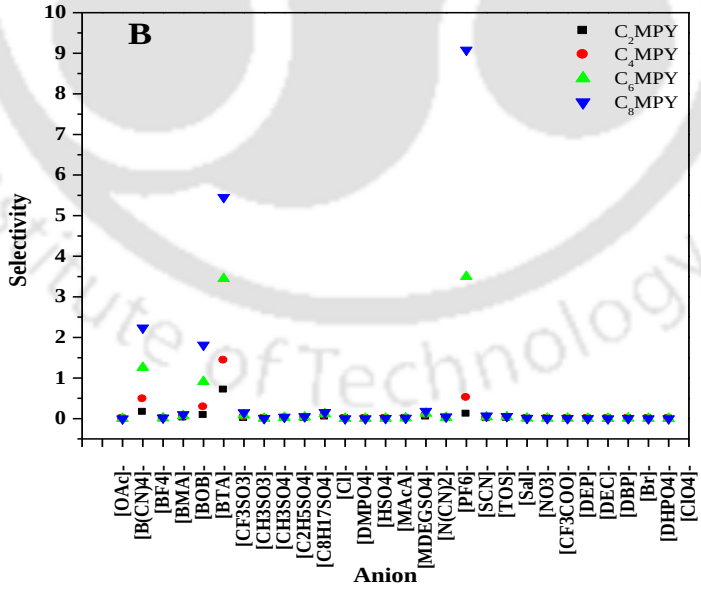


**Figure 4.1.2(b).** Selectivity at infinite dilution and at ambient temperature (T=25 °C) for pyridinium based IL with DDT.

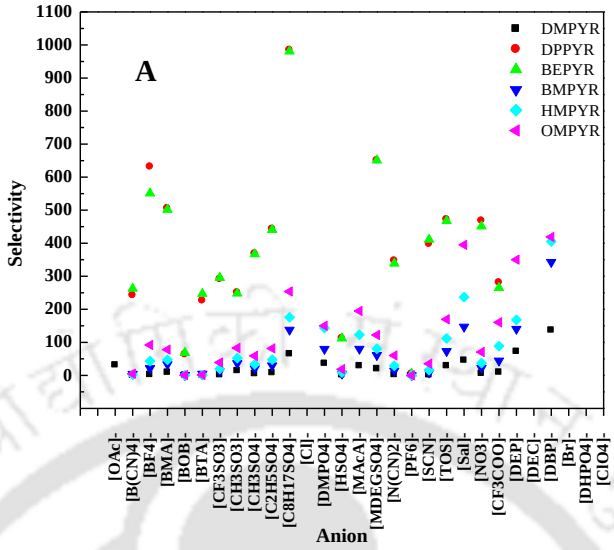


**Figure 4.1.3(a).** Selectivity at infinite dilution and at ambient temperature (T=25 °C) for pyrrolidinium based IL with PCP.

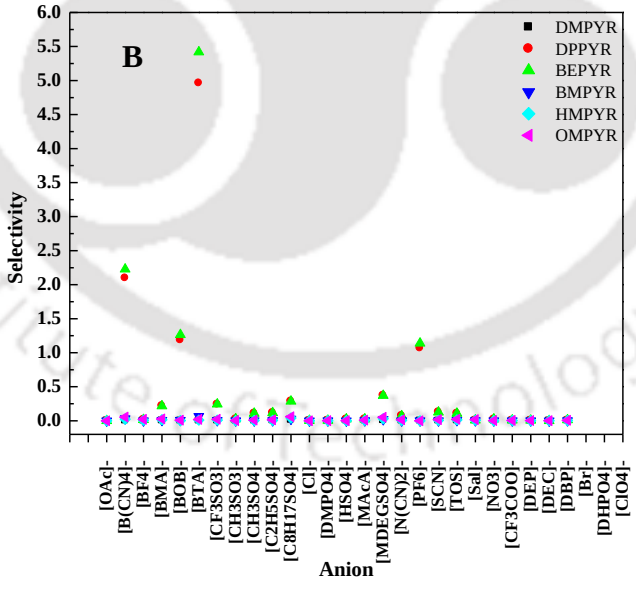


**Figure 4.1.3(b).** Selectivity at infinite dilution and at ambient temperature (T=25 °C) for pyrrolidinium based IL with DDT.

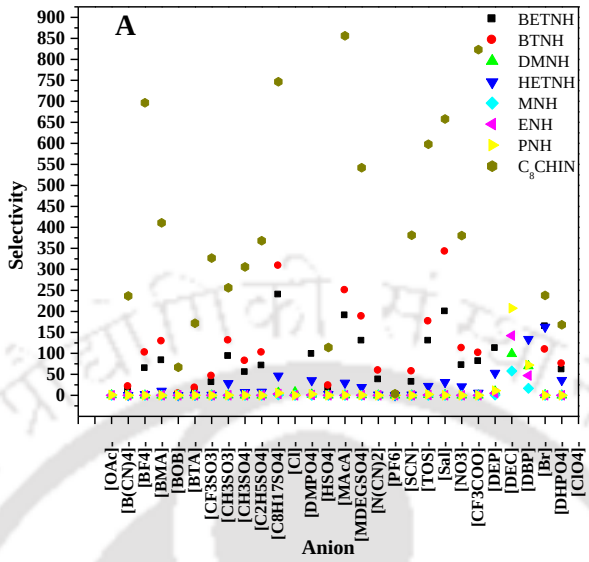


**Figure 4.1.4(a).** Selectivity at infinite dilution and at ambient temperature (T=25 °C) for ammonium based IL with PCP.

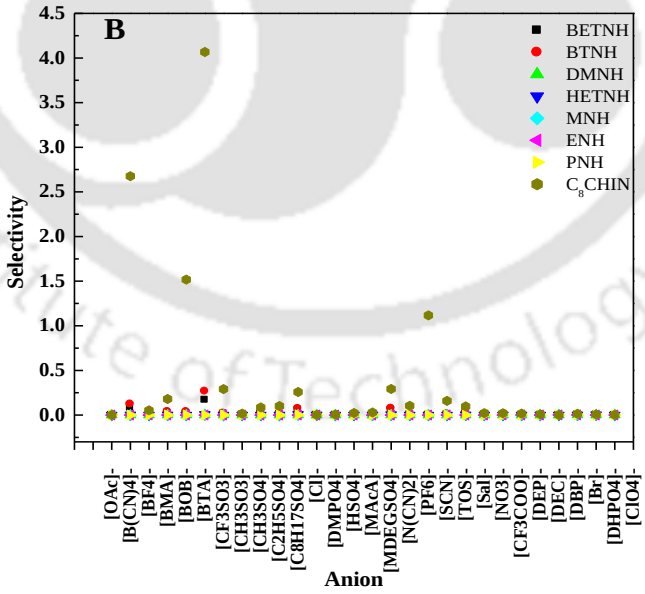


**Figure 4.1.4(b).** Selectivity at infinite dilution and at ambient temperature (T=25 °C) for ammonium based IL with DDT.

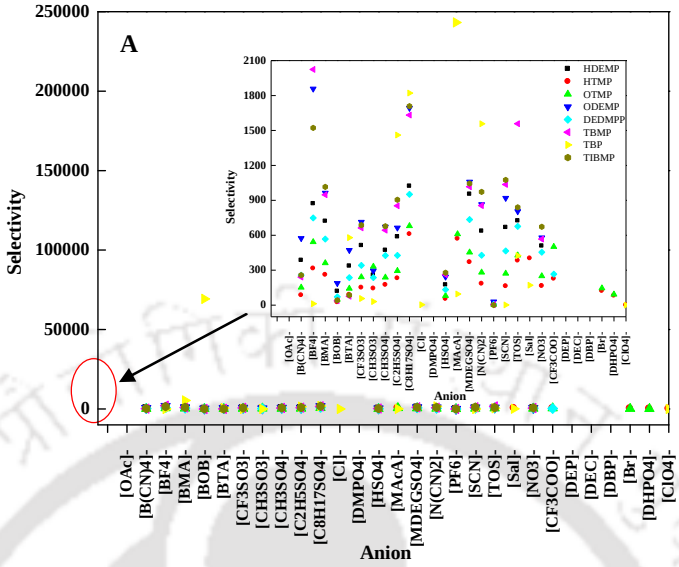


**Figure 4.1.5(a).** Selectivity at infinite dilution and at ambient temperature, (T=25 °C) for phosphonium based IL with PCP.

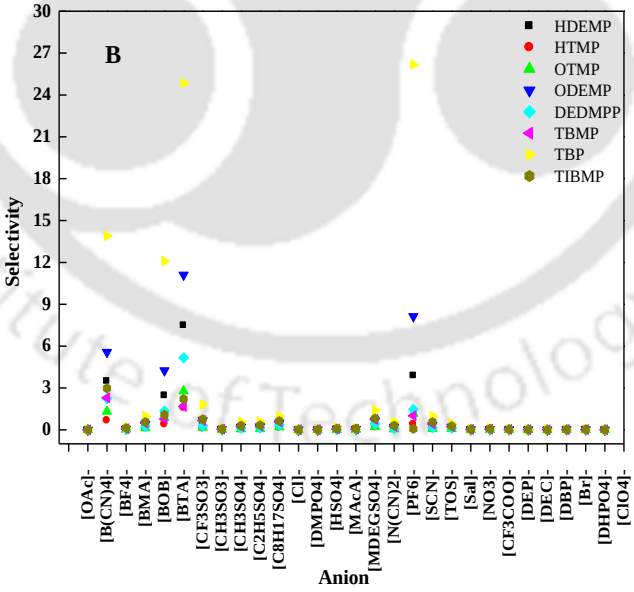


**Figure 4.1.5(b).** Selectivity at infinite dilution and at ambient temperature, (T=25 °C) for phosphonium based IL with (a) PCP and B) DDT.

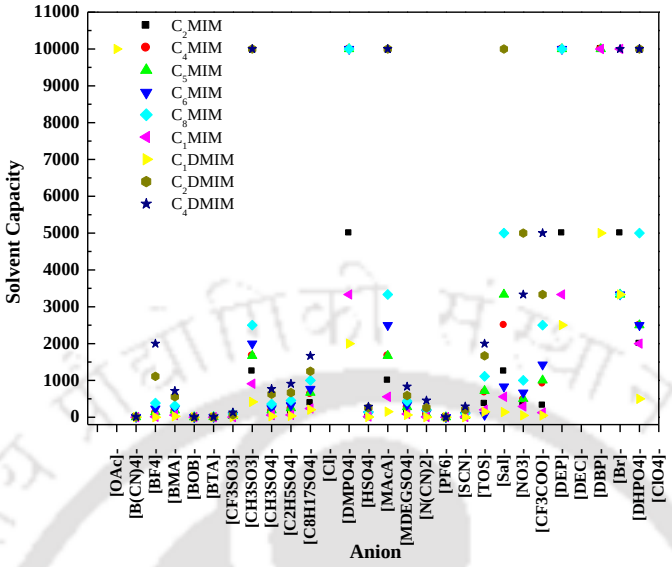


**Figure 4.1.6.** Solvent capacity values at infinite dilution and at ambient temperature (T=25 °C) for imidazolium based IL with PCP.

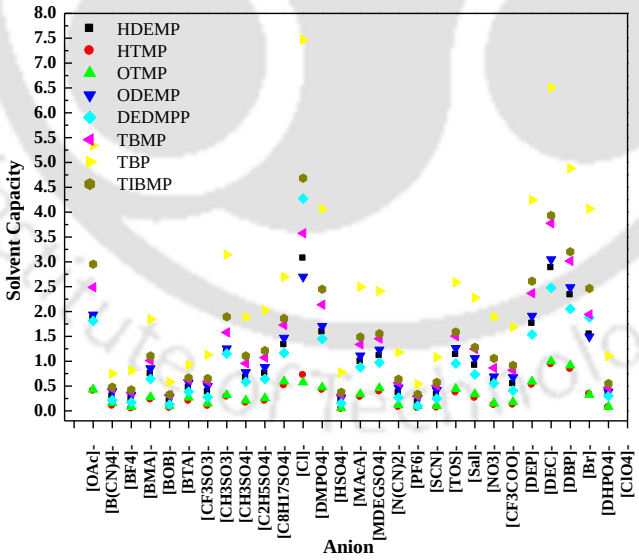


**Figure 4.1.7.** Solvent capacity values at infinite dilution and at ambient temperature (T=25 °C) for phosphonium based IL with DDT.

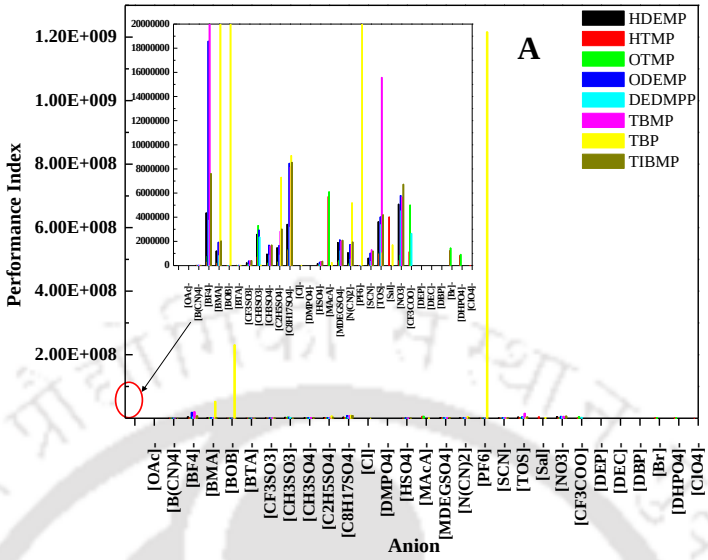


**Figure 4.1.8(a).** Performance index values at infinite dilution and at ambient temperature (T=25 °C) for phosphonium based IL with PCP.

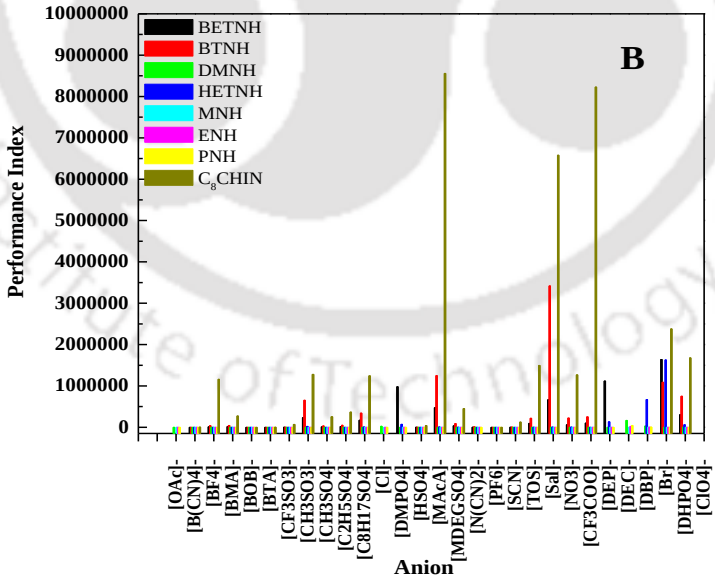


**Figure 4.1.8(b).** Performance index values at infinite dilution and at ambient temperature (T=25 °C) for ammonium based IL with PCP.

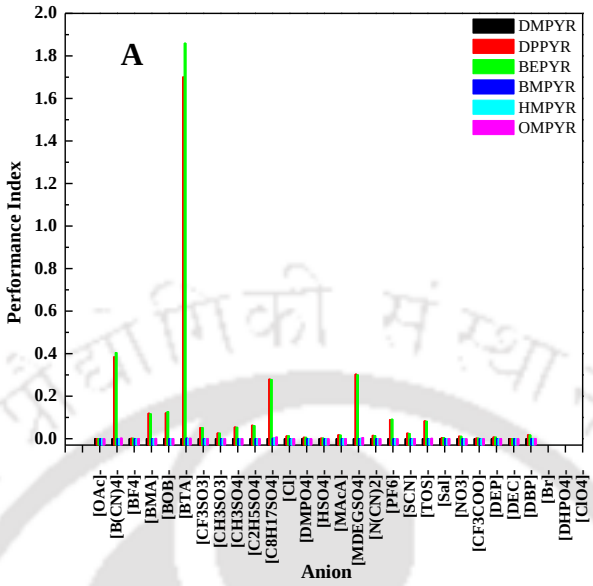


**Figure 4.1.9(a).** Performance index values at infinite dilution and at ambient temperature (T=25 °C) for pyrrolidinium based IL with DDT.

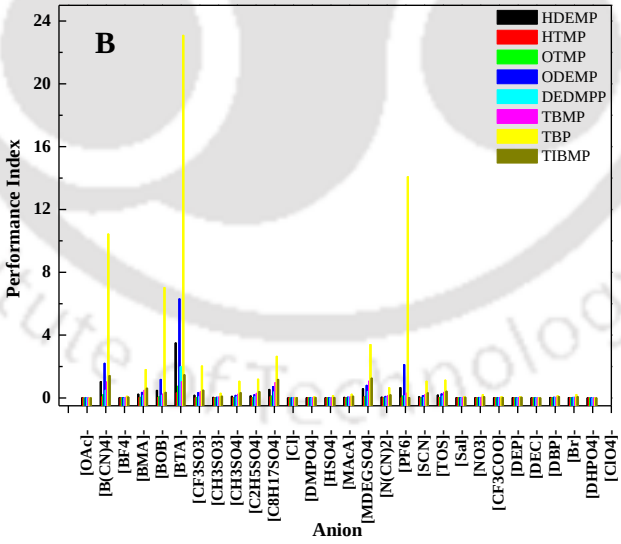


**Figure 4.1.9(b).** Performance index values at infinite dilution and at ambient temperature (T=25 °C) for phosphonium based IL with DDT.

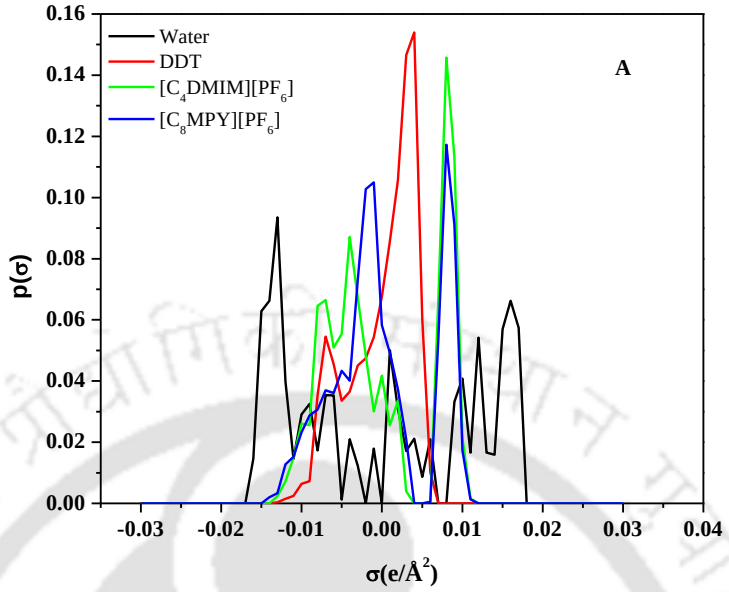


**Figure 4.1.10(a).** Sigma profiles for water, DDT, [$C_4$DMIM][$PF_6$], and [$C_8$MPY][$PF_6$].

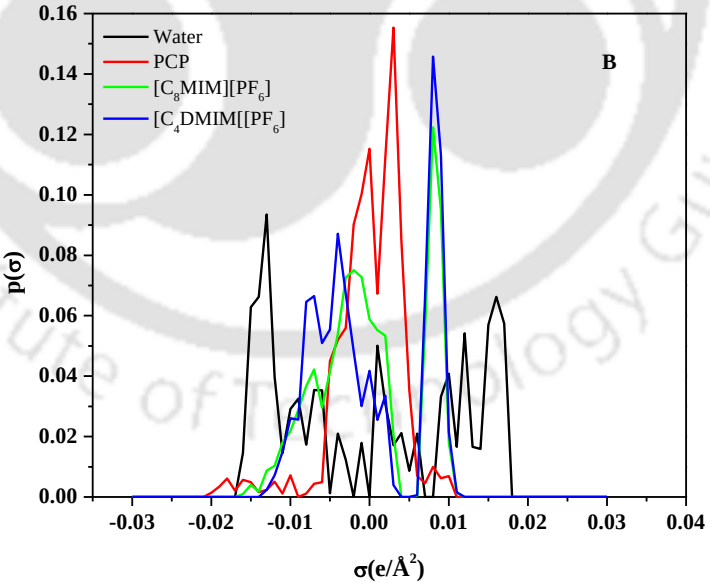


**Figure 4.1.10(b)** Sigma profiles for water, PCP, [$C_8$MIM][$PF_6$] and [$C_4$DMIM][$PF_6$].

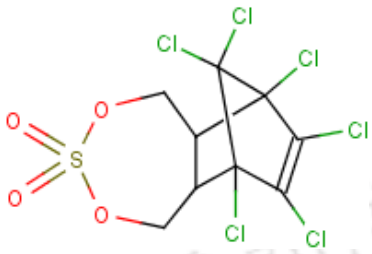


Endosulfan sulfate–$C_9H_6Cl_6O_4S$

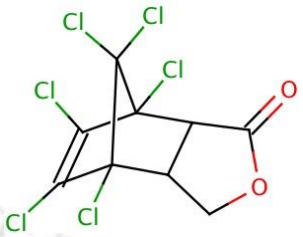


Endosulfan lactone–$C_9H_4Cl_6O_2$

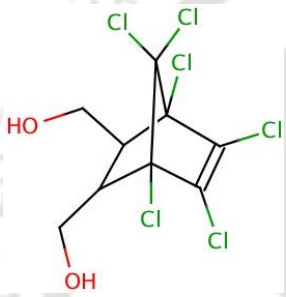


Endosulfan alcohol–$C_9H_8Cl_6O_2$

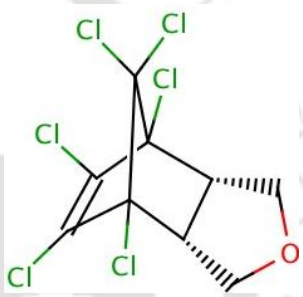


Endosulfan ether–$C_9H_6Cl_6O$

**Figure 4.2.1.** Chemical structures of different Endosulfan metabolites.

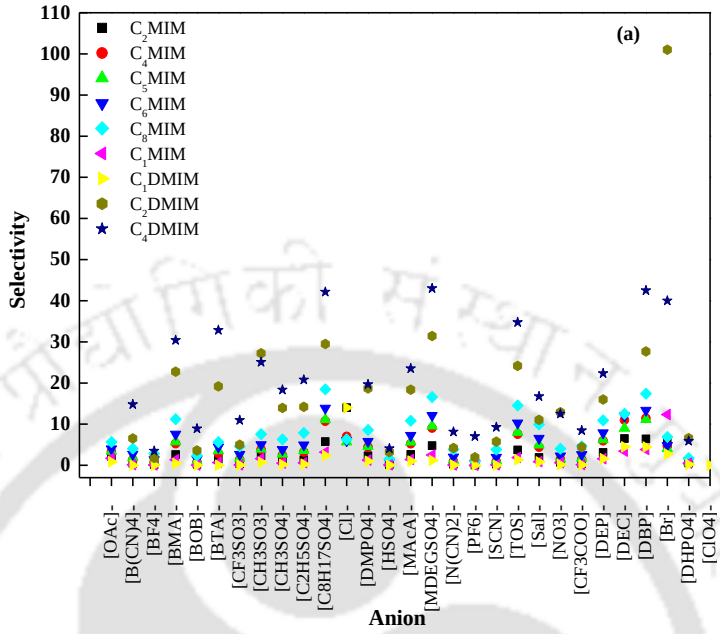


**Figure 4.2.2(a).** Selectivity values at infinite dilution and at ambient temperature (T=25 °C) for imidazolium based IL with α–Endosulfan.

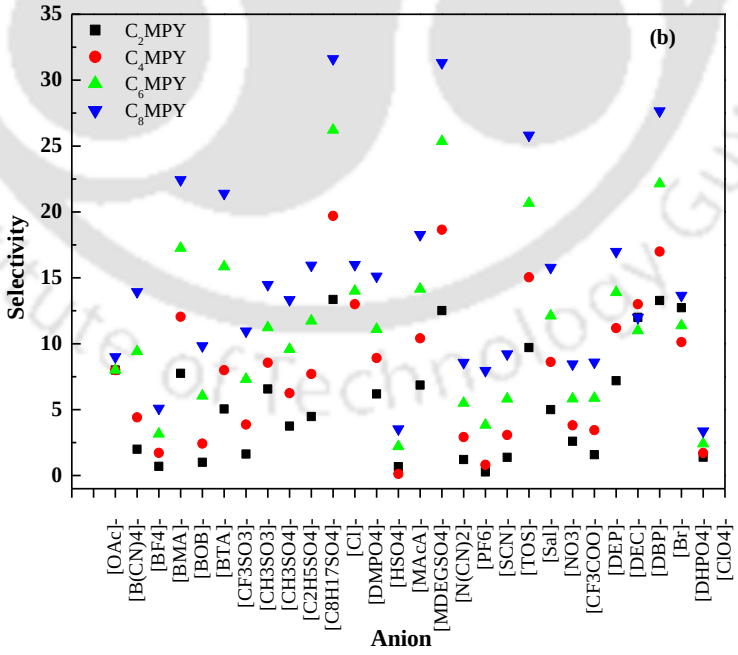

**Figure 4.2.2(b).** Selectivity values at infinite dilution and at ambient temperature (T=25 °C) for pyridinium based IL with α–Endosulfan.

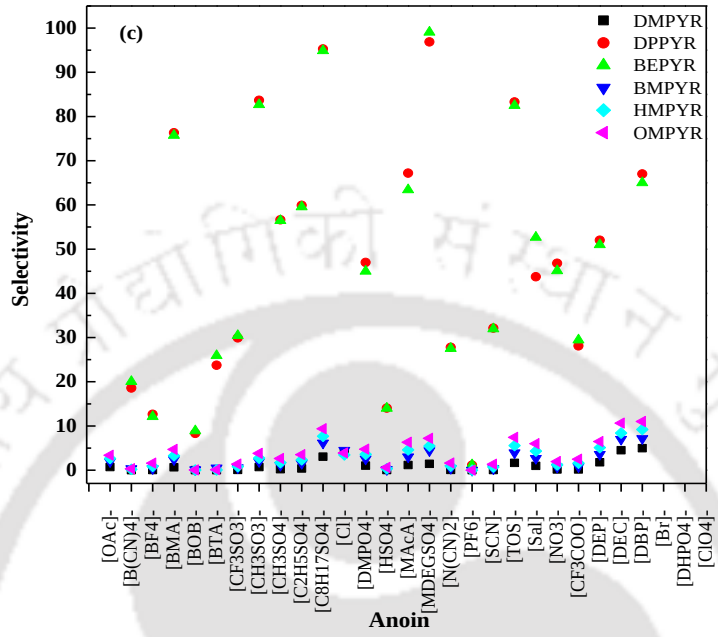


**Figure 4.2.2(c).** Selectivity values at infinite dilution and at ambient temperature (T=25 °C) for pyrrolidinium based IL with α–Endosulfan.

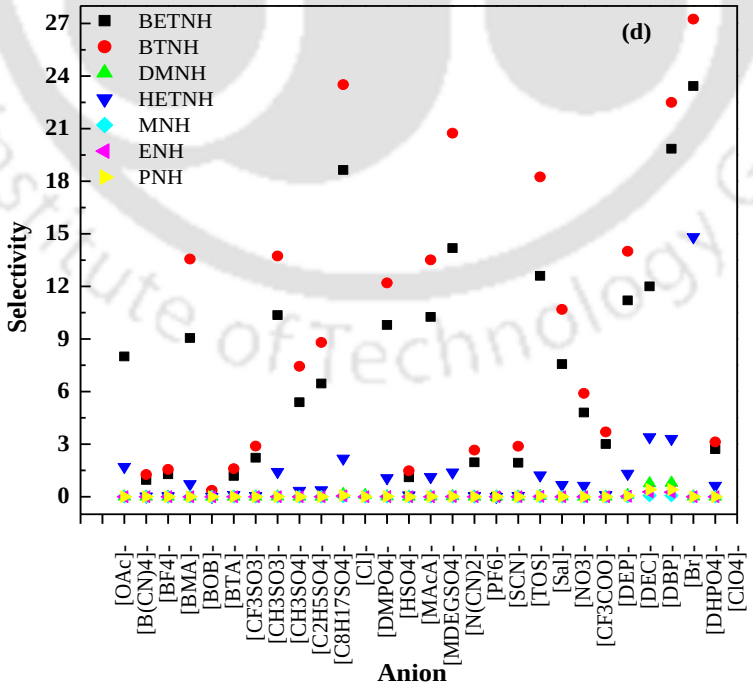

**Figure 4.2.2(d).** Selectivity values at infinite dilution and at ambient temperature (T=25 °C) for ammonium based IL with α–Endosulfan.

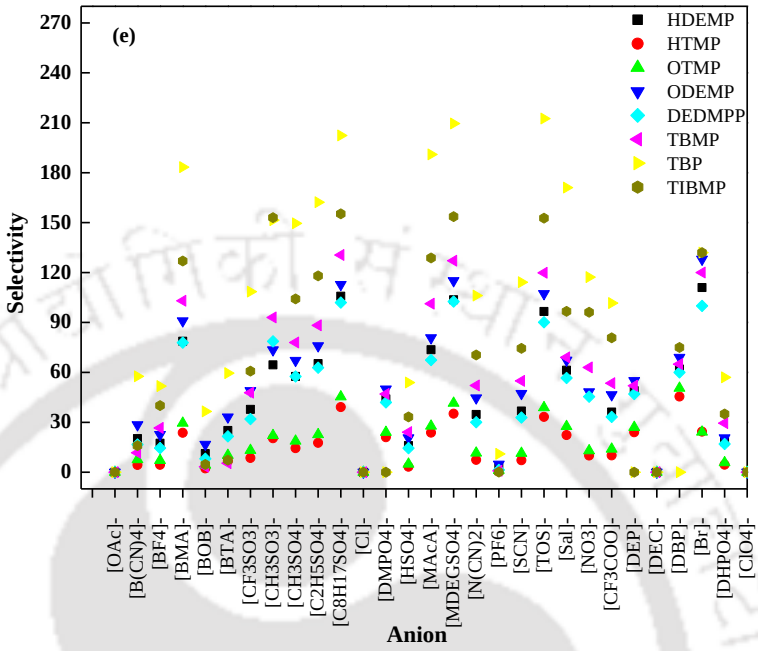


**Figure 4.2.2(e).** Selectivity values at infinite dilution and at ambient temperature (T=25 °C) for phosphonium based IL with α–Endosulfan

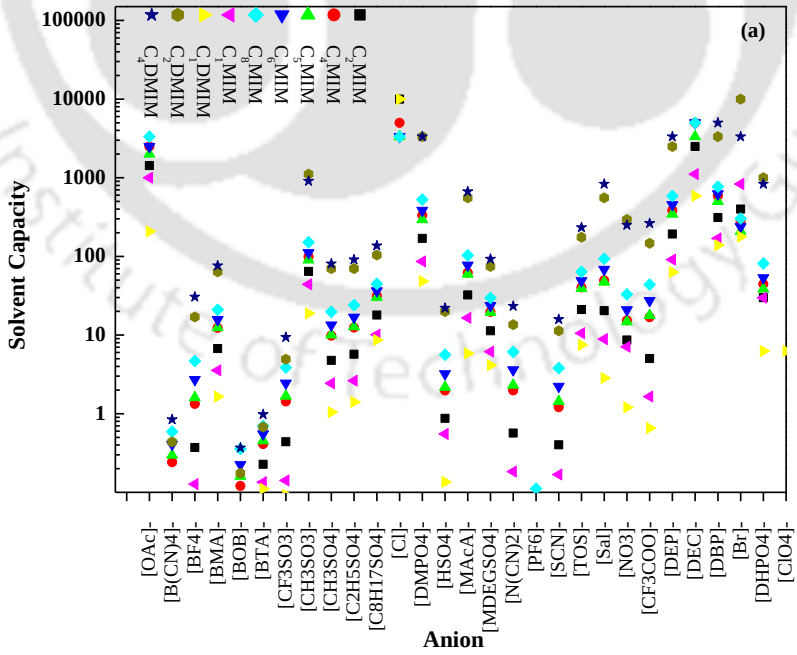

**Figure 4.2.3(a).** Solvent capacity values of α–Endosulfan at infinite dilution and at ambient temperature (T=25 °C) for imidazolium based ILs.

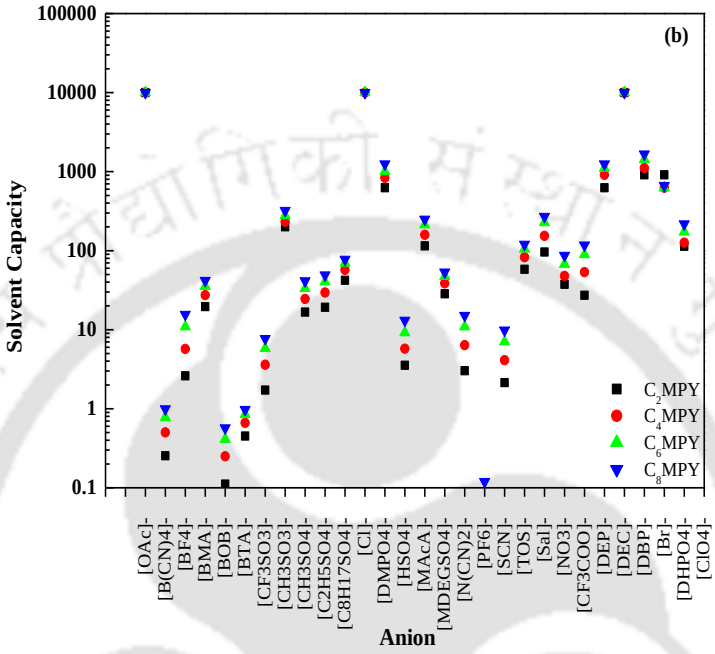


**Figure 4.2.3(b).** Solvent capacity values of α–Endosulfan at infinite dilution and at ambient temperature (T=25 °C) for pyridinium based IL.

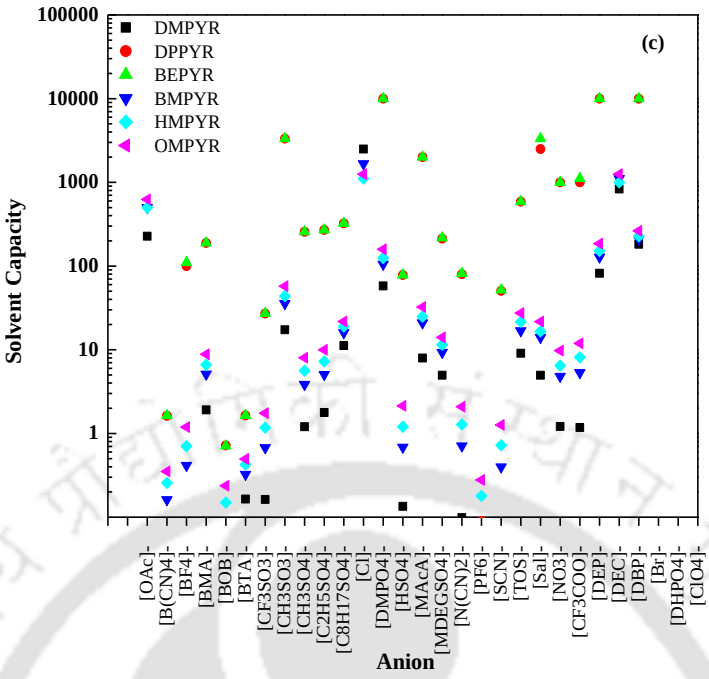


**Figure 4.2.3(c).** Solvent capacity values of α–Endosulfan at infinite dilution and at ambient temperature (T=25 °C) for pyrrolidinium based IL.

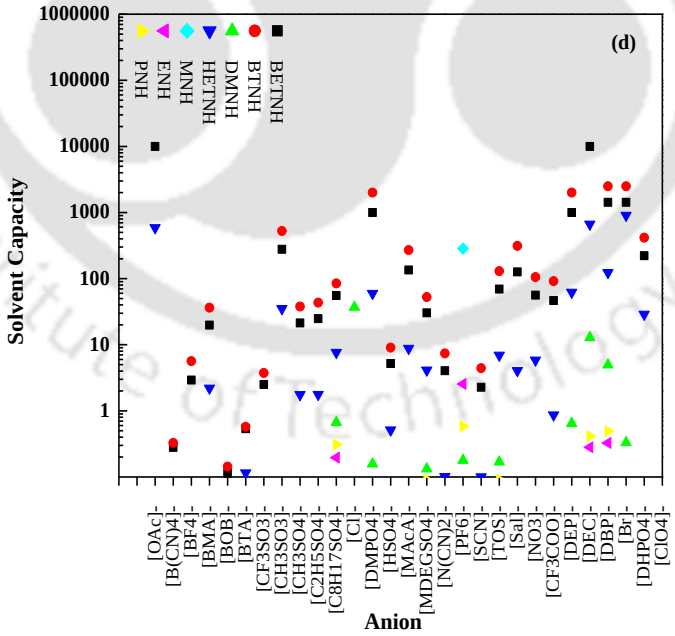


**Figure 4.2.3(d).** Solvent capacity values of α–Endosulfan at infinite dilution and at ambient temperature (T=25 °C) for ammonium based IL.

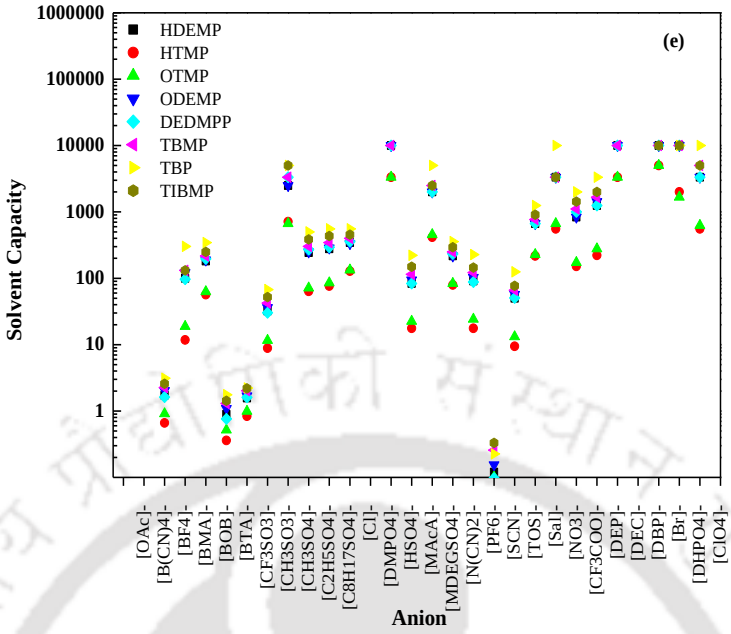


**Figure 4.2.3(e).** Solvent capacity values of α–Endosulfan at infinite dilution and at ambient temperature (T=25 °C) for phosphonium based IL.

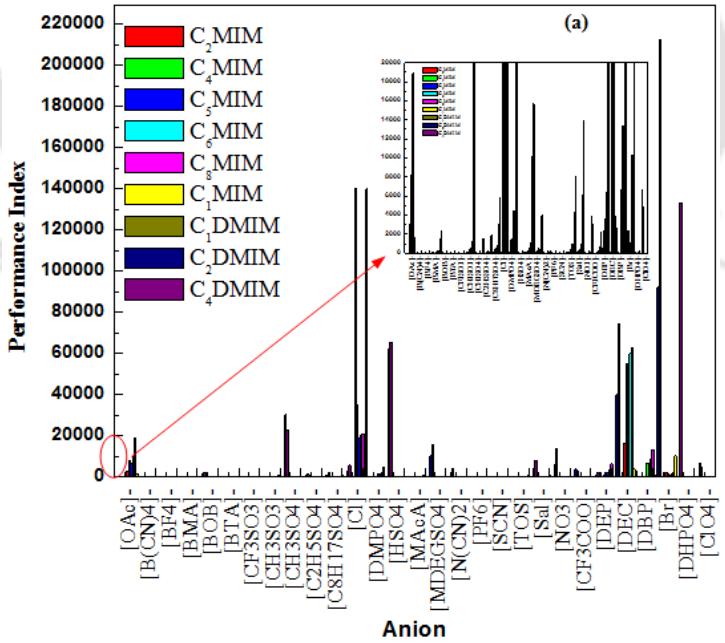


**Figure 4.2.4(a).** Performance index values of α–Endosulfan at infinite dilution and at ambient temperature (T=25 °C) for imidazolium based IL.

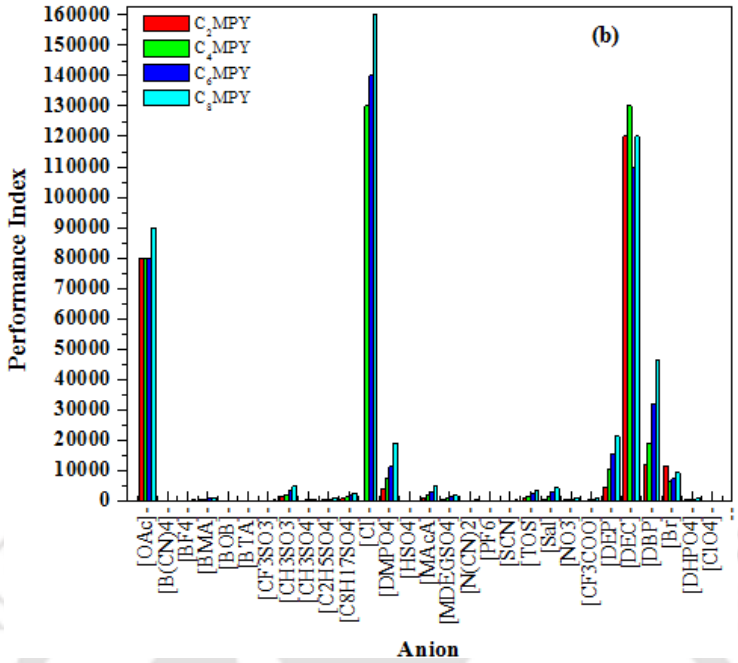


**Figure 4.2.4(b).** Performance index values of α–Endosulfan at infinite dilution and at ambient temperature (T=25 °C) for pyridinium based IL.

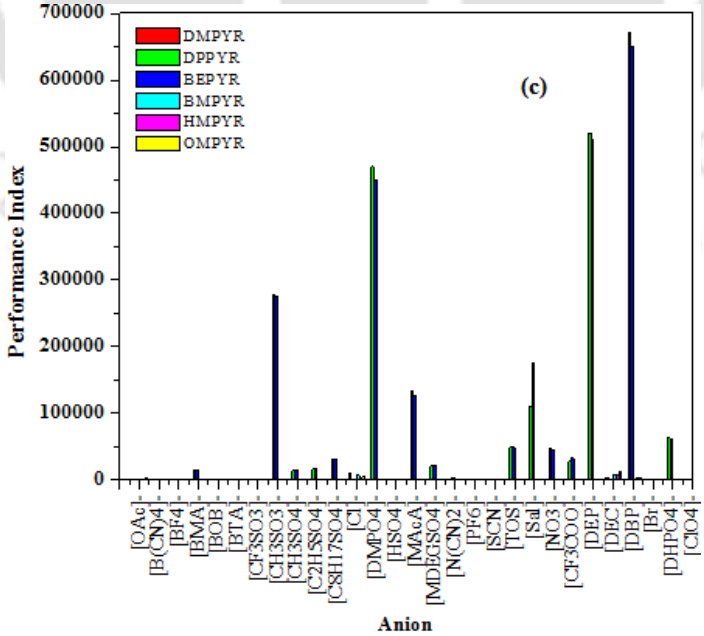

**Figure 4.2.4(c).** Performance index values of α–Endosulfan at infinite dilution and at ambient temperature (T=25 °C) for pyrrolidinium based IL.

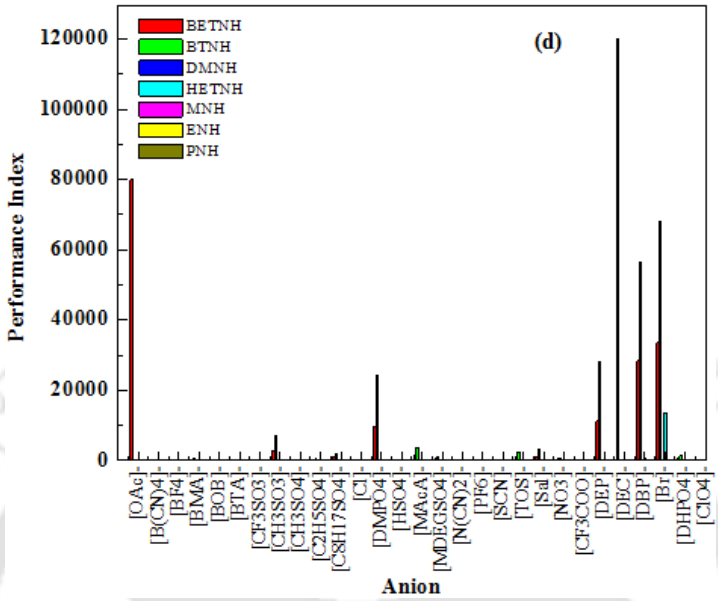


**Figure 4.2.4(d).** Performance index values of α–Endosulfan at infinite dilution and at ambient temperature (T=25 °C) for ammonium based IL.

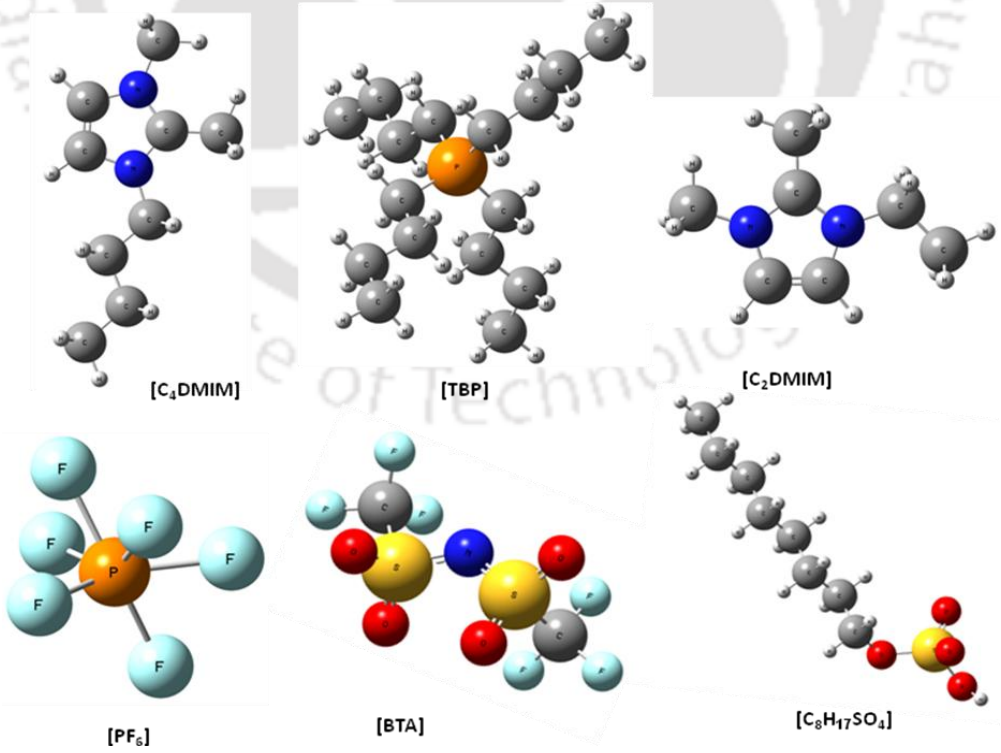

**Figure 4.3.1.** 3D structures of cations and anions studied.

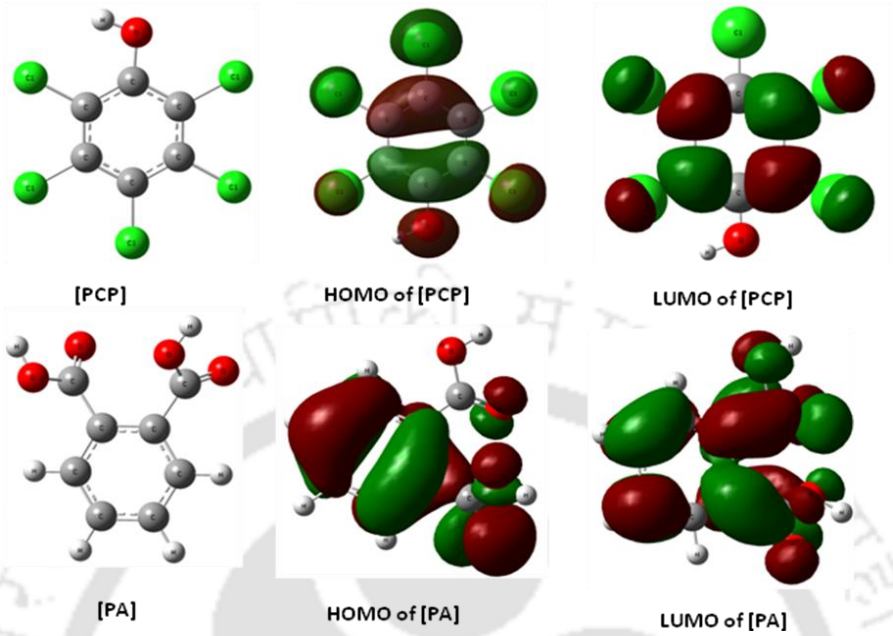


**Figure 4.3.2(a).** 3D structures and HOMO–LUMO energies projected on the van der Waals surface for [PCP] and [PA] using B3LYP/6-31G* method (green and dark red isosurfaces of HOMO and LUMO indicates positive and negative values, respectively).

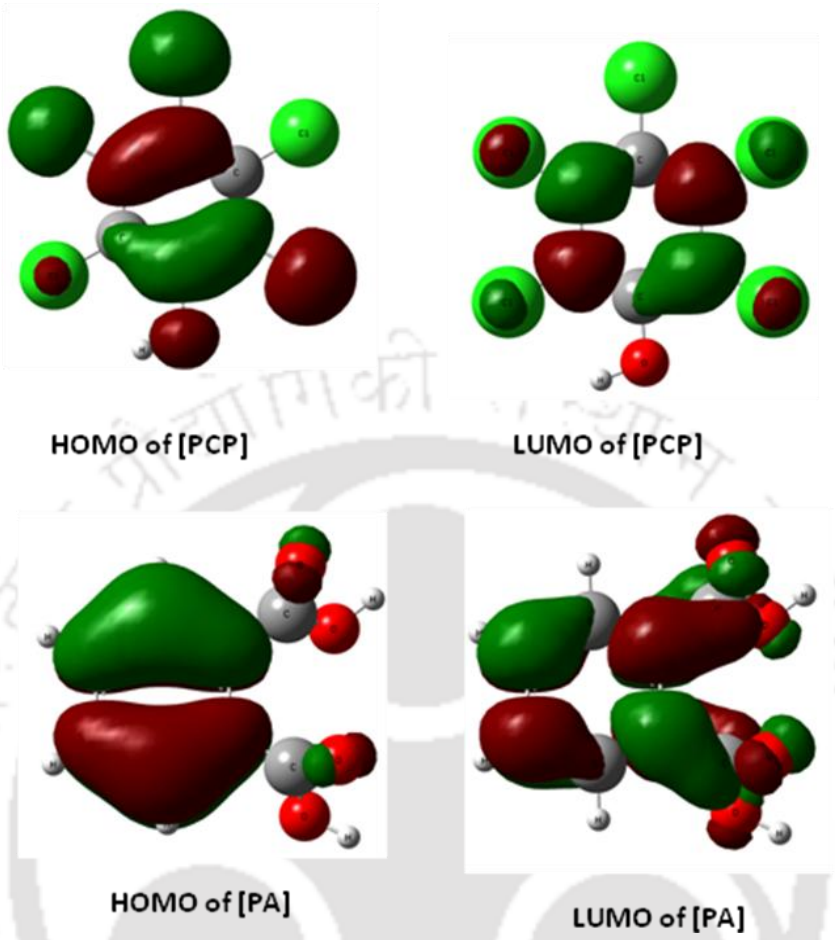


**Figure 4.3.2(b).** HOMO–LUMO energies projected on the van der Waals surface for [PCP] and [PA] using PM3/6-31G* method (green and dark red isosurfaces of HOMO and LUMO indicates positive and negative values, respectively).

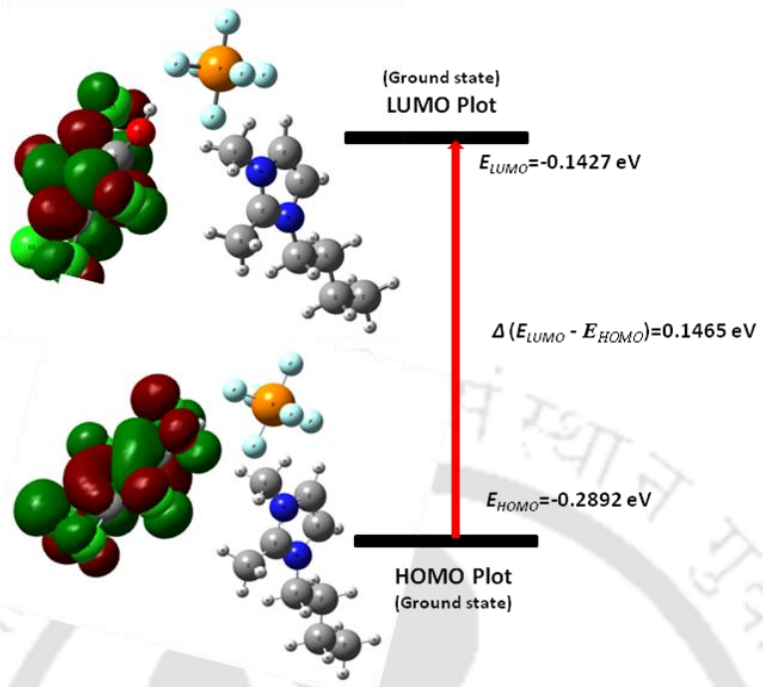


**Figure 4.3.3 (a).** Molecular orbital energy diagram projected on the van der Waals surface for the HOMO and LUMO of [PCP]+[$C_4$DMIM][$PF_6$] using B3LYP/6-31G* method.

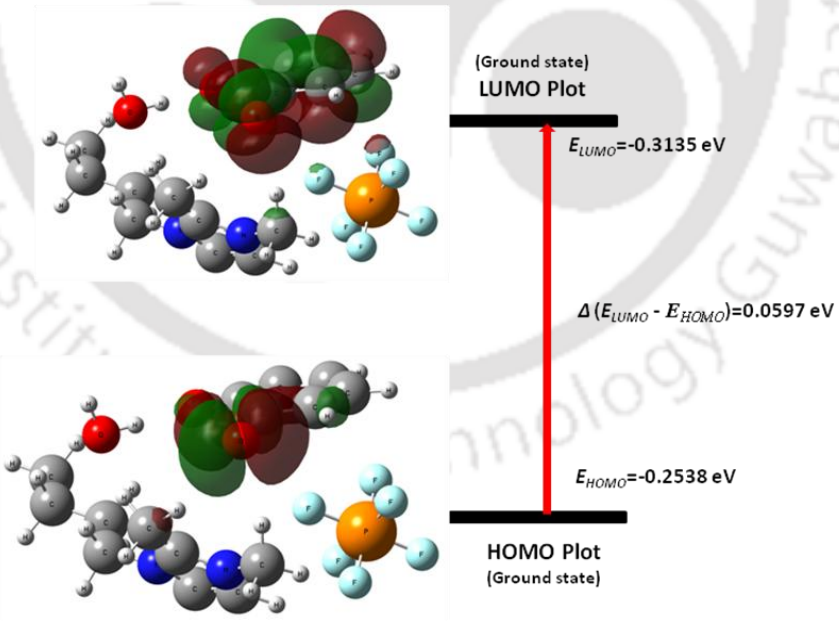


**Figure 4.3.3 (b).** Molecular orbital energy diagram projected on the van der Waals surface for the HOMO and LUMO of [PA]+[$C_4$DMIM][$PF_6$] using B3LYP/6-31G* method.

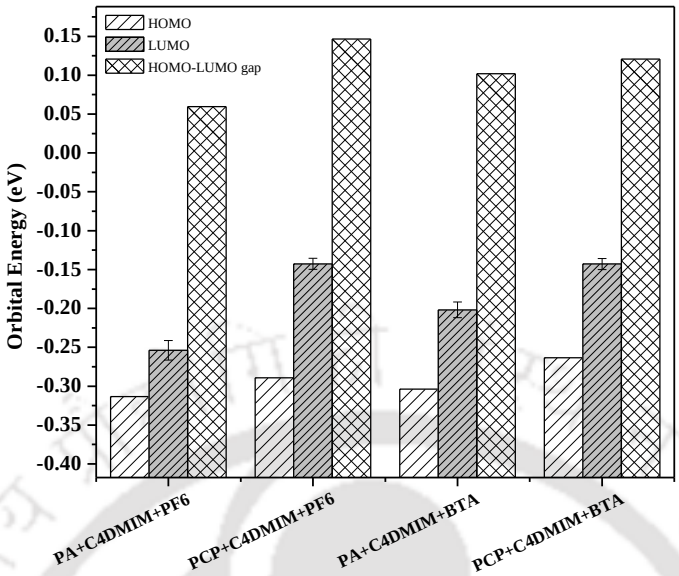


**Figure 4.3.4(a).** Energy level diagram (HOMO and LUMO energies and HOMO–LUMO energy gaps) of PA/PCP–IL complex molecules used in this study.

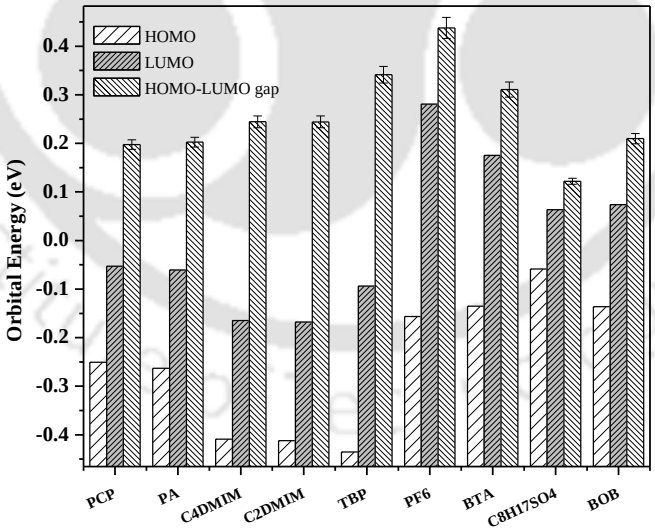


**Figure 4.3.4(b).** Energy level diagram (HOMO and LUMO energies and HOMO–LUMO energy gaps) of individual molecules used in this study.

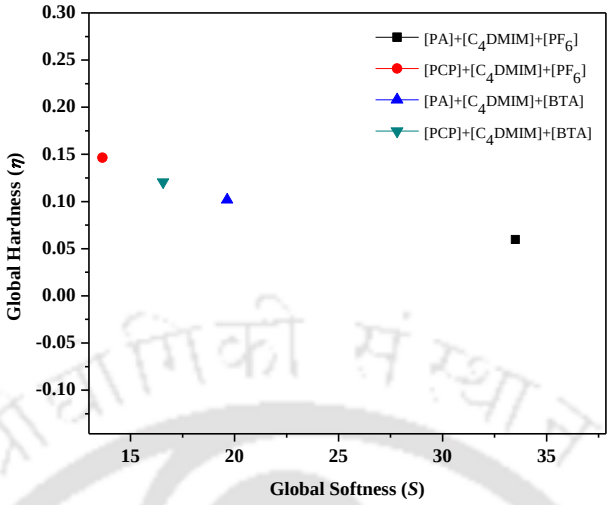


**Figure 4.3.5 (a).** Global hardness and softness of [PA] and [PCP] with [C4DMIM][PF6] ionic liquid complex.

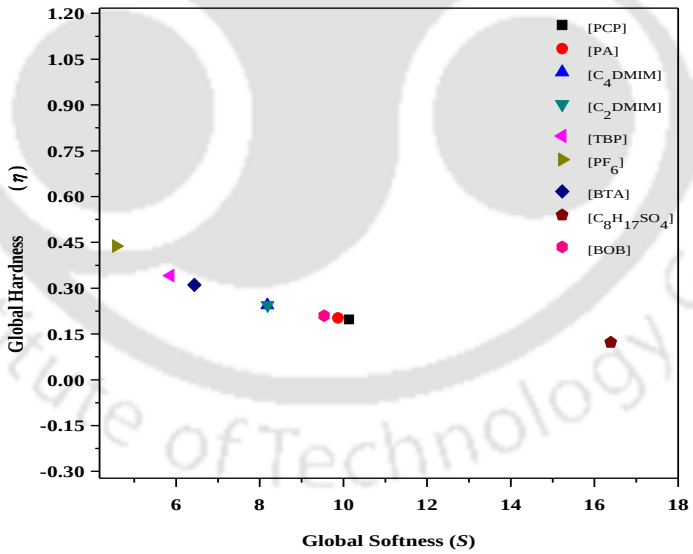


**Figure 4.3.5 (b).** Global hardness and softness of individual molecules used in this study.

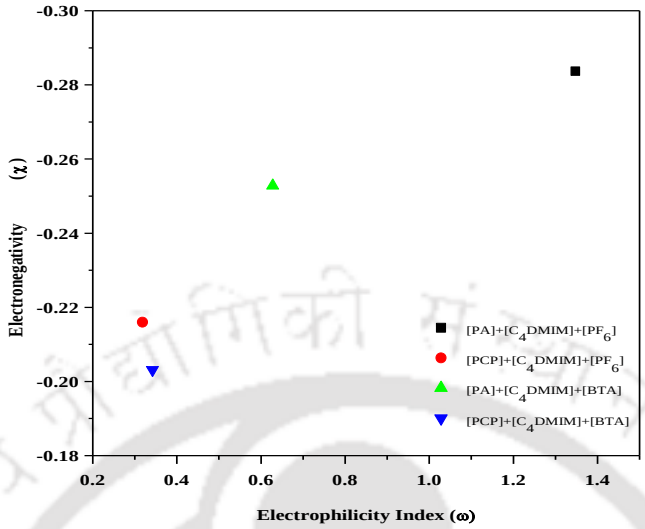


**Figure 4.3.6 (a).** Electrophilicity index vs Electronegativity of complex molecules used in this study.

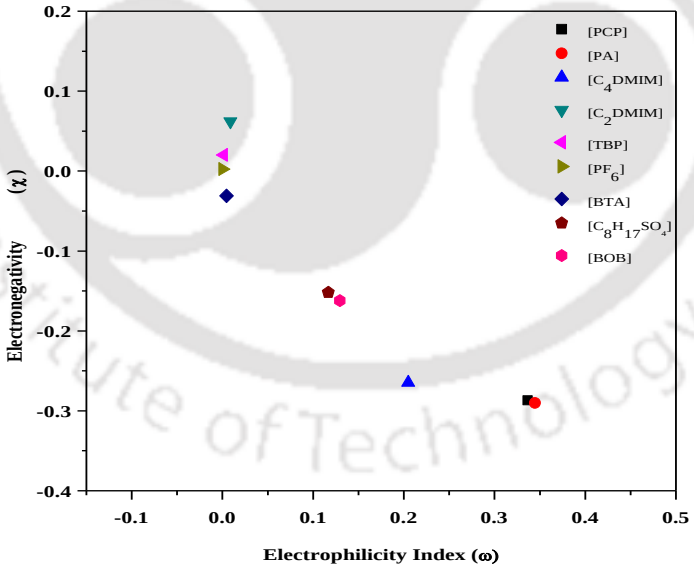


**Figure 4.3.6 (b).** Electrophilicity index vs Electronegativity of individual molecules used in this study.

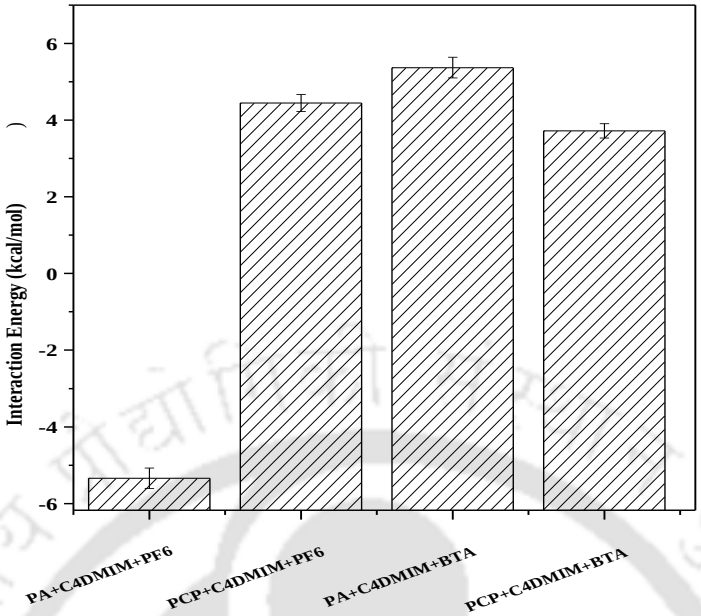


**Figure 4.3.7.** Interaction energy of PA/PCP–IL complex molecules.

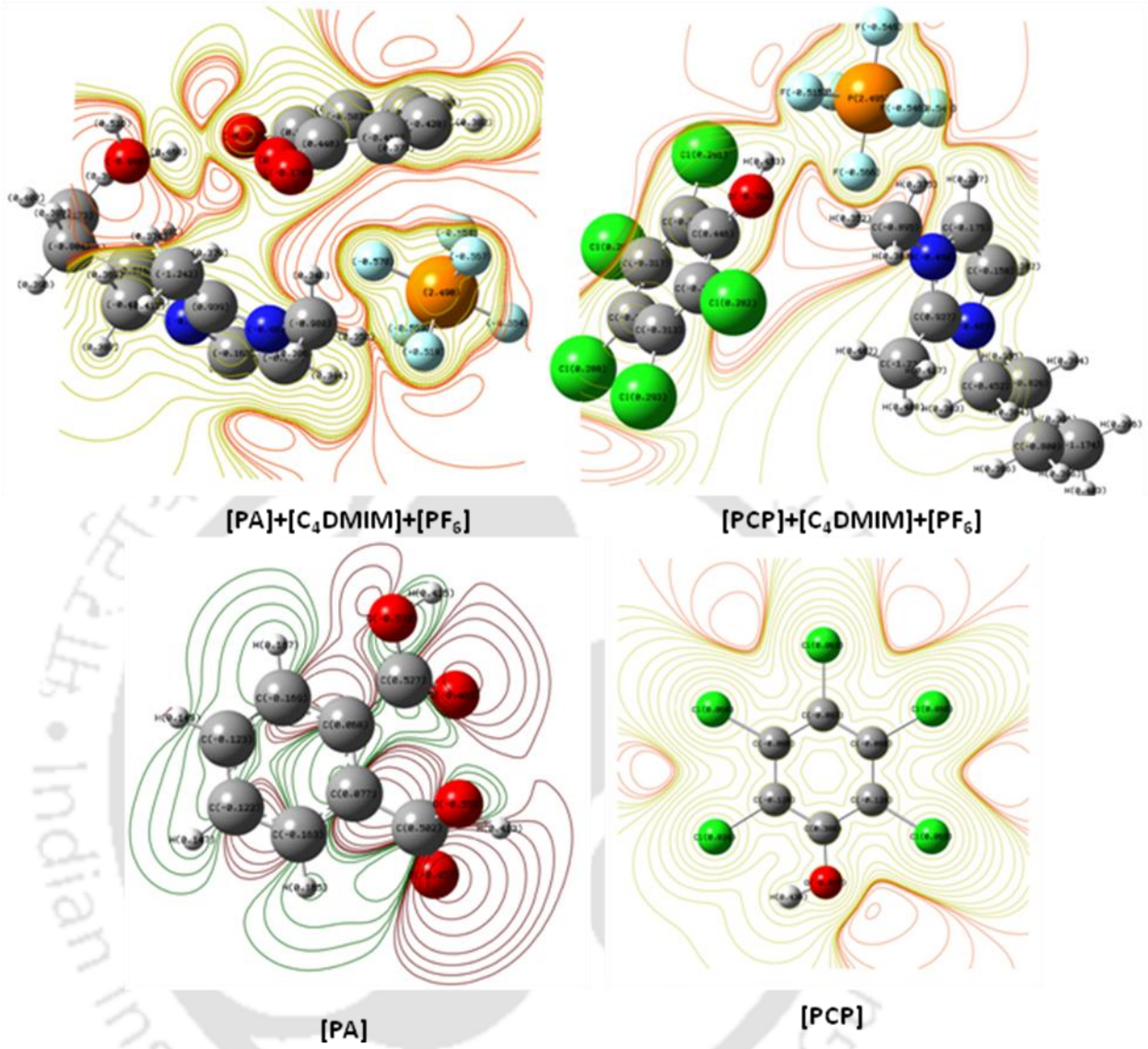


**Figure 4.3.8.** Contours of deformation of electron density of [PA] and [PCP] with [C4DMIM][PF6] with CHELPG charges using B3LYP/6-31G* method.

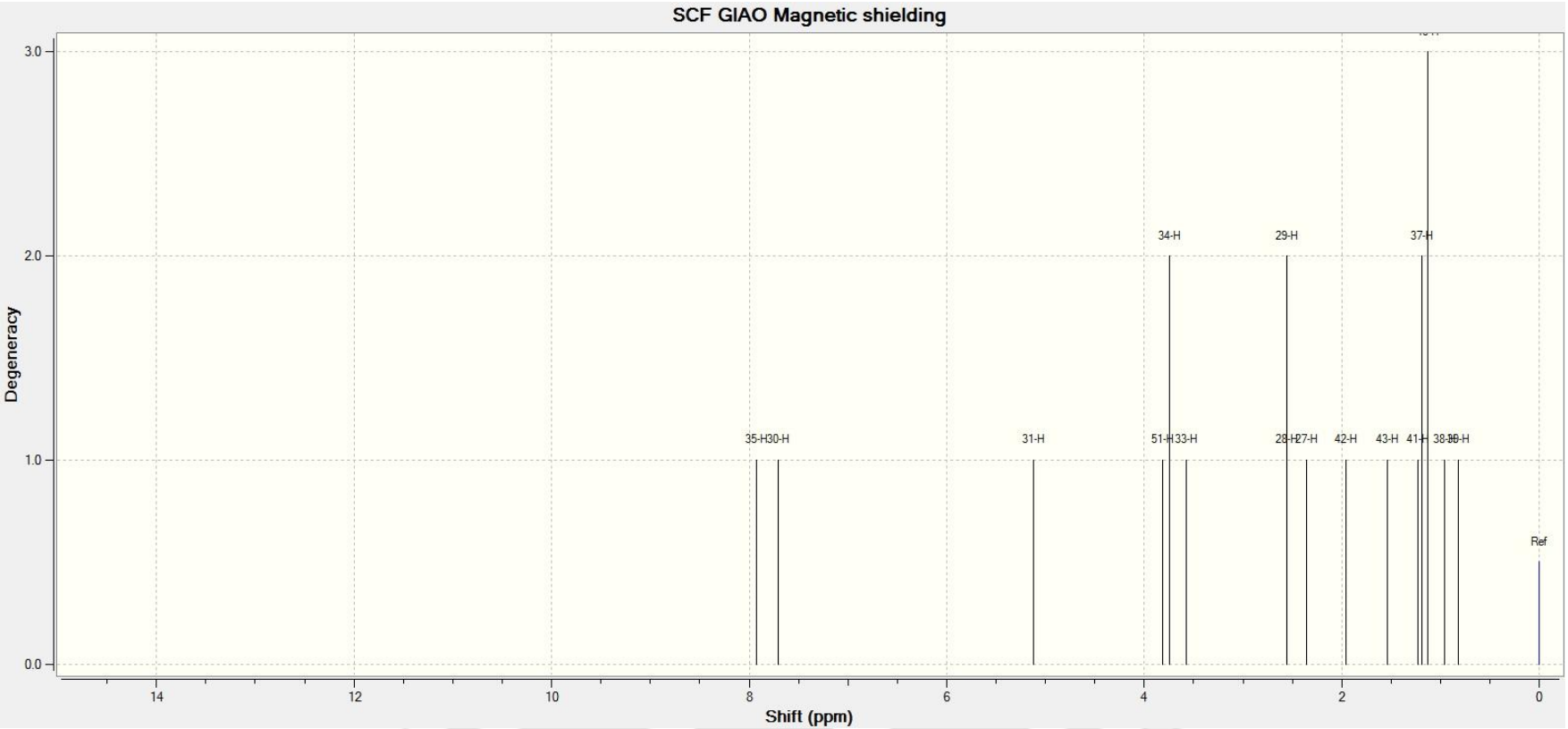


**Figure 4.3.9(a).**Theoretical $^{1}H$ NMR spectra of [PCP]+[$C_4$DMIM][$PF_6$] calculated using B3LYP/6-31G*.

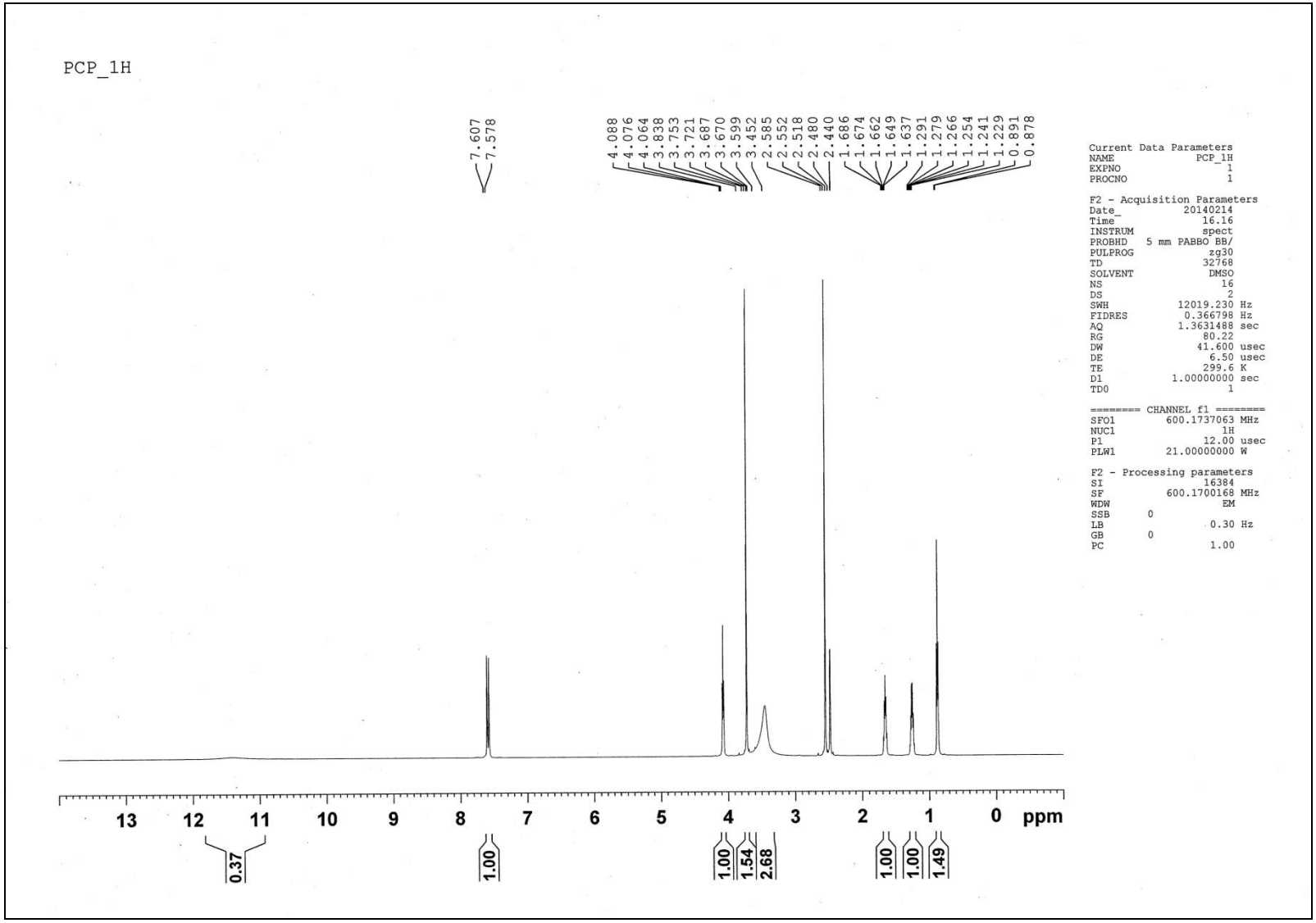


**Figure 4.3.9(b).** Experimental $^{1}H$ NMR spectra of [PCP]+[$C_4$DMIM][$PF_6$].

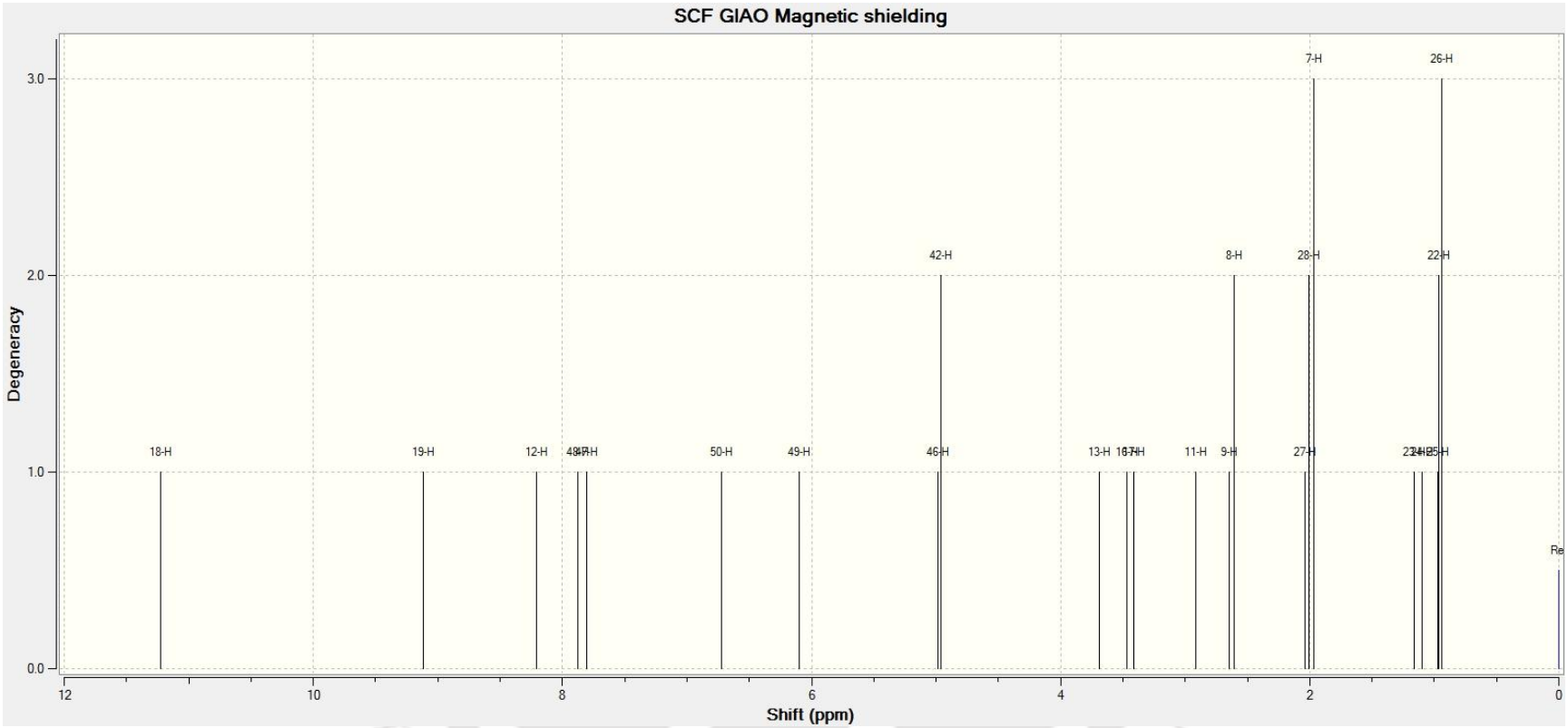


**Figure 4.3.10(a).** Theoretical $^{1}H$ NMR spectra of [PA]+[$C_4$DMIM][$PF_6$] calculated using B3LYP/6-31G*.

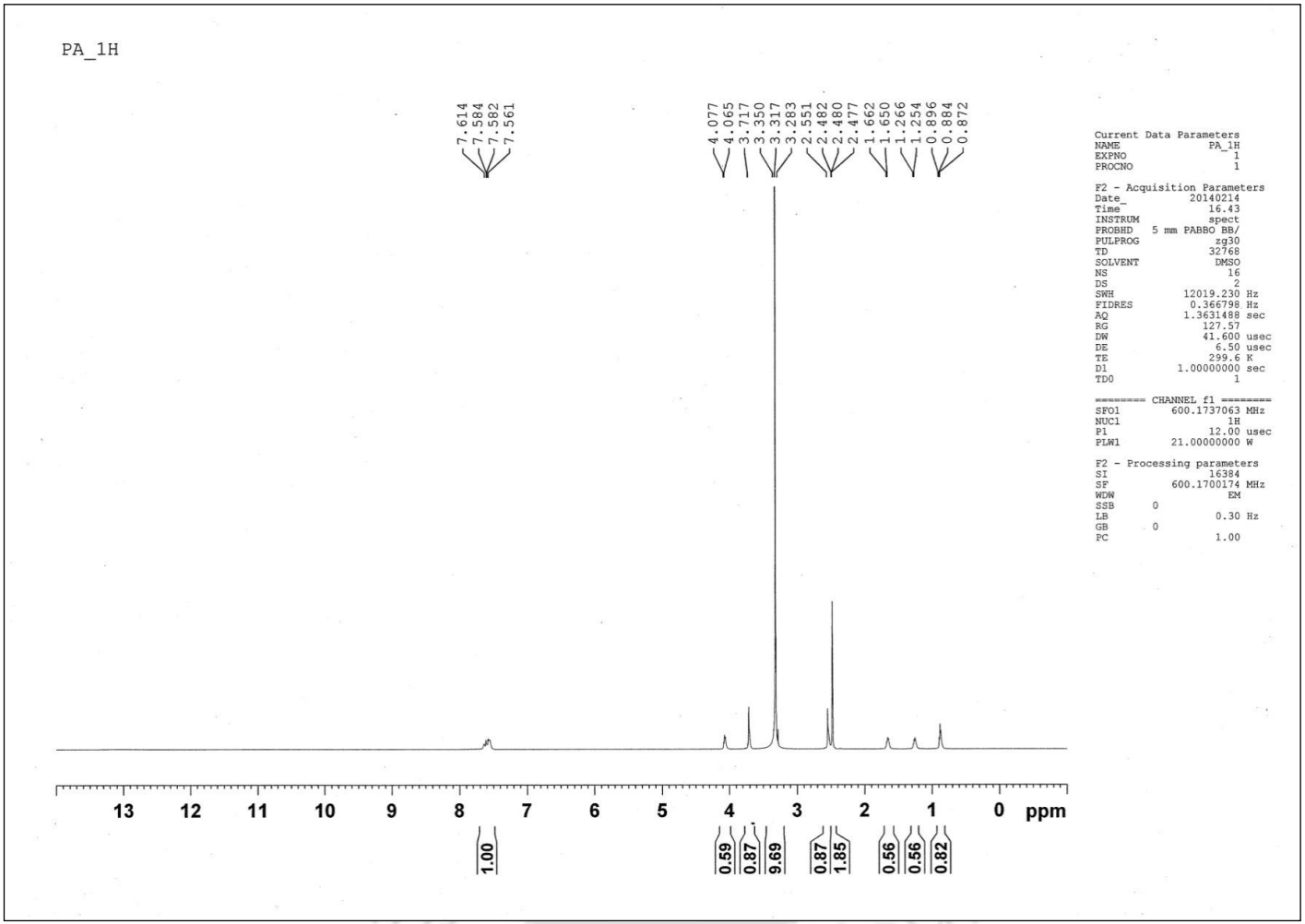


**Figure 4.3.10(b).** Experimental $^{1}H$ NMR spectra of [PA]+[$C_4$DMIM][$PF_6$].

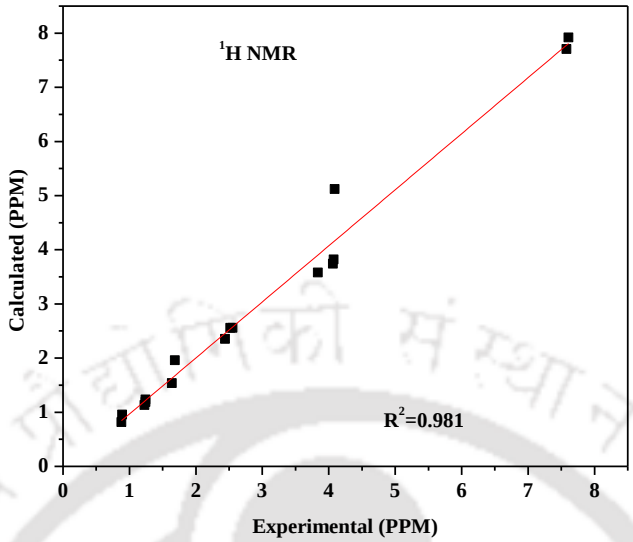


**Figure 4.3.11(a).** Correlation graphic between the experimental and calculated (B3LYP) chemical shifts of [PCP]+[$C_4$DMIM][$PF_6$] molecule.

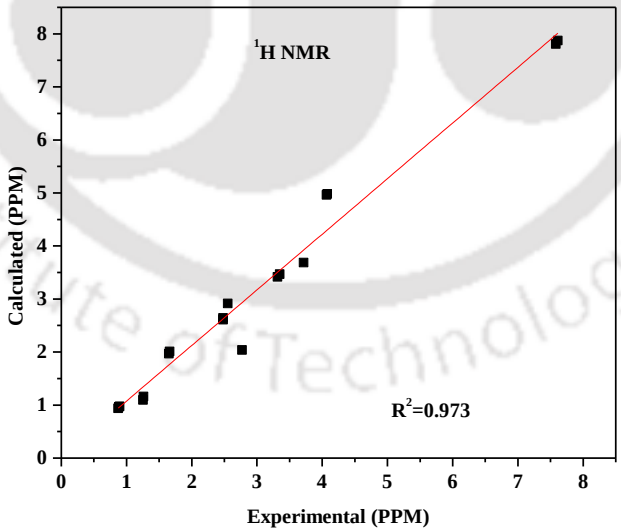


**Figure 4.3.11(b).** Correlation graphic between the experimental and calculated (B3LYP) chemical shifts of [PA]+[$C_4$DMIM][$PF_6$] molecule.

# CHAPTER 5

## LLE AND SILM EXPERIMENTS FOR EXTRACTION OF ENDOCRINE DISRUPTING COMPOUNDS FROM AQUEOUS SOLUTION

Chapter 5 puts an emphasis on the experimental work carried out in this thesis based on the results obtained in chapter 4. It covers the experiments conducted through LLE and SILM methods. As discussed in chapter 1, selected EDCs namely, phenol, endosulfan and PCP/PA were chosen for experimentation. The selection of ILs was on the basis of COSMO–RS method as explained in chapter 4. This chapter consists of four sections: LLE of PCP and PA (section 5.1), removal of phenol (section 5.2), removal of endosulfan (section 5.3) and removal of PCP (section 5.4) from aqueous solution using SILM experiments.

Liquid-Liquid extraction is a method by which a compound is extracted from solvent A to solvent B where solvents A and B are not miscible. This method is based on their relative solubilities in two different immiscible liquids, usually water and an organic solvent (IL). LLE works on the principle of chemical structure difference. Extraction methods differ depending upon the *density* of the solvent being used. It often offers a process with significantly reduced energy requirement, and as such can provide a cost effective process which has minimal energy utilization, a key factor for effective extraction of toxic compounds such as EDCs and also recovery and reuse of solvent. Section 5.1 reports the extraction of EDC compounds namely, PCP and PA from aqueous phase using imidazolium based IL [$C_4$DMIM][$PF_6$]. The IL was selected based on the selectivity as reported in section 4.1. An experimental study of LLE behavior of [$C_4$DMIM][$PF_6$](1)+PCP(2)+water(3) and [$C_4$DMIM][$PF_6$] (1) +PA (2)+water(3) was carried out at $T$=298.15 K and $p$=1 bar.

Further sections (5.2 to 5.4) discuses the SILM technology for the removal of phenol, endosulfan and PCP. Membrane based separation processes are getting appreciable attention

due to easy scaling, capability of integration with other process (hybrid processes) and adjustable characteristics of the membrane. Liquid membranes in general have certain advantages such as generation of large surface area in small equipment, simultaneous extraction and stripping in single step and high selectivity. Supported liquid membranes are especially favorable in terms of the stability problem associated with liquid membranes.

Extractants used in liquid membranes are mainly organic solvents such as aromatic and aliphatic hydrocarbons, amines, esters, ethers, ketones, and nitrated or chlorinated hydrocarbons. Most of these solvents are carcinogens as recognized by NIOSH, volatile at room temperature, non-biodegradable and are flammable. Search for better and greener solvents ends with room temperature ionic liquids (ILs) which have several advantages over the conventional organic solvents. More details and advantages and properties of ILs were already discussed in chapter 1. An experimental study was carried out for the removal of phenol, endosulfan and PCP from aqueous solutions using supported liquid membranes containing ionic liquid (IL) as the carrier solvent. The supported liquid membrane was prepared using hydrophilic polyvinylidene fluoride (PVDF) support immobilized in selected ILs and henceforth known as supported ionic liquid membrane (SILM). Vacuum immobilization method was used to prepare the SILM for the removal of EDCs. The details of the SILM preparation can be found from chapter 3. The effect of various parameters such as initial feed phase concentration, feed phase pH, operation time, stirring speed and membrane flux on the removal of EDCs have been investigated by using the different ILs. Additionally, the transport mechanism involving SILMs has also been elucidated. Moreover, characterization of SILM using SEM, EDX and FTIR was carried out in detail. The

operational stability of the SILM was tested continuously for an experimental run of 30 to 48 h.

## 5.1. LLE of PCP and PA from aqueous phase

In this work LLE experiments were carried out for two systems i.e. [$C_4$DMIM][$PF_6$] (1) + PCP (2) + water (3) and [$C_4$DMIM][$PF_6$] (1) + PA (2) + water (3) at 298.15 K. The obtained experimental tie lines for PA and PCP are given in Tables 5.1 and 5.2, respectively. Experimental and correlated tie lines are shown in ternary plots i.e. Figs. 5.1.1(a,b)–5.1.2(a,b). The LLE experiments were carried out to show the potential capability of [$C_4$DMIM][$PF_6$] for the extraction of PA and PCP from water. Important parameters in solvent extraction are the distribution coefficient (β) and the selectivity (*S*). The separation efficiency was examined by calculating the *S* and β which measures the difference in solubility of the compounds in two phases. The selectivity (*S*) (Eq. 5.1) and distribution coefficient (β) (Eq.5.2) can be defined as:

$$\text{Selectivity } (S) = \frac{\left(x^{E}_{effluent}\right) * \left(x^{R}_{water}\right)}{\left(x^{R}_{effluent}\right) * \left(x^{E}_{water}\right)} \tag{5.1}$$

$$\text{Distribution coefficient } (\beta) = \frac{\left(x^{E}_{effluent}\right)}{\left(x^{R}_{effluent}\right)} \tag{5.2}$$

Where, $x_{effluent}$ is the mole fraction of PA/PCP in the extract (E) and raffinate (R) phase respectively and $x_{water}$ is the mole fraction of water. The selectivity and distribution coefficients of the studied ternary systems are given in Tables 5.1 and 5.2. Here the selectivity values indicate a better ability for the IL to extract effluent from water phase,

where as the distribution coefficient concerns to the amount of IL used to achieve the separation. The distribution coefficient values lesser than unities are effectively useful and it also suggests lower solvent to feed ratio.

The IL ($[C_4DMIM][PF_6]$) used in this study was hydrophobic in nature which explains the it's negligible presence in the water rich phase (Tables 5.1-5.2). Thus, the points of raffinate phase will lie on the binary axis connecting water and PCP/PA. This also becomes economical and potential attractive technique as IL does not contaminate the aqueous phase as it simply extracts PA/PCP from the aqueous phase. The experimental and the correlated tie–lines for the system at (298.15 K) are shown in Fig. 5.1.1(a,b)–5.1.2(a,b). It is also observed from these figures that the point near to the 100% water suggests that entire PA/PCP is transferred to the extract phase. From the experiments it was also observed that the mole fraction of water in IL rich phase is approximately 18% in case of PA as noted in Table 5.1 and Fig. 5.1.1(a) and 5.1.2(b), whereas for PCP it ranges from 13–19% (Table 5.2 and Fig. 5.1.1(b) and 5.1.2(b). The selectivity values of PCP are higher than that of PA for all obtained mole fractions in the feed for $[C_4DMIM][PF_6]$ IL. The distribution coefficient and selectivity are particularly higher for most of lower concentrations of PCP and PA in the feed. Fig. 5.1.3 and 5.1.4 represents the plots of comparison of experimental selectivity and distribution coefficient versus mole fraction of PA and PCP respectively. As the quantity of PCP and PA in water samples are usually in trace (ppm level), these results are favorable for analyzing the potential of $[C_4DMIM][PF_6]$ for wastewater treatment.

Two different thermodynamic activity coefficient models namely NRTL and the

UNIQUAC models were used for the correlation of the experimental equilibrium data. These thermodynamic models have been used, since they are known to be able to explain the performance of IL based systems [Banerjee et al., 2005a]. The NRTL model [Renon and Prausnitz, 1968], gives the non–ideal liquid phase activity coefficient ($\gamma$) of component *i* by the following Eq.:

$$\ln \gamma_i = \frac{\sum_{j=1}^{c} \tau_{ji} G_{ji} x_j}{\sum_{k=1}^{c} G_{ki} x_k} + \sum_{j=1}^{c} \left[ \frac{G_{ij} x_j}{\sum_{k=1}^{c} G_{kj} x_k} \left( \tau_{ij} - \frac{\sum_{i=1}^{c} \tau_{ij} G_{ij} x_i}{\sum_{k=1}^{c} G_{kj} x_k} \right) \right] \tag{5.3}$$

where,

$$G_{ji} = \exp(-\alpha_{ji} \tau_{ji}) \tag{5.4}$$

The non–ideal activity coefficient for component *i* by UNIQUAC model [Abrams and Prausnitz, 1975] is represented by the following Eq.:

$$\ln \gamma_i = \ln\left(\frac{\Phi_i}{x_i}\right) + \frac{z}{2} q_i \ln\left(\frac{\theta_i}{\Phi_i}\right) + l_i - \frac{\Phi_i}{x_i} \sum_{j=1}^{c} x_j l_j + q_i \left( 1 - \ln \sum_{j=1}^{c} \theta_j \tau_{ji} - \sum_{j=1}^{c} \frac{\theta_j \tau_{ij}}{\sum_{k=1}^{c} \theta_k \tau_{kj}} \right) \tag{5.5}$$

where $$\tau_{ji} = \frac{g_{ji} - g_{ii}}{RT} = \frac{A_{ji}}{T} \tag{5.6}$$

$$\theta_i = \frac{q_i x_i}{q_T} \tag{5.7}$$

$$q_T = \sum_k q_k x_k \tag{5.8}$$

$$\Phi_i = \frac{r_i x_i}{r_T} \tag{5.9}$$

$$r_T = \sum_k r_k x_k \tag{5.10}$$

$$l_i = \frac{z}{2}(r_k - q_k) + 1 - r_k \tag{5.11}$$

In the above Eqs. (5.3–5.9), $\theta$, $\tau$ and $\Phi$ correspond to the area fraction, interaction parameter and segment fraction, respectively. In Eq. (5.6), $g_{ij}$ represents the average interaction energy for the interaction of molecules of component $j$ with molecules of component $i$, $R$ stands for the gas constant and $T$ is the temperature in K. The surface area parameter of pure-component and the volume parameter of the pure-component in the UNIQUAC model are represented by $r$ and $q$, respectively, where, $r$ is the relative van der Waals volume and $q$ *is* the surface area of the pure component. The coordination number can be represented by $z$ (=10) and the mole fraction in the liquid phase is represented by $x$. The detailed methodology and applications were given elsewhere [Banerjee et al., 2005a].

The objective function ($F$) for minimizing the total error between the experimental and correlated mole fractions was defined as:

$$\text{Maximize}: \quad F_{\left(\begin{array}{l}\text{with respect to } A_{ij} \\ \text{where } i,j=1,2,3 \\ \text{and } j\neq i\end{array}\right)} = -\sum_{k=1}^{m}\sum_{l=I}^{II}\sum_{i=1}^{c} w_{ik}^{l}\left(x_{ik}^{l} - \hat{x}_{ik}^{l}\right)^2 \quad , \quad w_{ik}^{l} = 1 \tag{5.12}$$

$$\text{RMSD}\,(\%) = \left(-\frac{F}{2mc}\right)^{1/2} = \left[\sum_{k=1}^{m}\sum_{l=I}^{II}\sum_{i=1}^{c}\frac{\left(x_{ik}^{l} - \hat{x}_{ik}^{l}\right)^2}{2mc}\right]\times 100 \tag{5.13}$$

The binary interaction parameters were obtained from the experimental LLE data by minimizing the objective function, which was defined as the sum of the square of errors between the experimental and calculated compositions of all the components over the entire

set of tie lines as per Eq. (5.12). The deviation of the fit was measured by the root mean square deviation (RMSD) as defined in Eq. (5.13). The modified Rachford–Rice algorithm [Seader and Henley, 2005] was used to compute the tie lines. For the UNIQUAC model, the UNIQUAC structure parameters $r$ and $q$ of the IL were predicted using the Polarizable Continuum Model (PCM) with GEPOL algorithm as given in the previous works [Rao, 1997; Banerjee et al., 2005b]. The estimation of $r$ and $q$ values of the IL has been calculated using the following Eq.:

$$r_{pred} = \frac{\left(V^{PCM} \text{ in Å}^3\right)\left(1\times10^{-8} \text{ cm}\right) N_{av}}{V_{ws}} \tag{5.14}$$

$$q_{pred} = \frac{\left(A^{PCM} \text{ in Å}^2\right)\left(1\times10^{-8} \text{ cm}\right)^2 N_{av}}{A_{ws}} \tag{5.15}$$

where, $N_{av}$ is the Avogadro's number. The standard segment volume $Vws$ (15.17 $cm^3$ $mol^{-1}$) and area $Aws$ (2.5 × 109 $cm^2$ $mol^{-1}$) are also reported in literature [Banerjee et al., 2005a]. The output file of PCM contains the overall surface (APCM) and the overall volume (VPCM) of the ionic liquid under consideration. The $r$ and $q$ values for the components were used in predictions as represented in Table 5.3. It has been noted that the parameters $\tau_{ij}$ and $A_{ij}$ are fitted parameters for both NRTL and UNIQUAC models, and has thus no physical interpretation. Different runs of GA [Banerjee et al., 2005b] with number of generations 200 and the population size of 100 will gave different values of parameters. The experimental data was fitted by maximizing the objective function via Eq. (5.14). In the present calculations, $\alpha_{ij}$= $\alpha_{ji}$=0.2 has been used, where α is NRTL non-randomness parameter. It can be seen from Figs. 5.1.1(a,b) and 5.1.2(a,b) that the NRTL and UNIQUAC correlated tie–

lines overlaps with the experiment tie–line data. Fig. 5.1.1(a) and Fig. 5.1.2(b) represents the experimental and NRTL correlated tie lines for [$C_4$DMIM][$PF_6$] (1) + PA (2) + water (3) and [$C_4$DMIM][$PF_6$] (1) + PCP (2) + water (3) systems at 298.15 K. Similarly, Fig. 5.1.1(b) and Fig. 5.1.2(a) shows the experimental and correlated tie-lines using UNIQUAC model for [$C_4$DMIM][$PF_6$] (1) + PCP (2) + water (3) and [$C_4$DMIM][$PF_6$] (1) + PA (2) + water (3) systems respectively at 298.15 K. The RMSD values of both systems are 0.35% and 0.46% respectively as reported in Table 5.4. The RMSD values of both systems are 0.54% and 0.41% respectively as described in Table 5.4. The NRTL and UNIQUAC binary interaction parameter values are shown in Table 5.4. Similarly, Table 5.5(a), 5.5(b), 5.6(a) and 5.7(b) represents the calculated UNIQUAC and NRTL tie–line values for water and IL rich phase for corresponding experimental values in mole fraction for [$C_4$DMIM][$PF_6$] (1) + PA (2) + water (3) at $T$=298.15 K and for [$C_4$DMIM][$PF_6$] (1) + PCP (2) + water (3) at $T$=298.15 K.

Finally, the reliability of tie–line data was validated by using two different models, i.e. Othmer–Tobias (Eq. 5.16) and Bachman (Eq. 5.17) correlation Eqs. [Chen et al., 2007].

$$\left(\frac{1-x_R}{x_R}\right) = A + B\ln\left(\frac{1-x_E}{x_E}\right) \tag{5.16}$$

$$x_R = A + B\left(\frac{x_R}{x_E}\right) \tag{5.17}$$

The correlation parameters of the Othmer–Tobias and Bachman models are presented in Table 5.7. The Bachman correlation is an empirical equation describing the distribution of components in the three–component of two phase liquid system. From Fig. 5.1.5 and 5.1.6, the Othmer–Tobias and Bachman plots exhibit a good linear fit and indicate the excellent

quality of the obtained experimental LLE results in this work. The observed correlation factor ($R^2$) was 0.955 and 0.969 for [$C_4$DMIM][$PF_6$] (1) + PA (2) + water (3) and [$C_4$DMIM][$PF_6$] (1) + PCP (2) + water (3) respectively. Similarly, the reliability of tie–line data for [$C_4$DMIM][$PF_6$] (1) + PA (2) +water (3) and [$C_4$DMIM][$PF_6$] (1) + PCP (2) +water (3) was validated for Bachman correlation, where correlation factor ($R^2$) values are 0.94 and 0.855 respectively. A correlation factor of unity suggests a higher degree of consistency of the related data.

## 5.2. Removal of phenol from Aqueous phase using SILM

The effects of concentration of phenol in feed phase with time, effects of concentration of phenol in stripping phase with time, rates of permeation of phenol with different ILs, rate of permeation of phenol at different pH conditions were studied and the results are discussed in this section.

### *5.2.1. Effect of time on phenol concentrations in feed and stripping phase for different ionic liquids*

The change in concentration of phenol in feed phase and stripping phase with respect to time are shown in Figs. 5.2.1 and 5.2.2. The initial feed concentration of phenol was fixed at 100 mg $L^{-1}$. Fig. 5.2.2 shows the effect of feed phase concentration with time for different ILs at feed phase pH of 5.6 (natural pH of the feed). From Fig. 5.2.2, it can be seen that the concentration of phenol decreased very sharply in feed side within 12 h of transport experiment while reaching a steady state at around 24 h. Thereafter no variation was

observed with operating time. Out of the six ionic liquids used, approximately 53.2 mg $L^{-1}$ (73.63%) of phenol present in the feed phase was transported to permeate side within 24 h via SILM consisting of [CYPHOS® 104] at feed pH of 5.6. Table 5.9 gives the complete details of the different ionic liquid membranes used and their corresponding feed concentration and percentage rate of permeation after 24 h of transport experiment. For phosphonium based ionic liquids, it was observed that the concentration of phenol decreased with time with an increase in the length of alkyl chain on the cation of the phosphonium ionic liquid. The anion bis(2,4,4-trimethylpentyl) phosphinate gave better separation than that of chloride anion. This was due to stronger hydrogen-bonding between bis(2,4,4-trimethylpentyl) phosphinate and phenol compound. The chloride anion gave very poor separation, may be due its high solubility in water.

The order the permeation rate of ILs for a given phenol concentration at a feed pH of 5.6 was as follows: [CYPHOS® 104] > [CYPHOS® 103] > [CYPHOS® 102] > [CYPHOS® 101] > [$C_8$MIM][$PF_6$] > [Aliquat 336®] under the same experimental conditions. On the other hand, Fig. 5.2.2 shows the effect of phenol concentration in stripping side with respect to time for the six different ILs used. 0.1 N NaOH was used as stripping agent. The concentration of phenol in the stripping phase increased with increasing time (Fig. 5.2.2). It was observed that the concentration of phenol in the stripping phase increased sharply within first 8-12 h of transport experiment thereby slowly reached to equilibrium. Hence, the phenol present in the feed phase was transported to the permeate side after 24 h of the transport experiment. As mentioned above highest rate of permeation of (at pH=5.6) was observed for [CYPHOS–104].

Among the six ILs used, [CYPHOS–104] gave the highest extraction of phenol (53.21 mg $L^{-1}$) from feed phase. Similarly, [Aliquat–336] was gave poor (44.47 mg $L^{-1}$) performance when compared with phosphonium based ILs. Marták *et al.*, [Marták et al., 2008] reported that phosphonium based ILs were highly hydrophobic which ultimately improves the stability of SILM. More details about the stability of the supported liquid membranes were reported elsewhere [Kemperman et al., 1996].

### *5.2.2. Rate of permeation and membrane flux*

The permeation rate was calculated as per the following formula:

$$\text{Rate of permeation (\%)} = \frac{C_{R,24h}}{C_{F,0}} \times 100 \tag{5.18}$$

where $C_{R,24\ h}$ is the concentration of phenol in receiving phase after 24 h, $C_{F,0}$ is initial concentration of phenol in feed phase.

The rate of permeation of phenol in different ILs through the SILM is presented in Fig. 5.2.3(a). [CYPHOS–104] was observed to give better permeation, whereas other ILs such as [Aliquat–336] and [$C_8$MIM][$PF_6$] did not give good permeation as compared to phosphonium ILs. Lowest rate of permeation of phenol was given by Aliquat–336 and [$C_8$MIM][$PF_6$] with the corresponding values of 32.43% and 35.11% respectively. The permeation rates followed the order: [CYPHOS® 104] > [CYPHOS® 103] > [CYPHOS® 102] > [CYPHOS® 101] > [$C_8$MIM][$PF_6$] > [Aliquat 336®]. From the literature [Stannett, 1978] important observations made for the rate of permeation are: (i) permeation is independent of pressure, (ii) increase in temperature lead to decrease in penetrant solubility,

but made the membrane more permeable, (iii) prolonged exposure to elevated temperature affected the retention capacity of the membrane; (iv) variation in membrane thickness altered the permeation rate but not the separation characteristics of the polymer

The membrane flux measures the number of moles or amount of substance diffusing per unit time and unit effective contact area of the membrane. The flux can be calculated by the following Eq.

$$J = -\left(\frac{V}{A}\right) \times \left(\frac{dC}{dt}\right) \tag{5.19}$$

Where, $V$ is the stripping phase volume in $m^3$; $A$ is the contact area of the membrane in $m^2$; $C$ is the concentration of phenol in the receiving phase in mol $L^{-1}$ and $t$ is the time elapsed in $s$. The SI unit of membrane flux is mol $m^{-2}$ $s^{-1}$. The membrane fluxes were measured every time with fresh membrane, feed as well as stripping solutions so that the same driving force for each flux measurement can be obtained. [CYPHOS-104] ionic liquid was used as the membrane phase for flux measurements. Fig. 5.2.3(b) describes the variation of permeate flux with operation time. The initial feed phenol concentration used was 100 mg $L^{-1}$. 0.1 N NaOH was used as the stripping phase and the feed phase pH was 5.6. From Fig. 5.2.3(b), it can be seen that the permeate flux decreased sharply within 10 h of operation and later on reached to steady state. Severe flux decline was observed which could be due to the membrane fouling. Vigorous membrane fouling may thus require cleaning or replacement of membrane.

### 5.2.3. *Effect of stirring speed*

The rotation speed of the magnetic spinbars in feed phase and stripping phase compartments of the permeation cell was controlled by magnetic stirrer. The concentration polarization at the interface of the ionic liquid membrane can be avoided by continuous mechanical stirring of the feed as well as stripping phase. Stirring speed was varied from 100 to 400 rpm (Fig. 5.2.4) to find out the optimum stirring speed that permits effective diffusion of phenol through the SILM. Permeability was increased when the stirring speed was increased from 100 to 300 rpm. This shows that the aqueous boundary layer thickness decreased by increasing the stirring speed. For stirring speed above 300 rpm the permeation rate started to decrease. This was due to the high speeds that lead to the displacement of ionic liquid from pores of the support. The optimum rotation speed reduces the mass transfer resistance and due to this reason 300 rpm was chosen as the optimum rotation speed throughout the investigation. Thus the mass transfer rate from feed to permeate side will be affected by solubility and the diffusivity of the phenol in the immobilized IL phase. The separation rate is also influenced by the properties of solid support such as porosity of the membrane, thickness of the membrane and tortuosity of the membrane pores [Adnan,et al., 2012].

### 5.2.4. *Effect of feed phase pH on rate of permeation*

Fig. 5.2.5 shows the effect of feed phase pH on the performance of SILM. In this experiment the feed phase pH was varied from 4 to 7.5 by adjusting with 1 M HCl or 1 M NaOH solution, 0.1 N NaOH was used as a stripping agent as mentioned above. From Fig. 6

it was noted that the pH of feed phase did not have much positive effect on the removal of phenol. The highest permeation rate of 75.70% was achieved by [CYPHOS-104] at pH 4. Similarly, at pH 7.5 the rate of permeation was 69.86% for the same ionic liquid. It was found that phenol permeation rate was increased only by ~6% when the feed phase pH was varied from 4–7.5. Phenol exists in two different forms in aqueous phase depending on it's $pK_a$ value. The $pK_a$ value of phenol is approximately within 9.2-9.6 as reported elsewhere [Fan et al., 2008]. If the pH of the solution containing phenol is higher than the $pK_a$ value, then phenol dissociates to form phenolate ions ($C_6H_5O^-$) and below it's $pK_a$ value, phenol exists in it's molecular form [http://en.wikipedia.org/wiki/Phenol]. It was reported by several earlier researchers that at pH ≥ $pK_a$, there was drastic decrease in phenol removal. That is why in this work, feed phase pH was varied between 4 to 7.5. Shen *et al.* [Shen et al., 2009] have come up with similar conclusion for the phenol recovery with tributyl phosphate in a hollow fiber membrane contactor. The extraction process decreased because of the increase in the dissociation of phenol at pH > pKa which is in agreement with the results reported by Reis *et al.* [Reis et al., 2007]. Similar kind of phenomenon was also observed in literature [Fan et al., 2008; Vidal et al., 2005; Khachatryan et al., 2005].

### *5.2.5. Phenol transport mechanism*

Fig. 5.2.6 illustrates the detailed transport mechanism of phenol in SILM. It was envisaged that diffusion of phenol from feed phase to stripping phase through SILM occurred via simple permeation process. From the previous section it was confirmed that phenol remains in it's molecular form under pH < $pK_a$, hence phenol in molecular form was

transported via SILM. The proposed mechanism (Fig. 5.2.6) consists of molecular form of phenol dissolved in SILM due to its high distribution coefficient between trihexyl(tetradecyl)phosphonium bis(2,4,4-trimethylpentyl)phosphinate ([CYPHOS® 104]) and water. The extraction of phenol depends on formation of H–bonding between the molecular phenol and the anion of the ionic liquid. The ionic liquid here may act as H–donor. Molecular phenol in the feed solution diffused towards the interface. The formation of a complex between phenol and ionic liquid takes place which then permeates through the membrane to the receiving phase due to the concentration gradient, where it reacts with 0.1 N NaOH to produce sodium phenolate ($C_6H_5O^-Na^+$) (Eq. 4). In most cases the phenolic compounds have very weak tendencies to lose the $H^+$ ions from the hydroxyl group, leading to the formation of sodium phenolate ion and water [http://en.wikipedia.org/wiki/Phenol]. Since sodium phenolate is insoluble in membrane phase, thus it was trapped in the stripping phase and under the present experimental conditions it cannot diffuse back to the feed phase.

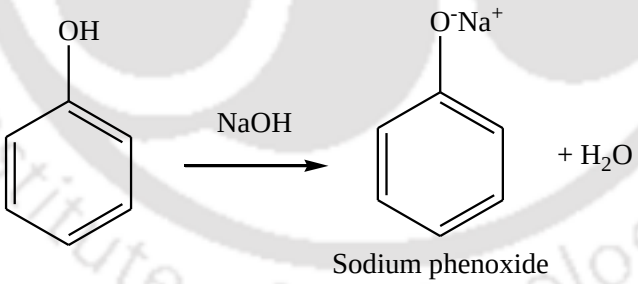


Sodium phenoxide (5.20)

Sodium hydroxide concentration (stripping phase) was varied from 0 to 0.5 N to study the effect of concentration of the stripping agent. The phenol removal percentage at these concentrations for the experimental run of 4 to 10 h showed that the concentration of NaOH is not a significant factor for phenol removal. This agrees well with the findings of literature [Wang et al., 1994; Venkateswaran and Palanivelu, 2006].

### *5.2.6. Characterization of PVDF membrane*

Characterization of the membrane surface morphology was done by scanning electron microscope (SEM, *LEO, Model 1430VP)* and energy dispersive X–ray (EDX) analysis. The characterization of membrane was used to study the influence of the vacuum immobilization method on the SILMs performance [de los Ríos, et al., 2007]. SEM micrographs gave the morphological information of the distribution of the IL within the membrane pores where as the EDX spectra gave elemental composition of the membrane. Fig. 5.2.7(a) and (b) shows examples of SEM micrographs of a blank PVDF membrane and supported liquid membranes based on $[C_8MIM][PF_6]$ respectively. From Fig. 5.2.7(a) it can be observed that pores of the PVDF membrane were completely unfilled and no material was present inside the pore. Fig. 5.2.7(b) shows the morphological study of membrane after vacuum immobilization technique with $[C_8MIM][PF_6]$. The surface morphology study showed that the ionic liquid was homogeneously distributed within the smaller pores of the membrane whereas the larger macropores were partially filled with ionic liquid. From Fig. 5.2.7(b), it can be seen that a small amount of excess ionic liquid was found to settle on the external surface of the membrane. The ILs are predominantly viscous in nature which is the reason that some amount of ionic liquid accumulated and settled on the surface of the membrane. In this case low viscous ionic liquids are more desirable as they can completely fill the pores of the membrane but do not settle on the surface of the membrane. Nevertheless, low viscosity ionic liquids suffer from mechanical stability.

The energy dispersive X-ray spectrum of the PVDF membranes were analysed before

and after immobilization with the IL as shown in Fig. 5.2.8(a) and Fig. 5.2.8(b) respectively. The EDX comparison study of SILMs was based on the selection of characteristic elements of interest in ionic liquid. In case of Fig. 5.2.8(a), identified elements were C and F, where as F is common in both the spectra, since membrane is made of the fluorosurfactant perfluorononanoic acid. From Fig. 5.2.8(b) it was clear that, elements P and N were observed as it originated from $[C_8MIM][PF_6]$ composed of sodium hexafluorophosphate and 1-octyl-3-methylimidazolium chloride. This confirmed that the IL remains in the pores of the PVDF membrane support throughout the experiments for 24 h.

Fig. 5.2.9(a–c) shows the IR spectra (Shimadzu, Japan, model: IRAffinity–1) of pure phenol, pure ionic liquid (CYPHOS–104) and mixture of phenol and ionic liquid. All the IR peaks of phenol (Fig. 5.2.9(c)) are broadened and shifted from their parent positions because of the solubility of phenol in ionic liquid. There is also large change in intensities of IR peaks. Some additional bands appeared in the spectra of combination of phenol and CYPHOS–104 (Fig. 5.2.9(c)) compared with individual spectra's of phenol (Fig. 5.2.9(a)) and CYPHOS–104 (Fig. 5.2.9(b)) such as stretching band at 3640, 2936, 2600 and 1624 $cm^{-1}$ which indicated the presence of O–H (H-bonded), =C–H, $=CH_2$ and substituted C-O. The additional peaks observed were due to the impurities present.

## 5.3. Removal of Endosulfan from Aqueous phase using SILM

The application of ILs as a novel and stable carrier for the transport of ES through SILM was investigated against various experimental parameters. A series of permeation experiments were conducted to examine the influence of ES concentration in feed and stripping phase solution. Different stripping phase solutions were tested in this work. The following sections describe the obtained results.

### *5.3.1. Control experiments*

Series of control experiments (PVDF membrane without ionic liquid) were performed to find out the transport of ES through the PVDF membrane. The observed effective transport of ES was very small in this case. Control experiments were performed with initial ES feed concentration of 50 mg $L^{-1}$ (pH=6.5 ± 0.1). Different strip phase solution (0.1M NaOH, 0.1M KOH and 0.1M $NH_4OH$ at feed pH=5.6 ± 0.1) were used in this work. A maximum permeation rate of 36% (at feed pH=6.5) was observed for 0.1 M NaOH as a stripping phase after 30 h of experimental run. This is followed by 32% for 0.1M KOH as shown in Fig. 5.3.1. In case of 0.1 M $NH_4OH$ as stripping phase, a minimum permeation rate of 29.5% (at feed pH=6.5±0.1) was observed for 30 h of experimental run. The control experiments were also run for 30 h using deionized water as a striping phase. In this case, the rate of permeation was only 21.6% at feed pH of 6.5 ± 0.1 (Fig. 5.3.1). All the experimental runs were conducted further up to 48 h, however from Fig. 3 it can be seen that there is hardly any improvement in ES transport. It was also noted that after 20 h of operation time both feed and receiving phases attained equilibrium as shown in Fig. 5.3.1. The uncertainties

in case of control experiments were within 10 to 15%. The ES analysis was done by HPLC after the completion of experiments (after 48 h) and this might have lead to mild precipitation of ES. Moreover, in control experiments, ionic liquid was not present; hence the movement of ES from feed to permeate and vice-versa was not restricted. However, in case of experiments with ionic liquid, analyses were carried out immediately after drawing the samples in a given time interval.

### *5.3.2. Selection of IL*

The IL properties such as high viscosity and high surface tension offer stability to supported liquid membranes. A key characteristic of IL is that their unique properties can be designed by judicious selection of cation, anion, and its substitutes. In an earlier report, Seddon and co-workers [Seddon et al., 2000] provided a selection procedure on the choice of anion on the miscibility of ILs and water. It was found that an increase in alkyl chain length of the cation increases the hydrophobic nature of IL, thereby reducing water solubility. The physical and chemical properties can be different, significantly by the selection of anion, such as halide ions [$Cl^-$, $Br^-$, $I^-$], nitrate [$NO_3^-$], acetate [$CH_3CO_2^-$], tetrafluoroborate [$BF_4^-$], hexafluorophosphate [$PF_6^-$], and bis(trifluoromethyl–sulfonyl)imide [$(CF_3SO_2)_2N^-$] [Brennecke, and Maginn, 2011]. In this work various combinations of cations and anions were selected and were screened for the removal of ES by using the COSMO–RS based process as reported in our previous work [Pilli et al., 2013]. It was reported that 1-Butyl-2,3-dimethylimidazolium hexaflourophosphate gave the highest selectivity for the extraction of endosulfan from water and hence has been used in this experimental work.

### *5.3.3. Transport experiments*

Fig. 5.3.2. shows the variation in initial ES ion concentration in feed and stripping solution as a function of time. Initial feed concentration of ES studied in the transport experiments were in the range of 10–50 mg $L^{-1}$. The rate of permeation of ES through SILM increased with increasing feed phase concentration. At higher initial feed concentration of 50 mg $L^{-1}$, the rate of permeation of ES was around 72%. However, the rate of permeation decreased to 59% when the initial feed concentration was 10 mg $L^{-1}$. A higher permeation usually at higher initial feed phase resulted in a large molecular gradient across the membrane barrier. From Fig. 5.3.2, it was observed that the rate of permeation was constant after 24 h of experiment; which may be due to the saturation of membrane pores with ES molecules which resulted in a film on the membrane interface. This film or layer enhanced the retention of ES compounds on the feed side and thus, may be the reason for the constant permeation rate [Venkateswaran and Palanivelu, 2005]. The uncertainty in case of SILM experiments are 2 to 5%.

Fig. 5.3.3 represents the variation in ES concentration in feed and stripping phase solution as a function of operation time for different stripping phase solutions. In this experiment strip phase solution such as 0.1M NaOH, 0.1M KOH and 0.1M $NH_4OH$ were used to find out the best stripping agent. From Fig. 5.3.3, it was clear that the concentration of ES in feed decreased gradually with operation time. Similarly, strip solution concentration of ES increased slowly with operation time. Both feed and permeate side concentrations reached a steady-state after 24 h of operation time. From Fig. 5.3.3, it can be seen that a maximum 35.76 mg $L^{-1}$ of ES was transported to strip phase from 50 mg $L^{-1}$ of initial feed

concentration using 0.1 M NaOH as strip phase. Approximately 34 mg $L^{-1}$ of ES was transported from feed to strip phase when 0.1M KOH as a stripping agent was used for the same initial feed concentration. Similarly, for 0.1M $NH_4OH$, a maximum of 31 mg $L^{-1}$ of ES was transported. In a recent work, behavior of hydrophobic ionic liquids as liquid membranes on phenol removal by Ng et al., 2011 described that in bulk liquid membrane process, the viscosity of the membrane solvent was significant on governing the stripping rate due to its high membrane thickness. This may be due to high hydrophobic property of ionic liquid ($[C_4DMIM][PF_6]$) which contributes to higher boundary layer thickness between the membrane phase and the aqueous stripping phase, resulting in a lower stripping efficiency. The amount of permeated ES that varied with the types of stripping agent could be due to the ionic strength difference between different stripping agents used. Nevertheless, the authentic reason for this observation remains unclear.

From Fig. 5.3.4, it can be seen that about 72% of the initial ES feed concentration was transported to the receiving phase by using $[C_4DMIM][PF_6]$ ionic liquid with 0.1M NaOH as the stripping phase. In case of 0.1M of KOH, 68% of ES feed concentration were transported into the striping phase. Similarly, for 0.1M $NH_4OH$ around 62% of ES was transported from feed to strip phase. For all those experiments, the initial feed concentration was kept constant at 50 mg $L^{-1}$ and pH 6.5. From this experiment it was confirmed that 0.1M NaOH was the best stripping solution in comparison to 0.1M KOH and 0.1M $NH_4OH$. Fig. 5.3.5 illustrates the variation of membrane flux with operation time. From Fig. 5.3.5, it can be seen that the feed flux decreased sharply within 12 h, and then reached steady-state. In case of permeate fluxes; the decline was not very sharp and reached steady-state within 12 h. Thereafter the

change in membrane flux was almost negligible. Vigorous flux decline may be resulted due to membrane fouling which impacts on quality of the permeate solution. Severe membrane fouling might require cleaning or replacement of membrane. The membrane weights before and after the transport experiment, rate of permeation at different pH values and corresponding feed and strip phase flux values are given in Table 5.8.

### *5.3.4. Effect of feed phase pH on endosulfan separation*

The initial pH of the aqueous solution considerably influences the transport of ES through SILM. The effect of pH on ES feed solution concentration is shown in Fig. 5.3.6. Initially the 50 mg $L^{-1}$ of ES solution was prepared by adjusting the pH to 2–10 by using HCl or NaOH. This helped us in studying the effect of pH on ES separation through SILM. Maximum of 43 mg $L^{-1}$ of ES was transported to stripping phase after 30 h of operation time at pH 2.

Similarly, for pH 4, 6.5, 8, and 10 the strip phase concentrations were 39, 36, 30 and 27 mg $L^{-1}$ respectively, for 30 h of experimental run. The results suggest that the rate of permeation decreased with increasing pH value from 2 to 10 (87–55%, Fig. 5.3.7). Over the range of experimental pH from 2 to 6.5, the rate of permeation decreased around 16% which may be due to the deprotonation of the surface functional (carbonyl and hydroxyl) groups. Further, the deprotonation increased with increase in pH which may be due to the availability of more negatively charged membrane surface at this pH. Further with the increase in feed pH to 10, the extent of extraction decreased to 55%. As a result, pH 6.5 was chosen as the optimum pH throughout the study as at this pH the permeation rate was around 71.53%.

Similar results were also observed by Gupta and Ali (Gupta and Ali, 2008) for adsorption for endosulfan and methoxychlor using carbon slurry.

### *5.3.5. Effect of Stirring Speed*

In order to investigate the ES transport from feed phase to strip phase through SILM system, it is important to study the result of diffusion process and diffusion fluxes. The rotation speed of the magnetic spinbars in feed phase and stripping phase compartments of the permeation cell were controlled by magnetic stirrers for continuous agitation. The effect of stirring speed in bulk solution on the diffusion of effluent ions is also an essential factor in order to minimize the diffusion layer at the interfaces of the SILM. The concentration polarization at the interface of the ionic liquid membrane can be prevented by the continuous mechanical stirring of the feed and stripping phases simultaneously. Therefore, the aqueous feed and strip phases were independently agitated over the range of 100–500 rpm to find out the optimum stirring speed that permits effective diffusion of ES in the SILM setup. Fig. 5.3.8 represents the effect of stirring speed on ES transportation. The % rate of permeation increased in the range of 100–500 rpm (68–74%), which suggested a decrease in the thickness of the diffusion layer. However, the rate of permeation was very small comparatively in the range of 300–500 rpm (71.5–74%). Further increase in stirring speed decreased the transport due to the high turbulence induced by stirring, which perhaps resulted in the displacement of IL molecules from the membrane pores. An optimum rotation speed of 300 rpm was chosen. Thus, the mass transfer rate from feed to permeate side will be affected by solubility and the diffusivity of the effluent in the immobilized IL phase. The

separation rate also depends on the properties of solid support i.e. porosity of the membrane, thickness of the membrane and tortuosity of the membrane pores [Adnan et al., 2012].

### *5.3.6. Mechanism of endosulfan separation*

Endosulfan does not contain any readily dissociable groups so that it can readily gain or lose a proton over the pH range of 5 to 9 [Gupta and Ali, 2008]. Fig. 5.3.9 is an example of the detailed transport mechanism of ES in SILM. It was assumed that permeation of ES from feed to stripping phase through SILM took place via simple permeation process (concentration diffusion). It is a well known fact that ES remains in it's molecular form even at acidic pH. Hence, ES in molecular form is transported via SILM since it does not possess readily dissociable groups. Fig. 5.3.9 is a proposed mechanism which explains that the molecular form of ES dissolved in SILM due to its high distribution coefficient between $[C_4DMIM][PF_6]$ immobilized on PVDF membrane and water. Owing to the molecular polarizibility of ES, it is clear that there exists a huge scope for hydrogen bonding with the IL. The cation of ionic liquid here may act as H–donor. $H^+$ reacts to provide energy for the release of ES. Molecular form ES in the feed solution then diffuses towards the interface. The formation of a complex between 7–membered dioxothiepin–oxide ring of ES and cation (as shown in Fig. 5.3.10) of the ionic liquid takes place which then permeates through the membrane phase to the stripping phase due to the concentration gradient, where it reacts with NaOH to produce $[Na]^+[ES]^-$. Endosulfan sorption by electrodialysis membranes was reported by Banasiak *et al.,* [Banasiak et al., 2011]. They suggested that ES sorption is a result of membrane catalyzed ES degradation, hydrogen bonding and cation–π interactions between ES and membrane (due to ionic liquid) functional groups. Since, the charge

separation is well established in such a π–bonded molecule apart from the assistance available from the membrane, the ES gets highly polarized and thereby enables the separation. In another work, Fan *et al.*, [Fan et al., 2008] reported that H–bonding and hydrophobic interactions between ionic liquid and phenol can facilitate the transfer of phenols from aqueous solution towards the membrane phase. In conclusion, both the hydrogen bonding as well as the hydrophobic action of cation plays a vital role in ES separation. The aromatic ring group compounds have very weak tendencies to lose the $H^+$ ions from the hydroxyl group, leading to the form of $[Na]^+[ES]^-$ ion and water. Since $[Na]^+[ES]^-$ is insoluble in membrane phase, so it was entrapped in the strip phase under the present experimental conditions and thus cannot be transported back to the feed phase.

### *5.3.7. Characterization of PVDF membrane by FTIR*

Fig. 5.3.11(a-c) explains the additional stretching bands appearing on IR spectra of aqueous phase ES, pure ionic liquid ($[C_4DMIM][PF_6]$) and mixture of ES and $C_4DMIM][PF_6]$ respectively. All the IR characteristics of endosulfan are extended and shifted from their parent positions because of solubility of ES in ionic liquid. Large change has been observed in intensities of IR peaks. Some additional bands appear in the spectra of combination of ES and $[C_4DMIM][PF_6]$ as compared to the individual spectra of ES and $C_4DMIM][PF_6]$ such as stretching band at 3674, 2878, 2747, 2420, 1726 and 560 $cm^{-1}$. These peaks indicate the presence of O–H (H-bonded), =C–H, $=CH_2$ and substituted C-O bonds. The stretching band at 1726 $cm^{-1}$ was due to the α,β-unsaturated carbonyl compounds. The carbonyl group of these compounds was conjugated with an alkene from which they

derive special properties [Rauhut and Currier, 1963]. The carbonyl group draws electrons away from the alkene, and the alkene group is, therefore, deactivated towards an electrophile, such as hydrochloric acid. As a general rule with asymmetric electrophiles, $H^+$ attaches itself at the α–position in an electrophilic addition. The additional peaks observed may be attributed due to impurities.

### *5.3.8. Characterization of PVDF membrane by SEM and EDX*

Characterization of the membrane surface morphology was done by scanning electron microscope (SEM) and energy dispersive X–ray (EDX) analysis. The immobilization of IL onto PVDF membrane was confirmed through SEM micrographs. The influence of vacuum immobilization method on the SILMs performance was studied and clarified by characterization of membrane. SEM images give the morphological information of the distribution of the IL within the membrane. Fig. 5.3.12(a) is a SEM micrograph of a blank PVDF membrane where as Fig. 14(b) is a PVDF membrane immobilized with $[C_8MIM][PF_6]$ respectively. From Fig. 5.3.12(b) the surface morphology analysis shows that smaller pores are uniformly dispersed with ionic liquid. The ionic liquid is homogeneously distributed within the pores of the membrane. But the larger macropores are partially filled with ionic liquid. From Fig. 5.3.12(b), it can be seen that a small amount of excess ionic liquid was found to settle on the external surface of the membrane. The ILs are predominantly viscous in their nature for the reason that some amount of the ionic liquid accumulates and settles on the surface of the membrane. This accumulation of ionic liquid on the membrane leads to higher amount of IL remaining on the surface of the membrane. In this case low viscous

ionic liquids are more desirable as it can totally fill the pores of the membrane but will not settle on the surface of the membrane. However, low viscosity ionic liquids suffer from mechanical stability.

Fig. 5.3.12(c) and (d) gives the EDX spectra of elemental composition of the membrane before and after immobilization. The EDX comparison study of SILMs is based on the selection of characteristic elements of interest in ionic liquid. In case of Fig. 5.3.12(c), identified elements were C and F, where as F is common in both the spectra, since membrane is made of the fluorosurfactant perfluorononanoic acid. From Fig. 5.3.12(d), P and N were observed as it originated from $[C_4DMIM][PF_6]$, which comprises of 1-Butyl-2,3-dimethylimidazolium cation and hexafluorophosphate anion. This confirms that the IL remains in the pores of the PVDF membrane support and are not displaced from the pores of membrane after 24 h of successive transport experiments.

## 5.4. Removal of Pentachlorophenol from Aqueous phase using SILM

As discussed in section 3.4.5 of chapter 3, prior to the supported liquid membrane experiment, the selection of ionic liquid was carried by judicious screening of ionic liquids using a well–known quantum chemical based theoretical model called COSMO–RS. The detailed methodology and approaches followed in COSMO–RS model was systematically explained in chapter 2 followed by screening results in chapter 4 from section 4.1 to 4.2. In addition, the selection of ionic liquid was also considered based on hydrophobicity and commercial availability after successful screening. Previously, Seddon and his co–workers [Seddon et al., 2000] furnished a selection process on the choice of anion on the miscibility

of ionic liquid and water. It was observed that an increase in alkyl chain length of the cation increases the hydrophobic nature of ionic liquid, thereby reducing water solubility which is more important when dealing with aqueous medium. In this case the chosen ILs were used in supported liquid membrane experiments. Below sections explain the detailed results obtained from PCP removal using SILM technology.

### *5.4.1 Membrane liquid loss*

After completion of SILM experiment, the membrane liquid (IL) loss was measured by weighing method i.e. by weighing the membrane before and after the transport experiment. The % weight loss of the membrane was calculated by the following Eq.

$$\text{Membrane \% Wt. loss} = \left(\frac{\text{Membrane wt. before-Membrane wt. after}}{\text{Membrane wt. before}}\right)\times 100 \qquad (5.21)$$

Prepared membrane weights were noted before and after the transport experiment for each SILM experiment. The maximum percentage of weight loss of the membrane was 2.28% for membrane prepared with [TBP][$PF_6$], in case of [$C_4$DMIM][$PF_6$] the percentage of weight loss of the membrane was 1.79% as shown in Table 5.10. This shows that the loss of IL from the pores of the membrane was not major. This may the evidence that liquid membranes were stable after 24 to 30 h of transport experiment. In addition, viscosity of the IL plays a very significant role in the stability of the SILMs. The less viscous RTILs were more prone to displacement from the pores of the support. This is in good agreement with the well–known fact that ionic liquids are not easily moved from the pores under a cross–

membrane pressure difference as they are immobilized by large Van der Waals forces due to their high viscosities [Kislik, 2010; Matsumoto et al., 2010].

### *5.4.2 Permeation rate*

Transport experiments were carried for two different SILMs prepared by [TBP][$PF_6$] and [$C_4$DMIM][$PF_6$] ionic liquids. The PCP separation process was observed through change of solute concentration in the feed and permeate phase. The initial feed phase concentration of 50 mg $L^{-1}$ and receiving phase contains 0.1M NaOH or KOH (pH~13), feed pH=6.5, at stirring speed 300 rpm and temperature 25 °C was studied. Two stripping phase solutions such as 0.1M NaOH (~pH = 13 ± 0.1), 0.1M KOH (~pH = 13 ± 0.1) were checked for few experiments and 0.1M NaOH was found to be the best among both stripping phase solutions. In previous work Yahaya et al., was also studied the 0.1M NaOH as stripping agent for the separation of lactic acid from aqueous phase using SILM [Yahaya et al., 2000]. Fig. 5.4.1 shows the PCP concentration in the feed and permeates solutions as a function of time. It is well–known that the concentration of PCP in feed side decreases (Fig. 5.4.1), whereas, in the receiving phase (permeate side) increases with operation time. This is due to the fact that PCP diffuses through the membrane from the feed phase into the permeate phase. From Fig. 5.4.1, it was observe that PCP concentration in feed side was decreased to 12.36 mg $L^{-1}$ from initial feed concentration of 50 mg $L^{-1}$ in 30 h using the ionic liquid [$C_4$DMIM][$PF_6$] as membrane carrier. In case of permeate side PCP concentration was increased from 0 to 36.55 mg $L^{-1}$ in 30 h of time interval. The rate of permeation after 30 h was 73.11% for [$C_4$DMIM][$PF_6$]. Similarly in case of [TBP][$PF_6$], the PCP concentration in

feed side was decreased to 12.6 mg $L^{-1}$ from initial feed concentration of 50 mg $L^{-1}$ in 30 h using the ionic liquid [$C_4$DMIM][$PF_6$] as membrane carrier. In permeate side PCP concentration was increased from 0 to 40.22 mg $L^{-1}$ in 30 h of operation time. The rate of permeation of 80.52% after 30 h for [TBP][$PF_6$] which was 7% higher permeation rate than [$C_4$DMIM][$PF_6$]. All the transport experiments were carried by 0.1M NaOH as stripping phase solution until unless stated.

### *5.4.3 Effect of feed phase concentration*

Fig. 5.4.2 describes the variation in effect of initial concentration in feed and stripping solution as a function of time. Initial feed PCP concentrations considered for this study were 10, 30 and 50 mg $L^{-1}$. With increasing of PCP concentration in supply feed phase, the concentration in stripping phase increased, later it reached equilibrium within 30 h. At initial feed concentration of 50 mg $L^{-1}$, the strip phase concentration of PCP was 36.55 mg $L^{-1}$ after 30 h of operation time, in case of feed concentration, 30 and 10 mg $L^{-1}$, strip phase concentrations were 23.38 and 8.37 mg $L^{-1}$ respectively as shown in Fig. 5.4.2. However, the rate of permeation of 50, 30 and 10 mg $L^{-1}$ initial feed concentrations were 73.11%, 77.95% and 83.71% respectively after successful experimental run of 30 h. A higher permeation rate usually at low initial feed phase results in a large molecular gradient across the membrane barrier, since the effective area of membrane and time are fixed. It was observed that the permeation rate is almost constant after 20 h of experiment; this may be due to both feed and strip phases saturated with PCP molecules and reached equilibrium. The saturation of membrane pores with PCP molecules forms a layer on membrane interface which increases

retention of PCP molecules on the feed side resulting in a constant permeation rate [Venkateswaran and Palanivelu, 2005]. The permeation rate was calculated using Eq. (3.4).

### *5.4.4 Flux measurement*

The flux ($J$ mol $m^{-2}$ $s^{-1}$) measures the number of moles or amount of substance diffusing per unit time and unit effective contact area. The membrane fluxes were measured with fresh feed and stripping solutions (Eq. 3.2). Every time new membrane was used in each flux measurement; which provided the same driving force for each set of experiment.

Fig. 5.4.3 describes the membrane flux in the feed and permeate solutions as a function of operation time. It was observed from Fig. 5.4.3, the membrane flux for feed phase both [$C_4$DMIM][$PF_6$] and [TBP][$PF_6$] ionic liquids used in SILMs gave $1.9\times10^{-9}$ mol. $m^{-2}$ $s^{-1}$ and $1.75\times10^{-9}$ mol. $m^{-2}$ $s^{-1}$ respectively. Initially first 5 h the membrane flux was very sharp in both feed and permeate sides. After 30h of time flux reaches to almost saturation. Fig. 5.4.4 describes the flux as function of initial feed concentration. From Fig. 5.4.4 the membrane flux is almost linearly proportional to the initial PCP concentration in the range of 10–50 mg $L^{-1}$. Yahaya *et al.,* [Yahaya et al., 2000] reported similar observations for the flux of lactic acid and its ethyl ester through supported liquid membrane containing functionalized polyorganosiloxanes. In another work, phenol through n-decanol SLM [Zha et al., 1994] and uranium through SLM of bis(2-ethylhexyl) hydrogen phosphate [Elhassadi and Do, 1986]. This linear increase in the flux was attributed to enhance in the facilitating effect, therefore resulting in an increase in the concentration gradient of the PCP–carrier complex within the membrane and hence an increase in the rate of permeation. Though it is not evidently

observed here, the flux at high feed concentrations would reach a plateau value at high feed concentrations. The plateau value was assigned to the complexation reaction rate becoming faster thus a complete loading of the carrier would take place and consequently the membrane phase would become saturated with the solute-carrier complex species and any further increase in the initial PCP concentration will not affect the flux. However, once the membrane becomes saturated with PCP–carrier complex species, PCP molecules are expected to diffuse through the membrane before a new molecule can interact with the carrier in the membrane.

### *5.4.5 Effect of pH on feed phase and membrane transport mechanism*

The feed pH of the aqueous solution significantly affects during the transport experiment particularly when acidic or basic solutes are separated. The effect of pH on PCP feed solution concentration is described in Fig. 5.4.5(a). Primarily the 50 mg $L^{-1}$ of PCP solution was prepared by adjusting the pH 4–8 using 0.1M NaOH to study the effect of pH on PCP removal through SILM. The maximum permeation rate of 86.74% was obtained at feed pH 4.0 when SILM prepared with [TBP][$PF_6$], at 30 h of operation time. High removal efficiency by using ionic liquids containing longer alkyl chain was also reported in recent study by Zhao *et al.*, where an ionic liquid based headspace single-drop micro extraction teqniques using GC for sensitive identification of phenols [Zhao et al., 2008]. In case of [$C_4$DMIM][$PF_6$] the rate of permeation was observed to be 78.82% after 30 h at a feed of pH 4.0. Fig. 5.4.5(a) shows that the rate of permeation decreases with increasing pH value from 4 to 8 (86.74–73.77%) for [TBP][$PF_6$]. Similarly for [$C_4$DMIM][$PF_6$], rate of permeation was

also decreases with increasing pH from 4 to 8 (78.82–68.48%). The rate of permeation decreases around 6% which may be owing to the deprotonation of the surface functional (carbonyl and hydroxyl) groups at feed pH from 4 to 6.5. Further, the deprotonation increases with increase in pH which may be due to the availability of more negatively charged membrane surface at this pH. Further increase in feed pH to 8, the extent of extraction decreases to 10–12% for both [TBP][$PF_6$] and [$C_4$DMIM][$PF_6$] ionic liquids. These results recommend that for a given PCP solute, its rate of permeation increase with increasing alkyl chain length on the cations of the ionic liquids used as extraction medium under acidic conditions than basic pH. Under acidic environment the dissociation of phenolic compounds can be suppressed and phenols exist primarily as neutral molecules. The observed pH dependence of separation efficiency clearly suggests that PCP species are preferably partitioned into ionic liquid phase as un–dissociated species. Therefore, it was found that even at pH 8 (Fig. 5.4.5(a)) the PCP extraction still relatively significant. In earlier study, it was also described that in case of removal of hydrophobic phenols, the effect of pH on distribution ratios into imidazolium and ammonium based ionic liquids was very small [Li et al., 2009]. The pH range from 5–6.5, maximum PCP removal was also achieved as reported earlier [Zheng et al., 2004] for sorption of chlorophenols using chitosan. As a result, pH 6.5 was chosen as the optimum pH throughout the study.

Fig. 5.4.5(b) gives the detailed PCP transport mechanism from feed to stripping phase trough membrane. The PCP species dissolved in SILM due to its high distribution coefficient between [TBP][$PF_6$] and [$C_4$DMIM][$PF_6$] immobilized on PVDF membrane and water. Assumption made in this figure that the PCP permeation was took place from feed to

stripping phase through SILM via simple diffusion process. Due to the molecular polarizibility of PCP, there is a scope for existence of $H^+$ bonding with the ionic liquid.

The tendency of increasing removal efficiency with increasing linear alkyl chain length can be ascribed to increase the cation hydrophobicity. Evidence from literature states that the extraction of phenolic compounds by magnetic room temperature ionic liquids suggested that higher distribution ratios were achieved at more acidic conditions [Deng et al., 2011]. In earlier work Mohanty *et al.*, stated that the increased interaction facilitates the accommodation of the phenol molecules by ionic liquids [Mohanty et al., 2010].

Recently, Banasiak *et al.*, suggested that the hydrogen bonding and cation–π interactions between aromatic compounds and membrane (due to ionic liquid) functional groups enhances the separation efficiency [Banasiak et al., 2011]. Because the charge separation is well recognized in such a π–bonded molecule separately from the support available from the membrane, hence PCP molecule becomes highly polarized and thereby alters the separation process. As reported in literature, the H–bonding and hydrophobic interactions between ionic liquid and phenol can help the transfer of phenols from water in the direction of the membrane phase [Fan et al., 2008]. This statement clarifies that both the $H^+$ bonding as well as the hydrophobic interaction of cation shows very significant role on separation of PCP.

The cation present in ionic liquid may act as hydrogen–donor. $H^+$ ions react to provide energy for the release of PCP. Then PCP species in the feed solution starts to diffuse towards the interface. Due to the concentration gradient, PCP permeates through the

membrane phase to the stripping phase by interconnection between aromatic ring structure of PCP and cation of the ionic liquid. Then the diffused PCP reacts with 0.1 M NaOH to produce $[C_6Cl_5O^-]^-[Na]^+$. Phenolic compounds contains aromatic ring may have very weak propensities to lose the hydrogen ions from the –OH group leading to formation of $[C_6Cl_5O^-]^-[Na]^+ + H_2O$ as shown in mechanism (Fig. 5.4.5(b). Because $[C_6Cl_5O^-]^-[Na]^+$+ is insoluble in membrane phase, so it may trapped in the striping phase under the present experimental conditions and therefore, it remains in the strip phase and cannot diffuse back.

### *5.4.6 Zeta potential measurement*

Zeta–potential (ζ) measurements were conducted using a zeta potential analyzer (DelsaNano C., Beckman Coulter, USA). The stability of the SILM was carried out by measuring the zeta potential before and after immobilization of IL on PVDF membrane. Zeta potential is the potential dissimilarity between the dispersion medium and the stationary layer of fluid attached to the dispersed particle (IL molecule on membrane). Prior to zeta potential measurement, membrane filter containing ionic liquid was prepared as described in preparation of SILM section. During zeta potential analysis, the SILM was placed in the electrophoresis flat surface cell, which was thoroughly washed and rinsed with ultrapure water followed by rinsing with electrolyte solution (KOH). Electrophoretic light scattering (ELS) has been used to characterize the zeta potential. ELS measurements are many times faster than conventional manual techniques. The potential difference between the PVDF membrane before immobilization and after immobilization was calculated using an experimentally–determined electrophoretic mobility. A high zeta potential value denoted the high stability of SILM. Table 5.11 describes the zeta potential variation (negative or positive)

with stability behavior of ionic liquid in membrane pores. The importance of zeta potential is that its value can be connected to the stability of the IL impregnated on PVDF membrane. From Fig. 5.4.6(a), it can be seen that the zeta potential of blank PVDF membrane is 27.88 mV which denotes the incipient instability. Fig. 5.4.6(b) describes the zeta potential of SILM after immobilization with [$C_4$DMIM][$PF_6$]. Fig. 5.4.6(b) shows the maximum zeta potential of -93.24 mV which states the excellent stability of SILM. The unit of zeta potential value (positive or negative) can be taken as the arbitrary value that separates low charged surfaces from highly charged surfaces. The uncertainty of the zeta potential value was 2% to 4% in both experiments. This experiment suggested that the SILM stable enough to separate PCP from aqueous phase.

### *5.4.7 SEM and EDX analysis*

The surface morphological study of membrane was carried by scanning electron microscope (SEM), (*LEO, Model 1430VP)* and energy dispersive X–ray (EDX) analysis. SEM analysis gave the morphological information of the dispersion of the IL within the membrane pores where as the EDX spectra gave elemental composition of the membrane. The characterization of SILM determines use of the vacuum immobilization method on its performance [de los Ríos et al., 2007]. Fig. 5.4.7(a) and (b) indicates the examples of SEM images of a PVDF membrane before and after immobilization of supported liquid membranes based on [$C_4$DMIM][$PF_6$]. From Fig. 5.4.7(a) it can be seen that PVDF membrane pores were completely open and no ionic liquid was present inside the pore. Fig. 5.4.7(b) indicates the morphological study of membrane after immobilization with

[$C_4$DMIM][$PF_6$]. The surface morphology of SEM image demonstrated that the ionic liquid was homogeneously distributed within the smaller pores of the membrane. Some of larger macro pores were incompletely filled with ionic liquid. From Fig. 5.4.7(b), it was also observed that a small amount of excess ionic liquid appeared on surface of the membrane. The ILs are mainly viscous in character which may be the reason that some amount of ionic liquid settled on the membrane surface. This can be overcome by selecting the ionic liquids of mildly viscous in nature that they can be completely distributed within the pores of the membrane. However, ionic liquids that are low viscous in nature may have lower mechanical stability.

Fig. 5.4.8(a) and 5.4.8(b) show the EDX spectra of the PVDF membrane before and after immobilization with ionic liquids. This study gives the selection of characteristic elements of interest in ionic liquid. From Fig. 5.4.8(a), elements such as C and F are observed. Element F is common in both the spectra, as PVDF membrane is made of the fluorosurfactant perfluorononanoic acid. From Fig. 5.4.8(b) it was observed that, element P which was originated from [$C_4$DMIM][$PF_6$] composed of sodium hexafluorophosphate and 1-octyl-3-methylimidazolium chloride. This study supported that the ionic liquid stays in the pores of the PVDF membrane support throughout the experimental run of 24 h.

## 5.5. Conclusions

An experimental study of equilibrium behavior of liquid–liquid and ternary systems [$C_4$DMIM][$PF_6$] (1) + PCP (2) +water (3) and [$C_4$DMIM][$PF_6$] (1) + PA (2) + water (3) was carried out at $T$= 298.15 K and at $p$=1 bar as demonstrated in section 5.1. The selectivity

values of 24–29 and 106–293 for PA and PCP respectively, indicate easier separation of these organic effluents from wastewater. The IL becomes an economical and potential attractive technique as IL does not contaminate the aqueous phase. As the quantity of PCP and PA in water samples are usually found in trace, these results are favorable for analyzing the potential of $[C_4DMIM][PF_6]$ for wastewater treatment. The UNIQUAC and NRTL models were used to correlate the experimental data and calculate the phase compositions. The predictions based on both UNIQUAC and NRTL equations gave a good representation of the tie–line data for the systems studied. For each ternary system, the Othmer–Tobias and Bachman correlation plots proved excellent reliability of the experimental tie–line results.

The present study of section 5.2, confirmed that the phosphonium based ILs were alternative greener solvents for the removal of phenol from the aqueous solutions using supported liquid membrane technique. Initial feed concentration of 100 mg $L^{-1}$ of phenol was used for all the experiments. SILM was prepared through vacuum immobilization method. Effect of time on the concentration of phenol in both feed and stripping phase for different ionic liquids was analyzed. About 73.63% of the phenol present in the feed phase was transported to stripping phase within 24 h at feed phase pH of 5.6 using [CYPHOS® 104]. By adjusting the feed pH to 4, [CYPHOS®104] gave the maximum permeation rate of 75.70% over an experimental run of 24 h. It was noteworthy that the effect of feed phase pH on phenol removal by using SILM was negligible. The stirring speed of 300 rpm was found to be optimum for highest rate of permeation. [CYPHOS® 104] gave highest permeation rate among the six different ILs used. The concentration of NaOH used as stripping agent was found to be insignificant. The operational stability and performance of the supported liquid

membranes was studied.

The possibility of using supported liquid membrane based on ionic liquids for the selective separation of α–endosulfan is illustrated in section 5.3. PVDF membrane immobilized with [$C_4$DMIM][$PF_6$] IL was used as separating medium and the influence of the ionic liquid membrane on solute transport was studied. Series of control experiments were carried without ionic liquid. Different striping agents such as 0.1M NaOH, 0.1M KOH and 0.1M $NH_4OH$ were successfully used for the separation of α–endosulfan. Out of three stripping agents used 0.1 M NaOH gave the best permeation rate of 71% at an initial feed pH of 6.5 and 87% at an initial feed pH of 2. Favorable permeabilities were found for this SILM. Parameters affecting the rate of permeation such as pH, initial feed concentration and stirring speed were studied. It was confirmed that initially the interface shear forces due to high speed stirring was the main cause for membrane liquid loss leading to SILM instability. The characterization of PVDF membrane before and after the experiment was done using SEM, EDX and FTIR. The experimental results obtained from this study showed successful application of supported ionic liquid membrane for separation of ES from aqueous phase.

The aim of the section 5.4 is to study the removal of PCP from wastewater using SILM. Three different concentrations, 10, 30 and 50 mg $L^{-1}$ of PCP in feed and 0.1 M NaOH as strip phase solution as function of operation time was studied. Operating parameters such as pH, initial feed concentration and fluxes were studied. The characterization using scanning electron microscopy and EDX was studied. Two different ionic liquids [$C_4$DMIM][$PF_6$] and [TBP][$PF_6$] were used to prepare the SILM and 0.1M NaOH used as a stripping agent. The maximum permeation rate of 80.52% was obtained by [TBP][$PF_6$] followed by 73.11% for

$[C_4DMIM][PF_6]$ at feed pH of 6.5 on 30 h experimental run. Highest permeation of 86.74% was obtained by phosphonium based hydrophobic ionic liquids i.e. $[TBP][PF_6]$ at feed pH 4, whereas $[C_4DMIM][PF_6]$ gave 78.82% after 30 h experimental run at feed pH 4. The transport mechanism of PCP through SILM was explained by hydrogen bonding interactions, hydrophobic interactions and carbon–π bonding interactions thoroughly. Stability of membranes was also studied by measuring the zeta potential before and after immobilization of IL on PVDF membrane. The SILM characterization was done by scanning electron microscopy and was used to study the morphology before and after transport experiments with EDX spectra. Present work suggests that several polymeric membranes can be used as substitute supporting materials for the application of supported liquid membrane technology. An extensive study on extraction of PCP from wastewater using supported ionic liquid membrane was studied. This method can be a future alternative for extraction trace amounts of PCP from aqueous phase. Superior operational performance was found and results of this study indicated that the designed SILM may be used in future separation processes for removal of organic compounds.

**References**

Abrams, D.S., J.M. Prausnitz, Statistical thermodynamics of liquid mixtures: a new expression for the excess Gibbs energy of partly or completely miscible systems, *AIChE J.* 21 (1975) 116–128.

Adnan, S., M. Hoang, H. Wang, Z. Xie, Commercial PTFE membranes for membrane distillation application: Effect of microstructure and support material, *Desalination* 284 (2012) 297–308.

Banasiak, L.J., B. Van der Bruggen, A.I. Schäfer, Sorption of pesticide Endosulfan by electrodialysis membranes, *Chem. Eng. J.* 166 (2011) 233–239.

Banerjee, T., M.K. Singh, R.K. Sahoo, A. Khanna, surface and UNIQUAC interaction parameters for imidazolium based ionic liquids via Polarizable Continuum Model, *Fluid Phase Equilib.* 234 (2005a) 64–76.

Banerjee, T., M.K. Singh, A. Khanna, Genetic algorithm to estimate interaction parameters of multicomponent systems for liquid–liquid equilibria, *Comp. Chem. Engg.* 29 (2005b) 1712–1719.

Brennecke, J.F., E.J. Maginn, Ionic Liquids: Innovative Fluids for Chemical Processing, *AIChE J.* 47 (2011) 2384–2389.

Chen, D.C., H.Q. Ye, H. Wu, Measurement and Correlation of Liquid–Liquid Equilibria of Methylcyclohexane + Toluene + N-Formylmorpholine at (293, 303, 313, and 323) K, J. *Chem. Eng. Data.* 52 (2007) 1297–1301.

de los Ríos, A.P., F.J. Hern´andez-Fernández, F. Tomás Alonso, J.M. Palacios, D. Gómez, M. Rubio, G. Víllora, A SEM–EDX study of highly stable supported liquid membranes based on ionic liquids, *J. Membr. Sci.* 300 (2007) 88–94.

Deng, N., Min Li, Lijie Zhao, Chengfei Lu, Sergio L. de Rooy, Isiah M. Warner, Highly efficient extraction of phenolic compounds by use of magnetic room temperature ionic liquids for environmental remediation, *J. Hazard. Mater.* 192 (2011) 1350–1357.

Elhassadi, A.A., D.D. Do, Effects of a carrier and its diluent on the transport of metal across supported liquid membranes (SLM). II. Viscosity effects, *Sep. Sci. Technol.* 21 (1986) 285.

Fan, J., Y. Fan, Y. Pei, K. Wu, J. Wang, M. Fan, Solvent extraction of selected endocrine disrupting phenols using ionic liquids, *Sep. Purif. Technol.* 61 (2008) 324–331.

Greenwood, R., K. Kendall, Selection of Suitable Dispersants for Aqueous Suspensions of Zirconia and Titania Powders using Acoustophoresis, *J. Eur. Ceram. Soc.*19 (1999) 479–488.

Gupta, V.K., I. Ali, Removal of Endosulfan and Methoxychlor from Water on Carbon Slurry, *Environ. Sci. Technol.* 42 (2008) 766–770.

http://en.wikipedia.org/wiki/Phenol, accessed online on Nov. 2012.

Kemperman, A., D. Bargeman, T. Van Boomgaard, H. Strathmann, Stability of Supported Liquid Membranes: State of the Art, *Sep. Purif. Technol.* 31 (1996) 2733–2762.

Khachatryan, K.S., S.V. Smirnova, I.I. Torocheshnikova, N.V. Shvedene, A.A. Formanovsky, I.V. Pletnev, Solvent extraction and extraction–voltammetric determination of phenol using room temperature ionic liquid, *Anal. Bioanal. Chem.* 381 (2005) 464–470.

Kislik, V.S., Liquid membranes principles and applications in chemical separations and wastewater treatment, Elsevier First Edition 2010, ISBN: 978-0-444-53218-3, Elsevier B.V, Jordan Hills, Oxford OX2 8DP, UK.

Li, M., C.U. Pittman Jr., T. Li, Extraction of polyunsaturated fatty acid methyl esters by imidazolium-based ionic liquids containing silver tetrafluoroborate—extraction equilibrium studies, *Talanta.* 78 (2009) 1364–1370.

Marták, J., S. Schlosser, S. Vlcková, Pertraction of lactic acid through supported liquid membranes containing phosphonium ionic liquid, *J. Membr. Sci.* 318 (2008) 298–310.

Matsumoto, M., W. Hasegawa, K. Kondo, T. Shimamura, M. Tsuji, Application of supported ionic liquid membranes using a flat sheet and hollow fibers to lactic acid recovery, *Desal. Water Treat.* 14 (2010) 37–46.

Mohanty, S., T. Ranerjee, K. Mohanty, Quantum chemical based screening of ionic liquids for the extraction of phenol from aqueous solution, *Ind. Eng. Chem. Res.* 49 (2010), 2916–2925.

Ng, Y.S., N.S. Jayakumar, M.A. Hashim, Behavior of hydrophobic ionic liquids as liquid membranes on phenol removal: Experimental study and optimization, *Desalination.* 278 (2011) 250–258.

Pilli, S.R., T. Banerjee, K. Mohanty, Ionic Liquids as Green Solvents for the Extraction of Endosulfan from Aqueous Solution: a Quantum Chemical Approach, *Chem. Prod. Process Model.* 8 (2013) 1–14.

Rao, Y.V.C., Chemical Engineering Thermodynamics, 01 Edition, Universities Press, 1997.

Rauhut, M., H. Currier, (American Cyanamide Co.). U.S. Patent 3,074, 999, Chem. Abstr. 1963, 58, 11224a.

Reis, M.T.A., O.M.F. de Freitas, M.R.C. Ismael, J.M.R. Carvalho, Recovery of phenol from aqueous solutions using liquid membranes with Cyanex 923, *J. Membr. Sci.* 305 (2007) 313–324.

Renon, H., J.M. Prausnitz, Local compositions in thermodynamic excess functions for liquid mixtures, *AIChE J.* 14 (1968) 135–144.

Seader, J.D., E.J. Henley, Separation Process Principles (2nd ed.) Wiley, New York (2005)196.

Seddon, K.R., A. Stark, M.J. Torres, Influence of Chloride, Water, and Organic Solvents on the Physical Properties of Ionic Liquids, *Pure Appl. Chem.* 72 (2000) 2275–2287.

Shen, S.F., K.H. Smith, S. Cook, S.E. Kentish, J.M. Perera, T. Bowser, G.W. Stevens, Phenol recovery with tributyl phosphate in a hollow fiber membrane contactor: experimental and model analysis, *Sep. Purif. Technol.* 69 (2009) 48–56.

Stannett, V., The transport of gases in synthetic polymeric membranes-An historic Perspective, *J. Membr. Sci.* 3 (1978) 97-115.

Venkateswaran, P., K. Palanivelu, Studies on recovery of hexavalent chromium from plating wastewater by supported liquid membrane using tri-n-butyl phosphate as carrier, *Hydrometallurgy*. 78 (2005) 107–115.

Vidal, S.T.M., M.J.N. Correia, M.M. Marques, M.R. Ismael, M.T.A. Reis, Studies on the use of ionic liquids as potential extractant of phenolic compounds and metal ions, *Sep. Sci. Technol*. 39 (2005) 2155–2169.

Wang, M.L., H.K. Hua, Extraction of Phenol Using Sulfuric Acid Salts of Trioctylamine in a Supported Liquid Membrane, *Ind. Eng. Chem. Res.* 33 (1994) 914–921.

Yahaya, G.O., B.J. Brisdon, R. England, Facilitated transport of lactic acid and its ethyl ester by supported liquid membranes containing functionalized polyorganosiloxanes as carriers, *J. Membr. Sci*. 168 (2000) 187–201.

Zha, F.F., A.G. Fane, C.J.D. Fell, Phenol removal by supported liquid membranes, *Sep. Sci. Technol*. 29 (1994) 2317.

Zhao, F., J. Li, B. Zeng, Coupling of ionic liquid-based headspace single-drop microextraction with GC for sensitive detection of phenols, *J. Sep. Sci.* 31 (2008), 3045–3049.

Zheng, S., Z. Yang, D. Hyun Jo, Y.H. Park, Removal of chlorophenols from groundwater by chitosan sorption, *Water Res.* 38 (2004) 2315–2322.

# TABLES AND FIGURES OF CHAPTER 5

**Table 5.1.** Experimental tie lines for the system [$C_4$DMIM][$PF_6$]+ [PA]+[water] at $T$= 298.15 K and $p$=1 bar.

| | Water rich phase | | | IL Rich phase | | | Selectivity | Distribution coefficient |
|---|---|---|---|---|---|---|---|---|
| S.No. | $X_{IL}$ | $X_{PA}$ | $X_{water}$ | $X_{IL}$ | $X_{PA}$ | $X_{water}$ | ($S$) | (β) |
| 1 | 0.0000 | 0.1200 | 0.8800 | 0.1924 | 0.6242 | 0.1834 | 24.9589 | 5.2017 |
| 2 | 0.0000 | 0.0874 | 0.9126 | 0.2936 | 0.5220 | 0.1844 | 29.5582 | 5.9725 |
| 3 | 0.0000 | 0.0820 | 0.9180 | 0.3404 | 0.4635 | 0.1961 | 26.4607 | 5.6524 |
| 4 | 0.0000 | 0.0794 | 0.9206 | 0.4524 | 0.3634 | 0.1842 | 22.8742 | 4.5768 |
| 5 | 0.0000 | 0.0622 | 0.9378 | 0.5065 | 0.3093 | 0.1842 | 25.3169 | 4.9727 |
| 6 | 0.0000 | 0.0469 | 0.9531 | 0.6063 | 0.2211 | 0.1726 | 26.0324 | 4.7143 |
| 7 | 0.0000 | 0.0410 | 0.9590 | 0.6340 | 0.1870 | 0.1790 | 24.4356 | 4.5610 |
| 8 | 0.0000 | 0.0388 | 0.9612 | 0.7114 | 0.1052 | 0.1834 | 13.7889 | 2.7113 |

**Table 5.2.** Experimental tie lines for the system [$C_4$DMIM][$PF_6$]+[PCP]+[water] at $T$= 298.15 K and $p$=1 bar.

| | Water rich phase | | | IL Rich phase | | | Selectivity | Distribution coefficient |
|---|---|---|---|---|---|---|---|---|
| S.No. | $X_{IL}$ | $X_{PCP}$ | $X_{water}$ | $X_{IL}$ | $X_{PCP}$ | $X_{water}$ | ($S$) | (β) |
| 1 | 0.0000 | 0.0566 | 0.9434 | 0.1189 | 0.7496 | 0.1315 | 95.0131 | 13.2438 |
| 2 | 0.0000 | 0.0476 | 0.9524 | 0.1500 | 0.7170 | 0.1330 | 107.8649 | 15.0630 |
| 3 | 0.0000 | 0.0399 | 0.9601 | 0.1777 | 0.6870 | 0.1353 | 122.1807 | 17.2180 |
| 4 | 0.0000 | 0.0295 | 0.9705 | 0.2040 | 0.6593 | 0.1367 | 158.6675 | 22.3492 |
| 5 | 0.0000 | 0.0145 | 0.9855 | 0.2536 | 0.6074 | 0.1390 | 296.9946 | 41.8897 |
| 6 | 0.0000 | 0.0128 | 0.9872 | 0.3215 | 0.5230 | 0.1555 | 259.3979 | 40.8594 |
| 7 | 0.0000 | 0.0108 | 0.9892 | 0.3628 | 0.4534 | 0.1838 | 225.9417 | 41.9815 |
| 8 | 0.0000 | 0.0070 | 0.9930 | 0.4317 | 0.3723 | 0.1960 | 68.4520 | 53.1857 |

**Table 5.3.** UNIQUAC structural parameters (*r* and *q*) for the pure components in the LLE system.

| S. No. | Component | Volume parameter (*r*) | Surface area parameter (*q*) |
|---|---|---|---|
| 1 | PA* | 5.457 | 4.282 |
| 2 | PCP* | 5.920 | 5.372 |
| 3 | $[C_4DMIM][PF_6]$# | 11.596 | 8.009 |
| 4 | Water* | 0.920 | 1.400 |

[*Rao et al., 1997; #Banerjee, et al., 2005b].

**Table 5.4.** UNIQUAC and NRTL interaction parameters for different systems at *T*= 298.15 K and *p*=1 bar (where α is NRTL non-randomness parameter $\alpha_{ij}= \alpha_{ji}=0.2$).

| System | NRTL model parameters | | | | UNIQUAC model parameters | | | |
|---|---|---|---|---|---|---|---|---|
| (*i*–*j*) | $\tau_{ij}$ | $\tau_{ji}$ | *F*[a] | RMSD[b] | $A_{ij}/K$ | $A_{ji}/K$ | *F*[a] | RMSD[b] |
| $[C_4DMIM][PF_6]$–[PA] | -0.02555 | 11.564 | -0.00062 | 0.35 | 71.806 | 572.35 | -0.0014 | 0.54 |
| $[C_4DMIM][PF_6]$–[water] | 1.8202 | 15.754 | | | 81.526 | 999.99 | | |
| [PA]–[water] | 16.917 | 2.4928 | | | -112.1 | -166.99 | | |
| $[C_4DMIM][PF_6]$–[PCP] | 1.6733 | 0.4244 | -0.00106 | 0.46 | 37.772 | 620.84 | -0.0008 | 0.41 |
| $[C_4DMIM][PF_6]$–[water] | -1.1445 | 20.000 | | | -453.81 | 687.29 | | |
| [PCP]–[water] | 8.3558 | 3.3150 | | | -398.68 | -114.91 | | |

[a]Calculated by Eq. (5.14)

[b]Calculated by Eq. (5.15)

**Table 5.5(a).** Correlated UNIQUAC and NRTL tie–line values for water rich phase in mole fraction for the $[C_4DMIM][PF_6]$+[PA]+[water] at $T$= 298.15 K and $p$=1 bar.

| | Water rich phase | | | | | | | | |
|---|---|---|---|---|---|---|---|---|---|
| | ($X_{IL}$) | | | ($X_{PA}$) | | | $X_{water}$ | | |
| S. No. | Exp | NRTL | UNIQUAC | Exp | NRTL | UNIQUAC | Exp | NRTL | UNIQUAC |
| 1 | 0.0000 | 0.0011 | 0.0016 | 0.1200 | 0.1139 | 0.1133 | 0.8800 | 0.8849 | 0.8850 |
| 2 | 0.0000 | 0.0003 | 0.0006 | 0.0874 | 0.0891 | 0.0849 | 0.9126 | 0.9104 | 0.9144 |
| 3 | 0.0000 | 0.0003 | 0.0005 | 0.0820 | 0.0841 | 0.0815 | 0.9180 | 0.9155 | 0.9178 |
| 4 | 0.0000 | 0.0002 | 0.0004 | 0.0794 | 0.0778 | 0.0818 | 0.9206 | 0.9218 | 0.9177 |
| 5 | 0.0000 | 0.0001 | 0.0002 | 0.0622 | 0.0649 | 0.0630 | 0.9378 | 0.9349 | 0.9367 |
| 6 | 0.0000 | 0.0000 | 0.0001 | 0.0469 | 0.0492 | 0.0443 | 0.9531 | 0.9506 | 0.9554 |
| 7 | 0.0000 | 0.0000 | 0.0001 | 0.0410 | 0.0430 | 0.0369 | 0.9590 | 0.9569 | 0.9629 |
| 8 | 0.0000 | 0.0000 | 0.0001 | 0.0388 | 0.0307 | 0.0268 | 0.9612 | 0.9692 | 0.9730 |

**Table 5.5(b).** Correlated UNIQUAC and NRTL tie–line values for IL rich phase in mole fraction for the $[C_4DMIM][PF_6]$+[PA]+[water] at $T$= 298.15 K and $p$=1 bar.

| | IL rich phase | | | | | | | | |
|---|---|---|---|---|---|---|---|---|---|
| | ($X_{IL}$) | | | ($X_{PA}$) | | | $X_{water}$ | | |
| S. No. | Exp | NRTL | UNIQUAC | Exp | NRTL | UNIQUAC | Exp | NRTL | UNIQUAC |
| 1 | 0.1924 | 0.1894 | 0.1861 | 0.1834 | 0.6255 | 0.6183 | 0.1834 | 0.1850 | 0.1954 |
| 2 | 0.2936 | 0.2939 | 0.2876 | 0.1844 | 0.5214 | 0.5164 | 0.1844 | 0.1845 | 0.1959 |
| 3 | 0.3404 | 0.3389 | 0.3370 | 0.1961 | 0.4600 | 0.4607 | 0.1961 | 0.2010 | 0.2021 |
| 4 | 0.4524 | 0.4521 | 0.4518 | 0.1842 | 0.3649 | 0.3609 | 0.1842 | 0.1828 | 0.1872 |
| 5 | 0.5065 | 0.5089 | 0.5073 | 0.1842 | 0.3077 | 0.3091 | 0.1842 | 0.1832 | 0.1835 |
| 6 | 0.6063 | 0.6142 | 0.6055 | 0.1726 | 0.2209 | 0.2234 | 0.1726 | 0.1648 | 0.1710 |
| 7 | 0.6340 | 0.6377 | 0.6365 | 0.1790 | 0.1857 | 0.1916 | 0.1790 | 0.1765 | 0.1717 |
| 8 | 0.7114 | 0.7012 | 0.7145 | 0.1834 | 0.1120 | 0.1175 | 0.1834 | 0.1866 | 0.1679 |

**Table 5.6(a).** Correlated UNIQUAC and NRTL tie–line values for water rich phase in mole fraction for the [$C_4$DMIM][$PF_6$]+[PCP]+[water] at $T$= 298.15 K and $p$=1 bar.

| | Water rich phase | | | | | | | | |
|---|---|---|---|---|---|---|---|---|---|
| | ($X_{IL}$) | | | ($X_{PCP}$) | | | $X_{water}$ | | |
| S. No. | Exp | NRTL | UNIQUAC | Exp | NRTL | UNIQUAC | Exp | NRTL | UNIQUAC |
| 1 | 0.0000 | 0.0002 | 0.0000 | 0.0566 | 0.0447 | 0.0578 | 0.9434 | 0.9549 | 0.9421 |
| 2 | 0.0000 | 0.0002 | 0.0000 | 0.0476 | 0.0383 | 0.0457 | 0.9524 | 0.9614 | 0.9542 |
| 3 | 0.0000 | 0.0002 | 0.0000 | 0.0399 | 0.0334 | 0.0360 | 0.9601 | 0.9664 | 0.9638 |
| 4 | 0.0000 | 0.0001 | 0.0000 | 0.0295 | 0.0281 | 0.0266 | 0.9705 | 0.9716 | 0.9733 |
| 5 | 0.0000 | 0.0001 | 0.0000 | 0.0145 | 0.0212 | 0.0145 | 0.9855 | 0.9786 | 0.9854 |
| 6 | 0.0000 | 0.0001 | 0.0000 | 0.0128 | 0.0178 | 0.0073 | 0.9872 | 0.9820 | 0.9925 |
| 7 | 0.0000 | 0.0001 | 0.0001 | 0.0108 | 0.0154 | 0.0037 | 0.9892 | 0.9844 | 0.9960 |
| 8 | 0.0000 | 0.0001 | 0.0004 | 0.0070 | 0.0120 | 0.0010 | 0.9930 | 0.9878 | 0.9984 |

**Table 5.6(b).** Correlated UNIQUAC and NRTL tie–line values for IL rich phase in mole fraction for the [$C_4$DMIM][$PF_6$]+[PCP]+[water] at $T$= 298.15 K and $p$=1 bar.

| | IL rich phase | | | | | | | | |
|---|---|---|---|---|---|---|---|---|---|
| | ($X_{IL}$) | | | ($X_{PCP}$) | | | $X_{water}$ | | |
| S. No. | Exp | NRTL | UNIQUAC | Exp | NRTL | UNIQUAC | Exp | NRTL | UNIQUAC |
| 1 | 0.1189 | 0.1177 | 0.1177 | 0.7496 | 0.7560 | 0.7419 | 0.1315 | 0.12616 | 0.1402 |
| 2 | 0.1500 | 0.1489 | 0.1487 | 0.7170 | 0.7222 | 0.7131 | 0.1330 | 0.12882 | 0.1381 |
| 3 | 0.1777 | 0.1766 | 0.1764 | 0.6870 | 0.6904 | 0.6861 | 0.1353 | 0.13284 | 0.1374 |
| 4 | 0.2040 | 0.2036 | 0.2032 | 0.6593 | 0.6600 | 0.6598 | 0.1367 | 0.13636 | 0.1368 |
| 5 | 0.2536 | 0.2542 | 0.2540 | 0.6074 | 0.6023 | 0.6085 | 0.1390 | 0.14336 | 0.1370 |
| 6 | 0.3215 | 0.3211 | 0.3214 | 0.5230 | 0.5175 | 0.5284 | 0.1555 | 0.16138 | 0.1501 |
| 7 | 0.3628 | 0.3655 | 0.3639 | 0.4534 | 0.4521 | 0.4621 | 0.1838 | 0.18229 | 0.1738 |
| 8 | 0.4317 | 0.4360 | 0.4242 | 0.3723 | 0.3709 | 0.3721 | 0.1960 | 0.19298 | 0.2036 |

**Table 5.7.** Othmer–Tobias and Bachman Eq. constants and the correlation factor ($R^2$) for two different ternary systems used at = 298.15 K.

| Ternary system | Othmer–Tobias correlation | | | Bachman correlation | | |
|---|---|---|---|---|---|---|
| | A | B | $R^2$ | A | B | $R^2$ |
| [C4DMIM][PF6]+ [PA]+[water] | 4.911 | 1.786 | 0.955 | 0.856 | 0.148 | 0.941 |
| [C4DMIM][PF6]+ [PCP]+[water] | 4.008 | 0.746 | 0.969 | 0.931 | 0.160 | 0.855 |

**Table 5.8.** Membrane weights before and after the transport experiment, Rate of Permeation at different pH values and corresponding feed and strip phase flux values.

| | IL used $[C_4DMIM][PF_6]$ | Membrane weights (g) | | Weight Loss | Rate of Permeation | Feed Flux after 30h | Strip Flux after 30h |
|---|---|---|---|---|---|---|---|
| Feed pH | Strip phase used | Before | After | % | (%) | mol $m^{-2}$ $s^{-1}$ | mol $m^{-2}$ $s^{-1}$ |
| 10 | 0.1NaOH | 0.8685 | 0.8564 | 1.4 | 55.25 | 3.962E-11 | 5.238E-11 |
| 8 | 0.1NaOH | 0.8417 | 0.8254 | 1.9 | 59.92 | 3.846E-11 | 5.680E-11 |
| 6.5 | 0.1NaOH | 0.8563 | 0.8346 | 2.5 | 71.53 | 2.682E-11 | 6.782E-11 |
| 4 | 0.1NaOH | 0.8756 | 0.8502 | 2.9 | 78.45 | 2.160E-11 | 7.438E-11 |
| 2 | 0.1NaOH | 0.8683 | 0.8403 | 3.2 | 86.74 | 2.205E-11 | 8.223E-11 |
| 6.5 | 0.1KOH | 0.8736 | 0.8422 | 3.6 | 68.00 | 2.743E-11 | 6.446E-11 |
| 6.5 | 0.1$NH_4OH$ | 0.8583 | 0.8203 | 4.4 | 62.00 | 2.735E-11 | 5.890E-11 |

**Table 5.9.** Weight of membrane before and after the transport experiment, rate of permeation of different SILMs used.

| S. No | Name of the Ionic liquid | Feed con. after 24h of expt. | Rate of Permeation (%) at pH 5.6 |
|---|---|---|---|
| 1 | [Aliquat-336] | 44.47 | 32.43 |
| 2 | [C8MIM][PF6] | 47.53 | 35.11 |
| 3 | [CYPHOS-101] | 48.84 | 50.00 |
| 4 | [CYPHOS-102] | 50.75 | 54.23 |
| 5 | [CYPHOS-103] | 51.62 | 59.74 |
| 6 | [CYPHOS-104] | 53.21 | 73.63 |

**Table 5.10.** Wt. before and after experiment and % Wt. loss of membrane.

| S. No. | Ionic Liquid | Wt. Before (g) | Wt. After (g) | % LOSS |
|---|---|---|---|---|
| 1 | $[C_4DMIM][PF_6]$ | 0.877 | 0.857 | 2.281 |
| 2 | $[TBP][PF_6]$ | 0.836 | 0.821 | 1.794 |

**Table 5.11.** Zeta potential vs stability [Greenwood and Kendall et al., 1999].

| Zeta potential [mV] | Stability behavior of the colloid |
|---|---|
| from 0 to ±5 | Rapid coagulation or flocculation |
| from ±10 to ±30 | Incipient instability |
| from ±30 to ±40 | Moderate stability |
| from ±40 to ±60 | Good stability |
| more than ±61 | Excellent stability |

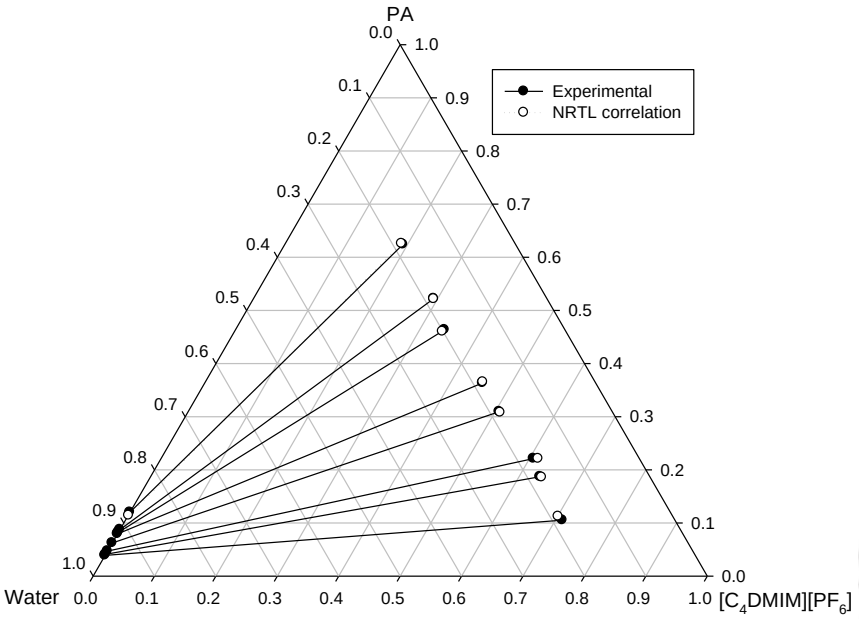


**Figure 5.1.1(a).** Experimental and NRTL correlated tie lines for $[C_4DMIM][PF_6]$ +[PA]+[water] at $T$= 298.15 K and $p$=1.

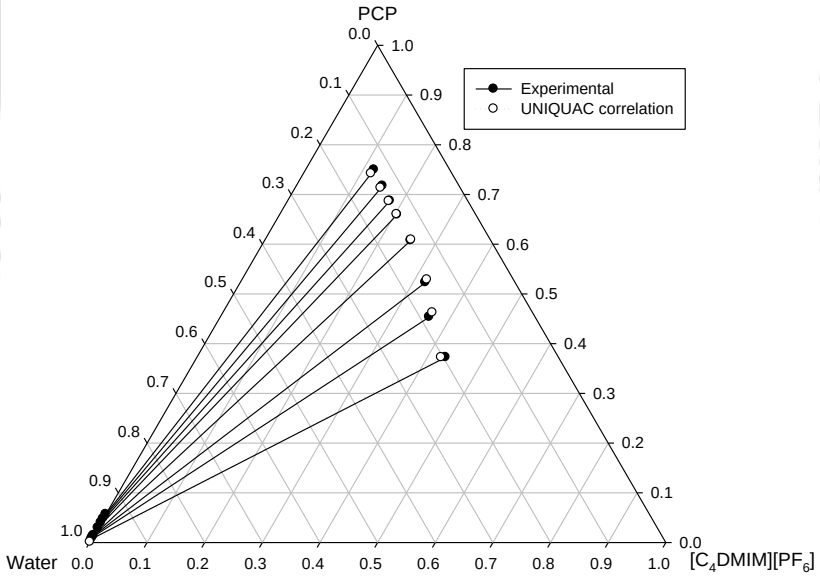


**Figure 5.1.1(b).** Experimental and UNIQUAC correlated tie lines for $C_4DMIM][PF_6]$+[PCP]+[water] at $T$= 298.15 K and $p$=1.

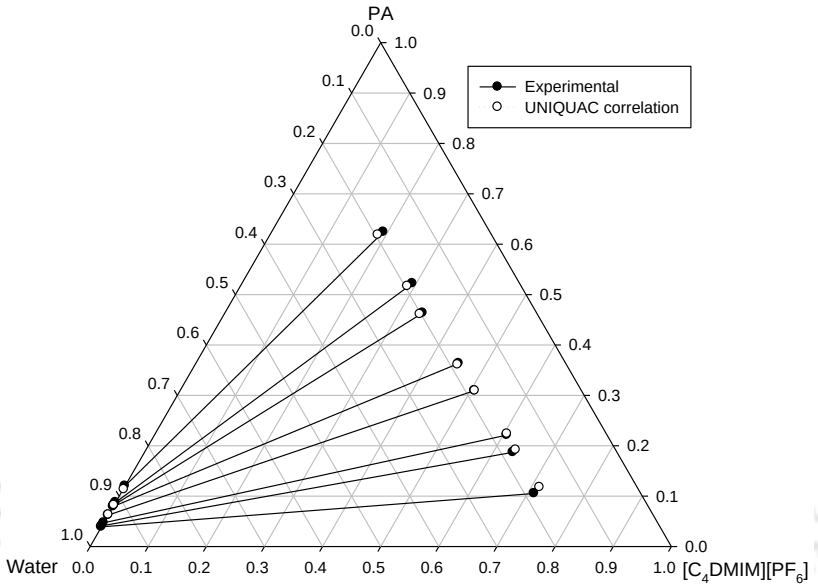


**Figure 5.1.2(a).** Experimental and UNIQUAC correlated tie lines for $[C_4DMIM][PF_6]$ +[PA]+[water] at $T$= 298.15 K and $p$=1.

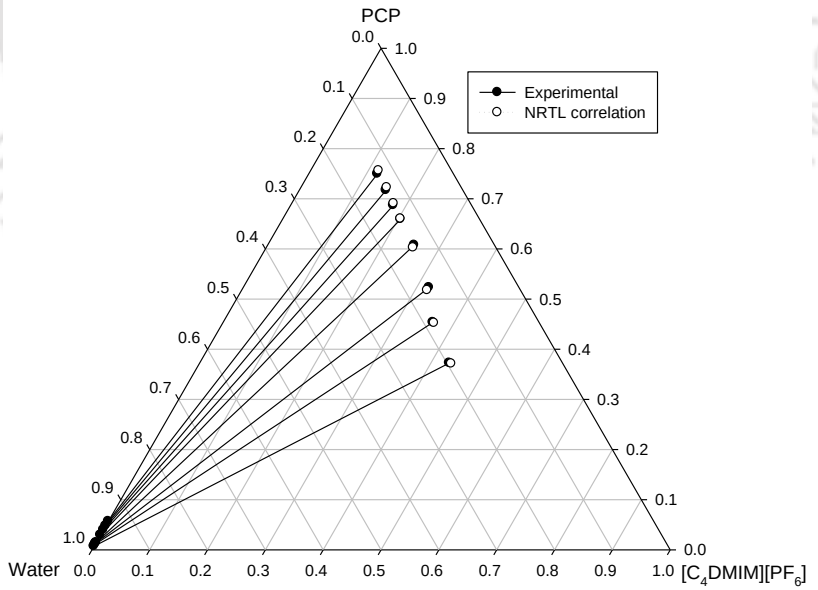


**Figure 5.1.2(b).** Experimental and NRTL correlated tie lines for $[C_4DMIM][PF_6]$ +[PCP]+[water] at $T$= 298.15 K and $p$=1.

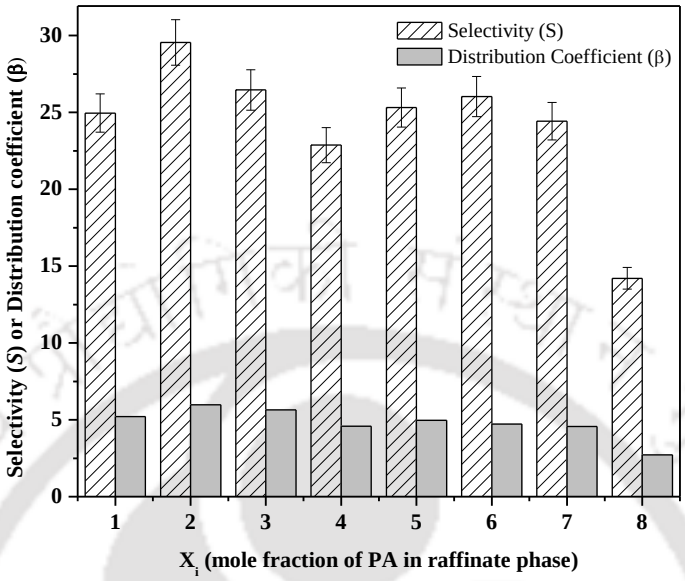


**Figure 5.1.3.** Comparison of experimental selectivity and distribution coefficient vs. mole fraction of PA in raffinate phase (x-axis corresponds to the mole fraction of PA: 1: 0.12; 2: 0.0874; 3: 0.0820; 4: 0.0794; 5: 0.0622; 6: 0.0469; 7: 0.0410; 8: 0.0388).

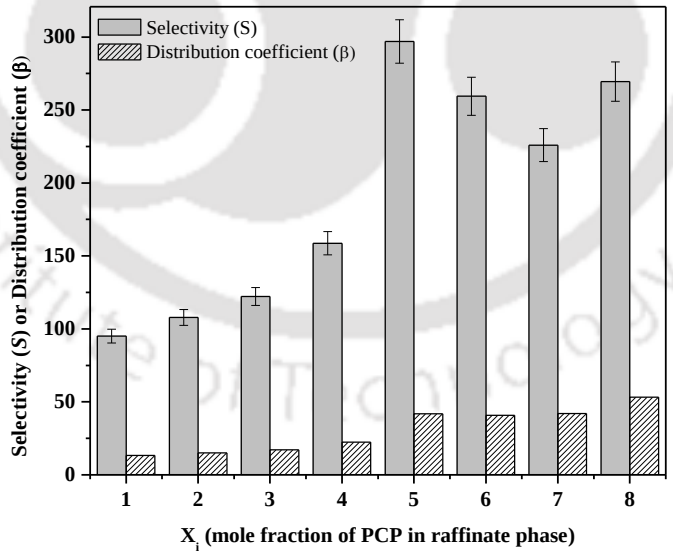


**Figure 5.1.4.** Comparison of experimental selectivity and distribution coefficient vs. mole fraction of PCP in raffinate phase (x-axis corresponds to the mole fraction of PCP: 1: 0.0566; 2: 0.0476; 3: 0.0399; 4: 0.0295; 5: 0.0145; 6: 0.0508; 7: 0.0388; 8: 0.0270).

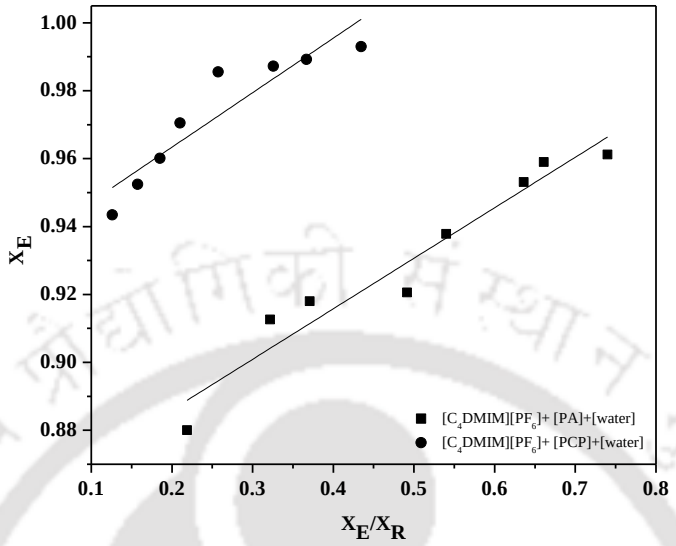


**Figure 5.1.5.** Bechman correlation for $[C_4DMIM][PF_6]$+[PA]+[water] and $[C_4DMIM][PF_6]$+[PCP]+[water] at 298.15 K.

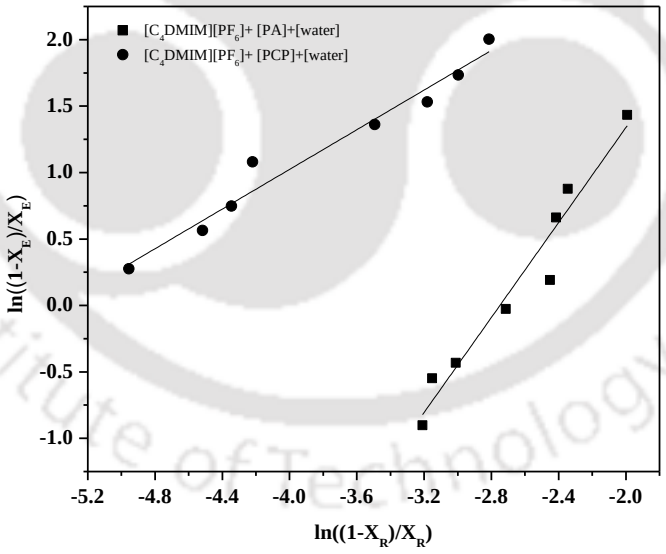


**Figure 5.1.6.** Othmer–Tobias correlation for $[C_4DMIM][PF_6]$+[PA]+[water] and $[C_4DMIM][PF_6]$+[PCP]+[water] at 298.15 K.

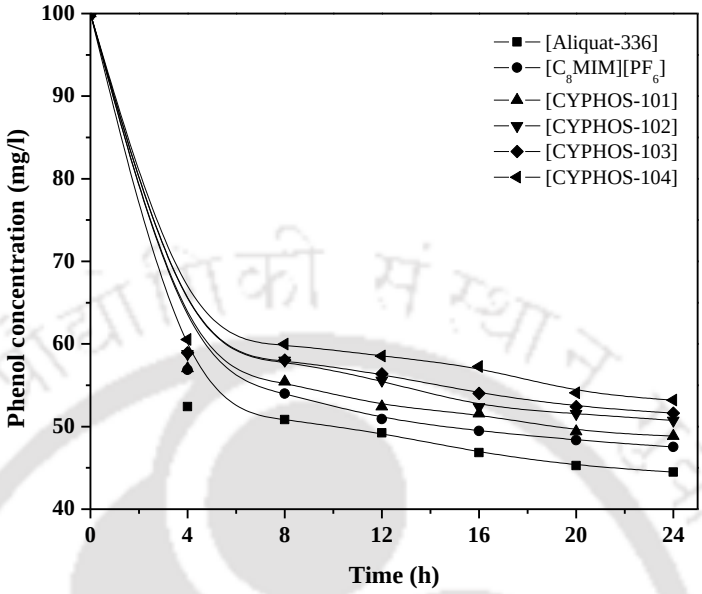


**Figure. 5.2.1.** Variation of feed phase concentration with time for different ILs for SILM transport experiment: (Conditions: initial feed phase concentration: 100 mg $L^{-1}$, pH: 5.6, stirring speed: 300 rpm and temperature: 25± °C).

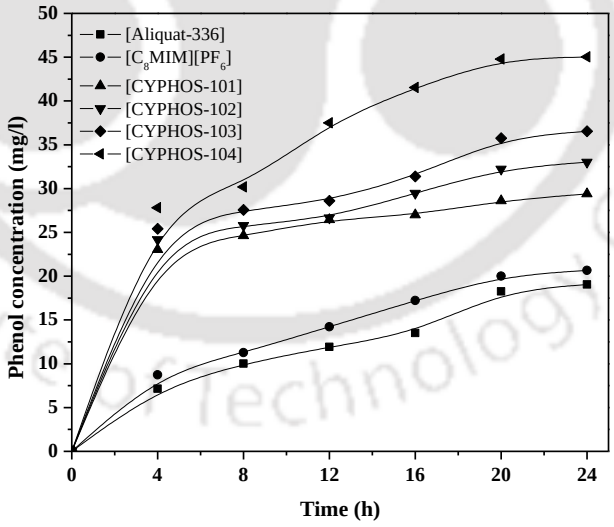


**Figure. 5.2.2.** Variation of stripping phase concentration with time for different ILs for SILM transport experiment: (Conditions: initial strip phase concentration: 100 mg $L^{-1}$, pH: 5.6, stirring speed: 300 rpm and temperature: 25± °C).

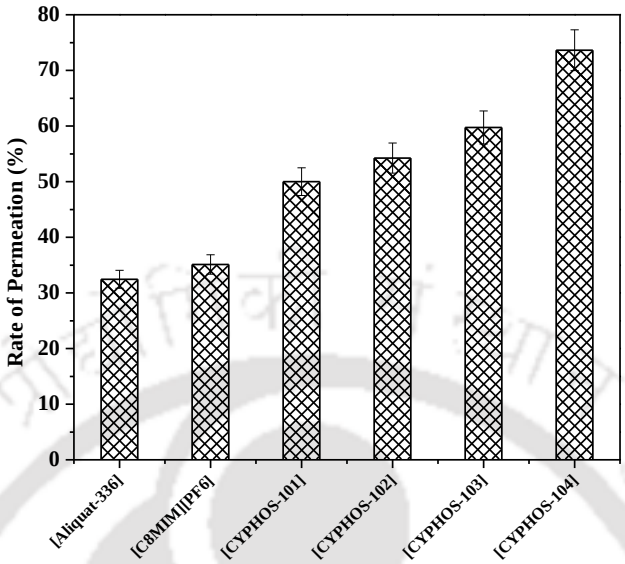


**Figure. 5.2.3(a).** Rate of permeation of different ILs: (Conditions: initial feed concentration: 100 mg $L^{-1}$, stripping phase concentration: 0.1 N NaOH, pH: 5.6, stirring speed: 300 rpm and temperature: 25± °C).

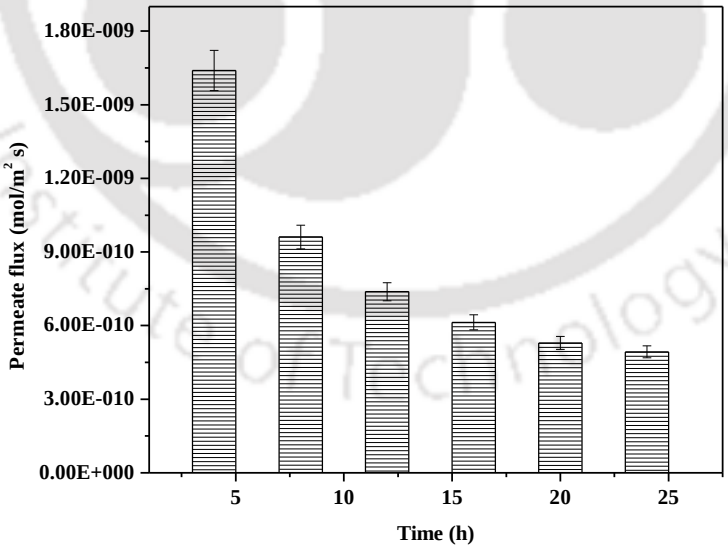


**Figure. 5.2.3(b).** Plot of permeate flux vs Time: (Conditions: initial feed concentration: 100 mg $L^{-1}$, stripping phase concentration: 0.1 N NaOH, pH: 5.6, temperature: 25± °C, and [CYPHOS-104] ionic liquid was used).

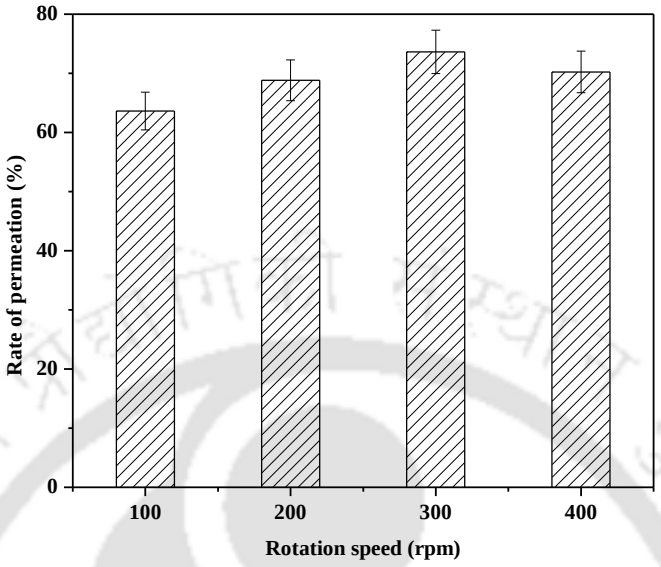


**Figure. 5.2.4.** Effect of stirring speed: (Conditions: initial feed concentration: 100 mg $L^{-1}$, stripping phase concentration: 0.1 N NaOH, pH: 5.6, temperature: 25± °C, and [CYPHOS-104] ionic liquid was used).

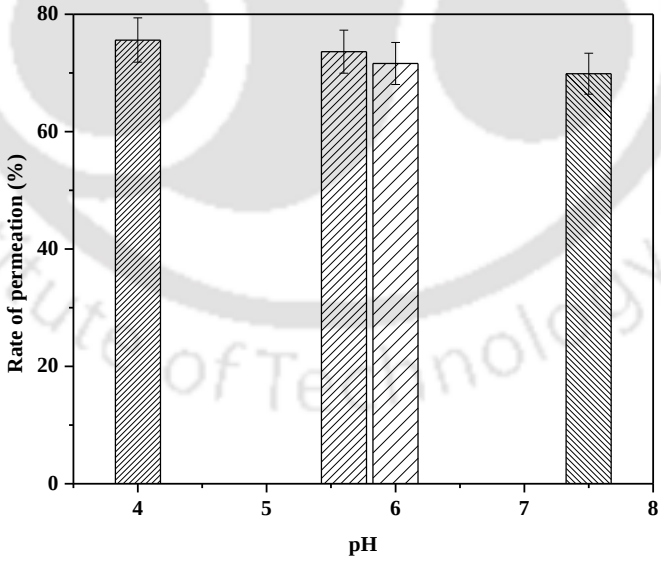


**Figure. 5.2.5.** Effect of feed phase pH on performance of SILM.

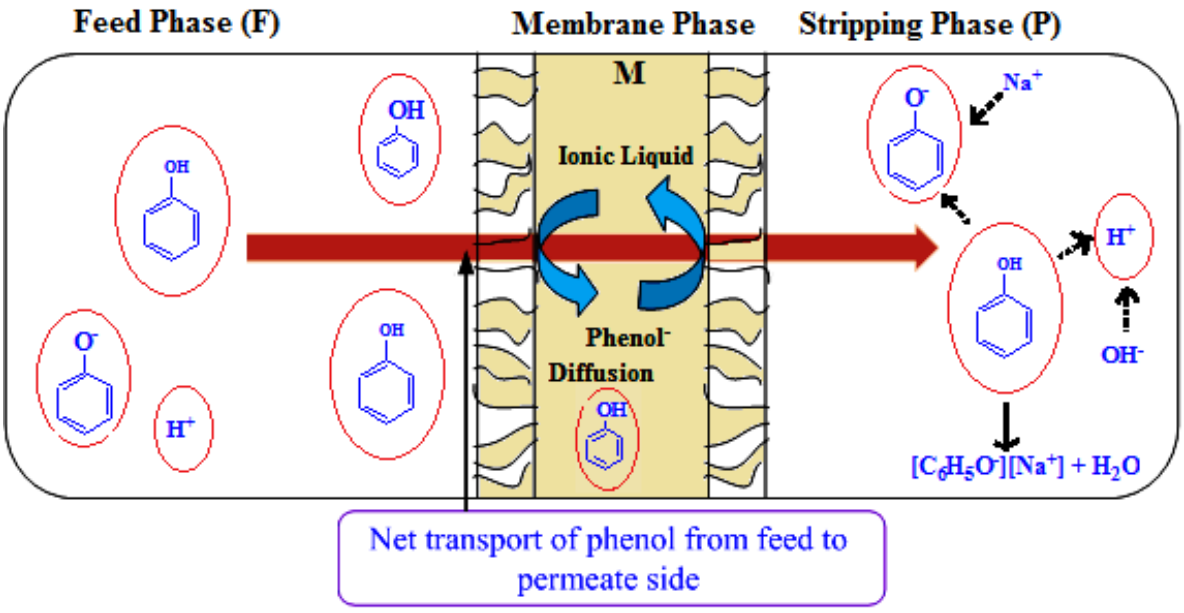


**Figure. 5.2.6.** Transport mechanism of phenol from feed to permeate side.

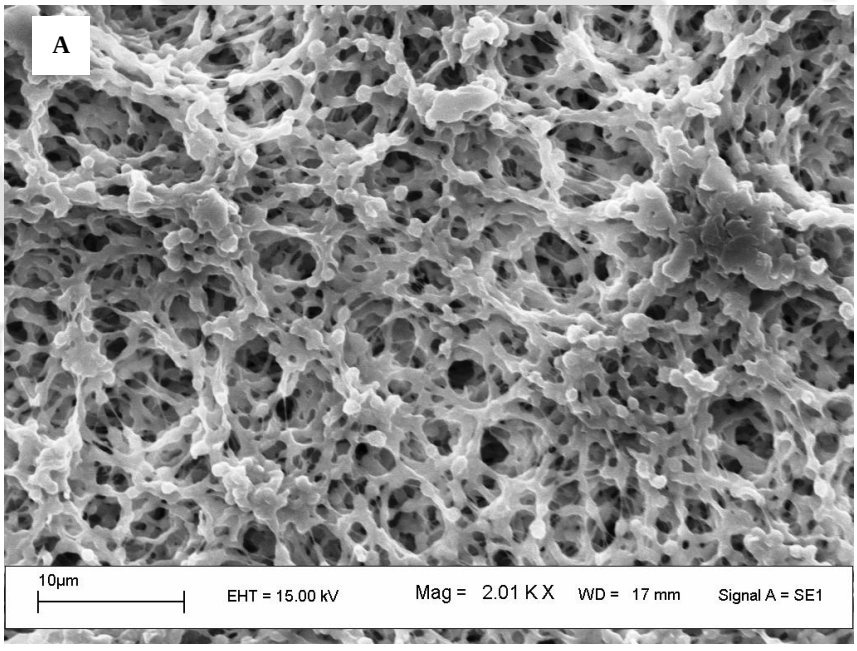


**Figure. 5.2.7(a).** Scanning electron micrographs of the blank PVDF membrane.

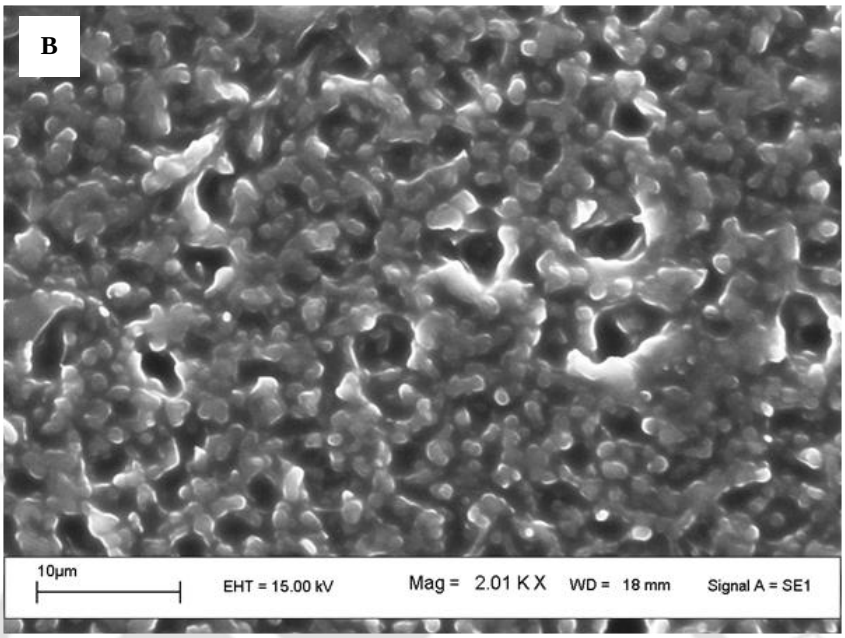


**Figure. 5.2.7(b).** Scanning electron micrographs of the PVDF membrane impregnated with $[C_8MIM][PF_6]$.

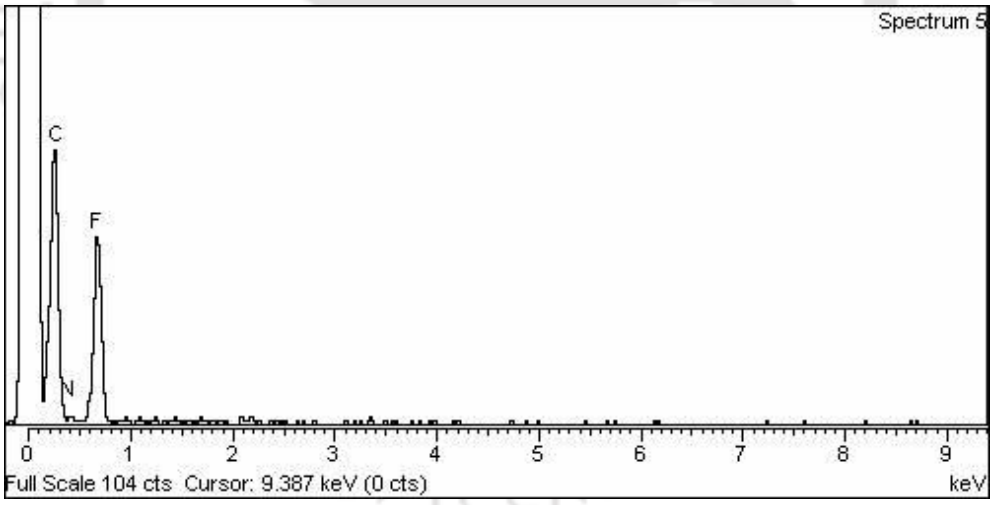


**Figure 5.2.8(a).** EDX spectra of the PVDF membrane without ionic liquid.

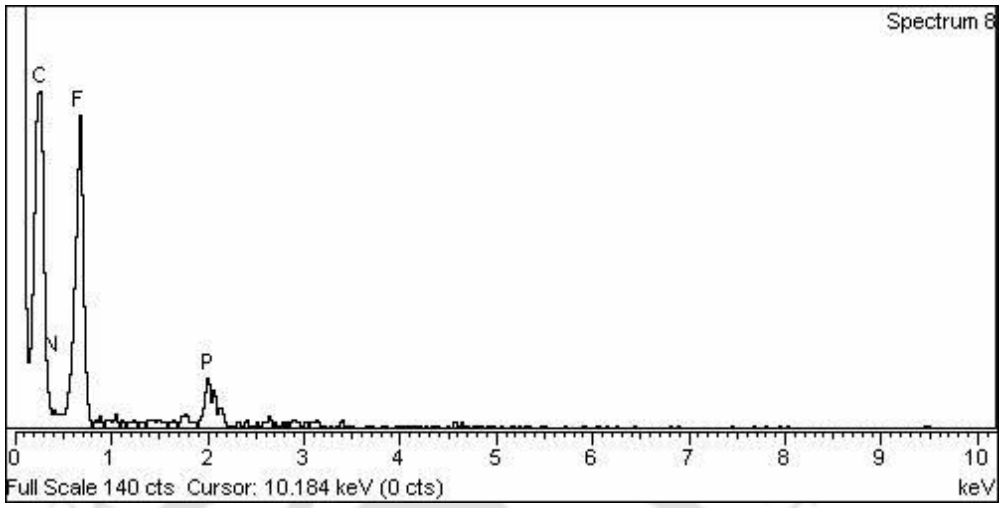


**Figure 5.2.8(a).** EDX spectra of the PVDF membrane without ionic liquid.

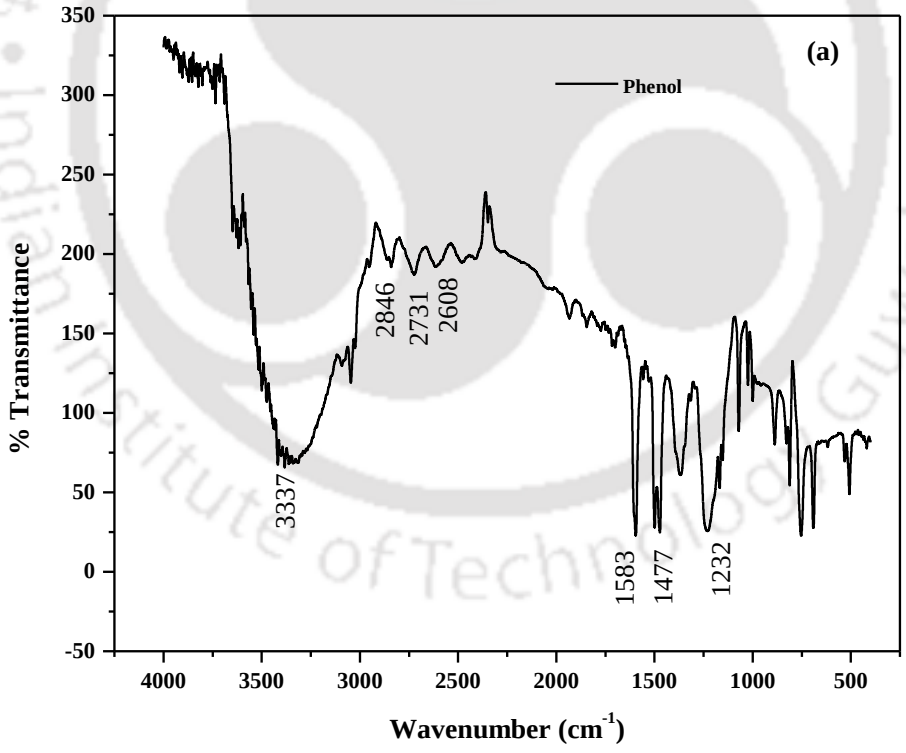


**Figure. 5.2.9(a).** The IR spectra of pure phenol.

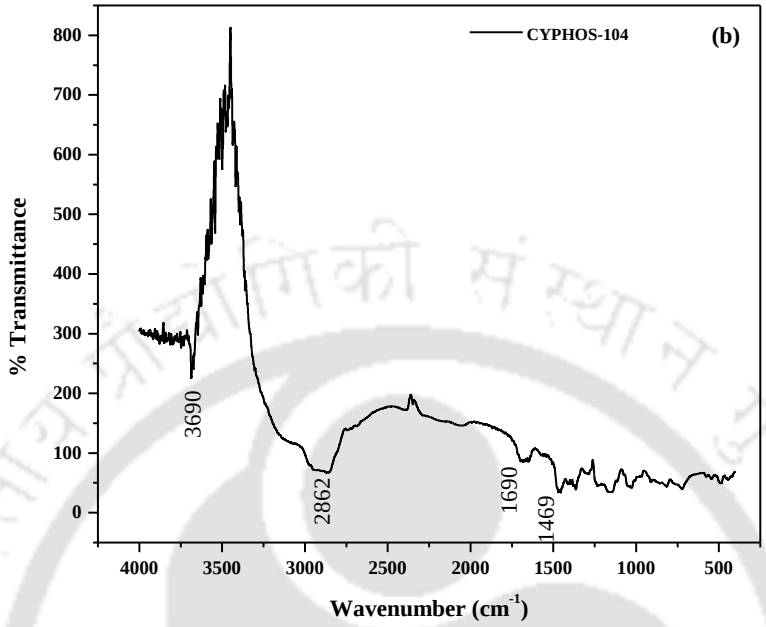


**Figure. 5.2.9(b).** The IR spectra of pure ionic liquid (CYPHOS-104).

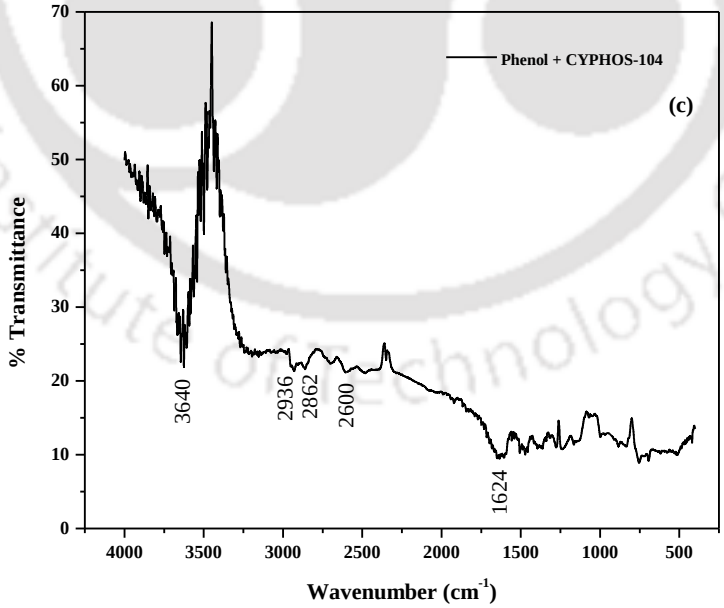


**Figure. 5.2.9(c).** The IR spectra of mixture of phenol and CYPHOS-104.

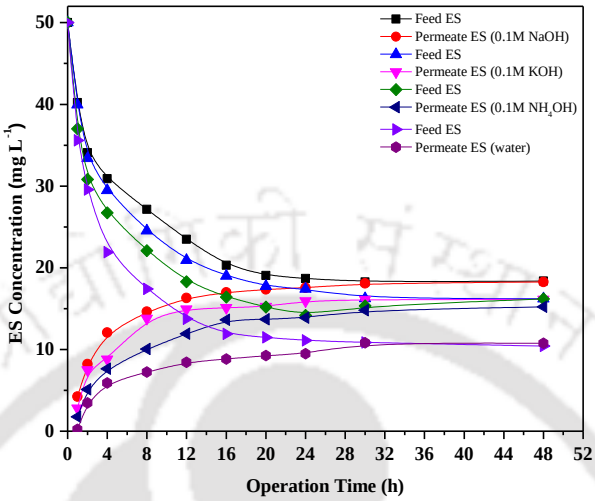


**Figure 5.3.1.** Variation in ES concentration in feed and strip solution as a function of operation time (effluent sample). (Initial ES concentration in feed = 50 mg $L^{-1}$, deionized water used as strip phase solution, blank PVDF membrane used (without ionic liquid) and temperature=25±1°C).

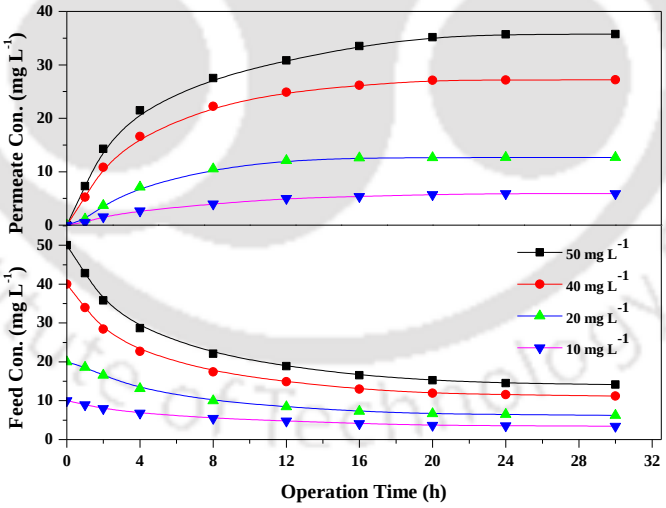


**Figure 5.3.2.** Effect Initial feed concentration as a function of operation time (effluent sample). (Initial ES concentration in feed = 50–10 mg $L^{-1}$, strip phase solution=0.1M NaOH, ionic liquid [$C_4$DMIM][$PF_6$] immobilized with PVDF membrane, feed pH=6.5 and temperature=25±1°C).

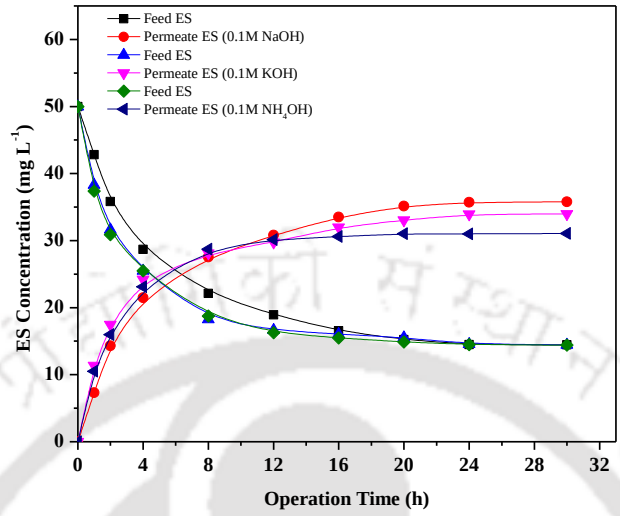


**Figure 5.3.3.** Variation in ES concentration in feed and strip phase solution as a function of operation time (effluent sample). (Initial ES concentration in feed = 50 mg $L^{-1}$, strip phase solution (0.1M NaOH, 0.1M KOH and 0.1M $NH_4OH$ at feed pH=6.5), ionic liquid $[C_4DMIM][PF_6]$ was immobilized with PVDF membrane and temperature=25±1 °C).

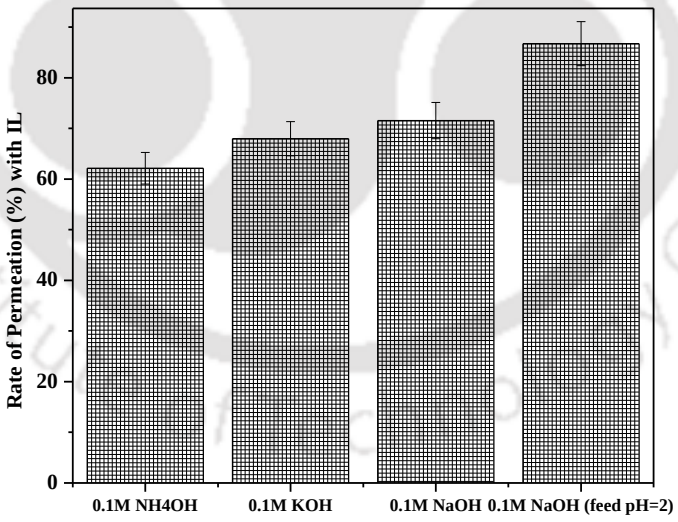


**Figure 5.3.4.** Variation in permeation rates of ES ion for different strip solution. (Initial ES concentration in feed = 50 mg $L^{-1}$, strip phase solution of 0.1M NaOH, 0.1M KOH and 0.1M $NH_4OH$ with feed pH=6.5 and 0.1M NaOH at feed pH=2, ionic liquid $[C_4DMIM][PF_6]$ immobilized with PVDF membrane and temperature=25±1 °C).

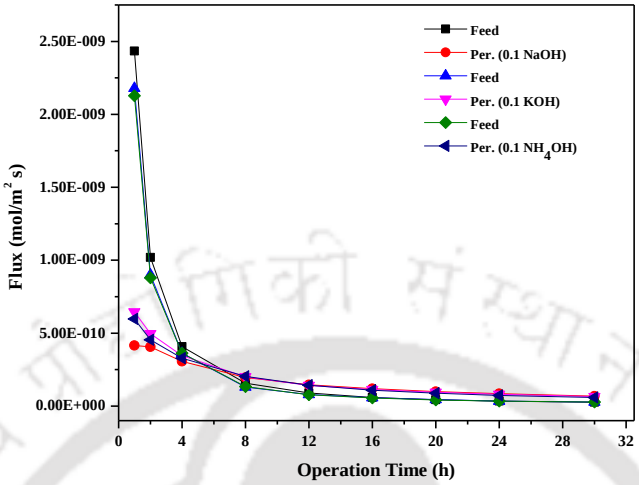


**Figure 5.3.5.** Flux as function of operation time. **(**Initial ES concentration in feed = 50 mg $L^{-1}$, strip phase solution=0.1M NaOH, ionic liquid [$C_4$DMIM][$PF_6$] immobilized with PVDF membrane, feed pH=6.5 and temperature=25±1°C).

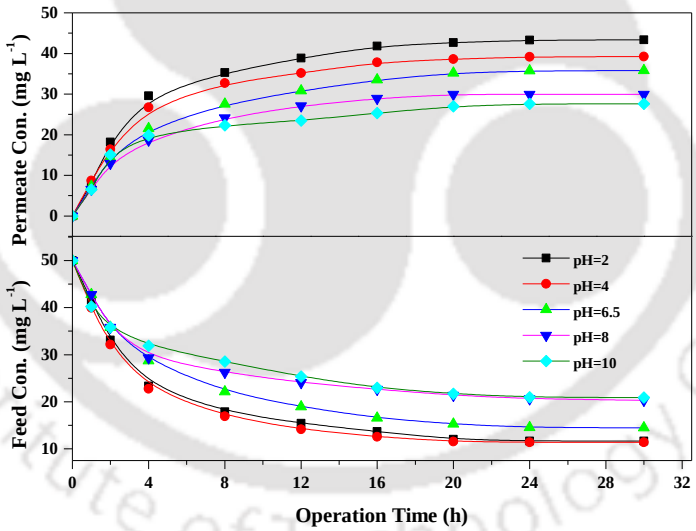


**Figure 5.3.6.** Variation in ES concentration in feed and strip phase solution at different feed pH conditions as a function of time (effluent sample). (Initial ES concentration in feed = 50 mg $L^{-1}$, strip phase solution= 0.1M NaOH, ionic liquid [$C_4$DMIM][$PF_6$] immobilized with PVDF membrane and temperature=25±1 °C).

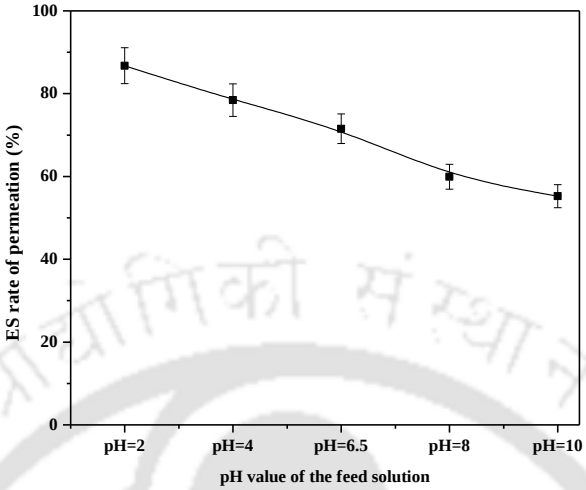


**Figure 5.3.7.** Variation of rate of ES permeation with feed solution pH value. (Initial ES concentration in feed = 50 mg $L^{-1}$, strip phase solution=0.1M NaOH, ionic liquid [$C_4$DMIM][$PF_6$] immobilized with PVDF membrane, feed pH=2–10 and temperature=25±1°C).

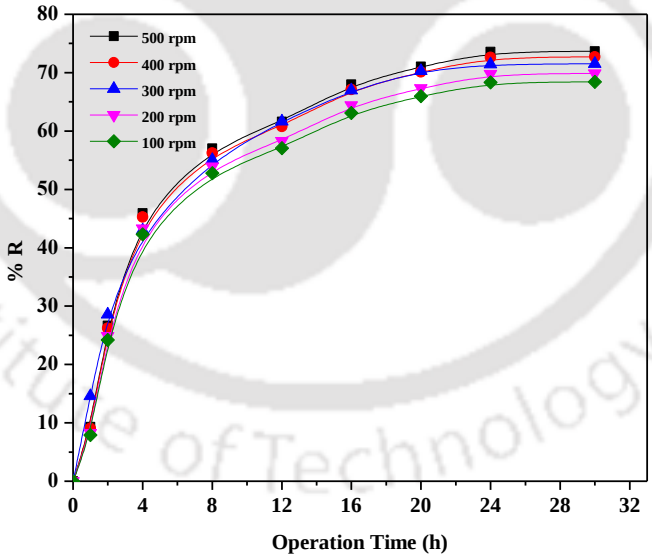


**Figure 5.3.8.** Effect of stirring speed in feed solution on the extraction of ES. (Initial ES concentration in feed = 50 mg $L^{-1}$, strip phase solution=0.1M NaOH, ionic liquid [$C_4$DMIM] [$PF_6$] immobilized with PVDF membrane, feed pH=6.5 and temperature=25±1°C).

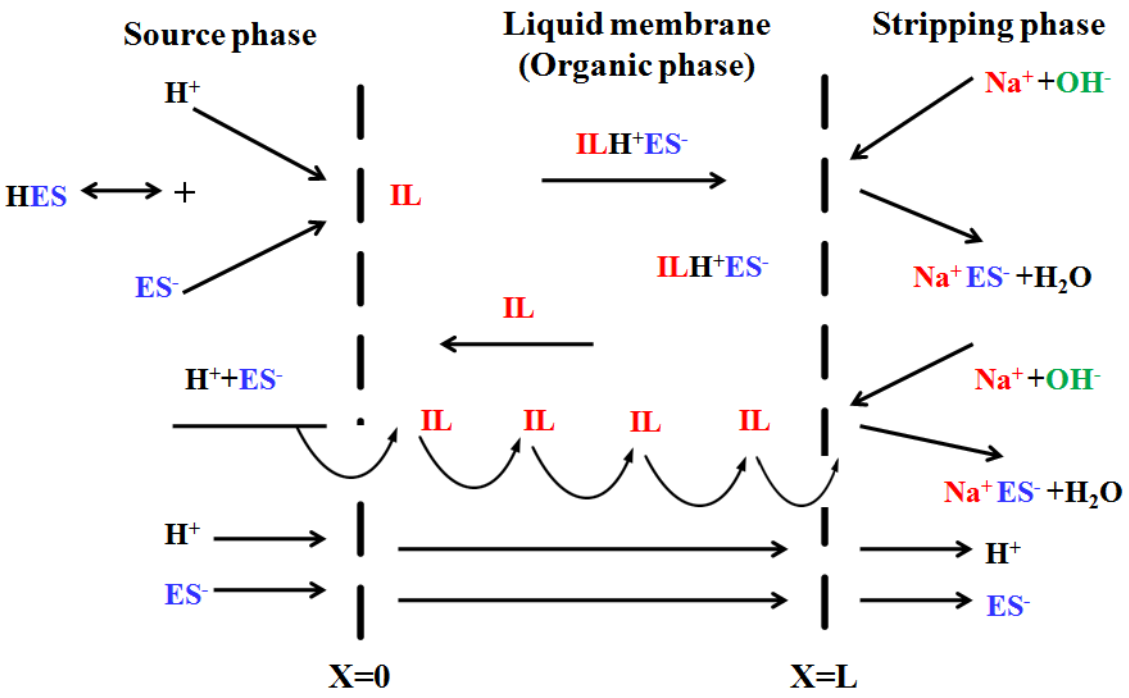


**Figure 5.3.9.** Transport mechanism of ES from feed to stripping phase trough SILM.

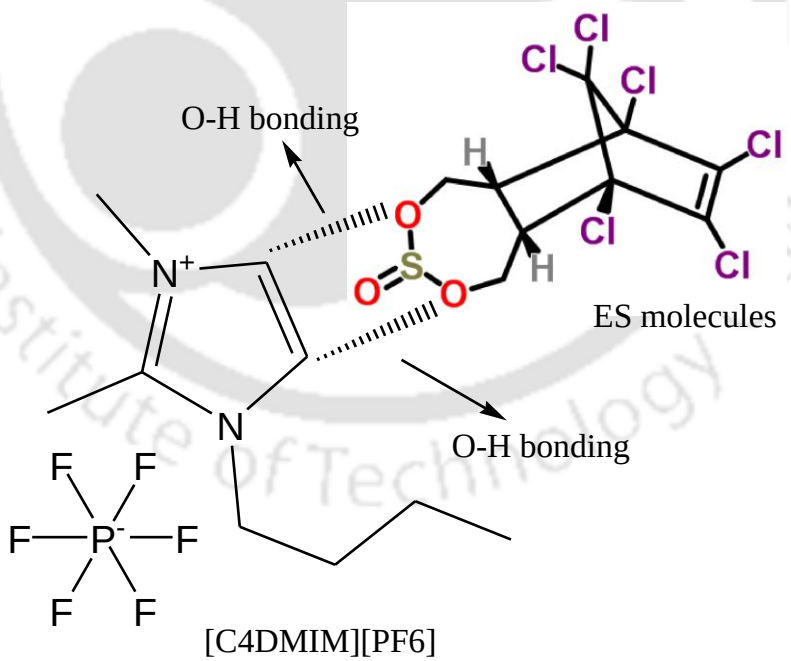


**Figure 5.3.10.** Schematic of possible interactions between ES molecules and [$C_4$DMIM][$PF_6$].

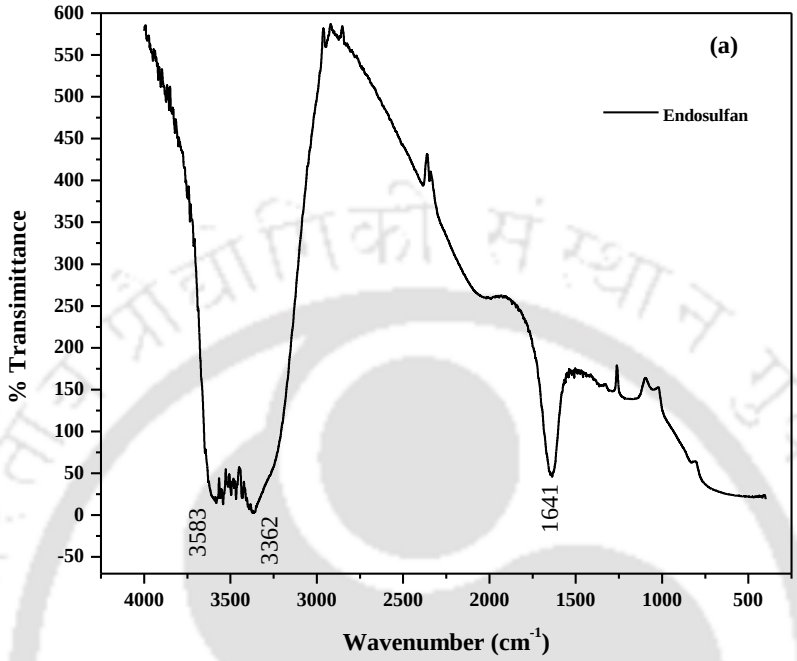


**Figure 5.3.11(a).** FT–IR spectra of pure aqueous phase endosulfan.

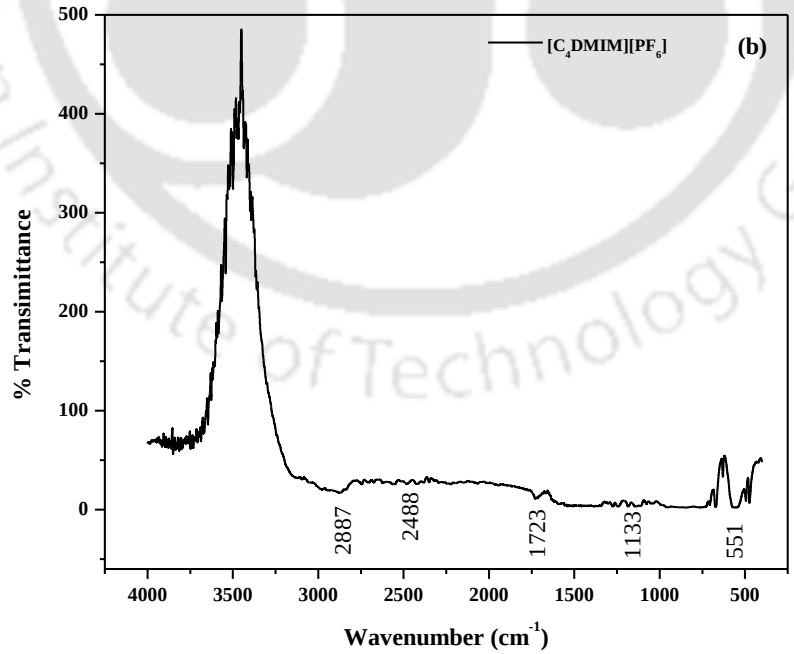


**Figure 5.3.11(b).** FT–IR spectra of pure $[C_4DMIM][PF_6]$ ionic liquid.

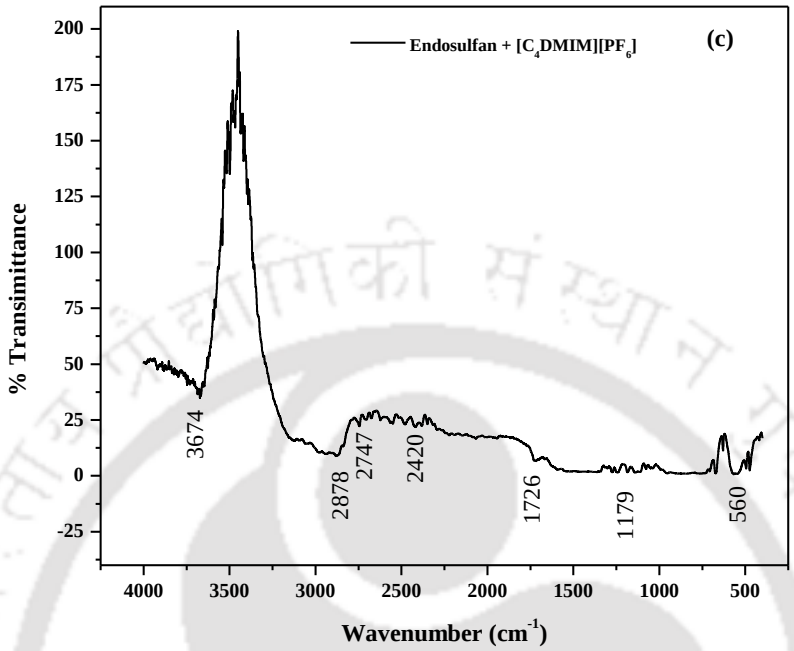


**Figure 5.3.11(c).** FT–IR spectra of mixture of aqueous phase endosulfan and $[C_4DMIM][PF_6]$.

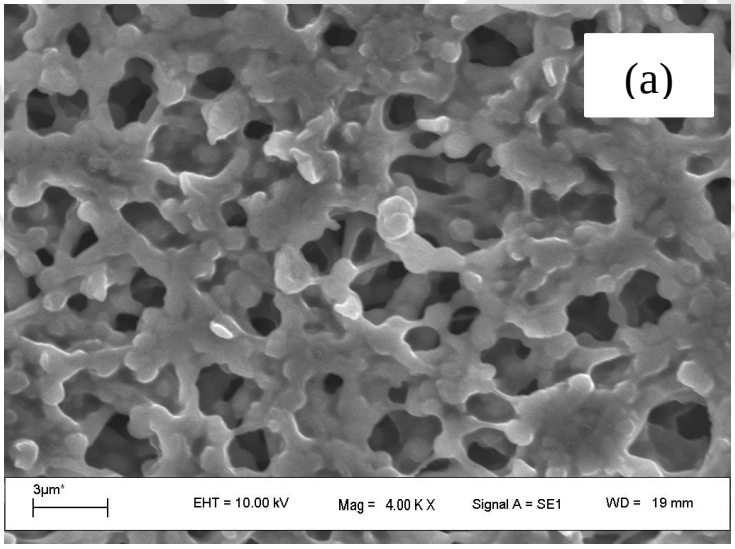


**Figure 5.3.12. (a)** SEM micrograph pure PVDF membrane.

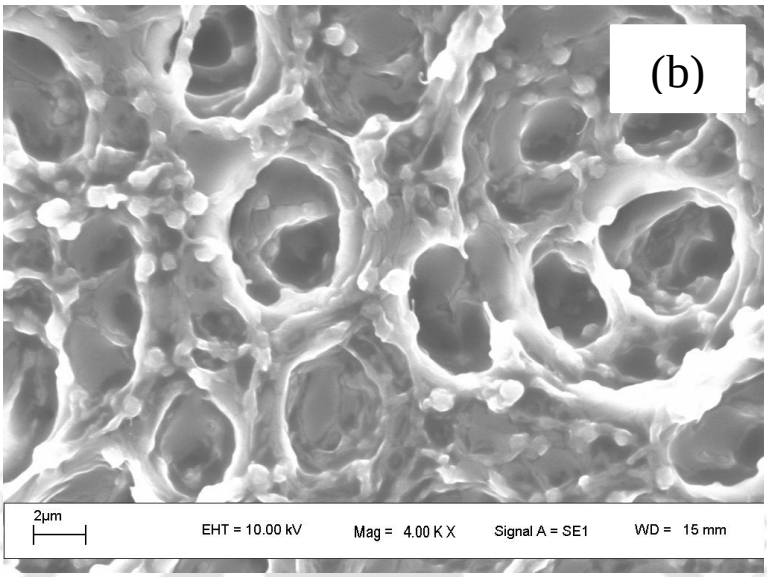


**Figure 5.3.12(a).** SEM micrograph PVDF membrane immobilized with $[C_4DMIM][PF_6]$.

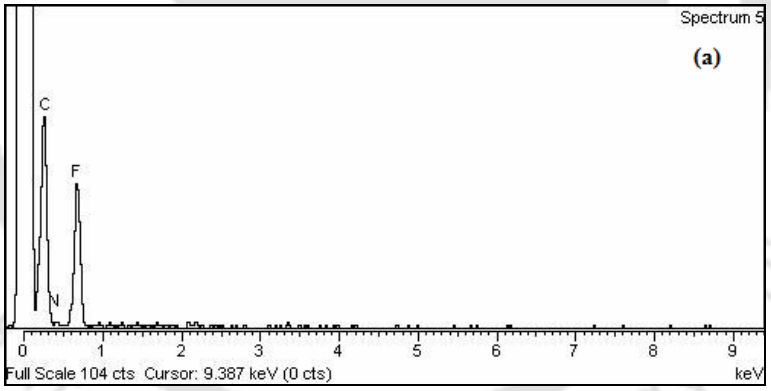


**Figure 5.2.12.** (c) EDX of pure PVDF membrane; (d) EDX of PVDF membrane immobilized with $[C_4DMIM][PF_6]$.

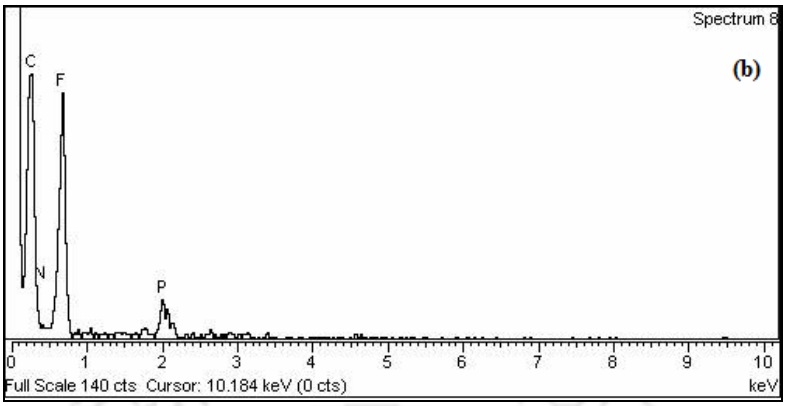


**Figure 5.2.12.**(c) EDX of pure PVDF membrane; (d) EDX of PVDF membrane immobilized with $[C_4DMIM][PF_6]$.

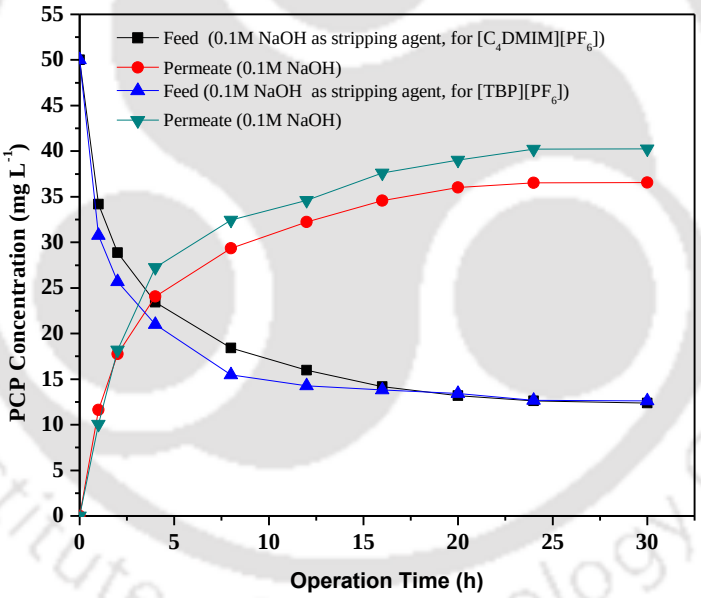


**Figure 5.4.1.** PCP concentration in the feed and permeate solutions as a function of time. (Conditions: feed phase concentration=50 mg $L^{-1}$, receiving phase=0.1M NaOH, feed pH=6.5, stirring speed=300 rpm and temperature=25°C).

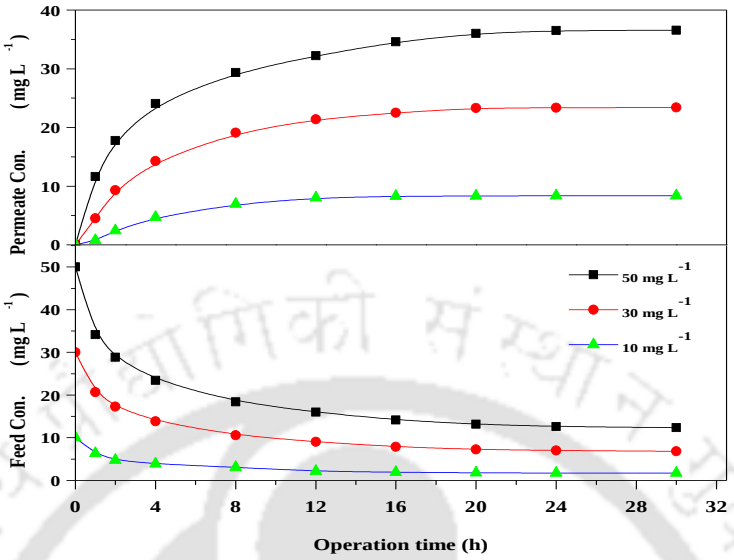


**Figure 5.4.2.** PCP concentration in the feed and permeate solutions as a function of time. (Conditions: feed phase concentration=10–50 mg $L^{-1}$, receiving phase=0.1M NaOH, feed pH=6.5, stirring speed=300 rpm and temperature=25°C).

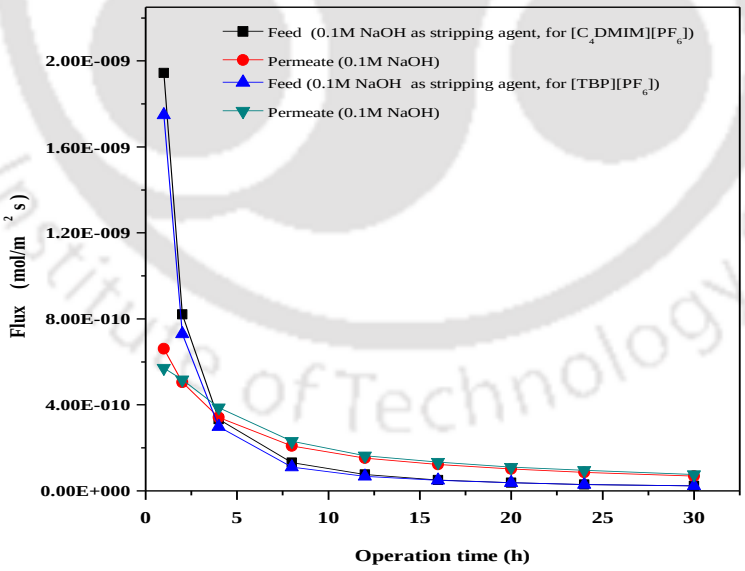


**Figure 5.4.3.** Membrane flux in the feed and permeate solutions as a function of time. (Conditions: feed phase concentration=50 mg $L^{-1}$, receiving phase=0.1M NaOH, feed pH=6.5, stirring speed=300 rpm and temperature=25°C).

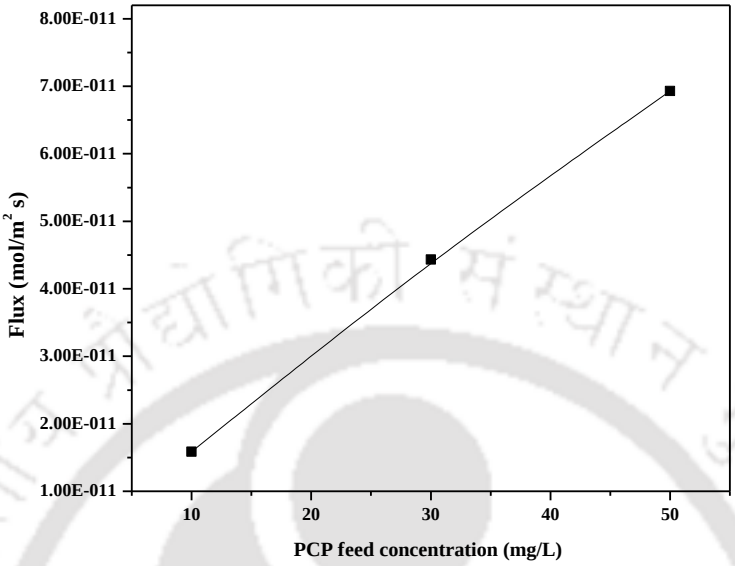


**Figure 5.4.4.** Membrane flux as a function of initial PCP feed concentration.

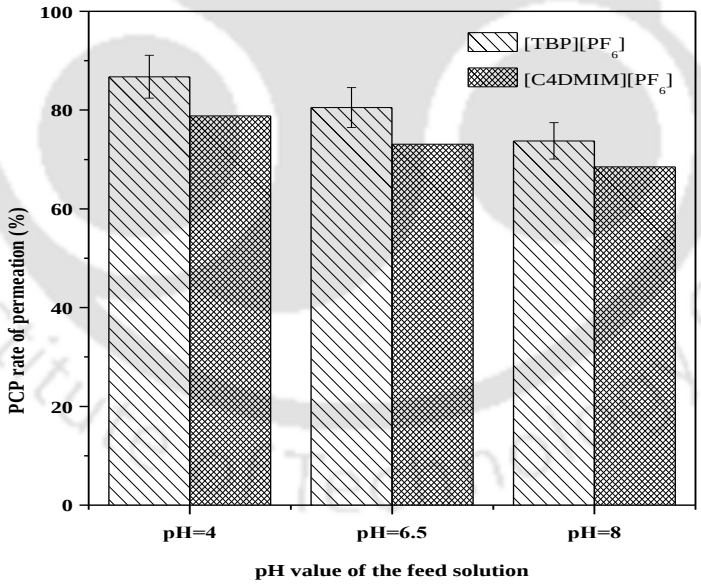


**Figure 5.4.5(a).** The rate of permeation PCP as a function of feed pH, (Conditions: feed phase concentration=50 mg $L^{-1}$, receiving phase=0.1M NaOH, feed pH=4–8, stirring speed=300 rpm and temperature=25°C).

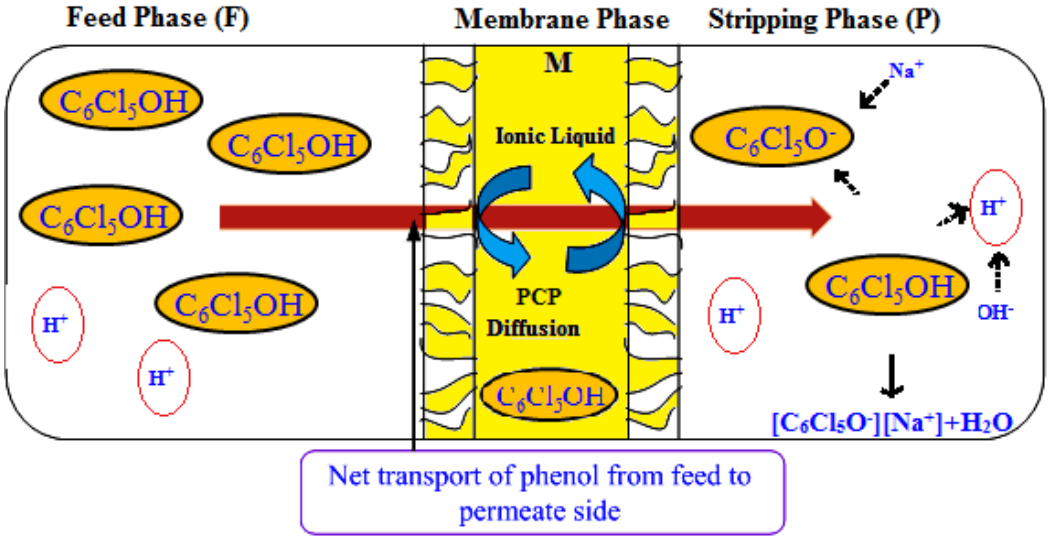


**Figure 5.4.5(b).** PCP transport mechanism from feed to stripping phase trough SILM.

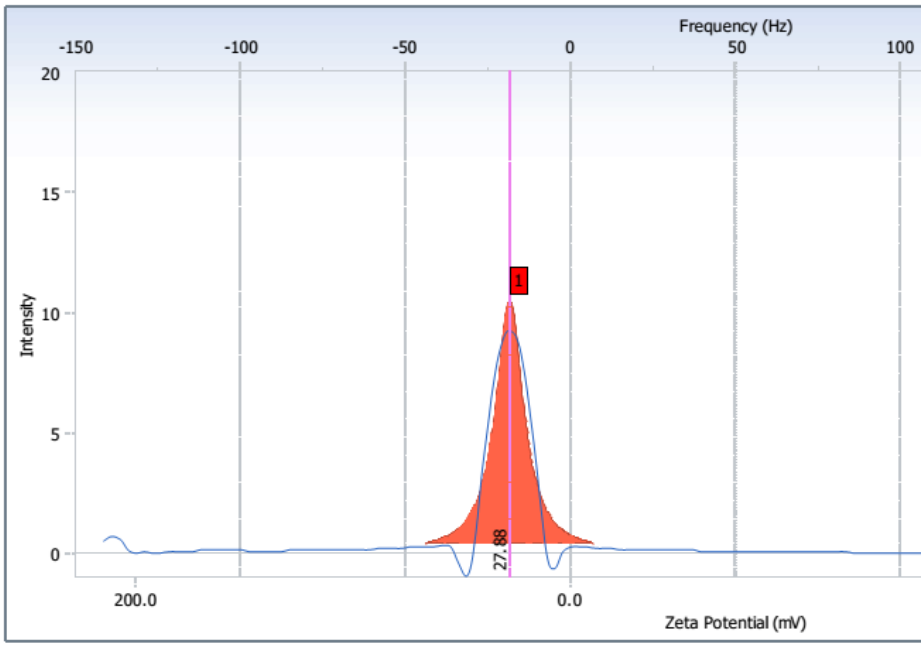


**Figure 5.4.6(a).** Zeta potential chromate gram of (a) blank PVDF membrane.

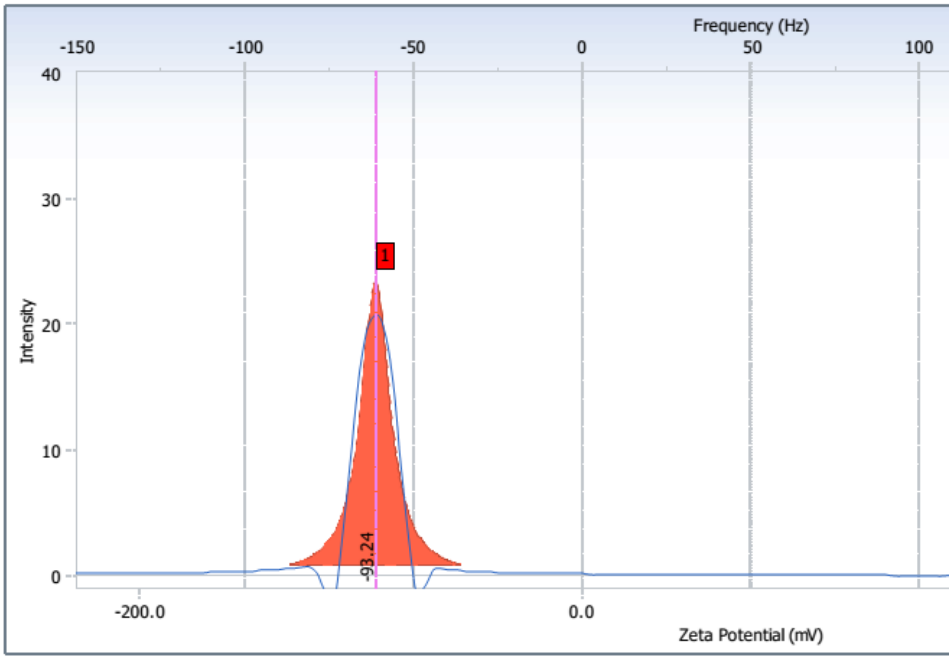


**Figure 5.4.6(b).** Zeta potential chromate gram of PVDF membrane after immobilization with $[C_4DMIM][PF_6]$.

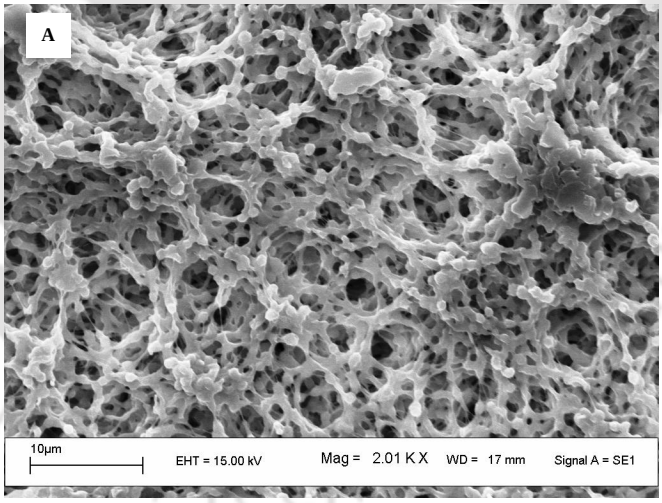


**Figure 5.4.7(a).** SEM image of pure PVDF membrane.

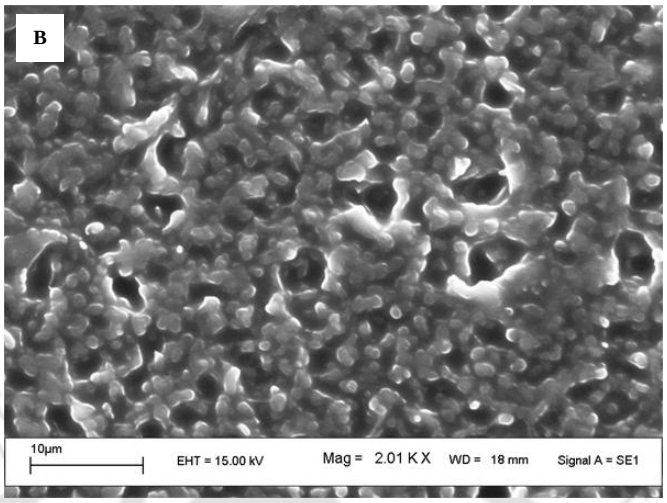


**Figure 5.4.7(b).** SEM image of PVDF membrane immobilized with $[C_4DMIM][PF_6]$.

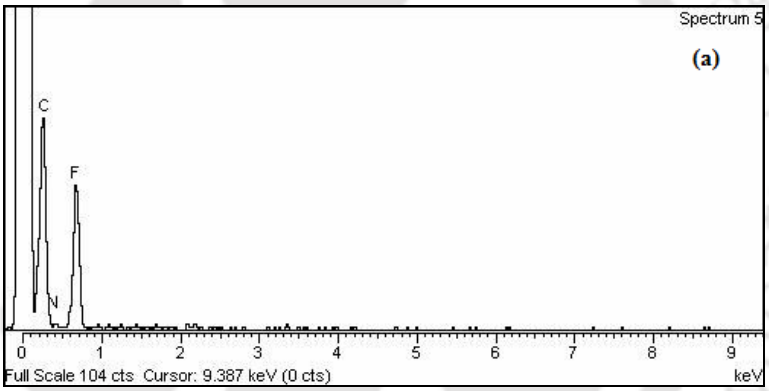


**Figure 5.4.8(a)** SEM micrograph pure PVDF membrane.

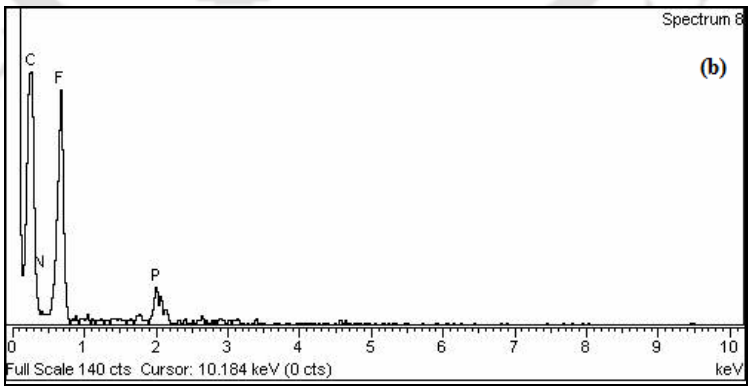


**Figure 5.4.8(b).** SEM micrograph PVDF membrane immobilized with $[C_4DMIM][PF_6]$.

# CHAPTER 6

## CONCLUSION AND SCOPE FOR FUTURE WORK

## 6.1. Conclusions

Separation of EDCs such as PCP, DDT, ES and phenol were successfully carried out from aqueous solution both theoretically and experimentally. Further, SILM and LLE experiments were performed to separate EDCs. Initially, theoretical screening was carried using COSMO–RS based predictions at infinite dilution.

This thesis thus reports the judicious screening of various ILs for the extraction of EDCs from aqueous solutions. These screening results were then used for the application of LLE and SILM processes. After the screening process, the experimental and COSMO–RS validation was carried using the octanol–water partition coefficients ($K_{ow}$) of EDC's. From the screening studies, the IL [$C_4$DMIM][$PF_6$] was chosen as potential IL for HOMO–LUMO studies and experimental (LLE and SILM) measurements later.

The HOMO–LUMO interaction studies were carried to find out parameters like global hardness and softness, chemical potential, electronegativity and electrophilicity index, HOMO/LUMO energy. HOMO–LUMO energy gaps were predicted for two systems i.e. [PCP]+[$C_4$DMIM][$PF_6$] and [PA]+[$C_4$DMIM][$PF_6$] and also for individual species. Initially geometry optimization was carried for individual molecules of [PCP], [PA], cations, anions and [PCP]\[PA]+ILs complexes. DFT based B3LYP/6-31G* method was adopted to carry out geometry optimization and then determine the quantum chemical descriptors. The experimental and theoretical $^1$H NMR chemical shifts of [PCP]+[$C_4$DMIM][$PF_6$] and [PA]+[$C_4$DMIM][$PF_6$] were also carried out to benchmark our predictions. The highest and lowest HOMO–LUMO energy gap was obtained for [PCP]+[$C_4$DMIM][$PF_6$] (0.146 eV) and

[PA]+[$C_4$DMIM][$PF_6$] (0.0597 eV) respectively. Charge distribution using the NBO analysis was also studied in detail.

Further, experimental investigation of Liquid–Liquid Equilibrium (LLE) behavior of [$C_4$DMIM][$PF_6$](1)+PCP(2)+water(3) and [$C_4$DMIM][$PF_6$](1)+PA(2)+water(3) were carried at ambient conditions and plotted in ternary plots. Information obtained from the ternary plots indicates a favourable sloping of the tie lines towards the IL. The selectivity and distribution coefficients determined from the tie line data confirmed high values of selectivity ~ 24–29 for PA and ~106–293 for PCP. The UNIQUAC and NRTL models were then used to correlate the experimental data. Both the methods gave RMSD value less than unity. For each ternary system, the Othmer–Tobias and Bachman correlation was also studied to verify the reliability of the experimental tie–line results. The $R^2$ value was close to unity.

The concluding part of the thesis presents the removal of ES, phenol and PCP using SILM. The commercial grade ILs namely: [$C_4$DMIM][$PF_6$], [TBP][$PF_6$] were used for ES and PCP removal, while [CYPHOS® 101], [CYPHOS® 102], [CYPHOS® 103], [CYPHOS® 104], [Aliquat 336®] and [$C_8$MIM][$PF_6$] were used for phenol removal. Here ILs were immobilized with PVDF membranes for separation of EDCs from aqueous phase using SILM. Effect of operating parameters such as pH and feed concentration along with flux calculation and transport mechanism were presented. The transport mechanism of ES, phenol and PCP through SILM was explained by hydrogen bonding interactions, hydrophobic interactions and carbon–π bonding interactions. The characterization of membrane was carried by SEM and EDX analysis. Highest PCP permeation of 86.74% was obtained by

[TBP][$PF_6$] at feed pH of 4, followed by 78.82% for [$C_4$DMIM][$PF_6$] after 30 h experimental run at feed pH of 4. The maximum permeation rate of 80.52% was obtained by [TBP][$PF_6$] followed by 73.11% for [$C_4$DMIM][$PF_6$] without changing the feed pH (at 6.5) after 30 h. The maximum phenol permeation rate of 75.63% was achieved over an experimental run of 24 h at pH 4. High permeation rate was obtained by [CYPHOS® 104] among ILs studied in case of phenol.

Finally, the selective separation of Endosulfan was carried out via supported membrane (SLM) using the IL, [$C_4$DMIM][$PF_6$] as the membrane phase. In case of endosulfan SILM experiments, a maximum of 72% (at feed pH=6.5) of endosulfan permeation was observed using 0.1 M NaOH as stripping agent after 30 h of experimental run. The rate of permeation decreases with increase in pH from 2 to 10 (87–55%). Different stripping agents such as 0.1M NaOH, 0.1M KOH and 0.1M $NH_4OH$ were successfully used and their performance was evaluated. The transport mechanism involving SILMs has also been elucidated. From our studies, SILM and LLE methods have been shown potential for further development into a process for the removal of organic compounds from wastewater in the bench scale or in industry. The results of the present study are quite encouraging and suggest that different EDCs can be selectively separated using LLE and SILMs techniques.

## 6.2. Scope for future work

The research work presented in this thesis can be extended further for other heavy metals and pharmaceutical effluents that would strengthen the arguments made and conclusions reached in this thesis. Based on the research findings from this work, the following are recommended for further studies in future as follows:

(a) HOMO–LUMO studies for other EDC's such as Dioxin, Atrazine, Phthalates, Lead, Mercury and Arsenic.

(b) SILM can be applied for the investigations of chemical compositions on different heavy metals and textile dye removal from wastewater

(c) Mathematical modeling of SILM experiments may be helpful for better understanding of the kinetics of membrane separation based on established mass transfer and diffusion theories. Task Specific Ionic Liquids (TSIL) can be used as carrier solvents in SILM technology for the separation of industrial gases such as carbon dioxide and sulphur dioxide.

(d) The effect of co-ions such as Na, Ca and Mg in EDCs can be studied using SILM and Solid Liquid Extraction in (b).

(e) There is potential application for the COSMO–RS method to provide substantial benefits for the processing and pre–treatment of biomass for saccharification by depolymerization of lignin.

# APPENDIX A

## Peer–Reviewed International Publications

[1]. Santhi Raju Pilli, Tamal Banerjee, Kaustubha Mohanty, Liquid–liquid equilibrium (LLE) data for ternary mixtures of [C4DMIM][PF6]+[PCP]+[water] and [C4DMIM][PF6] +[PA]+[water] at T = 298.15 K and p = 1 atm, ***Fluid Phase Equilibria,*** **(2014)** (**accepted,** ***DOI: 10.1016/j.fluid.2014.08.004***).

[2]. Santhi Raju Pilli, Tamal Banerjee, Kaustubha Mohanty, 1-Butyl-2,3-dimethylimidazolium hexaflourophosphate as a Green Solvent for the Extraction of Endosulfan from Aqueous Solution Using Supported Liquid Membrane, ***Chemical Engineering Journal***, **257 (2014) 56–65.**

[3]. Santhi Raju Pilli, Tamal Banerjee, Kaustubha Mohanty, Performance of Supported Liquid Membrane for the Removal of Phenol using Ionic Liquids, ***Desalination and Water Treatment,*** **(2014)** (**accepted, doi: 10.1080/19443994.2014.907750**).

[4]. Santhi Raju Pilli, Tamal Banerjee, Kaustubha Mohanty, Extraction of Phthalic Acid from Aqueous Solution by Using Ionic Liquids: A Theoretical Study, ***International Journal of Thermodynamics,*** **17 (2014) 42–51.**

[5]. Santhi Raju Pilli, Tamal Banerjee, Kaustubha Mohanty, Ionic Liquids as Green Solvents for The Extraction ff Endosulfan from Aqueous Solution: a Quantum Chemical Approach, ***Chemical Product and Process Modeling,*** **8 (2013) 1–14**.

[6]. Santhi Raju Pilli, Tamal Banerjee, Kaustubha Mohanty, Extraction of Pentachloro–Phenol and Dichlorodiphenyltrichloroethane from aqueous Solutions using Ionic Liquids, ***Journal of Industrial and Engineering Chemistry,*** **18 (2012) 1983–1996.**

[7]. Santhi Raju Pilli, Tamal Banerjee, Kaustubha Mohanty, HOMO–LUMO Energy Interactions between PCP\PA and Ionic Liquids using Density Functional Theory: Evaluation and Comparison (**submitted to** ***Journal of Molecular Modelling***).

[8]. Santhi Raju Pilli, Tamal Banerjee, Kaustubha Mohanty, Potential Removal of Pentachlorophenol from Wastewater using Novel Supported Ionic Liquid Membranes (**to be submitted**).

## International/National Conferences/Proceedings

[1]. Santhi Raju Pilli, Tamal Banerjee, Kaustubha Mohanty**,** Theoretical Screening of Different Ionic Liquids for the Separation of Bisphenol A from Aqueous Solution: A COSMO–RS Approach, in **Recent Trends in Water Science and Technology**, Ch. 25, Charotar Publishing House Ltd. (ISBN 978-93-80358-90-1), **2014**, 166-175.

[2]. Santhi Raju Pilli, Tamal Banerjee, Kaustubha Mohanty, Preparation and Characteri–zation of PVDF based Supported Ionic Liquid Membranes for the Removal of Organic Pollutants, poster to be presented in **the first Symposium on Advances in Sustainable Polymers (ASP),** organized by IIT Guwahati, Assam on Jan 10–11, **2014**.

[3]. Santhi Raju Pilli, Tamal Banerjee*, Kaustubha Mohanty, Performance of Ionic Liquids to remove Phenol from Aqueous Phase using Supported Ionic Liquid Membranes, poster presented in **Indrapastha International Conference on Biotechnology,** organized by Guru Gobind Singh Indraprastha University, New Delhi, October 22–25, **2013**.

[4]. Santhi Raju Pilli, Tamal Banerjee, Kaustubha Mohanty**,** Supported Ionic Liquid Membranes for the Separation of Endosulfan from Aqueous Phase: Experimental and COSMO–RS Study, paper presented in ***9th World Congress of Chemical Engineering (WCCE9)*** at Seoul, South Korea, August 18$^{th}$–23$^{rd}$, **2013**.

[5]. Santhi Raju Pilli, Tamal Banerjee, Kaustubha Mohanty**,** Separation of Phenol from Aqueous Phase Using Supported Ionic Liquid Membrane, poster presented in ***9th World Congress of Chemical Engineering (WCCE9)*** at Seoul, South Korea, August 18$^{th}$–23$^{rd}$, **2013**.

[6]. Santhi Raju Pilli, Tamal Banerjee, Kaustubha Mohanty**,** Quantum Chemical based Screening of Ionic Liquids for the Extraction of Phthalic Acid from Aqueous Solution, poster presented in ***International Conference on Advances in Chemical Engineering*** (ACE–2013) at IIT Roorke, February 22$^{nd}$–24$^{th}$, **2013**.

[7]. Santhi Raju Pilli, Tamal Banerjee, Kaustubha Mohanty, Application of Supported Ionic Liquid Membrane to the Phenol Removal from Wastewater, ***"REFLUX" 1.0,*** Annual Chemical Engineering Technical Festival organized by **Department of Chemical Engineering, IIT Guwahati,** April 6$^{th}$–7$^{th}$, **2013.**

[8]. Santhi Raju Pilli, Tamal Banerjee, Kaustubha Mohanty, Quantum Chemical Based Screening of Ionic Liquids for the Extraction of Endosulfan from Aqueous Solution, ***National Conference on Environment and Biodiversity of India*** **[EBI 2011],** Jamia Millia Islamia, Jamia Nagar, New Delhi, December 30$^{th}$–31$^{st}$, **2011**.

[9]. Santhi Raju Pilli, Tamal Banerjee, Kaustubha Mohanty**,** Ionic Liquids as Green Solvents for the Extraction of EDCs From Aqueous Solution: A Theoretical Approach, ***CHEMCON–2011, 64th Annual Session of the Indian Institute of Chemical Engineers*****,** M S Ramaiah Institute of Technology (MSRIT), Banglore, December 27th–29th, **2011.**